

The life and times of **Photosystem I**

excitation energy transfer and trapping unravelled

Bas Gobets

This thesis has been reviewed by:

Prof.dr. R.E. Blankenship, Arizona State University, Tempe, USA

Prof.dr. G.R. Fleming, University of California at Berkeley, Berkeley, USA

Dr. A. Freiberg, Institute of Physics of Tartu, Tartu, Estonia

Prof.dr. R. van Grondelle, Vrije Universiteit, Amsterdam

Dr. I.H.M. van Stokkum, Vrije Universiteit, Amsterdam

VRIJE UNIVERSITEIT

The life and times of Photosystem I

excitation energy transfer and trapping unravelled

ACADEMISCH PROEFSCHRIFT

ter verkrijging van de graad van doctor aan
de Vrije Universiteit Amsterdam,
op gezag van de rector magnificus
prof.dr. T. Sminia,
in het openbaar te verdedigen
ten overstaan van de promotiecommissie
van de faculteit der Exacte Wetenschappen
op dinsdag 15 oktober 2002 om 13.45 uur
in het auditorium van de universiteit,
De Boelelaan 1105

door

Sebastiaan Gobets

geboren te Uithoorn

promotor: prof.dr. R. van Grondelle
copromotor: dr. J.P. Dekker

Aan Aron Machiel Gobets
(±1754-1810)

Contents

	Abbreviations	ix
1	Introduction	1
	In the beginning	2
	Cyanobacteria	4
	Photosynthesis	5
	Light-harvesting pigments	8
	Heterogeneity, homogeneity and inhomogeneity	12
	Excitonic coupling and energy transfer	13
	The Photosystem I core complex	14
	Experimental techniques: The streak camera	18
	Data analysis	21
	This thesis	25
2	Polarized site-selected fluorescence spectroscopy of isolated Photosystem I particles	29
3	Time-resolved fluorescence emission measurements of Photosystem I particles of various cyanobacteria: a unified compartmental model	49
4	Energy transfer and trapping in Photosystem I	81
5	Bridging the gap between structural and lattice-models: a parametrization of energy transfer and trapping in Photosystem I	113
6	Excitation wavelength dependence of the fluorescence kinetics in Photosystem I particles from <i>Synechocystis</i> PCC 6803 and <i>Synechococcus elongatus</i>	133
7	Light harvesting by chlorophylls and carotenoids in the Photosystem I core complex of <i>Synechococcus elongatus</i> : a fluorescence upconversion study	161
8	Excitation energy transfer in dimeric Light-Harvesting Complex I: a combined streak camera/fluorescence upconversion study.	185
	Summary	205
	Samenvatting	207
	List of publications	211
	Nawoord	213

Abbreviations

A ₀	primary electron acceptor chlorophyll(s) in Photosystem I
ADP	adenosine diphosphate
ATP	adenosine triphosphate
β-car	β-carotene
Bchl	bacteriochlorophyll
Car	carotenoid
CD	circular dichroism
chl	chlorophyll
chl _a	chlorophyll- <i>a</i>
chl _b	chlorophyll- <i>b</i>
Cyt _{b₆f}	cytochrome <i>b₆f</i>
DAS	decay associated spectrum
Fd	ferredoxin
FNR	ferredoxin-NADPH ⁺ reductase
FWHM	full width at half maximum
IDF	inhomogeneous distribution function
IRF	instrument response function
LH1, LH2	Light-harvesting Complexes in bacterial (non-oxygenic) photosynthesis
LHCI	Light-harvesting Complex I of green plants
LHCII	Light-harvesting Complex II of green plants
lut	lutein
MCP	microchannel plate
MES	2-(N-morpholino)ethane sulfonic acid
NADPH	nicotinamide adenine dinucleotide phosphate
OPA	optical parametric amplifier
P680	primary donor in Photosystem II
P700	primary donor in Photosystem I
PC	plastocyanin
P _i	orthophosphate
PMS	phenazine meta sulphate
PQ	plastoquinone
PSI	Photosystem I
PSII	Photosystem II
PW	phonon wing
RC	reaction centre
S	Huang-Rhys factor
SAES	species associated emission spectra
SPT	single photon timing
UPC	fluorescence upconversion
vio	violaxantin
ZPL	zero-phonon line

1

Introduction

Photosynthesis has been of vital importance to the evolution of life and it continues to be so for its perpetuation as it produces oxygen and carbohydrates, which are essential for almost all life-forms. Without photosynthesis there would be no plants and no oxygen breathing animals: without photosynthesis the Earth would be a completely different place. The primary reactions of photosynthesis rely on the interaction between a handful of protein complexes embedded in the thylakoid membrane and lead to the production of adenosine triphosphate (ATP) and nicotinamide adenine dinucleotide phosphate (NADPH), chemicals that are used by the organism as sources of free energy and reducing power.

Chlorophylls (chls) and carotenoids are pigment molecules that play an essential role in these primary steps. Their spectroscopic properties are modified considerably by interactions with each other and with the protein environment. This thesis focuses on Photosystem I (PSI), one of the two photosystems in oxygenic photosynthesis. The PSI core complex contains about 100 chl and 20 carotenoid molecules. In plants additional LHCI antenna complexes bind to this core complex. A unique property of both the PSI core and LHCI is the presence of a small number of low-energy chls that have a profound effect on the PSI excited state dynamics.

The object of this thesis is to gain a greater understanding of the processes of energy transfer and primary charge separation in PSI. Therefore the light-induced temporal evolution of the entire fluorescence spectrum has been recorded for various PSI preparations using a streak camera, with a (sub) picosecond (ps , 10^{-12} s) time resolution. Sophisticated techniques (global and target analysis) were used to analyse this data.

Most of the PSI preparations investigated in this thesis were isolated from cyanobacteria. These remarkably versatile organisms evolved more than 3 billion years ago and perform oxygen producing photosynthesis. In fact, they are the progenitors of the chloroplasts of plant photosynthesis.

IN THE BEGINNING

About 4.6 billion years ago our Earth was formed by the accretion of small bodies orbiting in the gravitational field of (what would become) our sun. Due to radioactive and gravitational heating the newborn Earth melted during the first few hundred million years of its existence. The temperature increase resulted in the outgassing of small molecules such as water, methane, ammonia, hydrogen, nitrogen and carbon dioxide into the atmosphere.

About 3.8 billion years ago, the Earth's crust solidified. At this time the Earth was a lifeless, inhospitable place: the atmosphere consisted mainly of methane and ammonia,¹ and the concentration of gaseous oxygen was low, since it was used in the combustion (oxidation) of the hot Earth and its atmosphere.

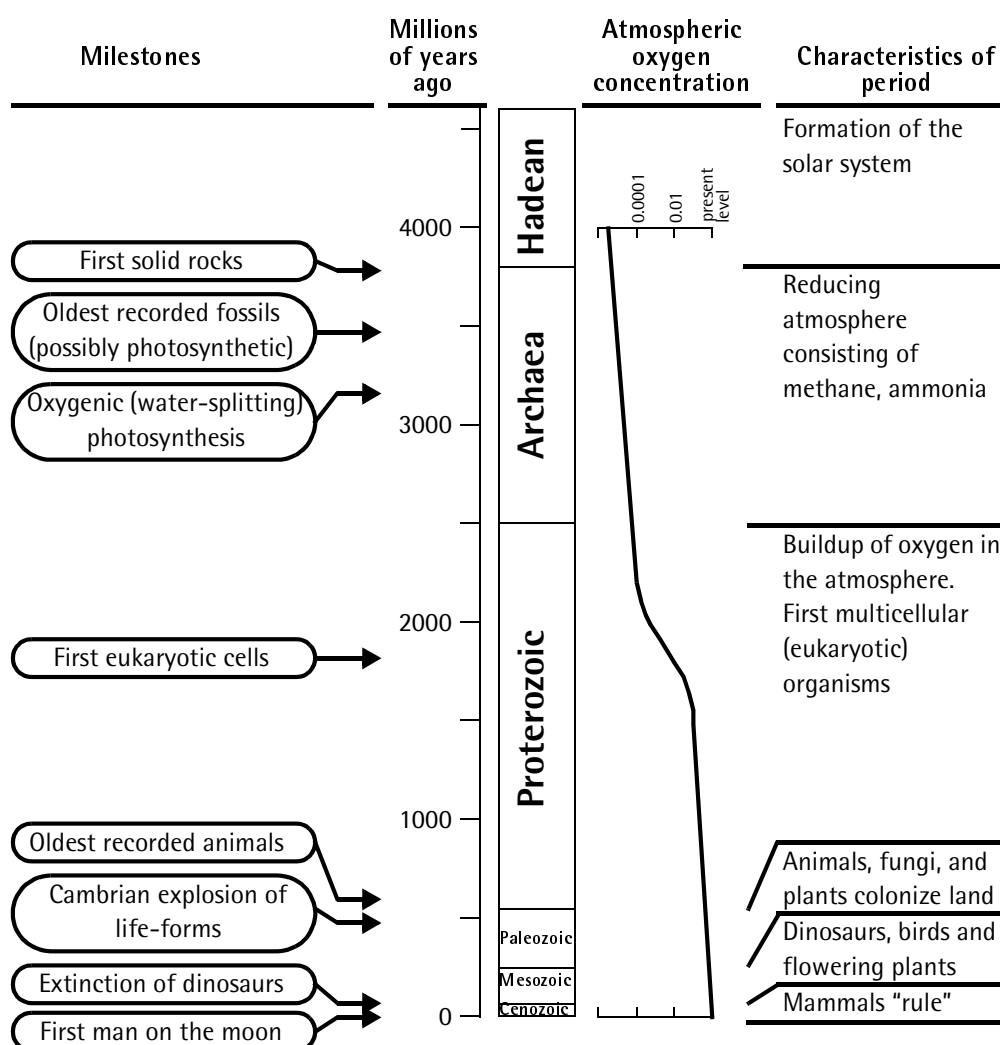
In the beginning of the first geological period, the Archaean, atmospheric water condensed on the Earth's surface. Chemical compounds were extracted from the rocks into pools of water, forming nutritious "soups" in which in the course of a few hundred million years the first organisms would develop. The earliest firm evidence of life, the oldest known fossils, dates back to roughly 3.5 billion years ago.² Life at this time was composed of prokaryotic (nonnucleated) microbes.

Some observations suggest that cyanobacteria, organisms capable of oxygenic photosynthesis, had already evolved at this time. This would imply that the complex process of oxygenic photosynthesis, in which light-energy is used to split water into protons and oxygen, had already developed surprisingly early in the history of life. The evidence for oxygen producing cyanobacteria existing around 3.2 billion years ago is stronger and about 3 billion years ago they must surely have been both abundant and widespread.²

With the arrival of the photosynthetic cyanobacteria on the scene the production of molecular oxygen gas is established, but it would take another billion years before the concentration of atmospheric oxygen showed an appreciable increase (fig. 1.1). The delay is caused by oxidative processes serving as oxygen sinks. The three foremost oxygen sinks are the result of micro-organisms carrying out aerobic respiration and the oxidation of both volcanic gasses and iron dissolved in the oceans. Whereas the first two sinks are still present today, the iron was depleted about 2 billion years ago, resulting in a spectacular increase of the level of atmospheric oxygen in the middle of the Proterozoic.² This atmospheric change had dramatic results for life on Earth. For many groups of bacteria oxygen was poisonous and lethal,¹ but, more importantly, the oxygen also resulted in the advent of the eukaryotic (nucleated) cell, the type of cell that makes up all multicellular organisms, including humans.

It appears that the eukaryotic cell originated from a collaboration of previously independently living prokaryotic cells. For instance the chloroplast, the intracellular site of photosynthesis in algae and plants, descends from a free-living cyanobacterial ancestor.² The evolution of prokaryotic and early eukaryotic cells proceeded at a relatively slow pace because reproduction at this time took place solely via cell division, and genetic diversification thus only occurred through random genetic mutations (although this included the process of lateral gene transfer³). About 1.1 billion years ago the capacity for sexual reproduction was developed: a method by which the offspring carries a combination of the genetic properties from two parental sources, rather than being an exact copy of a single, asexual parent cell.

This new innovation of life boosted both genetic diversity and the rate of evolution. After the appearance of the first multicellular (eukaryotic) organisms the first animals appeared toward the end of the Proterozoic. A true explosion of life-forms occurred in the beginning of the Paleozoic: the roots for all current forms of life were founded in a mere 40 million years.¹ During the Paleozoic life invades the land. The Mesozoic era (245-65 million years ago) is most well-known for the rise and fall of the dinosaurs, but it was a time of great changes in terrestrial vegetation too with the appearance of the first flowering plants.¹ In the Cenozoic, starting 65 million years ago and continuing to the present day, mammals are the largest animals around while in the last few million years humans develop.



1.1 A time-line of the history of life on Earth, from 4.6 billion years ago until present. Indicated are the geological eras and their characteristics, the concentration of atmospheric oxygen, and a number of important milestones in the evolution of life on Earth.

CYANOBACTERIA

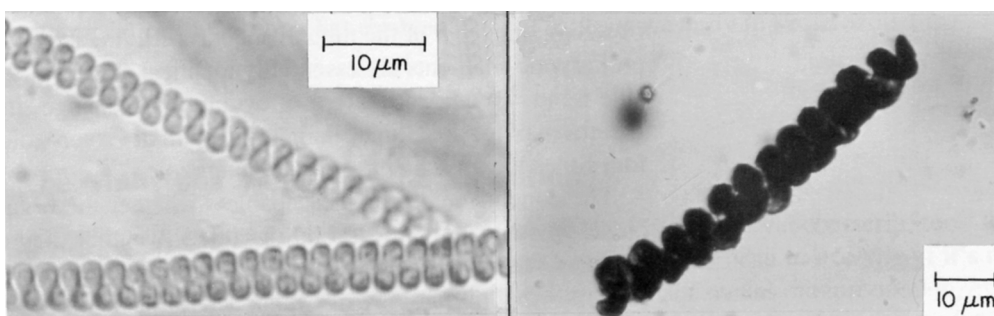
The most authoritative Dutch dictionary⁴ describes photosynthesis as: (translation from Dutch) "the formation of carbohydrates out of carbon dioxide and water by plants, mediated by light". This definition clearly manifests the terrestrial nature of us humans, since it entirely disregards the wealth of marine photosynthetic algae and bacteria. It may be worth noting that these undervalued marine photosynthetic organisms play a vital role in our biosphere. In fact, marine organisms are estimated to account for up to half of the yearly production of biomass,⁵ an amount that can hardly be called insignificant. Moreover, since life originated in the seas, all photosynthetic organisms have marine roots. In fact the chloroplast, the site where the photosynthetic apparatus in plants and algae is located, essentially is a (marine, prokaryotic) cyanobacterium that in the course of history took up residence within certain eukaryotic cells.²

Since this thesis deals almost exclusively with photosynthetic material isolated from cyanobacteria, this section is devoted to a review of some of the remarkable properties of these photosynthetic bacteria.

Cyanobacteria: built to last

All cyanobacteria are unicellular, though many grow in colonies or filaments.⁶ They are often named "blue-green algae" because of their colour, caused by the bluish pigment phycocyanin.⁷ However, cyanobacteria bear no direct relation to (eukaryotic) organisms called algae, although both are photosynthetic and aquatic. Cyanobacteria are prokaryotic bacteria, not eukaryotes. Moreover not all cyanobacteria are blue, some are red or pink from the pigment phycoerythrin.⁷

As noted in the first section, cyanobacteria may have originated as long as 3.5 billion years ago and thus are among the oldest life-forms around. Remarkably, they do not seem to have evolved much over the last 2 billion years of their existence, judging from the similarity between the appearance of some fossil cyanobacteria and that of contemporary relatives.² As an example figure 1.2 shows the comparison between the contemporary *Spirulina* and a 850 million year old fossil cyanobacterium, *Heliconema*.² The slogan "never change a winning team" may be the explanation for this lack of evolution: cyanobacteria have shown to be able



1.2 Left: *Spirulina*, a contemporary filamentous cyanobacterium having distinctive coiled filaments, right: *Heliconema*, a *Spirulina*-like fossil cyanobacterium about 850 Million years in age. (Reproduced from J.W. Schopf, 1992.²)

to live under the most extreme conditions and proven extraordinarily tough. They can live in deserts, tundra, forest floors, actually *within* rocks, in hot springs and snowfields, in freshwater, marine or extremely salt-rich environments, in aerobic and anaerobic habitats, in exceptionally acidic (pH ~3.5) and basic (pH 11 or even higher) settings. Cyanobacteria have been found at depths of 1000 m in the ocean, far below the level at which sunlight can penetrate. Many can survive in extremely dry environments: several species have been found near the town Calama in the Atacama Desert in Chile, a place where rainfall has never been recorded, the driest place on Earth. One species even made it into the Guinness Book of World Records, when it was revived with a bit of water after having been stored as a dried specimen in a museum for 107 years. Three other species have been shown to survive immersion in liquid helium (at -269°C) for 7.5 hours (also a world record) and several species have been shown to survive nuclear test-site explosions within a distance of about 1 km (No data is available any closer, since in this zone all soil was stripped away by the atomic blast).²

Cyanobacteria: Good guys or bad guys?

What can cyanobacteria do for you? Well, in first place you would not have been here if it were not for cyanobacteria. Performing photosynthesis for billions of years they paved the way for oxygen-dependent life-forms, such as humans. In the meantime they built up many of the world's oil deposits. Some species, the filamentous cyanobacteria, convert atmospheric nitrogen into forms that plants can use.^{7,8} In this way, they fertilize agricultural land throughout the world, in particular rice fields, where they are often added to the soil. The cyanobacterium *Spirulina* is highly valued as a food source;⁷ it is high in protein and can be cultivated in ponds quite easily. In tropical countries, it may be a very important part of the diet and it was eaten regularly by the Aztecs; it also serves in several oriental dishes. One variety of African flamingos⁷ specializes in feeding on *Spirulina*, that prospers in the soda lakes (pH 9.5–11.5) of their habitat. In fact the pink colouring of these flamingos arises from the pigments present in *Spirulina*.

So much for the positive aspects, but as always, there are also unfavourable aspects. Cyanobacteria may cause trouble as well; one species of *Lyngbya* is responsible for one of the skin irritations commonly known as "swimmer's itch".⁷ Some other cyanobacteria produce toxins. Under certain circumstances these species show explosive growth (known as waterblooms) forming thick floating scum layers. These blooms are responsible for dramatic die-offs of wild and domestic animals consuming the contaminated water.^{7,8}

In this thesis PSI preparations from three different kinds of cyanobacteria have been used: *Synechocystis* PCC6803, *Synechococcus elongatus* and *Spirulina platensis*.

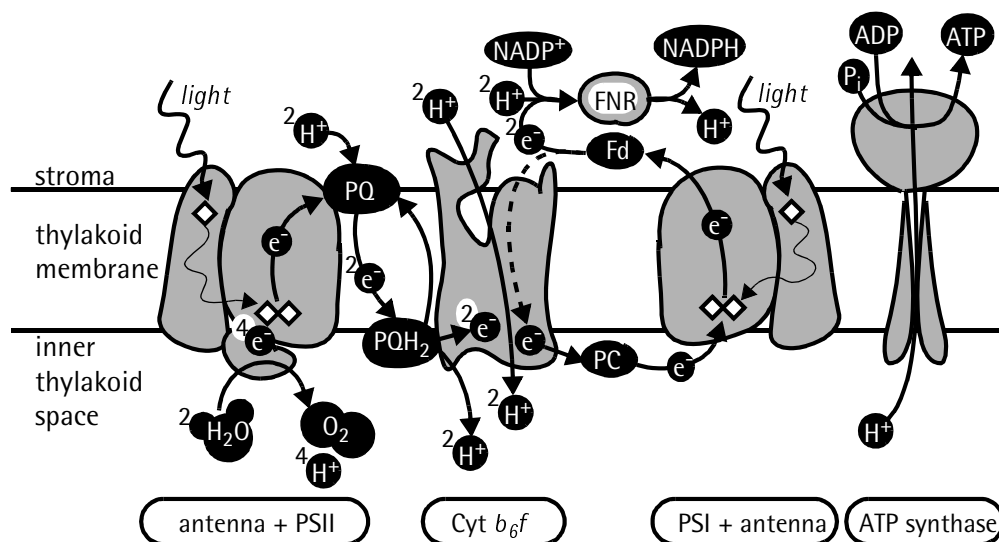
PHOTOSYNTHESIS

Photosynthesis is the process that enables certain organisms to use the energy of sunlight to fulfil their energy needs. Photosynthesis is one of the major developments of life: not only because it generated an environment in which oxygen-dependent life could evolve, but also since photosynthesis is at the base of the food-chain: practically all organisms in some way or other live on the energy stored by photosynthesis. Photosynthesis is a complex process,

studied in a range of scientific disciplines: physics, chemistry, biology, ecology etc. This thesis deals almost exclusively with the primary processes in photosynthesis belonging to the realm of physics. These primary processes start with the absorption of light by one of the pigment molecules in a light-harvesting antenna complex (LHC). The pigment, such as a chl or a carotenoid molecule, captures the energy of the light as the energy of its excited state. However, the excited state of a chl decays within a few nanoseconds (ns, 10^{-9} s) and that of a carotenoid even faster.⁹ To convert the captured energy to a more stable form, the fleeting excitation energy is transferred rapidly between the pigments in the LHC, to finally arrive at a special reaction centre (RC) site within the photosynthetic system where the excited state energy is stored by means of a stable (long lived) charge separation. The individual transfer steps between the antenna pigments typically take between 100 femtoseconds (fs, 10^{-15} s) and a few picoseconds, and the total time needed for the excitation to reach the RC is of the order of 100 ps or even shorter, significantly faster than the excited state lifetime of chl. The energy of the charge separation is subsequently used to drive a whole series of processes which ultimately lead to the production of ATP, the major source of free energy in biological systems, and NADPH, the major electron donor in reductive biosynthesis.¹⁰

Oxygenic photosynthesis

The general scheme of the first steps of photosynthesis, outlined above, applies to all types of photosynthetic systems: oxygen evolving photosynthesis that occurs in plants, algae and cyanobacteria, but also to non-oxygenic photosynthesis occurring in purple bacteria, green filamentous bacteria, heliobacteria and green sulphur bacteria.¹¹ Since this thesis deals with

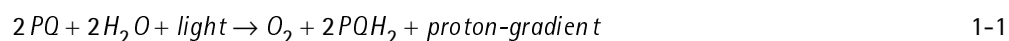


1.3 Simplified scheme of the light reactions and ATP synthesis in oxygenic photosynthesis. PQ: plastoquinone; PQH₂: plastoquinol; PC: plastocyanin; Fd: Ferredoxin; FNR: ferredoxin-NADPH⁺ reductase. Grey objects represent proteins and black objects represent other compounds. Thin lines indicate energy transfer within the light-harvesting antennas, and the bold lines electron and/or proton transfer. The dashed line represents the alternative cyclic electron transport pathway in PSI. The diamond shapes represent chlorophylls.

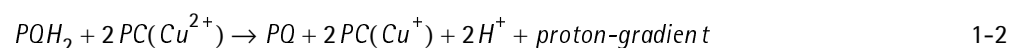
PSI, one of two photosystems that work together in oxygenic photosynthesis, this type of photosynthesis will be elaborated on before focusing on the specifics of PSI.

The machinery that performs photosynthesis is embedded in the thylakoid membrane (fig. 1.3) which is contained in the chloroplast in plants and the intracellular space in cyanobacteria. Four transmembrane protein complexes, PSI, Photosystem II (PSII), the cytochrome b_6f (Cyt b_6f) complex and ATP synthase each perform a specific task in the process.¹⁰

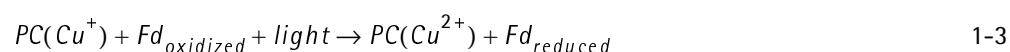
The actual oxygen evolution occurs in the PSII complex. After absorption of light by the light-harvesting antenna of PSII the excited state energy is transferred to a special pair of chls in the PSII RC, P680 (Primary electron donor absorbing light at 680 nm). Upon receiving an excitation an electron is released from P680 and transported to the other side of the thylakoid membrane, where it is ultimately donated to a plastoquinone (PQ) molecule. After receiving a second electron, from the next photocycle of P680, PQ takes up two protons (H^+) from the stromal space to form plastoquinol (PQH₂), which diffuses into the membrane towards the Cyt b_6f complex. P680⁺ is a very strong oxidant and extracts electrons from water, leading to the formation of O₂, the release of protons in the inner thylakoid space and the return of P680 to the neutral state. The net reaction catalysed by PSII therefore is:



Between PSI and PSII electrons flow through the Cyt b_6f complex. As the plastoquinol reaches this complex it is oxidized: two electrons are transferred through the Cyt b_6f complex to plastocyanin (PC) and two protons are released into the inner thylakoid space. The resulting plastoquinone is recycled to PSII. In addition the Cyt b_6f complex pumps another pair of protons across the membrane. The redox site of plastocyanin is a copper ion, that changes from the +2 to the +1 oxidation state upon receiving an electron. The effective reaction catalysed by the Cyt b_6f complex is:



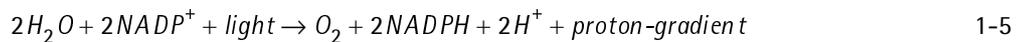
In PSI light is absorbed by the antenna pigments and the excitation energy is transported to the RC. As in PSII, a special pair of chls is present in the RC of PSI. This special pair, designated P700 (Primary electron donor absorbing light at 700 nm), upon excitation releases an electron that eventually ends up at an iron sulphur cluster on the other side of the protein. The final step is the reduction of ferredoxin (Fd), a water soluble protein. Meanwhile, reduced plastocyanin donates an electron to P700⁺ to return to P700, ready to be excited again. Thus, effectively PSI drives the reaction:



A flavoprotein, ferredoxin-NADPH⁺ reductase (FNR), uses two molecules of reduced ferredoxin and a stromal proton to form NADPH from NADP⁺ and thus effectively catalyses the reaction:



This concludes the set of reactions that is referred to as the "light reactions", since they only occur in the presence of light. The overall reaction that is catalysed by PSI, PSII, the Cyt_b₆f complex and FNR is given by:



In an alternative pathway, the electrons from ferredoxin are transferred back to plastocyanin via the Cyt_b₆f complex. This cyclic electron transport does not require the input of free energy by PSII and thus does not involve the production of O₂. In cyclic electron transport, which occurs when the stromal NADP⁺ concentration is too low to accept electrons from reduced ferredoxin, the energy input of PSI is effectively used to drive a proton pump.

The proton gradient generated by the light reactions is used by the protein ATP synthase to produce ATP out of adenosine diphosphate (ADP) and orthophosphate (P_i):



ATP is the principal immediate donor of free energy in biological systems. ATP cannot only be produced by photosynthesis, but also by the oxidation of fuel molecules. The turnover rate of ATP is high: a human at rest processes 40 kg of ATP a day, and during heavy exercise this may increase up to 0.5 kg per minute! Typically an ATP molecule is used within 1 minute on being formed.

For long-term storage of energy, CO₂ is reduced and converted to carbohydrates in the Calvin cycle, a process that requires both ATP and NADPH. Therefore the photosynthetic reaction is presented in many textbooks as:

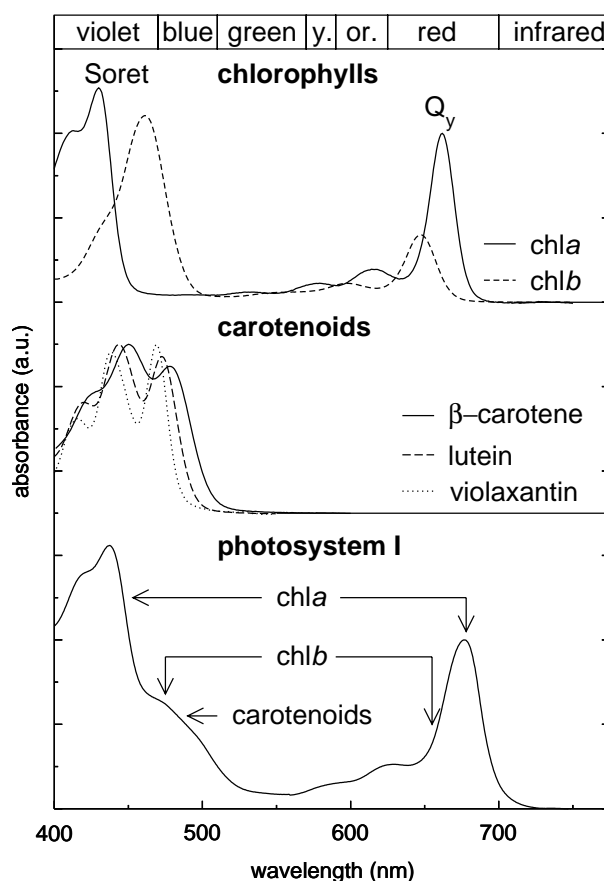


LIGHT-HARVESTING PIGMENTS

Pigment molecules play an essential role in the process of photosynthesis. They are responsible for the absorption (harvesting) of light and the primary steps in charge separation, but can also protect the photosystems and provide structural stability to the protein. The pigments present in PSI are chls and carotenoids.

Chlorophylls

Chlorophylls^{10,12} (from greek *chloros*, green and *phullon*, leaf) are the primary light-harvesting pigments in photosynthesis and in all photosystems a special pair of chls constitutes the primary electron donor of the electron transfer chain in the RC. In oxygenic photosynthesis two types of chls occur, chlorophyll-*a* (*chl**a*) and chlorophyll-*b* (*chl**b*). The absorption spectra of *chl**a* and *chl**b* in solution are shown in figure 1.4. The *chl**a* and *chl**b* absorption spectra do not fully overlap, which increases the spectral range over which light is absorbed, and thus increases efficiency of light-harvesting. Both chl species exhibit two major absorption bands in the visible spectrum. The red-most band represents the Q_y transition which peaks around 670 nm and 645 nm in *chl**a* and *chl**b* respectively. In the blue/violet part of the spectrum an absorption band appears which is caused by the Soret transitions. This structured band shows a maximum around 430 nm for *chl**a* and around 460 nm for *chl**b*. Both the Soret and Q_y transitions have very high extinction coefficients (in the order of $10^5 \text{ cm}^{-1} \text{ M}^{-1}$).^{10,12} Less clear from the spectrum is the weakly absorbing Q_x transition that appears around 580–640 nm and

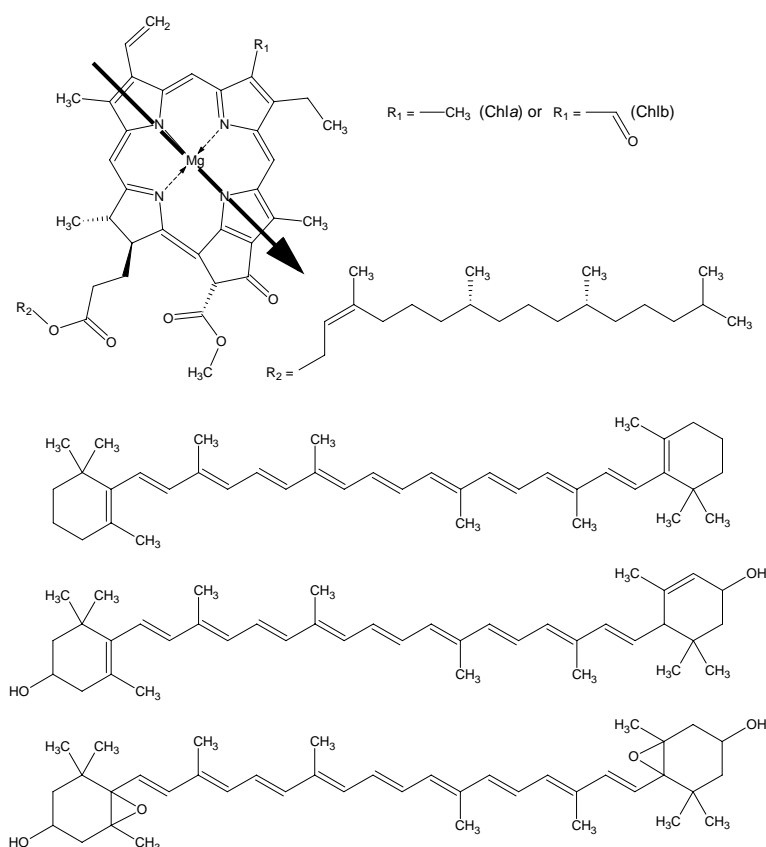


1.4 Room temperature absorption spectra of *chl**a* in pyridine and *chl**b* in acetone (top), of β -carotene in hexane and lutein and violaxanthin in methylpentane (middle) and the complete PSI complex isolated from maize (PSI-200). The spectra are not normalized to their relative oscillator strengths.

is masked by the Q_y vibronic bands. The strong absorption of both red and blue/violet light by the chls causes the green colour of most plants. The molecular structure of chl is shown in figure 1.5. It consists of a tetrapyrrole ring to which a long phytol tail is attached. The extensive conjugated π -electron system of the ring causes the strong absorption bands of the chls. The arrow indicates the approximate direction of the Q_y transition dipole moment in the plane of the ring. The weak Q_x transition dipole is also situated in the plane of the ring, but is oriented perpendicular to the Q_y transition dipole, whereas the Soret consists of several transitions. The fluorescence lifetime of chl *a* is 5 ns.⁹

Carotenoids

The carotenoids form the other important group of photosynthetic pigments. The carotenoids occurring in PSI are β -carotene (β -car), lutein (lut) and violaxantin (vio). β -car is the most abundant of the three, and the only type of carotenoid occurring in the core complex of PSI. Lut and vio, as well as β -car all occur in the peripheral light-harvesting complex of plant PSI.¹³ Unlike chls, carotenoid molecules are basically linear (fig. 1.5). They consist of a polyene chain with alternating single and double bonds, the number of which can vary between different



1.5 Structures of the pigments occurring in plant PSI. From top to bottom: chlorophyll-*a/b*, β -carotene, lutein and violaxantin.

species of carotenoids. The number of single/double bonds is 9 for all three carotenoids of PSI. Since the spectroscopic properties of carotenoids are mostly determined by the conjugated π -electrons of the polyene chain and the differences between the three species found in PSI only occur in the headgroups, the absorption spectra of the three carotenoid species are very similar (fig. 1.4). The transition to lowest excited state of the carotenoids, the S_1 state, was estimated to be positioned around 704 nm in β -car,¹⁴ but is optically forbidden as the S_1 state has the same symmetry as the ground state. The carotenoid absorption spectrum is therefore dominated by the strongly allowed S_2 transition (β -car: $\epsilon=1.3 \times 10^6 \text{ cm}^{-1} \text{ M}^{-1}$), which absorbs in the 400-500 nm region where it shows a number of vibronic bands. The fluorescence lifetimes of both the S_1 and S_2 states are much shorter than those of chls: in β -car, the S_2 state relaxes to the S_1 state in less than 200 fs,¹⁵ which in turn relaxes to the ground state in 8 ps.¹⁴ Similar lifetimes apply to the other carotenoids.

Carotenoids serve several purposes in photosynthesis. Despite the short excited state lifetimes they contribute in the light harvesting: a considerable fraction of the excitations of the carotenoids is transferred to chl. This implies that the rates of energy transfer from the carotenoids must be very high. The transfer may occur both through the S_1 and the S_2 state. As the S_2 state has a very large transition dipole moment, energy transfer from this state can proceed through the Förster mechanism (see below). The S_0 - S_1 transition is dipole forbidden and therefore energy transfer from this state cannot occur via the Förster mechanism. Possibly the transfer here proceeds through higher order electrostatic terms. For both processes the chls and carotenoids have to be in close proximity to achieve the fast energy transfer. Perhaps more important than light harvesting are the protective properties of carotenoids.¹⁶ Excited chls have a finite probability of intersystem crossing to triplet states. Such a chl triplet can transfer its energy to oxygen, which is a triplet in the ground state. The chl returns to the ground state and singlet excited oxygen is formed:



Singlet oxygen is a highly reactive free radical and can cause severe damage to the organism. Therefore quenching of chl triplets is imperative for its survival. This is just what carotenoids do: they accept triplet excitations from chl, returning the chl to the ground state and creating a triplet-excited carotenoid:



The triplet excited state energy of the carotenoid is lower than that of singlet excited oxygen, the formation of which is therefore prohibited.

Finally it has been shown that some photosynthetic proteins do not assemble (correctly) in the absence of carotenoids. This implies that in these proteins carotenoids are also important in assembling and stabilizing the structure of the proteins containing them.¹⁷

HETEROGENEITY, HOMOGENEITY AND INHOMOGENEITY

The spectroscopic properties of pigment molecules generally depend strongly on their interaction with the environment, such as a solvent or a protein. In a protein environment the (electronic) structure of pigments is modified due to interactions such as hydrogen bonding, ligation (to the central Mg in chl) and electrostatic interactions. This can have a profound effect on the spectroscopic properties of protein-bound pigments, such as the shift of absorption maxima over several tens of nanometers and a dramatic change of the absorption and emission line shapes.¹⁸

In a solvent each pigment experiences on average the same environment. In contrast to a solvent, a photosynthetic protein exhibits several specific pigment binding sites. Pigments in these different sites each experience a different interaction with their specific local protein environment and thus exhibit different spectroscopic properties. This heterogeneity can result in the appearance of several peaks and shoulders in the absorption bands of photosynthetic proteins.

Proteins do not form a rigid scaffolding for the pigments: they are dynamic structures. Consequently, even pigments located in identical positions in different proteins do not necessarily experience identical environments, and even the environment of an individual pigment in a specific site in a specific protein will vary in the course of time due to the motion of the protein. This results in a distribution of transition energies in the ensemble of these pigments, causing the ensemble absorption and emission bands to be broader than those of single individual pigment in the ensemble. This phenomenon is called inhomogeneous broadening. The shape of the absorption or emission spectrum of an individual pigment is called the homogeneous line shape. The absorption band of the ensemble is the convolution of this homogeneous line shape with an inhomogeneous distribution function (IDF) that accounts for the statistical variations in the transition energies. The homogeneous lineshape may also be modified by the pigment environment, for instance due to the coupling of the vibrational motions of the protein (phonons) to the electronic transitions of the pigment. If this electron-phonon coupling is significant, the homogeneous absorption and emission spectra will show a contribution due to a simultaneous electronic transition of the pigment and phonon transition of the protein, the phonon wing (PW), next to the absorption or emission due to the pure electronic transition, the zero-phonon line (ZPL). The strength of the electron-phonon coupling is given by the Huang-Rhys factor, S , which is defined by:^{18,19}

$$S = \ln \frac{A_{ZPL} + A_{PW}}{A_{ZPL}} \quad 1-10$$

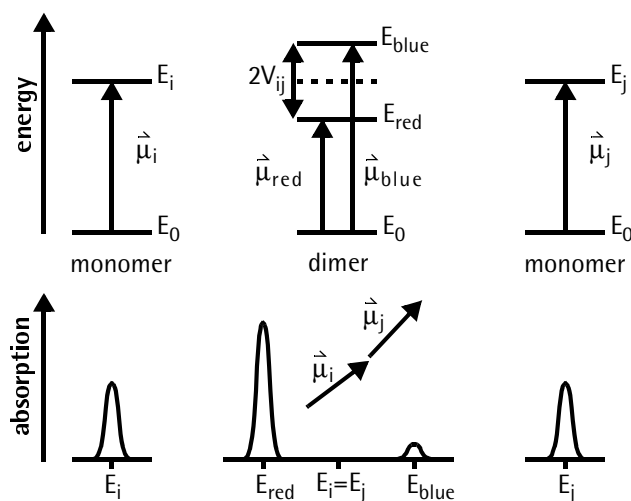
where A_{ZPL} and A_{PW} represent the integrated absorption of the zero-phonon line and the phonon wing, respectively.

EXCITONIC COUPLING AND ENERGY TRANSFER

The environment of a pigment may not only consist of protein or solvent, it may also interact with other pigment molecules. When pigment molecules are located sufficiently close to each other, electrostatic interactions result in the modification of the spectral and dynamic properties of these pigments. If the pigment molecules do not carry a permanent charge and the distance between the molecules is not too small, the interaction energy between the pigments i and j , can be approximated by the dipole-dipole term in the multipole expansion of the coulombic interaction, given by:

$$V_{ij} = \left(\frac{1}{4\pi\epsilon} \right) \frac{\vec{\mu}_i \cdot \vec{\mu}_j - 3(\vec{\mu}_i \cdot \hat{R}_{ij})(\vec{\mu}_j \cdot \hat{R}_{ij})}{R_{ij}^3} \quad 1-11$$

Here $\vec{\mu}_x$ is the transition dipole moment of pigment x , R_{ij} is the distance between pigments i and j and \hat{R}_{ij} is the normalized vector along the line connecting pigments i and j . If the magnitude of the interaction term exceeds the width of the individual transitions of the pigments, the combined spectrum will no longer simply be the sum of the individual (monomer) spectra, but will consist of new absorption bands that correspond to transitions from the unperturbed ground state to weighed combinations of the original individual excited



1.6 Excitonic interaction between two identical pigments. Top: energy levels; the monomers (left and right) have transition dipole moments $\hat{\mu}_i$ and $\hat{\mu}_j$ from the ground state at energy E_0 to the (first) excited state at energy $E_i=E_j$. In the dimer (middle) the original energy level is split symmetrically into two new energy levels E_{blue} and E_{red} that are separated by $2V_{ij}$. Associated with the new energy levels are two new transition dipole moments $\hat{\mu}_{\text{red}}$ and $\hat{\mu}_{\text{blue}}$. Bottom: absorption spectra of the monomers (left and right), centred around the energy $E_i=E_j$ and the absorption spectrum of the dimer (middle) exhibiting two new bands. The relative absorption strength of the two bands depends on the relative orientations of the dipole moments. Here an almost perfect head-to-tail dimer is shown for which the oscillator strength is concentrated in the red-most transition.

states. Excitations are no longer localized on one of the pigments, but delocalized over them. Effectively the interacting pigments now behave as one single super-pigment instead of individual pigments. In the simple case of two interacting identical pigments the original (single) absorption band of the monomers is split up into the two new absorption bands of the dimer that are respectively red- and blue-shifted by an energy V_{ij} , relative to the original absorption band. The distribution of oscillator strength between the two bands depends on the relative orientations of the transition dipole moments of the two pigments (fig. 1.6). This kind of strong coupling is called excitonic coupling, leading to coherent energy transfer.

In case the interaction term in equation 1-11 is small (but non-zero) the coupling is weak and the wave functions and excitations are essentially localized on the individual pigments. However, the coupling does facilitate the transfer of an excitation from one pigment to the other. Förster has derived an expression relating k_{DA} , the rate of energy transfer between a donor molecule D and an acceptor pigment molecule A , to the donor emission (fluorescence) spectrum and the acceptor absorption spectrum:²⁰

$$k_{DA} = \frac{9\kappa^2 c^4 \phi_D}{8\pi n^4 \tau_D R^6} \int_{\omega} \epsilon_A(\omega) f_D(\omega) \omega^{-4} d\omega \quad 1-12$$

with c the speed of light, n the refractive index of the medium,²¹ κ an orientational factor (see chapter 5), ϕ_D the fluorescence quantum yield of the donor, τ_D the fluorescence lifetime of the donor, R the distance between the donor and the acceptor, $\epsilon_A(\omega)$ the (homogeneous) molecular extinction coefficient of the acceptor, $f_D(\omega)$ the normalized (homogeneous) donor emission spectrum and ω the circular frequency of the light. Note that due to the Stokes' shift the rate of transfer from relatively blue absorbing pigments to relatively red absorbing pigments, downhill transfer, is faster than the reverse, uphill transfer process, eventually leading to an equilibrium with a preferential occupation of the lower energy levels, in accordance with the Boltzmann distribution. The Förster type of energy transfer that occurs in the weak interaction limit is often referred to as hopping, or incoherent energy transfer.

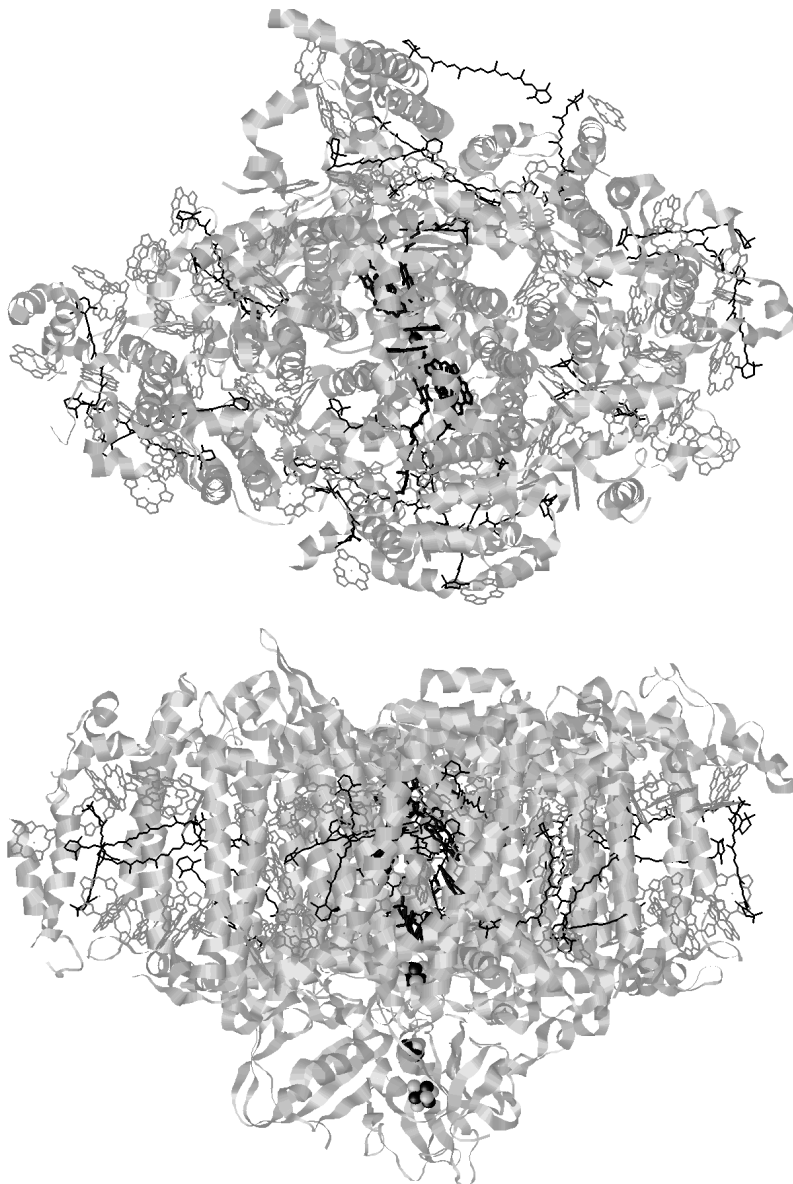
Throughout this thesis it will be assumed that the Förster mechanism is the dominant mechanism for energy transfer in PSI.

THE PHOTOSYSTEM I CORE COMPLEX

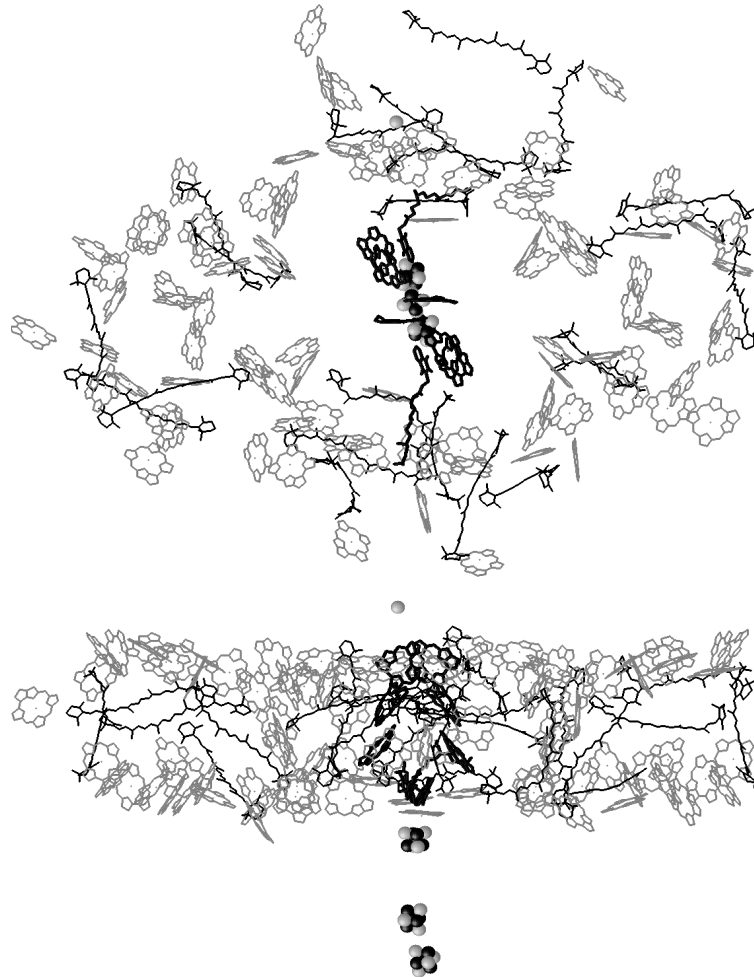
The heart of PSI is formed by the PSI core, a complex consisting of 11 to 13 proteins which binds the PSI RC as well as the PSI core light-harvesting antenna.²² *In vivo*, additional light-harvesting complexes bind to the core complex, enhancing the rate at which photons are captured (see below). The PSI core complexes of cyanobacteria can be isolated both as monomers and as trimers. It is very likely that both forms occur in the thylakoid membrane.²³ In contrast, trimers of PSI particles from plants have never been observed. Most of the work in this thesis has been performed on isolated PSI core complexes.

Photosystem I core structure

The molecular structure of the PSI core complex of the cyanobacterium *Synechococcus elongatus* has recently been resolved to a resolution of 2.5 Å.²⁴ It reveals a total of 12 protein subunits that bind 127 cofactors (figure 1.7 and figure 1.8): 96 chl a , 2 phylloquinones, 3 Fe $_4$ S $_4$ clusters, 22 carotenoids (modelled as β -carotene), 4 lipids and a putative Ca $^{2+}$ ion.²⁴

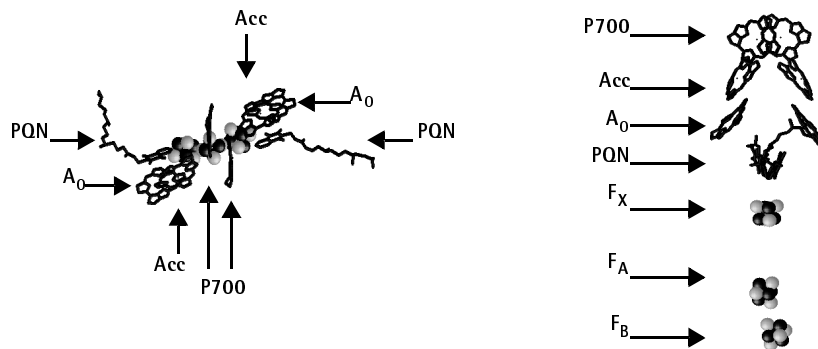


1.7 The structural model of PSI from *Synechococcus elongatus*. Top: Top view onto the membrane plane. Bottom: Side view in the membrane plane. The protein scaffolding is depicted as ribbons, clearly revealing the many α -helices.



1.8 As figure 1.7 but now with the protein removed, disclosing the antenna and RC cofactors. Antenna chls are in grey, β -carotenes in black, and the RC cofactors in bold black and spheres. Notice from the top view that the RC, although located in the centre, is not in close proximity to most of the antenna. The side view shows that in the central region chls are more or less evenly distributed, whereas in the outer domains the chls form quite distinct lumenal and stromal layers.

The electron transfer chain of the RC is bound between PsaA and PsaB, two large proteins that also bind the majority of the PSI core light-harvesting antenna. It consists of 6 chl*a* molecules, two phyloquinones and three iron-sulphur clusters (figure 1.9). Two parallel oriented chls on top constitute the primary electron donor P700 (figure 1.9) and the two other chls located on each side of P700 represent the primary electron acceptors, A_0 and the accessory chls. Two phyloquinones (PQN, vitamin K) form the secondary electron acceptor A_1 . The rest of the electron transfer chain is formed by the three Fe_4S_4 iron-sulphur clusters F_X , F_A and F_B . The latter donates the electron to ferredoxin (see above). Like the bacterial RC, the PSI RC is organized in two branches. In the bacterial RC, however, only one of these two branches is active, whereas in PSI electron transfer appears to occur through both branches.^{25,26}



1.9 As figure 1.8, but now with the antenna pigments also removed, such that only the RC cofactors remain. From top to bottom the electron transfer chain consists of three times two chls, representing the primary donor (P700), accessory chls (Acc) and the primary electron acceptor (A_0), two phylloquinones (PQN, vitamin K) and three Fe_4S_4 iron-sulphur clusters (F_X , F_A and F_B). In contrast to the purple bacterial RC, both electron transfer branches seem to be active in PSI.

The top view (figure 1.8b) shows that remaining 90 chls and the 22 carotenoids, which form the core light-harvesting antenna, are arranged in the shape of a more or less elliptical doughnut. The RC is positioned in the hole of the doughnut at a relatively large distance from most antenna pigments.

Light-harvesting Complex I

In plants the antenna size of PSI is increased by Light-harvesting Complex I (LHCI), bound to the PSI core complex. This peripheral antenna complex is composed of approximately equal amounts of four different proteins Lhca1-4 that assemble as dimers.²⁷ The Lhca1-4 proteins bind on average 8 chl a , 2 chl b and 2 carotenoid molecules (a mixture of violaxanthin, lutein and β -carotene).¹³

The LHCI proteins show a strong similarity to PSII light-harvesting proteins such as CP29 and LHCII, presently the only Lhca/b protein for which a high resolution (3.4 Å) structure exists.²⁸

In plants 3-4 or possibly 5 LHCI dimers bind to a PSI core particle to form PSI-200, a complex containing a total of 170-200 chls.^{29,30} It has long been thought that the LHCI dimers completely surround the PSI core, but recent electron microscopy experiments indicate that all LHCI dimers are located on one side of the core complex.²⁹

low-energy ("red") chlorophylls

The spectra of the PSI core complex and LHCI are highly heterogeneous due to the pigment-protein and pigment-pigment interactions described above. Although most photosynthetic antenna complexes exhibit such heterogeneity, the PSI complexes are unique in the sense that they generally exhibit at least one absorption band due to antenna chls absorbing at energies lower than that of the primary electron donor, i.e. P700. These chls are referred to as long-wavelength chls or red chls.

At first glance it may seem to be an imperfection of the system to contain these low-energy chls because they act as an energy sink that impedes the transfer of excitations to

where they should go: P700. However, excitations that reach the red* chls are not “trapped” there: at room temperature enough thermal energy is available to allow for a significant uphill transfer rate to the bulk antenna and P700. In this thesis it is shown that the low-energy chls have a very pronounced effect on the energy transfer and trapping in the whole PSI system and significantly slow down the effective rate of charge separation.³¹ This, however, does not result in a significant decrease of the efficiency of PSI, since the rate of charge separation remains much higher as compared to the rate at which excitations are lost. Therefore a small advantage of the system resulting from the red chls would already justify their presence. The most likely advantage proposed so far is the extension of the spectral window for light harvesting at the long wavelength end. Calculations indicate that under certain (shade-light) conditions the few percent of red chls in the antenna may be responsible for up to 40% of the total photon capture.³²

Although basically all PSI core particles exhibit a number of red chls, the exact numbers and energies differ from species to species. Plant PSI cores exhibit only two or three relatively moderately red-shifted chls (absorption maximum at ~705 nm at low temperatures), whereas trimeric PSI cores from the cyanobacterium *Spirulina platensis* carry about 10 red chls with absorption maxima up to 740 nm (at low temperatures).³³ There are, however, also important similarities between the red chls in different PSI cores: they all seem to be strongly coupled to their environment (strong electron-phonon coupling), resulting in a broad, almost featureless homogeneous line shape and a Stokes' shift which is much larger than for normal antenna chls. The bands of the red chls are also significantly inhomogeneously broadened. The absorption maxima of all red chls are also much more red-shifted at low temperatures as compared to room temperature. A common feature of the PSI-cores of the three different cyanobacteria studied in this thesis is a pool of red chls that absorbs at 708 nm at low temperatures and around 702 nm at ambient temperature.³¹

The properties of the red chls suggest that they are not monomeric chls, but excitonically coupled dimers or larger aggregates.³⁴ In fact, a number of dimers and a trimer are present in the structural model of the PSI core of *Synechococcus*.²⁴

The function of the red chls and the nature of their extreme red-shift, are some of the key issues in the spectroscopy of PSI and therefore a recurrent theme in this thesis.

* The name “red chls” may be somewhat confusing since it wrongly suggests that these chls are red as opposed of “normal” green chls. In reality the red chls at most would be “a different shade of green”. The term “red” in “red chls” is used merely to indicate that the red absorption band (Q_y) of these chls occurs at longer wavelengths than that of the primary electron donor.

EXPERIMENTAL TECHNIQUES: THE STREAK CAMERA

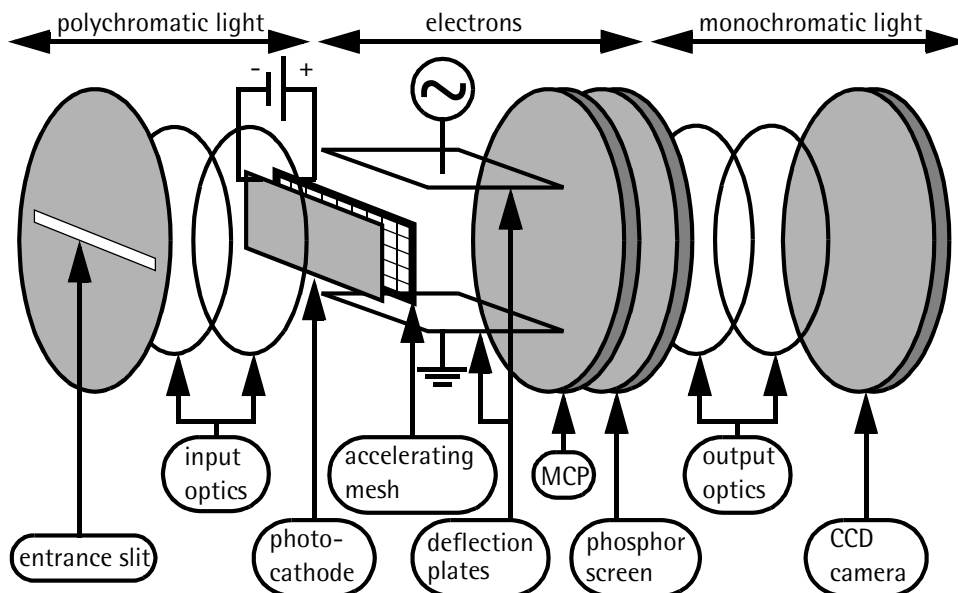
The key experiments in this thesis are time-resolved fluorescence measurements performed with a synchroscan streak camera. The use of streak cameras is not very common in the field of photosynthesis, somewhat surprisingly, since modern streak cameras (although quite expensive) exhibit a number of features that make them very useful for studying photosynthetic systems. They can be used to measure fluorescence kinetics, which are

generally easier to interpret (both qualitatively and quantitatively) than transient absorption kinetics, in which excited state absorption and stimulated emission contributions may hinder the extraction of the exact ground-state bleach of the various pigment species.

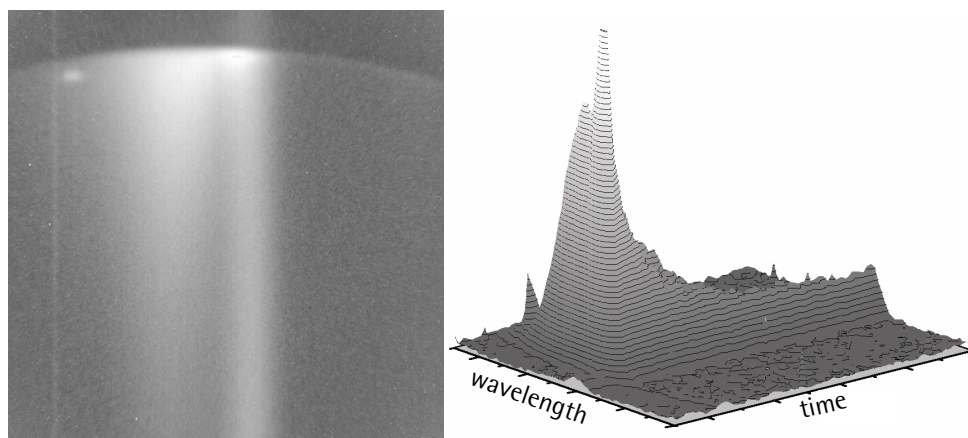
Other common techniques for recording fast fluorescence kinetics are fluorescence upconversion (UPC) and single photon timing (SPT). Of the three techniques UPC exhibits the best time resolution, in principle only limited by the cross-correlation between the excitation and gating pulses, typically in the order of 100 fs. However, the excitation densities and/or repetition rates needed for this technique are generally too high for a typical photosynthesis experiment, especially for studying PSI. Both synchroscan streak camera and SPT experiments can be performed using significantly lower excitation densities (sub nJ/pulse). This is, however, at the expense of time resolution: the width of the instrument response function of the streak camera used for the experiments presented in this thesis is about 3 ps and that of a typical SPT setup is about 50 ps. The huge advantage of using a streak camera over both other techniques is its intrinsic ability to perform two-dimensional spectroscopy, that is, to directly measure the temporal evolution of the entire fluorescence spectrum, rather than recording the kinetics at one single wavelength at a time. The only disadvantage of streak camera measurements, its somewhat lower time resolution, is overcome in some of the chapters in this thesis by a combined analysis of streak camera and UPC data.

The principle of operation of a streak camera relies on three physical processes:³⁷

- 1 The conversion of photons into electrons at a photocathode;
- 2 The linear acceleration of these electrons and subsequent deflection by a transverse electric field, the magnitude of which is swept in time;
- 3 The detection of the transverse position of impact of the electrons on a phosphor screen.



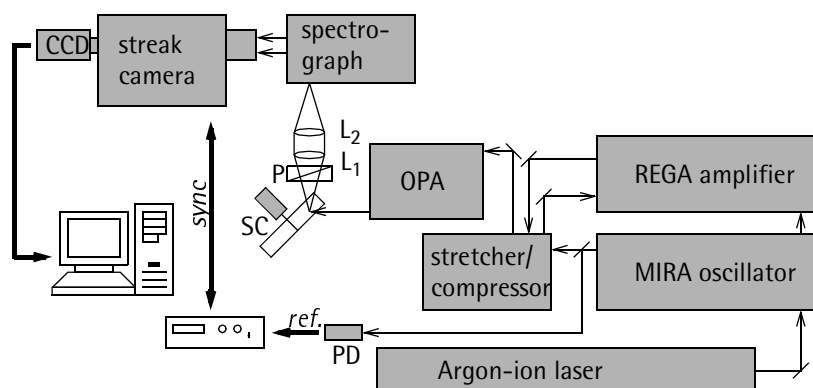
1.10 Schematic representation of a (synchroscan) streak camera. See text for details.



1.11 Left: A streak camera image as collected on the CCD camera displays the intensity of the fluorescence as a function of time (from top to bottom) and wavelength (from right to left). The curvature, reflecting a wavelength dependence of time zero, is an intrinsic property of the apparatus, which is corrected for, prior to the analysis. Right: the same data represented in a three dimensional intensity plot.

Figure 1.10 shows more details of the operation of the particular synchroscan streak camera system used in this work. Photons, dispersed by a spectrograph, enter the system through a horizontal entrance slit which is imaged onto a photocathode. Here electrons are released, proportional to the intensity of the incident light. These electrons are first linearly accelerated and subsequently pass between two deflection plates to which an oscillating electric field is applied. This results in a time dependent vertical deflection of the electrons. The electron flow is amplified several orders of magnitude in a microchannel plate (MCP) and the electrons are converted into photons on a phosphor screen. These photons are subsequently recorded with a high-sensitivity CCD camera. The oscillating field that is at the heart of the streak camera is synchronised to the repetition rate of the laser, such that the signal of a large number of successive laser pulses (synchroscan) can be accumulated on the CCD camera. The resulting "streak image", (fig. 1.11) represents the fluorescence intensity as a function of both wavelength and time.

The entire streak camera setup is depicted in figure 1.12. A 25 W Argon ion laser pumps the oscillator and the regenerative amplifier, which are both Ti-Sapphire based. The oscillator produces 50 fs, 800 nm pulses at a 76 MHz repetition rate. A part of the oscillator output is redirected to a PIN diode (PD) as a reference for the synchronisation of the streak camera oscillator. The major part of the oscillator output is directed into a pulse stretcher. In the regenerative amplifier selected pulses are amplified and the repetition rate is reduced from 76 MHz to 10-250 kHz. The amplified pulses are recompressed and directed into a double pass optical parametric amplifier (OPA). Here the colour of the 800 nm pulses can be tuned from $\sim 470\text{nm}$ to $\sim 720\text{nm}$. The pulses of the selected colour are focused into the sample, which is contained in a rotating measuring cell (SC). Fluorescence is collected at a right angle through a sheet polarizer (P) and focused into a spectrograph using two triplet achromatic lenses (L_1 and L_2). The output of the spectrograph is focused onto the entrance slit of the streak camera (see above).



1.12 Streak camera setup.

DATA ANALYSIS

Streak camera data sets are two-dimensional: the streak image collected on the CCD reflects the fluorescence intensity as a function of both time and wavelength (fig. 1.11). For convenient analysis the relevant part of a streak camera data set is "sliced up" into a (large) number of kinetic or time traces (fig. 1.13). Such large, multidimensional data sets require sophisticated methods of data analysis if all information contained in the measurements is to be extracted. Here the basic concepts of global (lifetime) analysis and (global) target analysis will be discussed. This discussion is definitely not intended as a thorough (mathematical) treatment of these methods of analysis. Rather it is meant for the reader, not familiar with these methods, to gain a basic understanding of concepts such as decay-associated spectra (DAS) and species-associated emission spectra (SAES), that constitute the pivots of most of the chapters contained in this thesis. Much of this section is based upon Holzwarth, 1996.³⁵ More details on the application of target analysis can be found in Hoff et al.³⁶

All systems studied in this thesis contain a number of pigments (chls, carotenoids) that transfer energy to each other, and that can exhibit specific excitation-quenching mechanisms. These systems have been studied by exciting them with a (short) laser pulse at the wavelength λ_{ex} and recording the fluorescence (although the following applies just as well to transient absorption) as a function of the emission wavelength (λ_{em}) and time (see previous section). In general the time dependence of the signal (I) for a certain emission wavelength can be described as a sum of exponentials:

$$I(t, \lambda_{ex}, \lambda_{em}) = \sum_{j=1}^n A_j(\lambda_{ex}, \lambda_{em}) \cdot e^{-t/\tau_j}, \quad 1-13$$

in which A_j and τ_j are the amplitudes and the lifetime of the j th component. Generally the number of lifetimes (components) equals the number of pigments, i.e. $n=N$, although not all may be distinguishable in an experiment. Conventionally the data would be analysed

than a handful of kinetic components, although PSI contains about 100 chls. The kinetic components therefore do not reflect the processes occurring between individual pigments, but the interaction between groups of pigments, which will be referred to as "species" from here on.

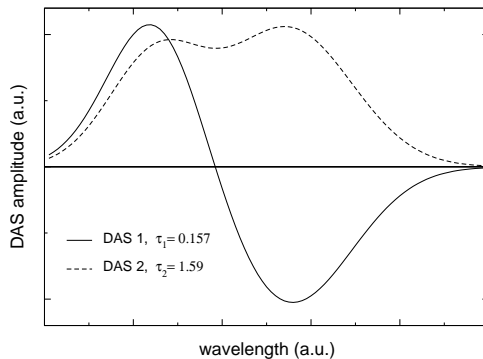
The plot of A_j as a function of λ_{em} is called the Decay Associated Spectrum (DAS) of the j th decay component. A DAS can be expressed as a linear combination of the Species Associated Emission Spectra (SAES), the emission spectra of the different species present in the system:

$$A_j(\lambda_{em}) = DAS_j(\lambda_{em}) = \sum_{k=1}^n c_{jk} \cdot SAES_k(\lambda_{em}) \quad 1-14$$

Examination of the DAS-es provides some insight in the processes that are taking place in the system after excitation. Often a distinction is made between two types of DAS-es: those reflecting energy transfer between different pigments and those reflecting a pure decay (due to, for instance, trapping in an RC). Pure energy transfer DAS-es exhibit both positive and negative regions. The positive regions reflect a decay (decrease) in fluorescence from the donor species and the negative regions represent a rise (increase) in fluorescence from the acceptor species. Note that negative regions in a DAS do not imply that the fluorescence is negative (which would be non-physical): the total fluorescence is the sum of a number of contributions (equation 1-13) and is always positive. A pure decay (or trapping) DAS is positive at all emission wavelengths. It represents the decay of excitations in a system after all energy transfer processes are completed, or the decay of fluorescence of a species that is not in contact with other species (such as a chromophore in a dilute solution). These "pure" decay DAS-es therefore generally represent the slower processes in the system, whereas energy transfer (equilibration) DAS-es are associated with shorter lifetimes. Often DAS-es represent neither pure energy transfer, nor a pure decay, but rather a mixture of both.³¹

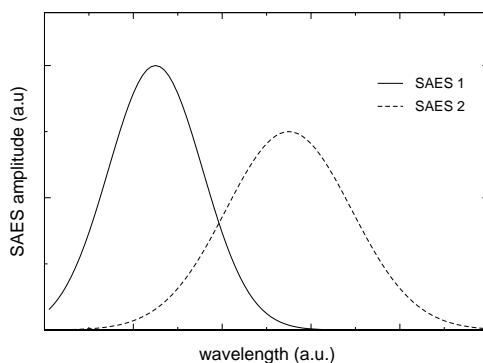
As an example figure 1.14 displays the analysis of a simple (fictitious) system. The global analysis of the kinetics of this system (top) yields two lifetimes with corresponding DAS-es. The DAS associated with the fastest process ($\tau_1=0.157$) has a clear energy transfer character: a decay at shorter wavelengths (positive region in DAS) and a rise at longer wavelengths (negative region in DAS) indicates a transfer of energy from a higher energy species to a lower energy species (downhill transfer). The slower process ($\tau_2=1.59$) is associated with a DAS that is positive at all wavelengths and therefore most probably reflects a pure decay. The maxima and minima of both DAS-es give some indication of the maxima of the SAES of the species involved.

The example of figure 1.14 demonstrates that the lifetimes and DAS spectra resulting from the global lifetime analysis can provide some insight in the physics of the system (equilibration lifetimes, approximate maxima of SAES-es). However, in principle these lifetimes and DAS-es represent no more than the mathematical parameters of a mathematical model describing the data. These mathematical parameters do not give direct information regarding the physics of the system. The physics, however, is what we are interested in: we would like to



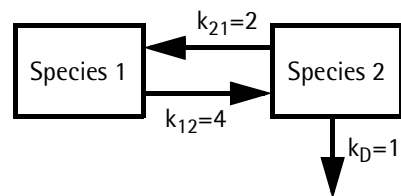
Global lifetime analysis (Mathematical model)

- Decay Associated Spectra (DAS)
- lifetimes



Target analysis (Physical model)

- Species Associated Emission Spectra (SAES)
- Physical parameters (i.e. rate constants)



1.14 Global lifetime analysis vs. target analysis of a particular (fictitious) data set. Top: Global Analysis results: an energy transfer DAS corresponding to $\tau=0.157$, decay, or trapping DAS corresponding to $\tau=1.59$. Below: Target analysis of the same kinetics using a 2-compartment model with reversible energy transfer, and decay (trapping) occurring from only one of the compartments. Species 1 is initially excited. The physical parameters (SAES-es, rate constants) are direct results from the analysis

know what the SAES-es for the different species are, what the uphill and downhill energy transfer rates between the species are, etc. Instead of the mathematical model, we would like to fit a physical model to the data, directly yielding the physical parameters of interest. This approach is called target analysis (or compartmental analysis, or kinetic modelling). Target analysis has several additional advantages: not only are the relevant physical parameters (and only those) directly derived from the data, one can also test different models, judge which one fits the data best and exclude those yielding physically unrealistic values. Moreover, some known physical properties can be used to restrict the degrees of freedom of the analysis (for instance regions where SAES-es are zero, relative oscillator strengths of SAES-es, initial excitation conditions, etc.).

The bottom part in figure 1.14 shows the target analysis of the same fictitious kinetics. A model is proposed consisting of two species (compartments). Energy transfer occurs between the two compartments with rates k_{12} and k_{21} and excitations disappear with a rate k_D , only from the second compartment. This could be the model of a very simple photosynthetic system: an antenna compartment that is in contact with an RC compartment, from which charge separation occurs. In an experiment the initial excitation conditions are generally known: here initially all excitations reside on species 1. The proposed model appears to fit the

kinetics well: two clearly resolved SAES-es appear (positive at all wavelengths) and it also directly yields the values of the three rate constants.

Clearly the target analysis approach is much more powerful than the global analysis (if a proper model can be found). The rates k_{12} and k_{21} can be used to calculate the energy difference between the two species and k_D directly gives the value of the quenching rate (trapping) from species 2. Also the entire emission spectra of both species are resolved, instead of just an estimate of the maxima.

THIS THESIS

The object of the research presented in this thesis is to gain greater insight into the way excitation energy transfer and trapping occurs in PSI. Therefore the spectroscopic and dynamic properties of a number of PSI core complexes (differing in their red chl content), as well as LHCl and to a lesser extent, PSI-200 were investigated.

In chapter 2 the spectroscopic properties of the low-energy chls in the PSI core of *Synechocystis* PCC6803 and PSI-200 were studied by energy selective fluorescence spectroscopy at low temperatures. We conclude that the bands of low-energy chls are both significantly homogeneously (electron-phonon coupling) and inhomogeneously broadened, and propose that the low-energy chls represent excitonically coupled dimers.

In chapter 3 time-resolved fluorescence measurements of 5 different PSI complexes are presented, each containing different amounts and types of low-energy chls. The target analysis of these 5 different data sets, using one general compartmental model, yields the room temperature absorption and emission properties of the different types of low-energy chls. Also the (longest) fluorescence lifetime is estimated for a hypothetical PSI particle, lacking low-energy chls.

Chapter 4 is a review of energy transfer and trapping in PSI, which features improved energy-selective emission spectra of the low-energy chls in *Synechocystis* PCC6803, that feature a structured phonon-progression. A low-temperature fluorescence excitation spectrum of PSI from *Synechococcus elongatus* reveals absorption features of the PSI RC, and demonstrates that even at low temperatures, where uphill energy transfer is blocked, still about 50% of the absorbed photons result in a charge separation in the RC. A simulation of energy transfer in PSI (lacking low-energy chls) is presented, based on the 4 Å structure model of PSI, and using the proposed dynamics of the hypothetical PSI particle from chapter 3.

In chapter 5 a similar simulation is performed, but now using the new 2.5 Å structural model, which reveals the orientations of all chls. It is shown that the main results of this simulation can be reproduced using a relatively simple lattice model. One of the merits of the lattice model is that it yields parameters that provide insight into the global energy transfer features of the system, rather than the microscopic parameters resulting from the structure-based simulation. The lattice model shows that the global rate of energy transfer from the bulk antenna chls to the RC is approximately equal to the rate of energy transfer from the bulk to the low-energy chls in *Synechococcus elongatus* PSI, found in chapter 3. This explains the fluorescence excitation results of chapter 4. Lattice models have been used extensively to model the excited state dynamics of various energy transferring systems, in the absence of

structural information. The comparison of such a model with the structure-based simulation, presented in this chapter, may serve to validate its general use.

In chapter 6, time-resolved fluorescence measurements of PSI are presented for different wavelengths of excitation. The results of the global analysis of these measurements are modelled by extending the structure-based simulation in chapter 5 to include the low-energy chls.

In chapter 7 the energy transfer in PSI from *Synechococcus elongatus* is studied in more detail, using the technique of fluorescence upconversion. This permits resolution of the elementary energy transfer steps (~160 fs) and equilibration (~360 fs) in the bulk antenna. Energy transfer from β -car to chl is found to proceed both via the S_2 and the S_1 state, resulting in an estimated overall yield of ~90%.

Finally, in chapter 8, the energy transfer in isolated LHCI dimers is studied. The difficulty in this study is that the preparation consists of a mixture of all different LHCI dimers, since separation is currently not possible. However, by using different wavelengths of excitation (in the chl a , chl b and carotenoid absorption regions) and by combining streak camera and fluorescence upconversion data, quite some details of the energy transfer processes can be resolved. It is concluded that, contrary to earlier reports, all LHCI dimers contain some low-energy chl form. Our analysis distinguishes between two distinct (classes of) LHCI dimers, based on their different excited state lifetimes.

REFERENCES

- (1) UCMP Exhibit Halls. Geologic Time: A temporal journey through Earth's history. <http://www.ucmp.berkeley.edu/exhibit/geology.html>
- (2) Schopf, J.W. 1992. The oldest fossils and what they mean. *In* Major events in the history of life. J.W. Schopf, editor. Jones and Bartlett. 29-63.
- (3) Ochman, H., J.G. Lawrence, and E.A. Groisman. 2000. Lateral gene transfer and the nature of bacterial innovation. *Nature*. 405:299-304.
- (4) Geerts, G., and H. Heestermans. 1992. *In* Groot woordenboek der Nederlandse taal. Van Dale, Utrecht-Antwerpen. 864.
- (5) Falkowski, P.G. and J.A. Raven. 1997. *In* Aquatic photosynthesis. Blackwell Science. 2.
- (6) More on morphology of the cyanobacteria. <http://www.ucmp.berkeley.edu/bacteria/cyanomm.html>.
- (7) Life history and ecology of cyanobacteria. <http://www.ucmp.berkeley.edu/bacteria/cyanolh.html>.
- (8) Carmichael, W.W. 1994. The toxins of cyanobacteria. *Scientific American*. Jan:64-72.
- (9) Brody, S.S., and E. Rabinowitch. 1957. Excitation lifetime of photosynthetic pigments *in vitro* and *in vivo*. *Science*. 125:555.
- (10) Stryer, L. 1995. Biochemistry. W.H. Freeman and Company, New York.
- (11) Schubert, W.D., O. Klukas, W. Saenger, H.T. Witt, P. Fromme, and N. Krauss. 1998. A common ancestor for oxygenic and anoxygenic photosynthetic systems: A comparison based on the structural model of Photosystem I. *J. Mol. Biol.* 280:297-314.
- (12) Scheer, H. 1991. Chlorophylls. CRC Press, Boca Raton, Florida.

- (13) Croce, R., and R. Bassi. 1998. The light-harvesting complex of Photosystem I: Pigment composition and stoichiometry. *In* Photosynthesis: Mechanisms and effects. G. Garab, editor. Kluwer Academic Publishers, Dordrecht, The Netherlands. 1:421-424.
- (14) Chynwat, V., and H.A. Frank. 1995. The application of the energy-gap law to the S-1 energies and dynamics of carotenoids. *Chem. Phys.* 194:237-244.
- (15) Koyama, Y., M. Kuki, P.O. Andersson, and T. Gillbro. 1996. Singlet excited states and the light-harvesting function of carotenoids in bacterial photosynthesis. *Photochem. Photobiol.* 63:243-256.
- (16) Cogdell, R.J. 1985. Carotenoids in photosynthesis. *Pure Applied Chem.* 57:723-728.
- (17) Horn, R., and H. Paulsen. 2002. Folding *in vitro* of light-harvesting chlorophyll-*a/b* protein is coupled with pigment binding. *J. Mol. Biol.* 318:547-556.
- (18) Van Amerongen, H., L. Valkunas, and R. van Grondelle. 2000. Photosynthetic excitons. World Scientific, London.
- (19) Jankowiak, R., J.M. Hayes, and G.J. Smal. 1993. Spectral hole-burning spectroscopy in amorphous molecular-solids and proteins. *Chem. Rev.* 93:1471-1502.
- (20) Förster, T. 1965. *In* Modern Quantum Chemistry. O. Sinanoglu, editor. Academic Press, New York. 2:93-137.
- (21) Knox, R.S., and H. van Amerongen. 2002. Refractive index dependence of the Förster resonance excitation transfer rate. *J. Phys. Chem. B.* 106:5289-5293.
- (22) Scheller, H.V., H. Naver, and B.L. Moller. 1997. Molecular aspects of Photosystem I. *Physiol. Plant.* 100:842-851
- (23) Kruij, J., D. Bald, E. Boekema, and M. Rögner. 1994. Evidence for the existence of trimeric and monomeric Photosystem I complexes in thylakoid membranes from cyanobacteria. *Photosynth. Res.* 40:279-286.
- (24) Jordan, P., P. Fromme, H.T. Witt, O. Klukas, W. Saenger, and N. Krauss. 2001. Three-dimensional structure of cyanobacterial Photosystem I at 2.5 angstrom resolution. *Nature.* 411:909-917.
- (25) Guergova-Kuras, M., B. Boudreaux, A. Joliot, P. Joliot, and K. Redding. 2001. Evidence for two active branches for electron transfer in Photosystem I. *Proc. Natl. Acad. Sci. USA.* 98:4437-4442.
- (26) Hastings, G., and V. Sivakumar. A Fourier transform infrared absorption difference spectrum associated with the reduction of A(1) in Photosystem I: Are both phylloquinones involved in electron transfer? *Biochemistry.* 40:3681-3689.
- (27) Jansson, S. 1994. The Light-harvesting chlorophyll *a/b* binding-proteins. *Biochim. Biophys. Acta.* 1184:1-19.
- (28) Kühlbrandt, W., D.N. Wang, and Y. Fujiyoshi. 1994. Atomic model of plant light-harvesting complex by electron crystallography. *Nature.* 367:614-621.
- (29) Boekema, E.J., P.E. Jensen, E. Schlodder, J.F.L. van Breemen, H. van Roon, H.V. Scheller, and J.P. Dekker. 2001. Green plant Photosystem I binds light-harvesting complex I on one side of the complex. *Biochemistry.* 40:1029-1036.
- (30) Croce, R., G. Zucchelli, F.M. Garlaschi, and R.C. Jennings. 1998. A thermal broadening study of the antenna chlorophylls in PSI-200, LHCl, and PSI core. *Biochemistry.* 37:17355-17360.
- (31) Gobets B., I.H.M. van Stokkum, M. Rögner, J. Kruij, E. Schlodder, N.V. Karapetyan, J.P. Dekker, and R. van Grondelle. 2001. Time-resolved fluorescence emission measurements of Photosystem I particles of various cyanobacteria: a unified compartmental model. *Biophys. J.* 81:407-424.

- (32) Rivadossi, A., G. Zucchelli, F.M. Garlaschi, and R.C. Jennings. 1999. The importance of PSI chlorophyll red forms in light-harvesting by leaves. *Photosynth. Res.* 60:209-215.
- (33) Gobets, B., and R. van Grondelle. 2001. Energy transfer and trapping in Photosystem I. *Biochim. Biophys. Acta.* 1507:80-99.
- (34) Gobets, B., H. van Amerongen, R. Monshouwer, J. Kruip, M. Rögner, R. van Grondelle, and J.P. Dekker. 1994. Polarized site-selected fluorescence spectroscopy of isolated Photosystem I particles. *Biochim. Biophys. Acta.* 1188:75-85.
- (35) Holzwarth, A.R. 1996. Data analysis of time-resolved measurements. *In* Biophysical techniques in photosynthesis. J. Amesz, and A. J. Hoff, editors. Kluwer, Dordrecht, the Netherlands. 75-92.
- (36) Hoff, W.D., I.H.M. van Stokkum, H.J. van Ramesdonk, M.E. van Brederode, A.M. Brouwer, J.C. Fitch, T.E. Meyer, R. van Grondelle, and K.J. Hellingwerf. 1994. Measurement and global analysis of the absorbance changes in the photocycle of the photoactive yellow protein from *Ectothiorhodospira halophila*. *Biophys. J.* 67:1691-1705.
- (37) Nordlund, T.M. 1991. Streak cameras for time-domain fluorescence. *In* Topics in fluorescence spectroscopy. J.R. Lakowicz, editor. Plenum press, New York and London. 1:183-260.

2

Polarized site-selected fluorescence spectroscopy of isolated Photosystem I particles

Bas Gobets, Herbert van Amerongen, René Monshouwer, Jochen Kruij, Matthias Rögner, Rienk van Grondelle and Jan P. Dekker

Polarized steady-state fluorescence spectra have been obtained from Photosystem I core complexes of the cyanobacterium *Synechocystis* PCC 6803 and from LHCI containing Photosystem I (PSI-200) complexes of spinach by selective laser excitation at 4 K. Excitation above 702 nm in *Synechocystis* and 720 nm in PSI-200 results in highly polarized emission, suggesting that pigments absorbing at these and longer wavelengths are not able to transfer excitation energy at 4 K. In both systems the peak wavelength of the emission (λ_{em}) depends strongly on the excitation wavelength (λ_{ex}). This indicates that in both systems the long-wavelength bands responsible for the steady-state emission are inhomogeneously broadened. The width of the inhomogeneous distribution is estimated to be about 215 cm^{-1} in *Synechocystis* and 400 cm^{-1} in PSI-200. We conclude that the peaks of the total absorption spectra of the long-wavelength pigments of *Synechocystis* and PSI-200 are at 708 and 716 nm, respectively, and therefore designate these pigments as C708 and C716. The results further show that C708 and C716 are strongly homogeneously broadened, i.e. carry broad phonon side-bands. The width of these bands is estimated to be about 170 and 200 cm^{-1} for C708 and C716, respectively. The Stokes' shifts appear to be large: about 200 cm^{-1} (10 nm) for C708 and about 325 cm^{-1} (17 nm) for C716. These values are much higher than usually observed for 'normal' antenna pigments, but are in the same order as found previously for a number of dimeric systems. Therefore, we propose that the long-wavelength pigments in Photosystem I are excitonically coupled dimers. Based on fitting with Gaussian bands the presence of one C708 dimer per P700 is suggested in the core antenna of *Synechocystis*.

INTRODUCTION

The two main functions of the light-harvesting antenna pigments in photosynthetic systems are the absorption of light of different wavelengths and the efficient transfer of excitation energy to one of the photochemical reaction centres. Both functions are highly optimized in photosynthetic organisms: the antenna usually absorbs as much as possible of the available light, and excitation energy transfer to the reaction centre is generally highly efficient.¹

In Photosystem I (PSI) of green plants, algae and cyanobacteria it has been shown that excitation energy transfer is indeed extremely rapid.² The most recent experiments suggest average single transfer times of about 180 fs³ and overall trapping times in the tens of picoseconds time-range.⁴⁻⁶ According to Trissl^{6,7} these processes in PSI are even more efficient than actually required, due to which the photosystem can afford a small number of antenna pigments absorbing at lower energy than the primary electron donor P700, thus increasing the absorption cross-section for red light (> 700 nm) and optimizing the balance between the two main functions. In addition, some of the long-wavelength pigments could help in guiding the excitations to P700.^{4,8} The long-wavelength pigments largely determine the steady-state emission properties at low temperatures. Such pigments in most of the PSI reaction centre core complexes of green plants, algae and cyanobacteria give rise to emission bands peaking near 720 nm at 77K, while most of the peripheral chlorophyll-*a/b* antenna complexes give rise to emission bands peaking near 735 nm.⁹

Despite substantial interest in the role of long-wavelength pigments of PSI in excitation energy transfer and trapping, there is still considerable lack of knowledge about their molecular properties. The number of red pigments per complex, the exact absorption maxima, the extent of homogeneous and inhomogeneous broadening and the possibility of energy transfer between the red pigments are, for instance, not well known. In a previous report, we analysed a number of isolated PSI preparations (monomeric and trimeric core complexes from the cyanobacterium *Synechocystis* PCC 6803 and LHCI containing PSI-200 complexes from spinach) by steady-state polarized light spectroscopy at 77 K and linear and circular dichroism characteristics were established.¹⁰ It was concluded that the possibility of energy transfer between the various long-wavelength pigments was very low in the monomeric and trimeric particles from *Synechocystis*, but high in PSI-200, in which significant downhill energy-transfer from the long-wavelength pigments of the core antenna to the peripheral antenna was proposed.

In this report, we extend this research by polarized site-selected fluorescence spectroscopy, provide new information on the spectroscopic properties of the long-wavelength pigments in the core and peripheral antenna of PSI, and propose that these pigments are arranged as excitonically coupled dimers of chl*a*.

MATERIALS AND METHODS

Monomeric and trimeric PSI core particles (P700-F_A/F_B) from *Synechocystis* sp. PCC 6803 were prepared as described before by Rögner and co-workers.^{11,12} Unlike the complexes studied in ref. 10, the absorption profiles at long wavelengths were similar for the monomeric

and trimeric complexes and the membranes studied in this contribution (see Section 3). For a possible explanation we suggested that the amplitude of the long-wavelength spectral component in the monomers varies per batch and depends on the severeness of the detergent treatment during the isolation procedure.¹⁰ Obviously, the monomeric complexes analysed in this contribution are more native. LHCl containing PSI-200 particles from spinach were prepared as described by Van der Lee et al.¹⁰ For the low-temperature measurements, the particles were diluted in 20 mM Mes-NaOH, 10 mM MgCl₂, 10 mM CaCl₂, 70% w/v glycerol and 0.05% dodecyl- β ,D-maltoside (pH 6.5) and cooled to 4 K in a He-flow cryostat (Oxford).

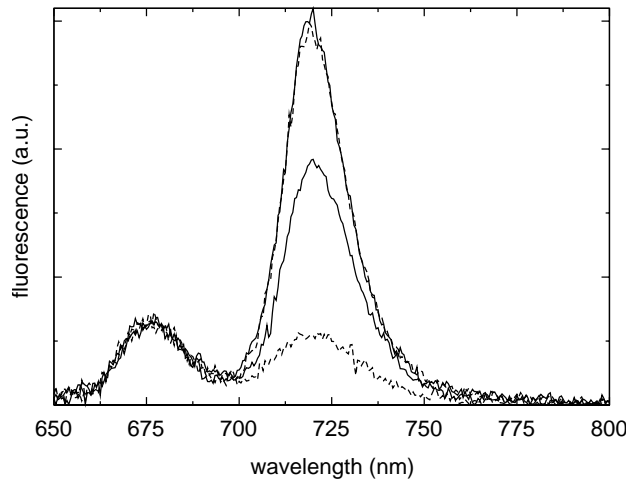
Fluorescence spectra were obtained on a home-built fluorimeter and corrected for the sensitivity of the detection system as in ref. 13. Site-selection was performed as in ref. 14, except that as light source for the site-selection excitation light a Ti-Sapphire laser was used (Coherent, model 890, spectral bandwidth $\sim 2 \text{ cm}^{-1}$). The laser was tuned between 693.5 and 733.5 nm at 1 nm intervals, using 4–20 mW/cm² energy. It was checked that no sample degradation took place during the measurements. Detection of the fluorescence was at right angle with respect to the excitation beam and was achieved with a double 1/8 m monochromator (Oriel) and a photomultiplier (S-20 photocathode, Thorn EMI 9658A). The spectral bandwidth for detection was 1.5 nm. The excitation light was vertically polarized (when sensitivity corrections were made horizontally polarized excitation was used as well) and a polarizer in the detection beam was either vertical or horizontal. The anisotropy of the emission is defined by $r = (I_{||} - I_{\perp}) / (I_{||} + 2I_{\perp})$, in which $I_{||}$ and I_{\perp} are the fluorescence intensities with vertical and horizontal detection beam polarizations, respectively. The site-selected spectra were recorded with $A_{680} \sim 1$. This high A was used to increase the fluorescence intensity. Self-absorption of the emitted light did not pose a serious problem, because the fluorescence appeared far away from the maximum of the absorption. Absorption spectra were measured on a Cary 219 spectrophotometer with 0.25 nm resolution.

RESULTS

Photosystem I core complexes from *Synechocystis*

Cyanobacteria like *Synechocystis* contain reaction centre core complexes of PSI, but lack peripheral chl*a/b* containing antenna complexes. Isolated cyanobacterial cores, including those of *Synechocystis*, have been isolated as monomeric and/or as trimeric complexes.^{15,18} There is increasing evidence that the trimeric association represents the *in vivo* organization of the cyanobacterial core under certain salt conditions,^{16–18} presumably in equilibrium with the monomer.¹⁸

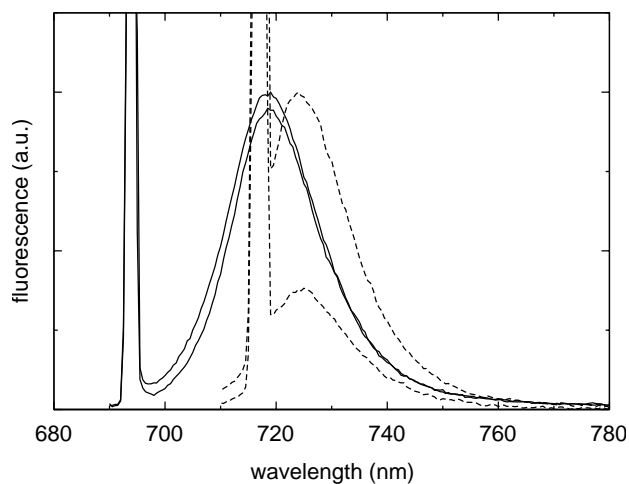
Figure 2.1 shows Soret-excited emission spectra from monomeric PSI core complexes from *Synechocystis* sp. PCC 6803 between 4 K and 120 K. The spectra are characterized by a strongly temperature-dependent contribution peaking at about 720 nm (the exact peak maxima are 720.5 nm at 77 K and at 718.5 nm at 4 K) and a small temperature-independent contribution peaking at 675.5 nm. We attribute the latter contribution to uncoupled chl absorbing at about 670 nm. The temperature-dependence of the 720 nm contribution is



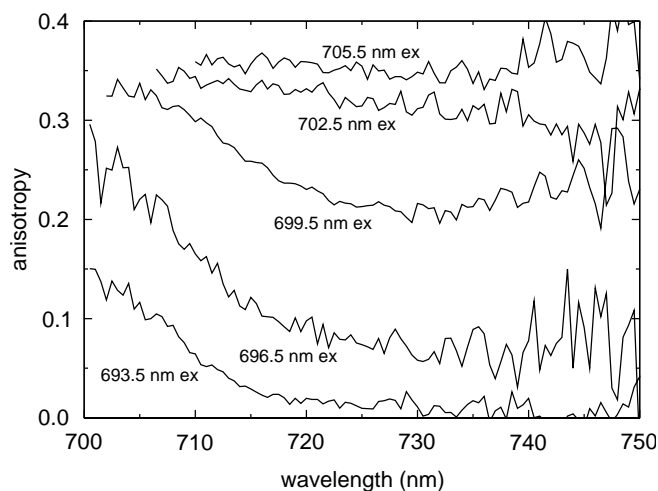
2.1 Soret excited (437 nm) emission spectra of monomeric PSI complexes from *Synechocystis* PCC 6803 at 4 K (full line, upper curve), 40 K (dashed line, upper curve), 77 K (full line, lower curve) and 120 K (dashed line, lower curve). The spectra were recorded with $A_{680} \sim 0.05$.

virtually identical to the dependence observed by Wittmershaus et al. for *Synechocystis* membranes.¹⁹

The nature of the emission at 4 K was further analysed by applying selective laser excitation in the red part of the chl $Q_{y(0-0)}$ absorption region. Figure 2.2 shows a typical result of the vertically and horizontally polarized emission spectra of monomeric complexes upon vertical excitation at 693.5 nm (continuous lines) and 716.5 nm (dashed lines). The spectra consist of sharp, high peaks at the laser excitation wavelength and broad features around



2.2 Emission spectra at 4 K of monomeric PSI complexes from *Synechocystis* PCC 6803, laser-excited at 693.5 nm (full lines) and at 716.5 nm (dashed lines). The laser excitation light was vertically polarized, and a polarizer in the detection beam selected either for vertically polarized light (upper curves) or for horizontally polarized light (lower curves). The spectra were recorded with $A_{680} \sim 1$ (see Materials and methods).

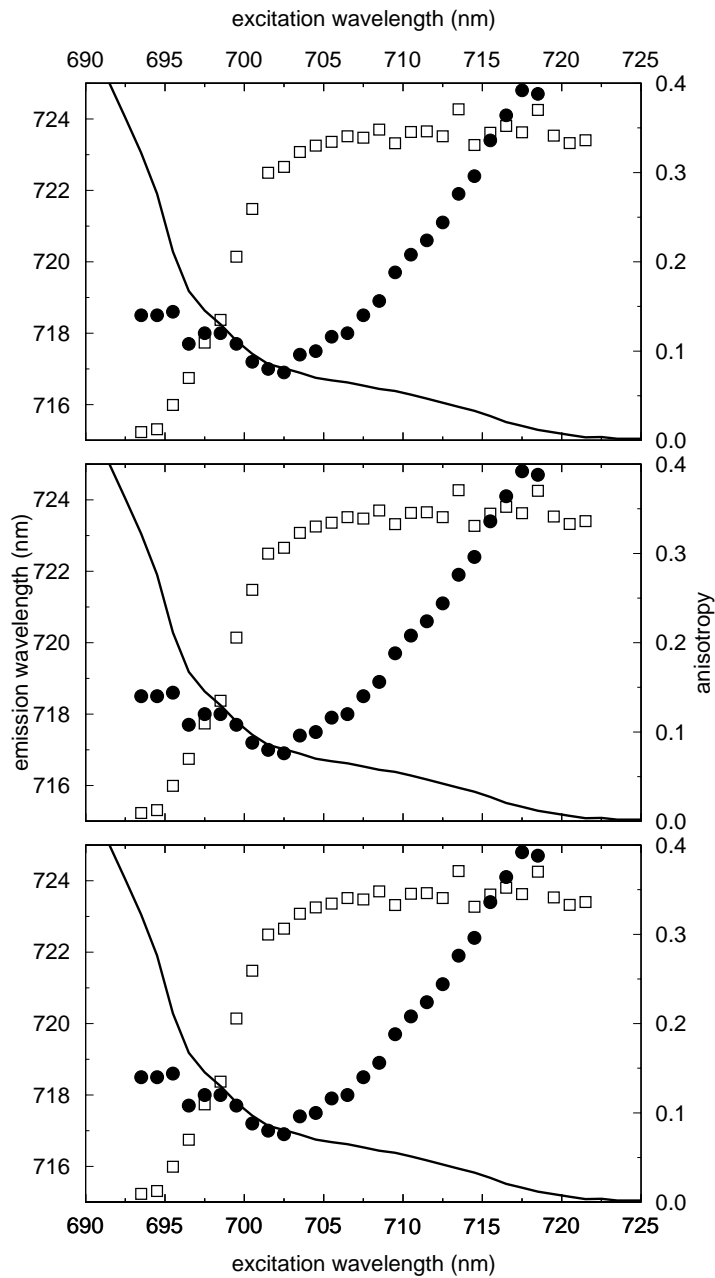


2.3 Anisotropy spectra at 4 K of monomeric PSI complexes from *Synechocystis* PCC 6803, laser-excited (from bottom-to-top) at 693.5, 696.5, 699.5, 702.5 and 705.5 nm.

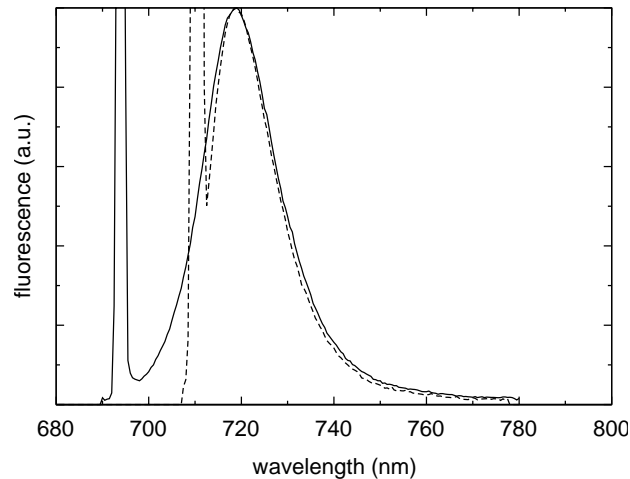
720 nm that resemble the PSI emission peaks obtained by excitation in the Soret absorption region of the chlorophylls (fig. 2.1). The contribution of uncoupled chl is not observed with both excitation wavelengths, which is expected because the excitation wavelength is well above their absorption maximum.¹⁴ The sharp features in figure 2.2 are largely due to elastic scattering of the laser excitation light. Also the contribution at the blue side of the scattering peak was found to originate from scattering, which was concluded from measurements on scattering samples without absorption at the wavelength of excitation.

It becomes immediately clear from figure 2.2 that the anisotropy of the emission depends strongly on the excitation wavelength. The vertically and horizontally detected emission spectra have about equal amplitudes upon 693.5 nm excitation, whereas they differ considerably upon 716.5 nm excitation. Figure 2.3 shows the anisotropy spectra of the emission upon selective excitation at wavelengths from 693.5 nm to 705.5 nm. At all excitation wavelengths at and above 705.5 nm the anisotropy is high (~ 0.34) and close to the theoretical maximum (0.4). This indicates that no depolarization due to energy transfer takes place at these wavelengths, although the possibility of energy transfer between pigments with almost perfectly aligned Q_y transitions cannot be ruled out. In figure 2.4a (open squares) the value of the anisotropy detected at 735 nm is plotted. It shows a steep rise from almost zero at 693.5 nm to about 0.34 above 705.5 nm and is almost identical to the fluorescence polarization spectra at 77 K.¹⁰ For excitation wavelengths between 693.5 and 705.5 nm the anisotropy of the emission depends on the detection wavelength; close to the scattering peak at the blue side of the emission band the anisotropy increases to some extent (fig. 2.3). This is not due to a contribution of polarized scattered light (anisotropy 1.0), because the region of increased anisotropy extends more to the red than the scattered light and because it is not observed upon excitation above 705.5 nm.

Another feature of the site-selected emission spectra of figure 2.2 is that the peak-wavelength of the emission depends on the excitation wavelength. The values of the emission maxima are plotted in figure 2.4a (closed circles) as a function of excitation



2.4 (A) Emission and absorption characteristics of monomeric PSI complexes from *Synechocystis* PCC 6803 at 4 K. Closed circles: wavelength of the emission maximum (λ_{em}) as a function of excitation wavelength (λ_{ex}). Open squares: value of the anisotropy of the emission detected at 735 nm. Line: 4 K absorption spectrum. (B) As A, but of trimeric PSI complexes from *Synechocystis* PCC 6803 at 4 K. (C) As A, but of thylakoid membranes from *Synechocystis* PCC 6803 at 4 K.



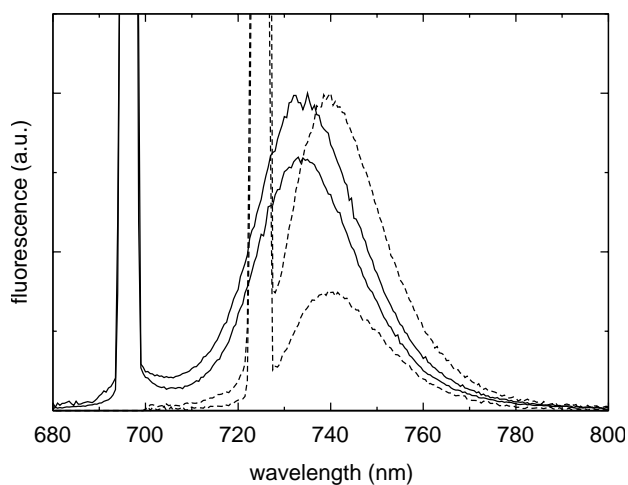
2.5 Comparison of the spectral shape of emission spectra of monomeric PSI complexes from *Synechocystis* PCC 6803 at 4 K excited at 693.5 nm (full line) and 712.5 nm (dashed line, blue-shifted by 2 nm). The spectra were normalized at the peak of the emission at 718.5 nm.

wavelength. Striking is the fact that upon red shifting the wavelength of excitation the emission maximum first blueshifts to about 717 nm upon excitation at 702 nm, and then red shifts with a slope of about 0.6. Figure 2.5 compares the shapes of the emission spectra obtained upon relatively blue (693.5 nm) and relatively red excitation (712.5 nm). The width and shape on the red side of the emission spectra are very similar, whereas the width on the blue side decreases upon far red excitation. The same phenomenon was also observed in the antenna of *Rhodospseudomonas viridis* (Monshouwer et al., unpublished observations).

Figure 2.4b and c show that site-selected fluorescence measurements on trimeric particles and thylakoid membranes from *Synechocystis* sp. PCC 6803 yield basically the same results as obtained for monomeric particles. This shows that the long-wavelength pigments that are responsible for the steady-state emission at 4 K are basically unperturbed during the isolation procedure. This also indicates that in the trimeric particles there is no excitation energy transfer among the long-wavelength pigments at 4 K (which confirms conclusions in ref. 10 at 77 K), because otherwise the anisotropy and peak wavelength of emission would show a dependence on excitation wavelength different from that observed in the monomers.

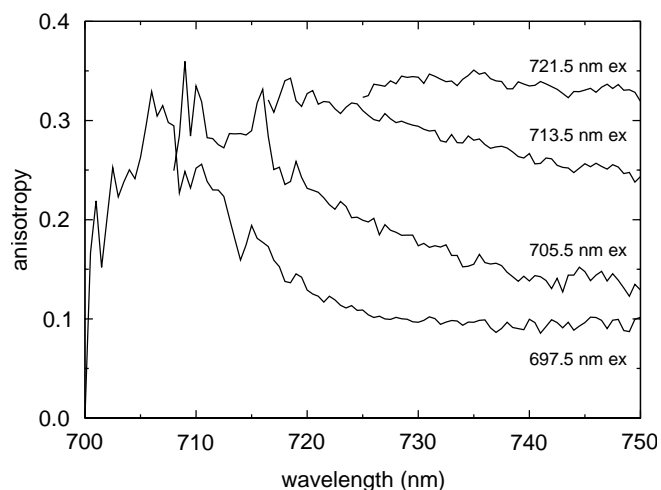
PSI-200 complexes from spinach

Polarized site-selected fluorescence experiments were also performed on PSI-200 complexes from spinach. These complexes consist of a monomeric PSI core surrounded by about 8 chl*a/b* containing LHCl proteins.²⁰ The latter proteins contain long-wavelength pigments that are responsible for steady-state fluorescence peaking at about 735 nm.⁹ These pigments absorb and fluoresce more to the red than the long-wavelength pigments of the core antenna of PSI. Van der Lee et al.¹⁰ suggested that excitations are effectively transferred from the long-wavelength pigments of the core antenna to the long-wavelength pigments of the peripheral antenna at low temperatures.

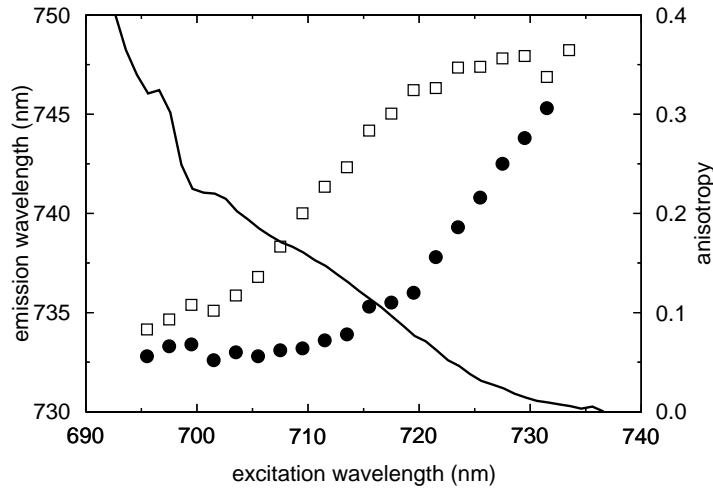


2.6 Emission spectra at 4 K of PSI-200 complexes from spinach, laser-excited at 695.5 nm (full lines) and at 723.5 nm (dashed lines). The laser excitation light was vertically polarized, and a polarizer in the detection beam selected either for vertically polarized light (upper curves) or for horizontally polarized light (lower curves). The spectra were recorded with $A_{680} \sim 1$ (see Materials and methods).

Figure 2.6 shows a typical result of polarized site-selected fluorescence experiments of PSI-200. Again, pronounced scattering peaks are observed around the excitation wavelength, as well as excitation-wavelength dependent anisotropies and peak wavelengths of the emission. The anisotropy spectra of the emission for a number of applied excitation wavelengths are shown in figure 2.7. For excitation wavelengths from 695.5 to 713.5 nm it shows a region of increased anisotropy close to the excitation wavelength, similar to excitation wavelengths below 705.5 nm in the PSI core particles from *Synechocystis*. As the excitation wavelength is shifted from the blue to the red side of this region, the red tail of the

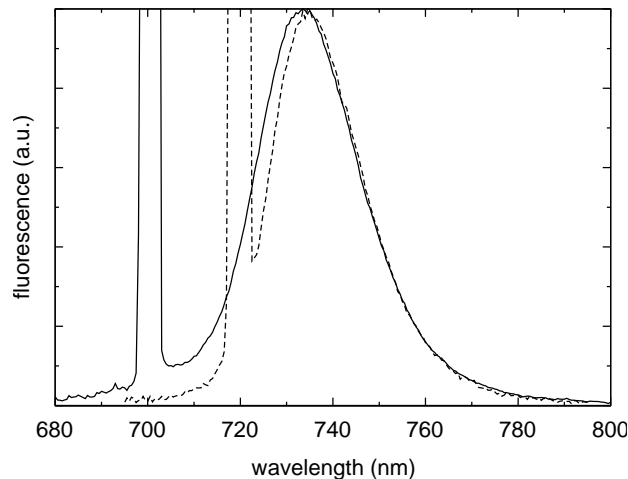


2.7 Anisotropy spectra at 4 K of PSI-200 complexes from spinach, laser-excited (from bottom-to-top) at 697.5, 705.5, 713.5 and 721.5 nm.



2.8 Emission and absorption characteristics of PSI-200 complexes from spinach at 4 K. Closed circles: wavelength of the emission maximum (λ_{em}) as a function of excitation wavelength (λ_{ex}). Open squares: value of the anisotropy of the emission detected at 750 nm. Line: 4 K absorption spectrum.

anisotropy rises until the anisotropy spectra are constant over the entire emission band. The flat, high anisotropy occurs with excitation wavelengths at and above 721.5 nm (see also figure 2.8, open squares). The peak wavelength of the emission is constant at excitation wavelengths below 715 nm (Figure 2.8, closed circles). Above 719 nm it starts to rise almost linearly upon red shifting the excitation with a slope of about 0.77. This slope is steeper than the slope observed in the PSI particles of *Synechocystis*, and a dip as in the corresponding experiments on *Synechocystis* (Figure 2.4a-c, closed circles) is not observed. Figure 2.9 compares the shapes of the emission spectra obtained upon relatively blue (699.5 nm) and



2.9 Comparison of the spectral shape of emission spectra of PSI-200 complexes from spinach at 4 K excited at 699.5 nm (full line) and 723.5 nm (dashed line, blueshifted by 5 nm). The spectra were normalized at the peak of the emission at 733.5 nm.

relatively red excitation (723.5 nm). As in *Synechocystis*, the width and shape on the red side of the emission spectra are the same, whereas the width on the blue side decreases upon far red excitation.

DISCUSSION

The polarized site-selected emission experiments of PSI reaction centre core and peripheral antenna complexes presented in this contribution show that anisotropy and peak wavelength of the emission depend on the excitation wavelength. Polarized site-selected emission experiments have also been performed on isolated LH1 antenna complexes from *Rhodobacter sphaeroides*,²¹ the B820 subunit of the LH1 antenna complex of *Rhodospirillum rubrum*,²² chl*a* in detergent¹⁴ and the isolated PSII reaction centre complex,²³ and results of these experiments have been explained in terms of downhill energy-transfer among a specific cluster of pigments and homogeneous and inhomogeneous broadening of spectral bands.

Inhomogeneous broadening

In general, spectral lines can be inhomogeneously and homogeneously broadened.²⁴⁻²⁶ Inhomogeneous broadening of the absorption bands (Γ_i) reflects variations in the energies of the electronic transitions of the pigments. These variations arise from slightly different conformations of the protein environment of the pigment. The various conformations will be frozen at very low temperatures, due to which pigments in those conformations can selectively be excited by steady-state laser light. Homogeneous broadening (Γ_h) is usually defined as broadening of the zero-phonon transition. Another form of broadening, which also may be regarded as a form of homogeneous broadening, stems from electron-phonon coupling, which leads to asymmetric broadening towards the high-energy side of the absorption band, reflected by a phonon side-band. The phonon side-band actually carries a significant part of the oscillator strength of the transition; it will also appear in the fluorescence spectrum but then on the low-energy side of the zero-phonon line. In the remaining part of this paper we will refer to Γ_h as the width of the phonon side-wing, since this wing is much broader than the zero-phonon line.

The site-selected emission spectra of the PSI core and peripheral antenna complexes presented in this contribution show that the optical transitions of the long-wavelength pigments responsible for the steady-state emission are considerably inhomogeneously broadened, since the shape and position of the emission spectrum depend on the excitation wavelength (see Appendix). We just note here that homogeneous broadening is also very significant for the description of the spectral properties of the long-wavelength pigments (see below).

The concept of inhomogeneous broadening has consequences for the shape of the PSI core emission spectra at intermediate temperatures (e.g., 77 K). At these temperatures there is slow uphill energy-transfer from the long-wavelength pigments to the primary electron donor P700, which forms a very efficient energy trap. The uphill transfer will be more efficient for long-wavelength pigments absorbing at the blue side of the inhomogeneous distribution than for those at the red side, due to which the red part will contribute more to the fluorescence.

The spectra presented in figure 2.1 show that indeed the emission red shifts upon raising the temperature from 4 K to 77 K, and therefore give further support to the inhomogeneous broadening of the long-wavelength pigments of PSI. This also shows that one has to be careful about assigning specific emission bands to specific pigments, because the emission spectrum may preferentially arise from a low-energy part of the inhomogeneous distribution.

Energy transfer in the PSI antenna from *Synechocystis*

The anisotropy data presented in ref. 10 and in figure 2.4 of this contribution suggest that the long-wavelength pigments in the core antenna of *Synechocystis* are either not connected by energy transfer or are connected but with almost parallel Q_y transition dipoles. However, the fact that anisotropy and peak wavelength of the emission start to rise and decrease, respectively, at the same excitation wavelength (~ 695 nm) rules out the option that parallel long-wavelength pigments are connected by energy transfer at 4 K. If two or more 'red' pigments would be coupled, the probability of energy transfer from a pigment on the blue side of the inhomogeneous distribution to another would be high, due to which the probability of emission at the blue side of the distribution would be low and the peak wavelength of emission would start to shift at a considerably longer excitation wavelength than the anisotropy (see also ref. 21).

The low anisotropy values of the emission obtained upon excitation at and below 695.5 nm are due to energy transfer from pigments which absorb below this wavelength and transfer their excitation energy to the long-wavelength pigments. Similarly, the high anisotropy values obtained upon excitation above 702 nm indicate the absence of energy transfer. Since just above 702 nm P700 should have significant absorption, it also indicates that there is no energy transfer from P700 to the long-wavelength pigments at 4 K, suggesting that P700 forms a perfect energy trap. At intermediate wavelengths a mixture of different types of pigments is excited. The resulting emission spectra revealed a relatively high anisotropy at the blue side of the emission band and a much lower anisotropy at the red side (fig. 2.3). The high anisotropy at the blue side may arise from pigments which form local energy traps and transfer the energy relatively slowly (in 10–20 ps see ref. 1) to P700 or to the long-wavelength antenna pigments.

The homogeneous bandwidth of the long-wavelength pigments in *Synechocystis*

The plot of the peak wavelength of emission versus excitation wavelength (fig. 2.4) also gives information about the relative width of the homogeneous lineshape of the long-wavelength pigments. From the anisotropy measurements it can be deduced that for excitation wavelengths above 702 nm the emission almost exclusively arises from directly excited long-wavelength pigments. The peak wavelength of the emission shifts from about 717 nm for 702 nm excitation to 725 nm for 719 nm excitation. It is remarkable that even at the latter wavelength at the far red end of the absorption spectrum the gap between excitation and peak of emission wavelength is rather high (about 6 nm, or 115 cm^{-1}). Since at this far-red excitation wavelength the pigments will be excited in their zero-phonon lines or in the red part of the phonon wing, a large proportion of this gap represents the energetic separation between the zero-phonon line and the peak of the corresponding phonon wing.

Also the spectrum obtained upon far-red excitation has a quite considerable width (see, for instance, the 716.5 nm excited spectra in figure 2.2, which are characterized by a fwhm of about 16 nm or 310 cm^{-1}).

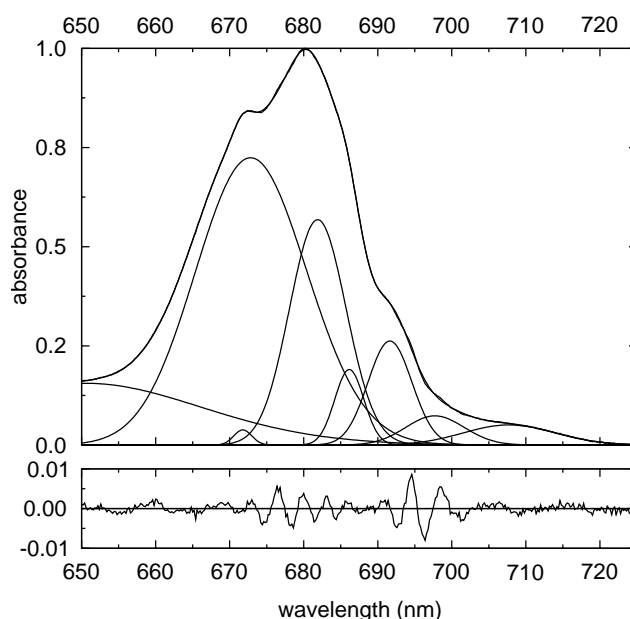
Excitation at 708 nm yielded an emission maximum at 718.5 nm. The same maximum is observed upon non-selective excitation, which suggests that the peak position of the complete absorption band of all longwavelength pigments is near 708 nm (see Appendix: $\lambda_{\text{em}} = \lambda_{0,\text{em}}$ at 718.5 nm, due to which $\lambda_0 = \lambda_{\text{ex}} = 708\text{ nm}$). We will therefore designate from now on the long-wavelength pigments of *Synechocystis* as C708.

From the slope of the λ_{em} vs. λ_{ex} plot estimates for the homogeneous (Γ_h) and inhomogeneous (Γ_i) bandwidths can be obtained (see Appendix). The slope is not very large ($s = 0.6$) and suggests $\Gamma_h/\Gamma_i \sim 0.8$. This means that C708 is characterized by a quite considerable homogeneous bandwidth. From the Gaussian fit of figure 2.10 (discussed in detail below) a value of $\sim 270\text{ cm}^{-1}$ is estimated for the total fwhm of C708 in absorption. Assuming Gaussian profiles for homogeneous and inhomogeneous broadening, this leads to values of ~ 170 and 215 cm^{-1} for Γ_h and Γ_i , respectively. The energetic separation between the peak wavelengths of absorption and emission is about 10 nm (or 200 cm^{-1}) for the total long-wavelength band, which largely represents the energetic separation between peak wavelengths of the phonon side bands in absorption and emission, i.e. the Stokes' shift δ . The difference in shape of the emission spectra upon relatively blue and red excitation (fig. 2.5) is attributed to the preferential excitation in the blue and red parts of the phonon wing, respectively.

The Stokes' shift of C708 appears much larger than of isolated chl a ($\sim 80\text{ cm}^{-1}$ - ref. 14). In principle, this large value could be due to specific interactions between the protein environment (e.g., charged amino acids) and monomeric chl a . However, we are not aware of any documented precedents. Alternatively, the large Stokes' shift of C708 may be caused by strong pigment-pigment interactions. An increased Stokes' shift was observed in the B820 subunit of the LH1 antenna of *Rhodospirillum rubrum* (about 120 cm^{-1} - ref. 27) and attributed to the dimeric nature of the Bchls. Also for the primary electron donor of the reaction centre of purple bacteria a large separation between zero-phonon line and peak wavelength of the phonon side band ($\sim 120\text{ cm}^{-1}$) was observed,²⁵ which predicts a Stokes' shift of about 240 cm^{-1} . Based on these results we propose that pigment-pigment interactions rather than pigment-protein interactions cause the large Stokes' shift of C708 and that C708 is a dimer of (excitonically coupled) chl a molecules (see also below). The CD is less than that of P700,¹⁰ which suggests that the electronic transition dipole moments of the individual molecules are more in one plane than those of P700. The transition dipole moment of the major exciton component of C708 was reported to make an angle between 17° and 28° with the plane of the particle.¹⁰

The number of long-wavelength pigments in *Synechocystis*

In our earlier report¹⁰ we mentioned that it was not possible to estimate the number of long-wavelength pigments per reaction centre by fitting the absorption spectra with Gaussian bands. Several good fits could be obtained in which peak wavelength and amplitude of the long-wavelength pigments varied quite considerably. The more accurate estimation of the peak wavelength of C708 in this contribution permits a better estimation of the oscillator



2.10 Fit with Gaussian bands of the absorption spectrum between 650 and 725 of monomeric PSI complexes from *Synechocystis* PCC 6803 at 4 K. The lower represents the (enlarged) difference between absorption spectrum and fit. Constraints: 8 Gaussians, each characterized by a certain peak wavelength (λ), FWHM and amplitude (a); all parameters were free fitting parameters. Result: band 1 (C708): $\lambda = 708.1$ nm, $fwhm = 13.5$ nm, $a = 0.049$; band 2 (P700): $\lambda = 697.9$ nm, $fwhm = 9.5$ nm, $a = 0.076$; band 3: $\lambda = 691.6$ nm, $fwhm = 7.0$ nm, $a = 0.262$; band 4: $\lambda = 686.1$ nm, $fwhm = 4.6$ nm, $a = 0.190$; band 5: $\lambda = 681.9$ nm, $fwhm = 9.0$ nm, $a = 0.567$; band 6: $\lambda = 672.8$ nm, $fwhm = 17.7$ nm, $a = 0.812$; band 7: $\lambda = 671.8$ nm, $fwhm = 2.9$ nm, $a = 0.007$; band 8: $\lambda = 650.6$ nm, $fwhm = 36$ nm, $a = 0.154$. The last band approximates a collection of vibrational bands of all spectral bands and is not included in the estimation of the oscillator strength in bands 1 and 2.

strength of C708. Figure 2.10 shows a fit with Gaussian bands of the 4 K absorbance spectrum of monomeric complexes. The result is a 13.5 nm broad Gaussian with an oscillator strength of 1.85 per 65 chls, suggesting one C708 dimer per monomeric reaction centre complex. The intensity of the P700 band at 698 nm was 2.05 per 65 chls, in agreement with its dimeric nature. We do not wish to attribute much significance to the remaining part of the fit. The fit is consistent, however, with the wavelength dependent behaviour of the anisotropy. Below 695 nm C708 has no absorption. Therefore, upon excitation below 695 nm almost all fluorescence arises after excitation energy transfer. On the other hand, the 'blue' antenna pigments do not absorb above 701 nm and excitation above 701 nm leads to highly polarized fluorescence from directly excited pigments, in agreement with the results presented in figure 2.4. The data suggest that the PSI core antenna does not contain a separate pool of antenna pigments that absorbs between C708 and the pool absorbing at 693 nm, and that C708 in *Synechocystis* may be regarded as a $N=1$ system.

Comparison with results from spectral hole-burning

It is worthwhile to compare our site-selected fluorescence data on PSI core particles with the hole-burning data by Small and co-workers.²⁸ These authors analysed PSI core particles from

spinach, which showed an absorption maximum at considerably shorter wavelength than our particles (~670 nm vs. 679 nm), but nevertheless are characterized by rather similar absorption profiles in the far red absorption region (compare, e.g., figure 2 from ref. 28 with figure 2.4 from this contribution). The hole-burning profiles were analysed in absorption, which means that (depending on the burning efficiencies) P700 and C708 may both contribute to the spectra and that the presented spectral parameters could arise from a mixture of both species. However, the presence of long-wavelength antenna pigments was not considered in ref. 28.

The hole-burning profiles obtained after irradiation at 702.6, 706.3 and 715.0 nm could reasonably well be described by a Huang-Rhys factor S of 4-6 and a mean phonon frequency ω_m of 35-50 cm^{-1} .²⁸ Because according to our fits (fig. 2.10) P700 will primarily be excited at 702.6 nm and C708 at 715 nm, we conclude that the spectral properties of both species do not differ very much. This suggests that the broad homogeneous linewidth of C708 observed in the present study is mainly caused by a large value of S , i.e., by a considerable reorganization of C708 in the excited state.

The product $S\omega_m$ approximately represents the energetic separation between the zero-phonon line and the peak of the phonon side-band.²⁵ This product was estimated by Gillie et al.²⁸ to be ~ 200 cm^{-1} , which is about twice as large as estimated from our site-selected fluorescence data. We do not have an appropriate explanation for this discrepancy. Nevertheless, both values are much larger than the value of $S\omega_m \sim 20 \text{ cm}^{-1}$ obtained after burning in the 'normal' antenna at 680.5 nm.²⁸ This emphasizes the different nature of the long-wavelength antenna pigments as opposed to normal antenna pigments.

Long-wavelength antenna pigments in PSI-200 from spinach

The situation in the core/peripheral antenna of PSI-200 is more complex than in the core antenna of *Synechocystis*. There are several pools of long-wavelength antenna pigments, and because the anisotropy starts to rise at a considerably longer wavelength than in the core antenna of *Synechocystis* and in isolated LHCl,²⁹ it is clear that at least some of these pools are connected by energy transfer. Excitation wavelengths longer than about 720 nm have to be applied in order to minimize the energy transfer.

The non-selectively excited steady-state emission spectrum is characterized by a broader bandwidth (FWHM ~470 cm^{-1} vs. ~340 cm^{-1} for *Synechocystis*). Because the slope of the λ_{em} vs. λ_{ex} plot is steeper (~0.77 in PSI-200 vs. ~0.6 in *Synechocystis*) we suggest that an increase of the inhomogeneous bandwidth is primarily responsible for the increased emission bandwidth of the red-most pool of long-wavelength pigments in PSI-200. According to calculations as in the Appendix, we estimate $\Gamma_h/\Gamma_i \sim 0.55$. With a somewhat higher value for Γ_h as in *Synechocystis* (200 cm^{-1}) and a 1/0.55 higher value for Γ_i (~360 cm^{-1}), the total bandwidth in absorption will be ~400 cm^{-1} , which seems a reasonable value.

The energetic separation between the zero-phonon line and the peak of the phonon wing (i.e. the value of $S\omega_m$) should be relatively large in PSI-200, since excitation at the far red end of the absorption spectrum (732 nm) still yielded a shift of 13 nm (240 cm^{-1}), which is about twice as large as in the core antenna of *Synechocystis*. Thus, the shape of the emission spectra upon far red excitation differs considerably for the two analysed systems: the value of $S\omega_m/\Gamma_h$ is about 0.57 in *Synechocystis* and 1.0 in PSI-200. Because the value of $S\omega_m$ is even larger in

PSI-200 than in *Synechocystis*, we propose, in line with the discussions described above for *Synechocystis*, that pigment-pigment interactions also determine the spectroscopic properties of the red-most long-wavelength pigments in PSI-200.

The data also permit an estimation of the peak wavelength of the total absorption band of the longwavelength pigments. Substituting values from the λ_{em} vs. λ_{ex} plot (for the region $\lambda_{ex} > 720$ nm - see figure 2.8) into equation 2-8 yields $\lambda_0 = 716$ nm. This value is somewhat less accurate than that of C708, because it is uncertain in which extent the long-wavelength pigments are connected by energy transfer. Introduction of energy transfer would shift the peak wavelength of the long-wavelength pigments to shorter wavelengths.²¹ A Stokes' shift δ of 17 nm, however, seems reasonable in view of the parameters described above. Therefore, we propose to denote the long-wavelength pigments in the peripheral antenna of PSI as C716.

ACKNOWLEDGEMENTS

This research was supported in part by the Netherlands Foundations for Chemical Research (SON) and for Biophysics (SvB), financed by the Netherlands Organization for Scientific Research (NWO). J.P.D. was supported by a fellowship from the Royal Academy of Arts and Sciences (KNAW). J.K. and M.R. were supported by a grant from the Deutsche Forschungsgesellschaft (DFG).

APPENDIX

In this appendix the fluorescence behaviour of a pool of non-transferring pigments upon site selected excitation is described. The position of the fluorescence maximum λ_{em} for excitation at a particular wavelength λ_{ex} depends on the relative contributions of homogeneous and inhomogeneous broadening to the absorption spectrum. In order to illustrate this we first consider two extreme cases:

- 1 The homogeneous broadening is negligible with respect to the inhomogeneous broadening. This is for instance the case when the absorption spectrum is solely determined by the zero-phonon line and the phonon sideband is absent. In that case both absorption and emission occur through the same zero-phonon transition and $\lambda_{em} = \lambda_{ex}$. This leads to a maximum value for the slope s defined as $d(\lambda_{em})/d(\lambda_{ex})$, namely $s=1$;
- 2 The inhomogeneous broadening is negligible with respect to the homogeneous broadening. In that case λ_{em} does not depend on λ_{ex} and $s = 0$. For pigments in a protein environment both types of broadening are significant and this leads to values of s between 0 and 1.

We consider now the case of individual pigments which do not transfer energy to each other. All pigments are assumed to have identically shaped absorption and emission spectra and the difference δ between the absorption and emission maxima (Stokes' shift) is also assumed to be identical. In all cases a wavelength scale is used. A frequency (energy) scale would be more appropriate but is not necessary at the current level of approximation. The maxima of the

absorption spectra of individual pigments are distributed according to a distribution function $IDF(\lambda)$, which is usually taken to be Gaussian:³⁰

$$IDF(\lambda) = \frac{1}{\sqrt{\pi}\sigma_i} e^{-(\lambda - \lambda_0)^2 / \sigma_i^2} \quad 2-1$$

Here λ_0 denotes the centre of the distribution and σ_i is proportional to the inhomogeneous width Γ_i (FWHM) of the distribution according to $\Gamma_i = 1.67\sigma_i$. At first, the zero-phonon line will be omitted. Its effect will be discussed later. Therefore, the absorption spectrum is fully determined by the phonon sideband. Its shape is chosen to be Gaussian (see also below), since this allows an easy mathematical treatment. For a single chromophore with its absorption maximum at λ , the absorption at a particular wavelength of excitation λ_{ex} is given by:

$$\varepsilon_\lambda(\lambda_{ex}) = \frac{1}{\sqrt{\pi}\sigma_h} e^{-(\lambda - \lambda_{ex})^2 / \sigma_h^2} \quad 2-2$$

σ_h is proportional to the width of the homogeneous broadening Γ_h (FWHM) according to $\Gamma_h = 1.67\sigma_h$. Note that the maximum of the total absorption spectrum is at λ_0 . The maximum of the total fluorescence spectrum $\lambda_{0,em}$ (which can be obtained upon non-selective excitation, e.g. in the Soret region) is then at $\lambda_{0,em} = \lambda_0 + \delta$.

The number of pigments $N(\lambda)$ with an absorption maximum at λ , excited by excitation light with wavelength λ_{ex} , is proportional to $P(\lambda)$ which is defined as

$$P(\lambda) = IDF(\lambda)\varepsilon_\lambda(\lambda_{ex}) \quad 2-3$$

and substitution of equations 2-1 and 2-2 into equation 2-3 leads to

$$P(\lambda) = \frac{1}{\pi\sigma_i\sigma_h} e^{\{-(\lambda - \lambda_0)^2 / \sigma_i^2 - (\lambda - \lambda_{ex})^2 / \sigma_h^2\}} \quad 2-4$$

$P(\lambda)$ also has a Gaussian shape with a maximum at $\lambda_0 + \{\sigma_i^2 / (\sigma_i^2 + \sigma_h^2)\}(\lambda_{ex} - \lambda_0)$. The wavelength $\lambda_{abs-max}$ where $N(\lambda)$ is largest is thus $\lambda_0 + \{\sigma_i^2 / (\sigma_i^2 + \sigma_h^2)\}(\lambda_{ex} - \lambda_0)$ and the maximum of the fluorescence spectrum (λ_{em}) is at $\lambda_{abs-max} + \delta$. This leads to:

$$\lambda_{em} = \lambda_0 + \delta + \frac{\sigma_i^2}{\sigma_i^2 + \sigma_h^2}(\lambda_{ex} - \lambda_0) \quad 2-5$$

Therefore,

$$s = \frac{d(\lambda_{em})}{d(\lambda_{ex})} = \frac{\sigma_i^2}{\sigma_i^2 + \sigma_h^2} \quad 2-6$$

and

$$\lambda_{em} = \lambda_0 + \delta + s(\lambda_{ex} - \lambda_0) = \lambda_{0,em} + s(\lambda_{ex} - \lambda_0) \quad 2-7$$

Note that $\sigma_i^2/(\sigma_i^2 + \sigma_h^2) = \Gamma_i^2/(\Gamma_i^2 + \Gamma_h^2) = \Gamma_i^2/\Gamma_{tot}^2$ where Γ_{tot} is the FWHM of the entire absorption band, caused by both homogeneous and inhomogeneous broadening.

From equation 2-7 the maximum λ_0 of the total absorption band and the Stokes' shift δ can be determined according to:

$$\lambda_0 = \lambda_{ex} - (1/s)(\lambda_{em} - \lambda_{0,em}) \quad 2-8$$

$$\delta = \lambda_{0,em} - \lambda_0 \quad 2-9$$

Clearly, these relations hold in the linear region of s . In the case of the red pigments in PSI, the contribution of the zero-phonon line is negligible (see Discussion and ref. 29) and the absorption spectrum is mainly determined by the phonon sideband. Although a Gaussian shape of this sideband is not realistic, this particular choice will not significantly influence the conclusions very much near the centre of the total absorption band. For instance, a Lorentzian shape will give very similar results as long as the extreme wings of the absorption spectrum are not taken into account (calculations not shown). Finally, we note that in case the contribution of the zero-phonon line is not negligible it will lead to an increase of s , since for very small homogeneous bandwidths (like that of the zero-phonon line) the slope $s=1$.

REFERENCES

- (1) Van Grondelle, R., J.P. Dekker, T. Gillbro, and V. Sundström. 1994. Energy-transfer and trapping in photosynthesis. *Biochim. Biophys. Acta.* 1187:1-65.
- (2) Lin, S., H. van Amerongen, and W.S. Struve. 1992. Ultrafast pump-probe spectroscopy of the P700-containing and F_x -containing Photosystem-I core protein from *Synechococcus* sp. PCC-6301 (*anacystis-nidulans*). *Biochim. Biophys. Acta.* 1140:6-14.
- (3) Du, M., X. Xie, Y. Jia, L. Mets, and G.R. Fleming. 1993. Direct observation of ultrafast energy-transfer in PSI core antenna. *Chem. Phys. Lett.* 201:535-542.
- (4) Werst, M., Y. Jia, L. Mets, and G.R. Fleming. 1992. Energy-transfer and trapping in the Photosystem-I core antenna - a temperature study. *Biophys. J.* 61:868-878.
- (5) Holzwarth, A.R., G. Schatz, H. Brock, and E. Bittersman. 1993. Energy-transfer and charge separation kinetics in Photosystem-I. 1. Picosecond transient absorption and fluorescence study of cyanobacterial Photosystem-I particles. *Biophys. J.* 64:1813-1826.

- (6) Trissl, H.-W. 1993. Long-wavelength absorbing antenna pigments and heterogeneous absorption-bands concentrate excitons and increase absorption cross-section. *Photosynth. Res.* 35:247-263.
- (7) Trissl, H.-W., and C. Wilhelm. 1993. Why do thylakoid membranes from higher-plants form grana stacks? *Trends Biochem. Sci.* 18:415-419.
- (8) Van Grondelle, R., H. Bergström, V. Sundström, R.J. van Dorssen, M. Vos, and C.N. Hunter. 1988. *In Photosynthetic LightHarvesting Systems*. H. Scheer, and S. Schneider, editors. Walter de Gruyter, Berlin. 519-530.
- (9) Holzwarth, A.R. 1991. Excited-state kinetics in chlorophyll systems and its relationship to the functional organization of the photosystems. *In Chlorophylls*. H. Scheer, editor. CRC Press, Boca Raton, FL. 1125-1151.
- (10) Van der Lee, J., D. Bald, S.L.S. Kwa, R. van Grondelle, M. Rögner, and J.P. Dekker. 1993. Steady-state polarized-light spectroscopy of isolated Photosystem-I complexes. *Photosynth. Res.* 35:311-321.
- (11) Rögner, M., P. Nixon, and B.A. Diner. 1990. Purification and characterization of Photosystem-I and Photosystem-II core complexes from wild-type and phycocyanin-deficient strains of the cyanobacterium *Synechocystis* PCC-6803. *J. Biol. Chem.* 265:6189-6196.
- (12) Kruij, J., E.J. Boekema, D. Bald, A.F. Boonstra, and M. Rögner. 1993. Isolation and structural characterization of monomeric and trimeric Photosystem-I complexes (P700_{F_a}/F_b and P700_{F_x}) from the cyanobacterium *Synechocystis* PCC-6803. *J. Biol. Chem.* 268:23353-23360.
- (13) Kwa, S.L.S., W.R. Newell, R. van Grondelle, and J.P. Dekker. 1992. The reaction center of Photosystem-II studied with polarized fluorescence spectroscopy. *Biochim. Biophys. Acta.* 1099:193-202.
- (14) Kwa, S.L.S., S. Völker, N.T. Tilly, R. van Grondelle, and J.P. Dekker. 1994. Polarized site-selection spectroscopy of chlorophyll-*a* in detergent. *Photochem. Photobiol.* 59:219-228.
- (15) Boekema, E.J., J.P. Dekker, M. van Heel, M. Rögner, W. Saenger, I. Witt, and H.T. Witt. 1987. Evidence for a trimeric organization of the Photosystem I complex from the thermophilic cyanobacterium *Synechococcus* sp. *FEBS Lett.* 217:283-286.
- (16) Hladik, J., and D. Sofrová. 1991. Does the trimeric form of the Photosystem-I reaction center of cyanobacteria *in vivo* exist? *Photosynth. Res.* 29:171-175.
- (17) Chitnis, V.P., and P.R. Chitnis. 1993. PsaL subunit is required for the formation of Photosystem-I trimers in the cyanobacterium *Synechocystis* sp. PCC-6803. *FEBS Lett.* 336:330-334.
- (18) Kruij, J., D. Bald, E.J. Boekema, and M. Rögner. 1994. Evidence for the existence of trimeric and monomeric Photosystem-I complexes in thylakoid membranes from cyanobacteria. *Photosynth. Res.* 40:279-286.
- (19) Wittmershaus, B.P., V.M. Woolf, and W.F.J. Vermaas. 1992. Temperature-dependence and polarization of fluorescence from Photosystem-I in the cyanobacterium *Synechocystis* sp PCC-6803. *Photosynth. Res.* 31:75-87.
- (20) Boekema, E.J., R.M. Wynn, and R. Malkin. 1990. The structure of spinach Photosystem-I studied by electron-microscopy. *Biochim. Biophys. Acta.* 1017:49-56.
- (21) Van Mourik, F., R.W. Visschers, and R. van Grondelle. 1992. Energy-transfer and aggregate size effects in the inhomogeneously broadened core light-harvesting complex of *Rhodobacter-sphaeroides*. *Chem. Phys. Lett.* 193:1-7.
- (22) Visschers, R.W., F. van Mourik, R. Monshouwer, and R. van Grondelle. 1993. Inhomogeneous spectral broadening of the B820 subunit form of LH1. *Biochim. Biophys. Acta.* 1141:238-244.

-
- (23) Kwa, S.L.S., N.T. Tilly, C. Eijkelhoff, R. van Grondelle, and J.P. Dekker. 1994. Site-selection spectroscopy of the reaction-center complex of Photosystem-II. 2. Identification of the fluorescing species at 4 K. *J. Phys. Chem.* 98:7712-7716.
- (24) Völker, S. 1989. Hole-burning spectroscopy. *Annu. Rev. Phys. Chem.* 40:499-530.
- (25) Reddy, N.R.S., P.A. Lyle, and G.J. Small. 1992. Applications of spectral hole burning spectroscopies to antenna and reaction center complexes. *Photosynth. Res.* 31:167-194.
- (26) Avarmaa, R.A., and K.K. Rebane. 1985. High-resolution optical spectra of chlorophyll molecules. *Spectrochim. Acta.* 41A:1365-1380.
- (27) Pullerits, T., F. van Mourik, R. Monshouwer, R.W. Visschers, and R. van Grondelle. 1994. Electron-phonon coupling in the B820 subunit form of LH1 studied by temperature-dependence of optical-spectra. *J. Luminescence.* 58:168-171.
- (28) Gillie, J.K., P.A. Lyle, G.J. Small, and J.H. Golbeck. 1989. Spectral hole burning of the primary electron-donor state of Photosystem-I. *Photosynth. Res.* 22:233-246.
- (29) Mukerji, I., and K. Sauer. 1990. Optical spectroscopy on a Photosystem I antenna complex. *In* Current research in photosynthesis. M. Baltscheffsky, editor. Kluwer, Dordrecht, the Netherlands. 2:321-324.
- (30) Jankowiak, R., and G.J. Small. 1993. Spectral Hole Burning: A window on excited state electronic structure, heterogeneity, electron-phonon coupling and transport dynamics of photosynthetic units. *In* The photosynthetic reaction center. J. Deisenhofer, and J. Norris, editors. Academic Press, New York. 2:133-176.

3

Time-resolved fluorescence emission measurements of Photosystem I particles of various cyanobacteria: a unified compartmental model

Bas Gobets, Ivo H.M. van Stokkum, Matthias Rögner, Jochen Kruij, Eberhard Schlodder, Navassard V. Karapetyan, Jan P. Dekker and Rienk van Grondelle

Photosystem I (PSI) contains a small fraction of chlorophylls (chls) that absorb at wavelengths longer than the primary electron donor P700. The total number of these long-wavelength chls and their spectral distribution are strongly species dependent. In this contribution we present room temperature time-resolved fluorescence data of five PSI core complexes which contain different amounts of these long-wavelength chls, i.e. monomeric and trimeric Photosystem I particles of the cyanobacteria *Synechocystis* sp. PCC 6803, *Synechococcus elongatus* and *Spirulina platensis*, which were obtained using a synchroscan streak camera. Global analysis of the data reveals considerable differences between the equilibration components (3.4–15 ps) and trapping components (23–50 ps) of the various PSI complexes. We show that a relatively simple compartmental model can be used to reproduce all the observed kinetics and demonstrate that the large kinetic differences are purely the result of differences in the long-wavelength chl content. This procedure not only offers rate constants of energy-transfer between and of trapping from the compartments, but also well-defined room temperature emission spectra of the individual chl pools. A pool of red-shifted chls absorbing around 702 nm and emitting around 712 nm was found to be a common feature of all studied PSI particles. These red-shifted chls were found to be located neither very close to P700 nor very remote from P700. In *Synechococcus* trimeric and *Spirulina* monomeric PSI cores a second pool of red chls was present which absorbs around 708 nm, and emits around 721 nm. In *Spirulina* trimeric PSI cores an even more red-shifted second pool of red chls was found, absorbing around 715 nm and emitting at 730 nm.

INTRODUCTION

PSI is one of two photosystems in oxygenic photosynthesis. It uses the energy of light to transfer electrons from plastocyanin or soluble cytochrome c_6 to NADP^+ .

In plants and green algae the PSI complex consists of two distinct functional units: The PSI core, and the LHCl peripheral antenna. Although cyanobacterial PSI lacks this peripheral antenna their PSI core complexes exhibit a strong homology to those of plants, and therefore the cyanobacterial PSI can be used as a model system to study the energy and electron transfer dynamics in the core of PSI.^{1,2}

The PSI core is a large protein complex consisting of at least 11 protein subunits, the largest two of which, PsaA and PsaB, form a heterodimer to which the largest fraction of the core antenna chls as well as most of the reaction centre (RC) co-factors are bound. Spectroscopic and structural data indicate that the core antenna and RC contain approximately 90 chlorophyll-*a* (chl*a*) and 10-25 β -carotene molecules in total.^{3,4}

Recently the structure of the PSI core complex of the cyanobacterium *Synechococcus elongatus* was resolved with 4 Å resolution.^{3,5,6} In this structure 89 chl molecules have been identified, including the 6 chl*a* molecules that constitute the first part of the electron transfer chain in the RC. The 83 core antenna chls were found to be arranged in a more or less elliptically shaped ring around the RC. The distance of most antenna chls to any of the RC chls was found to be larger than 20Å. However, two antenna chls, located at ~14Å from the closest RC chls, stood out in the structure, forming a structural, and possibly functional bridge between the other antenna chls and the RC. The 6 chls in the RC constitute P700, a pair of accessory chls and the primary electron acceptor A_0 . Also other components of the electron-transfer chain, including the three Fe_4S_4 iron-sulphur clusters F_x , F_A and F_B , could be assigned in the structure. Combining the structural data with single crystal EPR results allowed the localization of the two phylloquinones constituting A_1 .⁷

The ring-like organization of the antenna around the RC is a common feature in photosynthesis. The clearest example of such an arrangement is the light-harvesting I antenna of purple bacteria, which surrounds the bacterial RC. It can easily be shown that such an organization is a prerequisite for an efficient photosystem including a bulky RC. A system in which the RC is located in the centre with a relatively large average distance to each antenna chl, but in contact with many of them, is much more favourable than a system in which the RC is located at the periphery of the antenna to which it is linked by only a few antenna chls.⁸

The cyanobacterial core complexes can be isolated both as monomers and trimers, and since both are equally efficient in energy transfer and charge-separation⁹ it is not clear which is the native conformation; it may be that a dynamic equilibrium exists between monomers and trimers in the membrane, which can be regulated by for instance the salt-concentration.¹⁰ Energy transfer between the monomers within a trimer was found to be negligible at room temperature.¹¹

Low-energy ("red") chlorophylls

The PSI core absorption spectrum is spectrally highly heterogeneous, and varies from species to species.¹² The absorption maxima of most of the core antenna chls are distributed between 660-690 nm (bulk antenna)^{9,13-18} (see also below), which can be compared to the absorption

maximum of isolated chl a displaying a single broad maximum at ~662 nm in organic solvents.¹⁹ A conspicuous feature of all (intact) PSI cores is the presence of a relatively small number of red-shifted chl states that absorb at energies lower than that of the primary electron donor P700. The amounts and energies of these low-energy or "red" chls appear to be highly species-dependent^{13-15,17,20} (see also below).

Based upon energy selective emission spectra of PSI it has been proposed that the low-energy chls represent closely coupled dimers or larger aggregates of chl a .¹⁷

In monomeric PSI core preparations the number of red chls is generally found to be lower than in trimers. Especially the amplitude of the most red-shifted chl band may depend highly upon the aggregation state.^{21,22} This effect suggests that at least some of these chls are located in the periphery of the PSI core, and that the red shift of these chls may be induced by aggregation.⁴

At physiological temperatures the presence of the low-energy chls does not significantly decrease the quantum efficiency of charge separation. Even if these chls are excited directly, thermal energy of the surrounding enables efficient uphill transfer to P700. At lower temperatures, however, the red chls act as traps for excitations, thereby decreasing the quantum efficiency of charge separation.^{22,23}

Although the low-energy or "red" chls only account for 2-10% of the total absorption of the core antenna, they do have a very pronounced effect on the fluorescence properties of the system. In *Synechocystis* core complexes with only two C708 red chls,¹⁷ the room temperature fluorescence emission spectrum exhibits a peak around 685-690 nm (F685) with a broad shoulder due to red chls at ~710 nm. In contrast, in *Synechococcus* and *Spirulina* with more and longer wavelength absorbing red chls^{21,22} the room temperature emission peaks above 700 nm, with F685 only appearing as a shoulder.

At low temperatures the emission from the red chls fully dominates all fluorescence spectra, which peak at ~720 nm in *Synechocystis* (F720) and ~730 nm in *Synechococcus* trimers (F730). In trimers of *Spirulina* at low temperatures, one emission band is always present, peaking at ~730 nm (F730). A second emission band, with a maximum at ~760 nm (F760), may be observed depending on the oxidation state of P700: If P700 is pre-oxidized (using ferricyanide) F760 is absent, whereas it is present if the primary electron donor is reduced. The relatively strong spectral overlap of the F760 fluorescence with the absorption spectrum of P700⁺, resulting in quenching of F760 emission, is thought to be the cause of this remarkable feature.¹¹ Monomeric PSI cores of *Spirulina* only exhibit F730 fluorescence.

A decrease of the temperature also induces a dramatic increase of the fluorescence quantum yield of all PSI particles,^{17,22,24} due to the trapping of excitations by the low-energy chls at low temperatures (see above).

Energy transfer and trapping in PSI

The core antenna of PSI is intimately bound to the PSI RC and unlike in antenna-RC complexes of Photosystem II and purple-bacterial photosystems it is not possible to biochemically separate the core antenna from the RC. Therefore time-resolved experiments on native PSI have to be performed on systems with a large number (~100) of chl a molecules all connected by energy transfer. Time-resolved spectroscopic experiments on such large antenna-RC

complexes require the use of very low energy excitation pulses, to avoid the process of singlet-singlet annihilation (see for a review: Valkunas et al.²⁵ and Van Grondelle²⁶).

Even if experiments are performed very carefully, the details of the processes that can be distinguished are limited. In an antenna-RC complex containing 100 chl molecules, in principle 100 separate lifetimes are present in the excitation decay process. In reality one can at best resolve a fraction of those lifetimes but only if relatively selective excitation and detection is possible. Since the individual absorption and emission spectra of the 100 chls in PSI cores are strongly overlapping, this condition of selectivity can only be met to a very limited extent, and consequently only a small number of (average) kinetic processes can be discerned.

The fastest processes that occur are single energy-transfer steps between two chls. In PSI cores such single step transfer processes typically take place with time constants of a few 100 fs.^{27,28} Since the donor and acceptor chls do not necessarily absorb at significantly different wavelengths, these steps may not be resolved in isotropic measurements. Anisotropic pump-probe or fluorescence upconversion experiments can reveal energy transfer between iso-energetic chls, provided that the absorbing and emitting dipole moments of donor and acceptor are not parallel.

As the chls in PSI absorb at different energies, energy redistribution processes take place due to which the initial distribution of excited antenna molecules transforms into a more thermally equilibrated distribution. Because the initial donor and final acceptor chls absorb at different energies, equilibration appears as a decrease of fluorescence or bleaching in one part of the spectrum, and an increase in fluorescence or bleaching in another. It must be stressed that the observed equilibration lifetimes do not necessarily correspond to a one step energy-transfer process, but generally reflect the net result of a (large) number of those steps. In PSI core particles at room temperature, these equilibration components take place between the bulk antenna and the various pools of red chls in the 2 to 15 ps time range^{9,16,18,24,29-33} (see also below), and within the bulk antenna on a sub-ps time scale.^{28,32,33} In order to accurately record these processes, high time-resolution, spectrally-resolved techniques are required such as multicolour pump-probe, fluorescence upconversion, or streak camera fluorescence detection.

The slowest components that are observed are the so-called trapping components, which represent the overall rate at which excitations disappear from the system by charge separation in the RC, following equilibration processes that may have occurred in the antenna on a shorter time scale (see above). In time-resolved fluorescence spectroscopy experiments, trapping appears as the slowest rate of the system with a decay of fluorescence at all wavelengths of detection. In pump-probe transient absorption experiments trapping is observed as the rate at which the spectrum of P700⁺ is formed, which generally lives infinitely on the time scale of these experiments. Since the trapping component typically has a lifetime of tens of ps, it can be recorded quite accurately, even with moderate time-resolution techniques such as single photon timing (SPT) (for a review see: Van Grondelle et al., 1994¹²).

During the past decade PSI of a wide variety of species has been studied by several groups using (sub)picosecond time-resolved spectroscopic techniques including pump-probe,^{18,29,30,32-34} SPT,^{9,16,24,29-31} and fluorescence upconversion.^{27,28} Various rate

constants have been found for the energy redistribution within the main antenna, between main antenna chls and red chls, as well as trapping in the RC. It has been suggested¹⁸ that the variability of the results is more likely due to experimental differences rather than to real variation between the investigated species. To clarify this point we have decided to investigate the dynamics of different PSI cores of a number of cyanobacteria under identical experimental conditions. These time-resolved fluorescence experiments were performed using a synchroscan streak camera with a spectrograph, which has an instrumental response of ~ 3 ps and enables us to observe kinetics occurring significantly faster than 1 ps. In all studies referred to above, either time traces were measured sequentially for different detection wavelengths, or spectra were measured sequentially for different delay times. In contrast to this, our setup integrates spectral and temporal data simultaneously resulting in high quality spectra which allow quantitative analysis.

It will be shown that the experimentally observed kinetics are indeed quite different between the five PSI particles studied. However, we will clearly demonstrate that the dynamics in all these PSI cores are essentially the same, and that the observed differences are resulting entirely from differences in the amounts and energies of the red chls present in the various PSI cores.

MATERIALS AND METHODS

The *Synechocystis* sp. PCC 6803 PSI monomers and trimers were prepared as in Kruijff et al.,³⁵ the trimeric PSI complexes from the thermophilic cyanobacterium *Synechococcus elongatus* were isolated as in Fromme et al.³⁶ and monomeric and trimeric PSI particles from *Spirulina platensis* were prepared as described in Kruijff et al.³⁷

For the fluorescence experiments the concentrated samples were diluted to an OD_{680} of 0.6/cm with a buffer containing 20 mM $CaCl_2$, 20 mM $MgCl_2$, 10mM 2-(N-morpholino)ethane sulfonic acid (MES) and 0.05% W/V dodecyl- β -D-maltoside at a pH of 6.5 (*Synechocystis* and *Synechococcus*) or 10 mM $CaCl_2$, 10 mM $MgCl_2$, 10 mM Tris-HCl and 0.03% W/V dodecyl- β -D-maltoside at a pH of 7.8 (*Spirulina*). 10 mM Sodium Ascorbate and 10 μ M Phenazine Meta Sulphate (PMS) were added to all samples to avoid accumulation of P700⁺.

To avoid multiple excitation of the sample by successive laser flashes it was contained in a spinning cell (diameter 10 cm) rotating at 20 Hz. All experiments were performed at room-temperature (293 K).

The samples were excited using 100–200 fs pulses at 400 nm which were generated at a 100 kHz repetition rate using the frequency doubled output of a laser system consisting of a Titanium:sapphire based oscillator (Coherent MIRA) and a regenerative amplifier (Coherent REGA). The excitation light was collimated with a 15 cm focal length lens, resulting in a focal diameter of 150 μ m in the sample. Fluorescence was collected at right angle to the excitation using achromatic lenses and detected through a sheet polarizer set at magic angle (54.7°) with a Hamamatsu C5680 synchroscan streak camera and a Chromex 250IS spectrograph. The streak-images were recorded on a Hamamatsu C4880 CCD camera which was cooled to $-55^\circ C$.

The full width at half of the maximum of the overall time-response of this system was 3–3.5 ps. The spectral resolution was 8 nm. One streak image measured 315 nm in the spectral domain (1018 pixels) and 200 ps (1000 pixels) in the time-domain.

To avoid singlet-singlet annihilation the pulse energy was reduced to 1 nJ, thus exciting typically only 0.25% of all chls present in the focus.

The pathlength of the recorded fluorescence emission through the setup is wavelength dependent, resulting in a wavelength dependent position of time zero on the streak image. This time-dispersion was assessed by recording the streak-image of a (pulsed) white-light continuum which was scattered in a dilute solution of coffee-creamer, and combining this data with the intrinsic time-dispersion of this white-light continuum which was obtained in a pump-probe measurement of CS₂.³⁸

Before the global analysis the streak-images were background subtracted and corrected for difference in sensitivity in the time-domain by division by a streak-image of a halogen lamp (shading correction). Subsequently the dispersion correction was applied, and the relevant spectral region of the image was divided in 30–60 traces by spectral integration over 3–5 nm.

In the global analysis fitting a Gaussian shaped instrument response function was assumed. The width of this Gaussian was a free parameter of the fit (typically 3.5 ps). In some cases the fit was improved by allowing for a small additional contribution (~5%) of a broader Gaussian to the instrument response.

All measurements were analysed using a model with a number of parallel compartments, which yields Decay-Associated Spectra (DAS). The periodicity of the synchroscan with a period of 13.4 ns results in a "back and forth" sweeping of long lived (> 1 ns) components. By taking this into account in the analysis of the data, the lifetime and spectrum of a (single) long-lived component (such as some free chl present in the sample) could be estimated accurately on the 200 ps time scale. All the DAS shown were corrected for the spectral sensitivity of the apparatus.

The quality of the fit was judged by the root mean square error and by examination of the residual matrix with the help of singular value decomposition to extract the temporal and spectral structure.³⁹

The target analysis⁴⁰ yielded the Species-Associated Emission Spectra (SAES) of the different pools of red chls. In order to obtain these spectra a constraint had to be put on the SAES of the long-wavelength chls which were put to zero at wavelengths shorter than ~680 nm (1st pool) and ~690 nm (2nd pool).

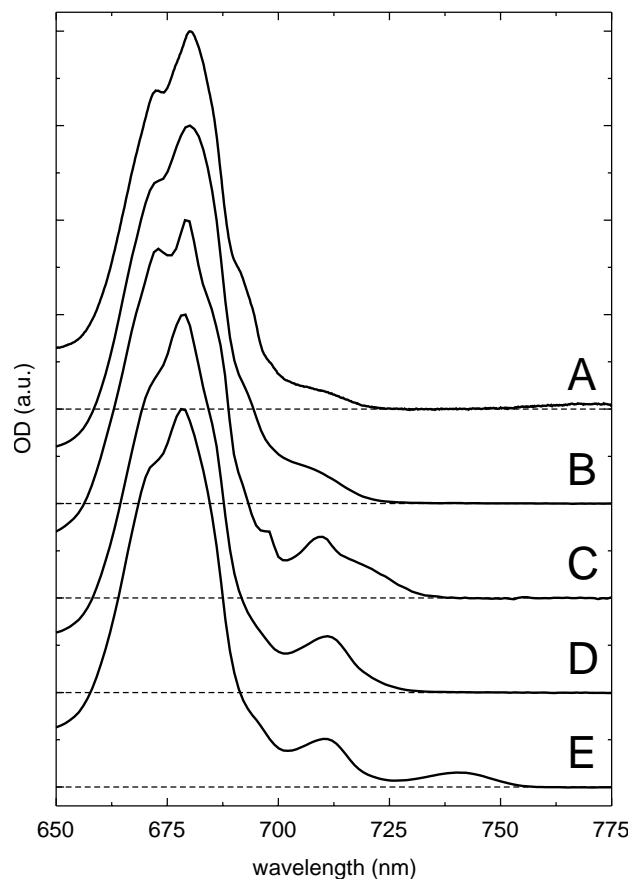
RESULTS

Absorption spectra

In figure 3.1 the 6K absorption spectra of the various investigated PSI particles are displayed. In the region below 700 nm the spectra of all particles are very similar, consisting of a large absorption band with a maximum at 680 nm and a shoulder around 673 nm. This spectral region is dominated by the absorption of the bulk antenna chls, which comprise 90% or more

of the total chl content. Pronounced differences between the various PSI species are observed only in the region above 700 nm, where the absorption of a relatively small number of red chls dominates the spectra. As the absorption bands of red chls are quite distinct at 6K, the maxima of these bands and the number of chls contained in them can be estimated by Gaussian deconvolution of the absorption spectra.

The spectrum of monomeric PSI core particles from *Synechocystis* (figure 3.1a) reveals an inhomogeneously broadened absorption band with a maximum at 708 nm (C708). This band was found to carry an oscillator strength of approximately 2 *chl a* molecules.¹⁷ This estimation was based on a total number of 65 chls in the core antenna. Since the true number of antenna chls is probably closer to 100, we now estimate the number of C708 chls in *Synechocystis* monomeric PSI to be close to 3. The spectrum of PSI trimers from *Synechocystis* (figure 3.1b) resembles the one reported by Rätsep et al.⁴¹ and exhibits significantly more long-wavelength absorption than monomeric PSI from this species. Hayes et al.⁴² suggested that 2 chls contribute to C706, and 2 other chls contribute to C714. We note however that the suggestion



3.1 6 K absorption spectra of different cyanobacterial PS I core particles. a) Monomeric core of *Synechocystis* sp. PCC 6803, b) Trimeric core of *Synechocystis* sp. PCC 6803 c) Trimeric core of *Synechococcus elongatus*, d) Monomeric core of *Spirulina platensis*, e) Trimeric core of *Spirulina platensis*.

of Hayes et al.⁴² that these pools are connected by energy transfer is at odds with the site-selected emission measurements of Gobets et al.¹⁷ on trimeric PSI particles from *Synechocystis*. From the 6 K OD spectrum of PSI trimers from *Synechocystis* we estimate that a total number of 4–5 C708 are present in these PSI cores. The exact number of C708 chls in this species, however, seems to vary somewhat between different isolations.

Two red absorption bands are found in the 6K absorption spectrum of the trimeric core particles of *Synechococcus* (figure 3.1c) with maxima at 708 nm (C708, corresponding to 4–5 chl α 's) and 719 nm (C719, corresponding to 4 chl α 's).²⁰ The monomers show a 50% reduction of C719 (not investigated in this study).²²

The monomeric complexes of *Spirulina* (figure 3.1d) exhibit a dominant absorption band at 708 nm corresponding to \sim 7 chls and a minor contribution of C719 (\sim 1 chl). The latter contribution is not very clear, and may also reflect a tail of a single band of red chls that exhibits a large and asymmetric inhomogeneous distribution. Trimeric PSI cores of *Spirulina* (figure 3.1e) exhibit an absorption band at \sim 708 nm which is similar to the one found in monomers (C708, corresponding to \sim 7 chl α) but also display an absorption band with a maximum at 740 nm (C740, corresponding to \sim 3 chl α), which constitutes the red-most absorbing species reported in any PSI complex.^{4,21,31}

The assignments and sizes of the red chl pools for the various PSI species are summarized in table 3.1. For comparison the red parts of the room temperature absorption spectra for the various PSI cores are shown in figure 3.2. At room temperature the red chls only appear as a long, featureless red tail to the absorption spectrum. Nevertheless some features are still

Table 3.1 6 K and room temperature low-energy chl α absorption and emission

species	first pool (C708)					second pool (C719, C740)				
	absorption (nm)		emission (nm)		# chls/100	absorption (nm)		emission (nm)		# chls/100
	6K	RT	6K	RT		6K	RT	6K	RT	
<i>Synechocystis</i> monomers	708	703	720	712	\sim 3	-	-	-	-	-
<i>Synechocystis</i> trimers	708	702	720	711	\sim 5	-	-	-	-	-
<i>Synechococcus</i> trimers	708	702		707	\sim 5	719	708	730	723	\sim 4
<i>Spirulina</i> monomers	708	699 (702)		712	\sim 7 (5)	719	719 (708)	730	721	\sim 1 (3)
<i>Spirulina</i> trimers	708	703		714	\sim 7	740	715	760	733	\sim 3

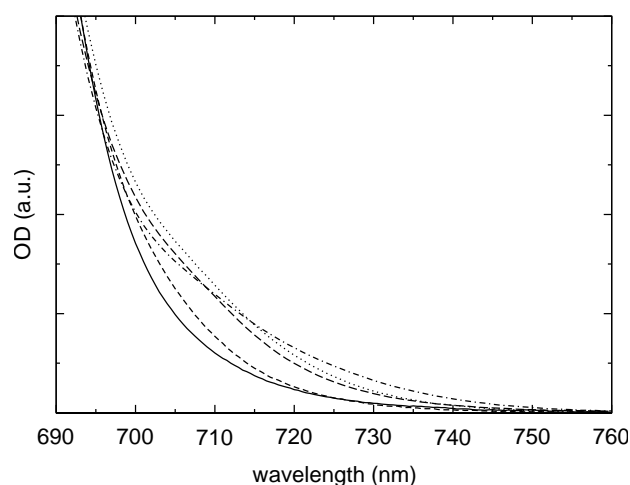
Except for the values in parentheses, the 6 K absorption properties of the low-energy chls were estimated from a Gaussian deconvolution of the absorption spectra. Room temperature absorption and emission properties were obtained from the target analysis of the time-resolved fluorescence data. For details, see text.

visible. The PSI cores of *Synechocystis* monomers (solid) show the least red absorption. PSI trimers of *Synechocystis* (dashed) show slightly more red absorption, but still much less than the other three PSI particles. *Synechococcus* trimeric PSI (dotted) and *Spirulina* monomeric PSI (long dashed) show a very similar red wing, although the latter appears to be slightly blue-shifted as compared to the former. *Spirulina* trimeric PSI (dot-dashed) also at room-temperature exhibits the most red-extended absorption of all studied PSI particles.

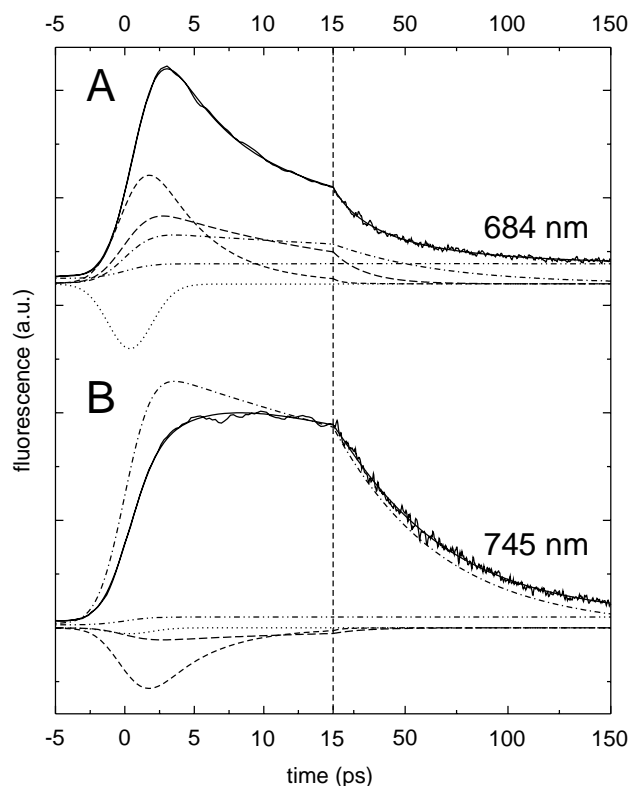
Time-resolved fluorescence measurements

We have recorded the time-resolved fluorescence kinetics of 5 different PSI preparations upon excitation at 400 nm, all under essentially identical conditions. In figure 3.3 we show typical time-resolved fluorescence traces of the *Spirulina* PSI trimers for two different wavelengths of detection. The raw data (noisy solid) and the fit (smooth solid) are shown along with the different lifetime contributions obtained in the global analysis of the data (other line types). We note that the global analysis involved a total of 30 to 60 wavelengths of detection.

Comparing the raw data for detection at 684 nm (figure 3.3a) and 745 nm (figure 3.3b) reveals some clear differences: the trace at 684 nm, which mainly represents the emission from the bulk chls, has a very distinct maximum in time, whereas the trace at 745 nm, which mainly represents emission from the "red" chls, does not exhibit such a well-defined maximum; the amplitude appears to be almost constant between 5 and 15 ps after excitation. At times later than 15 ps the kinetics for both detection wavelengths are very similar, decaying almost mono-exponentially to a constant value. The observed differences during the first 15 ps of both traces reflect the energy transfer from the bulk chls emitting around 684 nm to the red chls emitting around 745 nm, which causes a rapid initial decrease of the fluorescence at 684 nm, and a simultaneous increase of the fluorescence at 745 nm.



3.2 The red region of the room-temperature absorption spectra of monomeric core of *Synechocystis* sp. PCC 6803 (solid), trimeric core of *Synechocystis* sp. PCC 6803 (dashed), trimeric core of *Synechococcus elongatus* (dotted), monomeric core of *Spirulina platensis* (long dashed), and trimeric core of *Spirulina platensis* (dot-dashed).



3.3 Time-resolved fluorescence traces of *Spirulina* trimeric PS I, detected at a) 684 nm and b) 745 nm, for excitation at 400 nm. Data and fit (solid lines), and lifetime components of 0.4 ps (dotted), 3.9 ps (dashed), 15 ps (long-dashed), 50 ps (dot-dashed) and 5 ns (double-dot-dashed). Note the change of the scaling of the time axis at 15 ps.

The various lifetime contributions which were estimated by a global analysis fitting procedure, display this process in more detail. For 684 nm detection (figure 3.3a) all contributions but one (the 400 fs component (dotted) reflecting Soret- Q_y relaxation, see below) show a positive amplitude expressing a decay of fluorescence. The analysis demonstrates that the decay includes significant contributions by a 3.9 ps (dashed) and a 15 ps (long-dashed) lifetime component, which account for most of the dynamics observed in the first 15 ps after excitation. For 745 nm detection (figure 3.3b) the rapid decay during the first 15 ps after excitation is not present since the 3.9 ps and 15 ps contributions show a negative amplitude at this wavelength of detection, expressing an increase of fluorescence with these time constants. Since the 3.9 and 15 ps components show a decay at 684 nm and a rise at 745 nm, these components reflect energy transfer from the bulk chls to the red chls. The 50 ps (dot-dashed) component which is positive for both wavelengths of detection reflects the overall decay of excitations from the system (trapping component). The small 4.9 ns contribution (double-dot-dashed), which is positive at both wavelengths of detection can be attributed to a small fraction of uncoupled chls present in the preparation.

Results qualitatively very similar to those shown in figure 3.3 were obtained for all PSI species investigated in this study.

Global Analysis

We will now discuss in more detail the results of the global analysis of the data obtained for all PSI species studied, and for all wavelengths of detection. The Decay-Associated Spectra of the measurements of the 5 different PSI core particles are presented in figures 4a-e. All spectra have been scaled to the total number of excitations, and therefore not only the shapes, but also the amplitudes of the various components can be compared directly.

In all preparations a small decay component is found with a lifetime of about 5 ns, that was already mentioned with reference to figure 3.3 (figure 3.4a-e, dot-dashed). The lifetime of these components and the corresponding spectra, which peak at 675-678 nm and exhibit a long tail in the red region, are indicative of chl a in solution. We therefore assign these components to a fraction of chls in the preparation that is not attached to the protein. Hence, these components do not express a process in the intact systems.

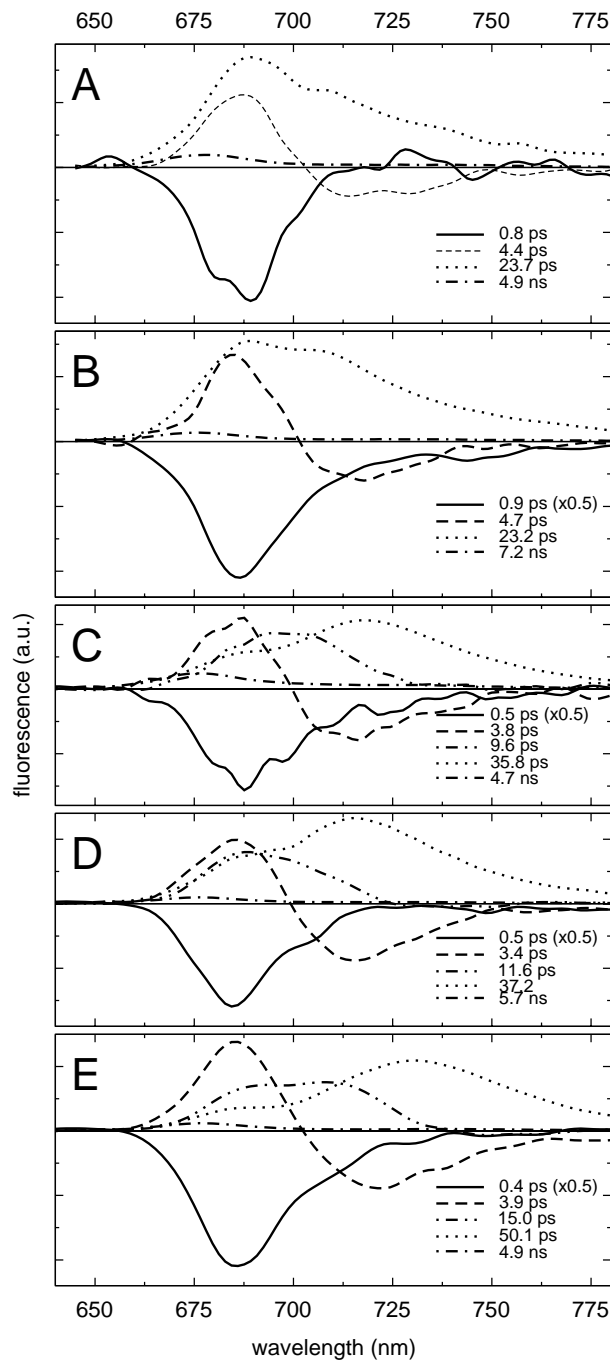
Monomeric and trimeric PSI from Synechocystis sp. PCC 6803

With 400 nm light, initially the Soret band, a higher electronic state of chl a , is excited. This state relaxes to the lowest singlet excited chl a state (Q_y) in a few hundred fs, like found for Bchl.⁴³ Therefore the fluorescence in the Q_y region does not appear instantaneously, but rises with a finite time-constant. In all PSI particles investigated in this study this is evident from a sub-picosecond component which exhibits an all-negative DAS (figure 3.4a-e, solid). This ingrowth is not observed for direct excitation in the Q_y region (data not shown). For *Synechocystis* monomeric PSI the lifetime of this component is fitted by a 0.8 ps lifetime (figure 3.4a, solid).

The second component in monomeric PSI from *Synechocystis* exhibits a lifetime of 4.4 ps and is represented by a DAS which is positive at short wavelengths with a distinct maximum around 686 nm, crosses zero at ~701 nm and exhibits a shallow negative region above this wavelength (figure 3.4a dashed). PSI from *Synechocystis* probably exhibits only one pool of long-wavelength chls peaking at 708 nm at 6K (see above), and the 4.4 ps component displays the net downhill energy-transfer from the bulk chls to this pool of long-wavelength chls, reflecting the relaxation of the initially excited chl distribution into a thermally more equilibrated distribution.

This equilibration spectrum is clearly not conservative: the area above zero is significantly larger than the area below. This shows that the spectrum is not a "pure" equilibration spectrum, but that also some (fast) trapping from the non-equilibrated state occurs during the equilibration process. Thus, the observed spectrum is the sum of a conservative "pure" equilibration contribution and a trapping contribution which is positive at all wavelengths. This feature can be reproduced both by simple compartmental models (see below) and by structure-based simulations.^{44,45}

The final component in monomeric PSI from *Synechocystis* is represented by a DAS which is clearly positive at all wavelengths of detection and which exhibits a lifetime of 23.7 ps, this being the longest lifetime actually occurring in the system (the ns lifetime is not due to intact systems, see above). Such a component is generally referred to as "the" trapping component of the system: the spectrum does not change any more, and decays with one single time-constant. The trapping DAS of *Synechocystis* monomeric PSI peaks at 688 nm



3.4 Decay-Associated Spectra of fluorescence decay of different cyanobacterial PS I core particles upon excitation at 400 nm. a) Monomeric core of *Synechocystis* sp. PCC 6803, b) Trimeric core of *Synechocystis* sp. PCC 6803 c) Trimeric core of *Synechococcus elongatus*, d) Monomeric core of *Spirulina platensis*, e) Trimeric core of *Spirulina platensis*.

(figure 3.4a, dotted), reflecting dominant emission from the bulk chls. The presence of the few red chls in this PSI species is revealed by a shoulder in the spectrum around 708 nm.

To distinguish between transfer components which may also incorporate some non-equilibrium trapping, and "the" trapping component as defined above, we will continue to refer to the former as equilibration or energy-transfer components.

The results for trimeric PSI particles from *Synechocystis* (figure 3.4b) are very similar to those found for monomers. The lifetimes do not differ significantly, and the DAS only display slight (but significant) differences. The ingrowth from the Soret is fitted with a 900 fs lifetime. The equilibration component is fitted with a 4.7 ps time constant (figure 3.4b, dashed) and the amplitude of the corresponding DAS is significantly higher in the trimers as compared to the monomers. Trapping in trimeric PSI of *Synechocystis* occurs in 23.2 ps and the corresponding spectrum (figure 3.4b, dotted) differs from that of monomers by a more pronounced shoulder around 708 nm. Both the enhanced amplitude of the downhill transfer component and the rise of the shoulder reflect the higher red chl content of the PSI trimers of *Synechocystis* as compared to monomers.^{17,41}

The lifetimes of the equilibration components found in this study correspond reasonably well with earlier SPT experiments^{9,30} and pump-probe experiments^{18,30} performed on *Synechocystis* PSI, in which equilibration upon aselective excitation was found to occur in 5 ps and 3.7 ps respectively. Recent pump-probe experiments performed on trimeric PSI cores from *Synechocystis*³² reveal a 4.8 ps component as well, although the authors also present a better fit of their data using 2 equilibration components with lifetimes 2 and 6.5 ps respectively. In another recent pump-probe studies on a mixture of PSI monomers and trimers from *Synechocystis*³³ equilibration is found to occur in about 2.3 ps. In our data there is no evidence of a (second) fast equilibration process occurring in ~2 ps. Of course the time resolution of the streak camera is less as compared to the above-mentioned pump-probe experiments, but the apparent discrepancy of our results with these experiments could also be due to the use of too high excitation powers in the latter resulting in singlet-singlet annihilation introducing non-physiological and non-exponential decay components.^{25,26} Savikhin et al.³² show a power dependence of a trace at 700 nm, but since there is still some difference between the lowest and the one-but-lowest energy trace, this does not convincingly rule out annihilation. Also their estimate of exciting one out of every 120 chls would imply that with each laser shot about one third of the excited PSI complexes would receive more than one excitation, resulting in annihilation (estimated using Poisson statistics, and 100 chls/PSI, assuming no significant amount of energy transfer between monomers in a trimer). The 1-3 nJ/pulse reported by Melkozernov et al.³³ could be relatively safe, although they do not specify the spot size of the focus of the excitation light. (In fact they state a pulse energy of 1-3 μJ/pulse, but this must certainly be 1-3 μW at a 1 kHz rep rate).

The lifetime and spectrum of trapping are consistent with earlier measurements on *Synechocystis* PSI.^{9,18,30,32,33}

Trimeric PSI particles from Synechococcus elongatus

The fluorescence DAS of trimeric PSI from *Synechococcus* following 400 nm excitation are shown in figure 3.4c. In this species the Soret Q_y relaxation also represents the fastest process, which is fitted with a 500 fs lifetime (figure 3.4c, solid).

For *Synechococcus* PSI trimers, which, in contrast to *Synechocystis* PSI, contain 2 pools of long-wavelength chls (C708 and C719), two separate energy-transfer components of 3.8 and 9.6 ps can be distinguished (figure 3.4c, dashed and double-dot-dashed). The 3.8 ps equilibration component exhibits a DAS of which the positive region displays a shape and amplitude which are very similar to the equilibration DAS of *Synechocystis* PSI, showing a maximum around 686 nm, and a zero crossing at 700 nm. The negative part is deeper, however, and shows a pronounced minimum around 715 nm. The spectrum is more or less conservative, indicating that in the trimeric PSI core of *Synechococcus* the amount of trapping occurring with the 3.8 ps time constant is negligible.

In contrast to the 3.8 ps equilibration component, the 9.6 ps component DAS is highly non-conservative and basically consists of a broad positive contribution peaking around 700 nm. The DAS is about zero above ~730 nm, but does not become distinctly negative. This shows that a significant amount of trapping occurs during the 9.6 ps process. The lack of a (clear) negative part in the spectrum does not imply that this spectrum is a pure trapping spectrum: the sum of an all positive pure trapping contribution and a conservative pure transfer component can easily be positive at all wavelengths. The differences between the 3.8 and 9.6 ps DAS indicate that in this PSI species energy transfer between the bulk antenna chls and the first (C708) pool of long-wavelength chls occurs on a fast time scale, and that the energy transfer from bulk chls and C708 to more red-shifted chls takes place on a slower time scale.

So far two distinct equilibration components have not been observed separately. In an early combined SPT/pump-probe study²⁹ only one equilibration component was revealed with a time constant of 8-12 ps (depending on the technique applied), although the authors suggested the existence of another, unresolved energy-transfer contribution. The spectrum of this single 8-12 ps component exhibited both pronounced positive and negative areas, and is therefore quite different from the (weighted) sum of the two equilibration spectra that were found in our experiments. We note that in particular this phenomenology recorded by Holzwarth et al.²⁹ was at the basis of the extensive modelling by Trinkunas et al.⁴⁶ Also in a very recent SPT study²⁴ only one energy-transfer component was observed, which had a lifetime of 13 ps, and a spectrum that showed a negative area which was much larger than the positive area, in clear contradiction with both our measurements, and those by Holzwarth et al., 1993.²⁹

The final component is fitted with a 35.8 ps time constant, and represents trapping from the equilibrated distribution of excitations (figure 3.4c, dotted). *Synechococcus* PSI trimers do not only contain a considerably larger number of red chls but about half of them also appear at lower energies than in *Synechocystis* (figure 3.1c, table 3.1). As a consequence the maximum of the trap spectrum is shifted to 719 nm, reflecting a dominant contribution of fluorescence from the red chls. The fluorescence of the bulk chls only appears as a shoulder around 690 nm.

The observed trapping lifetime and spectrum are consistent with the earlier results by Holzwarth et al.²⁹ and Byrdin et al.²⁴

Monomeric and trimeric PSI from Spirulina platensis

In PSI monomers of *Spirulina* the ingrowth from the Soret state is fitted with a 500 fs lifetime (figure 3.4d, solid), and the subsequent events include two equilibration processes taking place in 3.4 and 11.6 ps, respectively (figure 3.4d, dashed and double-dot-dashed). The 3.4 ps component peaks at 685 nm, has a zero crossing at 699 nm, exhibits a distinct minimum at 715 nm and is more or less conservative. The lifetime, spectral shape and amplitude of this component are virtually identical to the 3.8 ps component found in trimeric PSI of *Synechococcus*.

The DAS of the 11.6 ps equilibration component consists of a broad band positive contribution which peaks at ~688 nm, significantly more to the blue than the corresponding DAS in *Synechococcus* PSI. In contrast to the second equilibration DAS of *Synechococcus* PSI which does not exhibit a real negative region, the 11.6 ps DAS in *Spirulina* monomeric PSI slightly drops below zero above ~728 nm. Nevertheless this component is highly non-conservative, indicating that also in this species a significant amount of non-equilibrium trapping occurs during the second equilibration process. It seems obvious to associate the occurrence of two equilibration components in *Spirulina* monomeric PSI with the presence of two distinctly different chl pools. An alternative could be, however, that the long-wavelength region in *Spirulina* monomers does not consist of two distinctly different pools, but rather of a single (large) C708 pool which exhibits an exceptionally broad inhomogeneous distribution. (as suggested above in the discussion of the 6K absorption spectra). In this view the two distinct equilibration components that are observed may simply reflect the "two-pool approximation" of a broad distribution of lifetimes and spectra.

The trapping lifetime of 37.2 ps and the corresponding spectrum in *Spirulina* monomers (figure 3.4d, dotted) are very similar to that of *Synechococcus* PSI trimers. The spectrum peaks only slightly more blue (at 715 nm) than the latter (719 nm), and exhibits a slightly higher shoulder at 690 nm. These small differences reflect that, although the total amount of red chls in both species is comparable, their absorption is on the average slightly more blue in *Spirulina* monomeric PSI as compared to *Synechococcus* trimeric PSI (see above).

Our general observation is that all lifetimes and spectra found in *Spirulina* PSI monomers are remarkably similar to those found in *Synechococcus* PSI.

In contrast to PSI from *Synechocystis*, the results of monomeric and trimeric PSI of *Spirulina* differ significantly (figure 3.1d and e, figure 3.4 d and e). The 6K absorption spectrum of trimeric PSI complexes from *Spirulina* clearly exhibits two distinct pools of long-wavelength chls (see above): in addition to the C708 pool, which occurs throughout all PSI complexes investigated in this studies, trimeric PSI from *Spirulina* also exhibits an extremely red-shifted C740 pool, which is not present in monomeric PSI of this species.

For trimeric PSI from *Spirulina* the ingrowth from the Soret state is fitted with a 400 fs lifetime (figure 3.4e, solid).

In the kinetics of *Spirulina* trimeric PSI two equilibration components can be distinguished, occurring with time constants of 3.9 and 15 ps (figure 3.4d, dashed and double-dot-dashed), both slightly slower than found in the monomeric PSI complexes of this species.

The fast 3.9 ps DAS displays a shape which at first glance appears quite similar to the 3.4 ps DAS found in monomers. The amplitude is somewhat higher for trimers, however, and the zero crossing and the minimum of the spectrum are both significantly red shifted to 703 and 722 nm, respectively.

The 15 ps DAS, which represents the second equilibration process, clearly displays more significant differences with the monomers. In the trimer the spectrum of this component is also highly non-conservative, but in contrast to the monomers, the positive region clearly displays a double peaked structure with maxima at ~691 and ~706 nm. The zero-crossing is located at about 740 nm and the negative region at longer wavelengths is more pronounced than the corresponding DAS in monomers.

Trapping in *Spirulina* PSI trimers is by far the slowest of all the PSI species we investigated: 50 ps. Due to the extremely red-shifted chl forms that occur in *Spirulina* PSI trimers they exhibit a trapping DAS which is markedly red shifted, showing a maximum at 730 nm (figure 3.4e, dotted). The contribution of the bulk chls to this DAS is small, as reflected by the very low shoulder around 688 nm.

An earlier time-resolved emission study³¹ revealed one single 9 ps equilibration component as well as two all positive components with lifetimes of 28–31 ps and 65–69 ps, both in PSI monomers and trimers of *Spirulina*. The differences with our observations most probably can be ascribed to the much lower time-resolution of the earlier study, which may have caused some mixing of the different components, since all observed time constants are either equal to or significantly faster than the instrument response of the setup used by Karapetyan et al.³¹

DISCUSSION

Global analysis

Soret- Q_y relaxation

As mentioned above, in the time-resolved fluorescence experiments presented here, initially the Soret band, a higher electronic state of chl a , is excited which relaxes to the lowest singlet excited chl a state (Q_y) in a few hundred fs. Although the instrument response of the streakcamera is significantly longer than this relaxation process, it can clearly be distinguished, which is mostly due to the accurately determined (~100 fs) relative position of time zero for the different wavelengths of detection. The Soret Q_y relaxation is evident from an all-negative DAS, which is present in the kinetics of all PSI particles studied (figure 3.4a-e, solid). The fitted lifetime of the relaxation varies between 0.4 and 0.9 ps, but in view of the instrument response of our setup this variation is not significant. All fitted lifetimes are probably somewhat slower than the actual lifetime of Soret- Q_y relaxation.

Since the chl a molecules are excited aselectively at 400nm, independent of their Q_y absorption maximum, and since most likely the major part of the energy transfer occurs after Soret- Q_y relaxation, the ingrowth spectra are expected to resemble the Q_y region of the OD spectra (after changing the sign of the spectrum and taking into account an average Stokes' shift). The spectra corresponding to the rise (figure 3.4a-e, solid) indeed show a spectral shape

similar to that of the OD spectrum in the $Q_{y(0-0)}$ absorption region. The minima of the ingrowth spectra occur between 685 and 689 nm, suggesting a value of the Stokes' shift of 5-9 nm for the bulk antenna chls, which may be compared to the ~ 7 nm Stokes' shift found for chl a in solution.¹⁹ A Stokes' shift of 6.5 nm was also found for the single chl a in the cytochrome b_6f complex from *Synechocystis*.⁴⁷ These results suggest that in PSI no significant red shift of the emission spectrum occurs in the first few hundred fs.

The amount of carotenoids excited at 400 nm is less than 10%, as estimated from a comparison with an experiment in which the carotenoids were excited directly at 510 nm (results not shown). Since (most of) the transfer from the carotenoids to the chls occurs on a time scale comparable to the Soret Q_y relaxation,²⁸ the small fraction of carotenoids excited at 400 nm will have no significant effect upon our results.

Energy-transfer components

Since all experiments were performed under magic-angle conditions, no single step transfer kinetics between iso-energetic chls could be discerned, since these ultra-fast equilibration components can only be observed by high time-resolution anisotropic experiments. Also equilibration between spectrally different chls in the bulk antenna is not observed for this wavelength of excitation.

We do however observe components that are represented by a DAS which is positive at relatively short wavelengths and negative in the region of red chl emission (figure 3.4 a-e, dashed and double-dot-dashed), which reflect the transfer of excitation energy between the bulk and red chl pools in the PSI antenna.

In all studied PSI particles a fast 3.4 to 4.7 ps equilibration process is observed which mainly reflects energy transfer from the bulk chls to the C708 pool of red chls. The positive part of the spectra of this process is very similar in shape and amplitude for all PSI cores. The negative region of the spectra appears quite similar as well, although in *Synechocystis* monomeric and trimeric PSI this part is less pronounced than in other PSI particles. The spectrum of the fast equilibration component is slightly non-conservative in the PSI cores from *Synechocystis*, whereas it is basically conservative in the other PSI cores, indicating that some non-equilibrium trapping occurs in the former particles, which is absent in the latter. This is consistent with the observation that the transfer component in *Synechocystis* PSI cores is slightly slower (4.4-4.7 ps), than the fastest transfer component in the other PSI particles (~ 3.4 -3.9 ps).

The notion that the amount of non-equilibrium trapping increases with slower equilibration components is underlined by the spectra of the slower second equilibration processes in observed in the *Synechococcus* and *Spirulina* PSI particles (figure 3.4c-e, double-dot-dashed), that occur on a time scale of 9.6 to 15 ps, and which are consequently highly non-conservative.

The spectra of the second equilibration component in *Synechococcus* trimeric and *Spirulina* monomeric and trimeric PSI are qualitatively very similar: they exhibit a relatively large positive contribution in the blue part of the spectrum, and a red part which is only slightly negative. The maximum and width of the positive part, however, vary significantly between these three PSI species. These differences between the DAS of the second equilibration component in monomeric and trimeric PSI particles from *Spirulina* can be readily

explained by the differences in contents of long-wavelength chls. The second transfer component involves both non-equilibrium trapping from the bulk and C708 pools and transfer from these pools to the red-most chl pool. In monomeric PSI from *Spirulina* the emissions of the two long-wavelength pools are spectrally less separated as compared to trimers (see also below). Therefore in monomers the positive (decay) contribution of the emission of C708 to the spectrum of the slow transfer component is to a certain extent cancelled by the negative (rise) contribution of the emission of the C719 pool. This results in the slanting red wing, and the lack of a clearly negative region in the 11.6 ps DAS of the *Spirulina* monomers. In trimers the emissions of the two red pools are spectrally more separated, and consequently there is less cancellation of the emission of the C708 pool. This results in the two peaks in the positive part of the second transfer DAS in trimers, which can therefore be attributed to bulk and C708 emission. Furthermore it results in a more distinct negative region in the 15 ps DAS in trimers.

In view of the above explanation, one would expect the second equilibration DAS in *Synechococcus* trimeric PSI to be peaking even more to the blue than *Spirulina* monomeric PSI, since the former exhibits less C708 chls and more C719 chls than the latter, which would enhance the cancellation effect in the red part of the spectrum. However, this is not observed. A possible explanation for this apparent discrepancy is that in *Synechococcus* trimeric PSI more non-equilibrium trapping from the C708 chls occurs during the second equilibration step. The C708 contribution to the second equilibration process in *Spirulina* PSI may in its turn have been lowered since some additional bulk to C708 transfer, may have occurred along with the second equilibration process as well. An alternative explanation could be that the numbers and energies of the red chls that were found from the 6 K absorption spectrum may not be valid at room temperature.

Trapping components

For all PSI particles under investigation the slowest process is the so-called trapping component which exhibits a DAS that is clearly positive at all wavelengths (figure 3.4a-e dotted). As pointed out above the designation "trapping component" is somewhat misleading as (non-equilibrium) trapping also occurs on shorter time scales.

Both the trapping lifetime, which varies between 23 and 50 ps, and the trapping spectrum depend strongly on the numbers and energies of the red chls, present in the various PSI particles (figure 3.4a-e, dotted). This pronounced correlation can easily be understood in a qualitative manner. If the excitation density distribution reflected in the trap spectrum represents a (quasi) Boltzmann equilibrium of the excitation density over the PSI antenna chls, the exponential Boltzmann factor will cause the equilibrium to shift rapidly to lower energies if the energies of the red states are lowered. Likewise, the number ratio in the Boltzmann factor will shift the equilibrium dependent on the number of red chls relative to the bulk chl α . The shift of the equilibrium also accounts for the observed increase in trapping lifetimes. The emission of the low-energy chls has a lower spectral overlap with the absorption of P700 than the bulk chls (see also below). If the low-energy chls are not located exceptionally close to the RC, concentration of the excitations on these chls will consequently result in a decreased trapping rate.

It can therefore be concluded that effectively the presence of red chls lower the efficiency of charge separation, but it must be noted that slowing down trapping from 20 ps to 50 ps only results in a decrease of the quantum yield of charge separation of 99.6% to 99.0% (assuming an intrinsic fluorescence lifetime of chl *a* of 5 ns) which is not expected to seriously affect the organism.

We would like to point out that, although at shorter time-scales energy-transfer processes occur that lead to equilibration of the excitation energy throughout the antenna, this does not necessarily imply that the trap-spectrum reflects a fully Boltzmann-equilibrated distribution of excitations, but rather a so-called "transfer equilibrium".⁴⁸

At this stage we have not proven that all the differences that we observe between the different PSI species are entirely due to the differences in red chl contents. Below we will discuss a kinetic model to which we have fitted our data to explore in more detail the effects of the spectral composition of the antenna upon the experimentally observed spectral-temporal properties of the fluorescence of all PSI species studied.

Target analysis of the time-resolved fluorescence data: a compartmental model describing the kinetics of different PSI core complexes

In this section the differences and similarities underlying the variation in the experimentally recorded kinetics of the various PSI particles will be further explored.

Although the coordinates of the antenna chls are available from the crystal structure of PSI from *Synechococcus*^{5,3} and this has provided important new insight into the 3-D organization of this antenna-RC complex in relation to its function, a full calculation of energy transfer in PSI based on this structure is not straightforward. First of all information about the orientation of the transition dipole moments of the chls is currently missing. Secondly the positions of the different chl spectral forms are unknown. Finally the structure is known only for *Synechococcus* PSI: in view of the spectroscopic differences small variations of the protein structure and chl binding sites must be present between the different PSI species that we have investigated, although the global organisation of different PSI species is expected to be unchanged.

Even if these difficulties are overcome (by obtaining high resolution structures of the relevant proteins), relating the structure of a photosynthetic protein to spectroscopic data has proven to be very difficult, even for systems with a much smaller number of chls, such as for instance the FMO antenna complex⁴⁹ or LHCII.⁵⁰

Therefore we favour a relatively simple compartmental model over a structure-based calculation. This approach allows for a unified description of the dynamics in all studied PSI cores, and generates a relatively small number of rate constants which transparently reflect the macroscopic energy-transfer processes between spectrally different chl pools. The results of this analysis allow us to compare the various PSI cores quantitatively.

Since we choose to use discrete spectral pools, inhomogeneous broadening, although known to be large for the long-wavelength chls,^{17,20} is not explicitly included in our model.

The compartmental model, presented in figure 3.5, consists of 5 compartments, representing the Soret state (S) of all spectral forms, and the Q_y states of the bulk chl pool (B), two red-shifted chl pools (1 and 2) and a pool representing free chls which are not connected

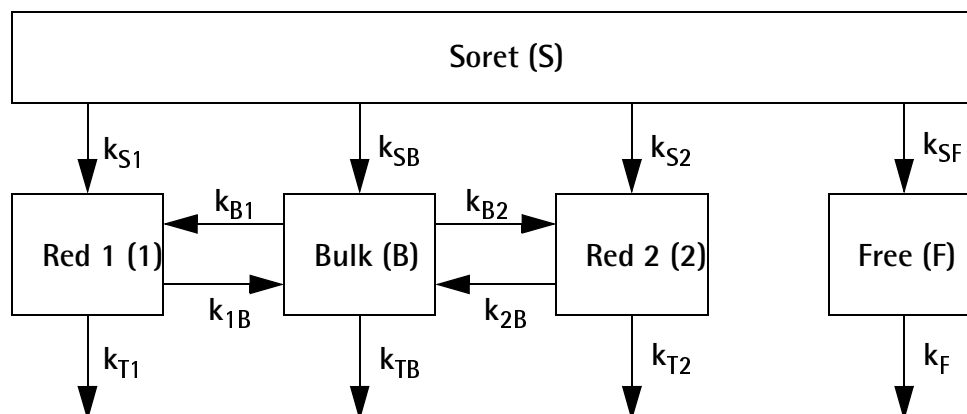
to the PSI core (F). For the modelling of *Synechocystis* PSI, the second pool of red-shifted chls was omitted from the scheme.

The following rate constants were included in the model:

1. From the Soret compartment irreversible energy-transfer occurs to the three or four Q_y compartments with the rate constants k_{SB} , k_{S1} , k_{S2} and k_{SF} . The sum of these rate constants represents the observed Soret- Q_y relaxation rate. The four individual rates do not have an actual physical meaning, they merely account for the initial distribution of the excitations over the different compartments, and scale with the total number of chls in each of the pools;
2. Uphill and downhill energy-transfer occurs between the red chl compartments and the bulk chl compartment with rate constants k_{B1} , k_{B2} , k_{1B} and k_{2B} ;
We have not included direct energy transfer between different pools of red chls since low-temperature fluorescence emission spectra of *Spirulina* trimeric PSI indicate that energy transfer between different pools of red chls is not very efficient.¹¹ Although energy transfer may occur between the two red pools in *Synechococcus* trimeric PSI,²⁰ we regard it as a secondary effect;
3. Trapping occurs from the bulk chls with a rate constant k_{TB} , and from the red chl compartments with rate constants k_{T1} and k_{T2} ;
4. Free chl emission decays with a rate constant k_F .

P700 was not included as a separate compartment in the target analysis of our data. Since both trapping and backtransfer to the antenna occur on a sub-picosecond time-scale (Gobets et al., unpublished results), the density of excitations on P700 is very small at all times, and hence the actual contribution of P700 to the total fluorescence is too small to be distinguished from our data.

The compartmental model was fitted to the data (target analysis), yielding the emission spectra of the different pools of chls, as well as the rate constants that were introduced above.⁴⁰ In order to solve the model, the number of free parameters had to be reduced by fixing or manually varying some of the rate constants. The free rates were the Soret to bulk relaxation rate k_{SB} , the energy-transfer rates k_{B1} , k_{B2} , k_{1B} , k_{2B} , and the free chl decay rate k_F .



3.5 Compartmental model describing the kinetics of different cyanobacterial PSI core particles upon excitation at 400 nm.

Two sets of fits were generated. In the first set the trapping rate from the bulk, k_{TB} , was a free parameter as well and could vary between different PSI species. In the second set k_{TB} was fixed to $(18 \text{ ps})^{-1}$ for all species. To solve the model, a constraint had to be imposed on the emission spectra of some pools, and therefore the emission spectra of the low-energy chls were forced to be zero below, respectively, ~ 680 , and ~ 690 nm for the first and second pool of red chls. Since the Soret state does not fluoresce in the spectral region that was recorded, its spectrum was set to zero at all wavelengths. Some of the parameters were varied manually to meet some boundary conditions that could not be implemented directly in the target analysis. First, the Soret to Q_y rates k_{S1} and k_{S2} were adjusted manually to k_{SB} to match the initial fraction of excitations on each Q_y pool to the number of chls contained in that pool (table 3.1), to account for the aselective excitation. Second, we required the SAES resulting from the target analysis to have equal areas. These areas reflect the relative oscillator strength per chl in each emitting pool, which is presupposed to be equal for all spectral forms. The areas of the spectra of the different pools were balanced by varying the trapping rates from the red chls k_{T1} and k_{T2} , as well as the free chl Soret to Q_y relaxation rate k_{SF} . For some of the data sets it was not possible to completely balance the areas of the spectra resulting from the target analysis. This problem mainly occurred for the fits in which the bulk trapping rate was fixed. In those cases we optimized the values of k_{T1} , k_{T2} and k_{SF} to get as close as possible to equal areas below the spectra. The final areas of the spectra deviated less than 10% from that of equal areas.

Under the constraints and conditions discussed above, the target analysis always converged to a unique optimal solution.

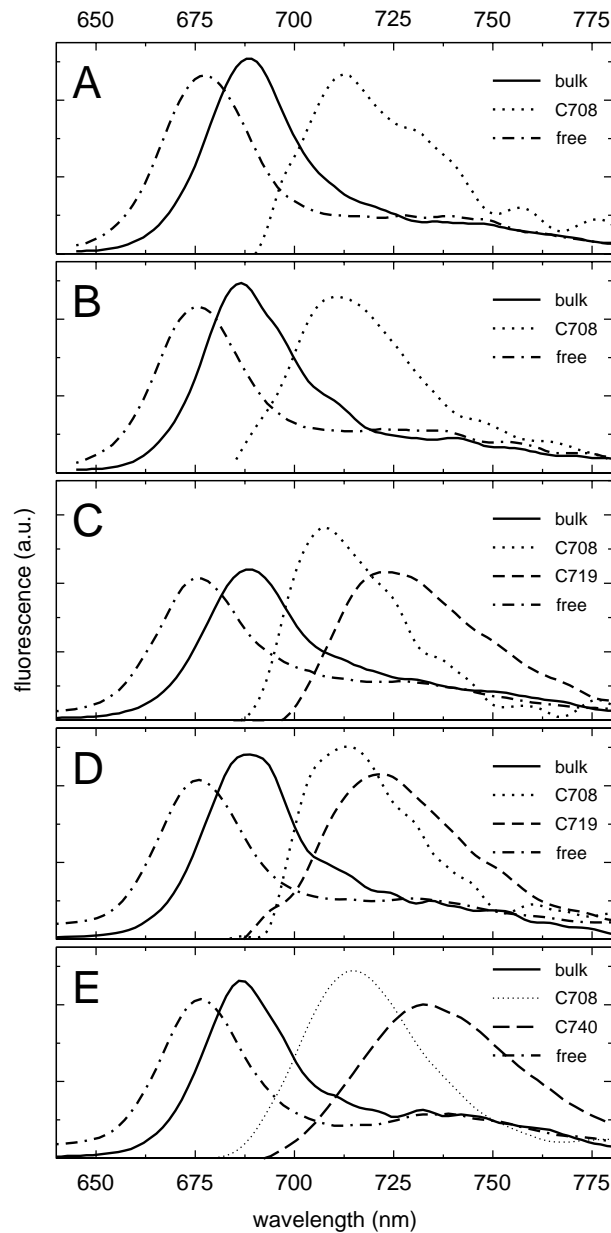
Due to the restrictions imposed by the model, the quality of the fit decreased slightly as compared to the analysis with parallel decaying components discussed above which is reflected by a small increase of the root mean square error by between 2% and 8%, and some temporal and spectral structure appearing in the residual matrix of the singular value decomposition. Nevertheless the quality of the fit remained very good. The kinetic parameters resulting from the target analysis resulted in system lifetimes which in almost all cases deviated less than 10% from those found using the model with parallel decaying components (see figure 3.4 and see above).

Species-associated emission spectra (SAES)

The SAES resulting from the target analysis of the five PSI species are presented in figure 3.6a-e. Since the SAES-es for the analysis with a free bulk trapping rate and a fixed bulk trapping rate of $(18 \text{ ps})^{-1}$ were virtually identical, we only show the latter. In the cases where the areas of the SAES could not be fully balanced (see above), the spectra were scaled afterwards for ease of comparison.

The compartment of the free chls is in all species represented by an identical spectrum (dot-dashed), which exhibits a maximum around 676 nm and shows a distinct long red tail which extends beyond the window of observation. This spectrum is very characteristic for the emission of monomeric chl a in solution.¹⁹

In all species the emission from the bulk compartment is represented by a rather characteristic shaped SAES (solid). We note that these bulk spectra are indistinguishable between the different PSI species, reflecting the lack of clear differences in the dominating band of the absorption spectra. The bulk SAES exhibits a maximum around 688 nm, and shows



3.6 Species-Associated Emission Spectra (SAES) of target analysis of fluorescence decay of different cyanobacterial PS I core particles upon excitation at 400 nm using a fixed 18 ps bulk trapping time k_{T_B} . a) Monomeric core of *Synechocystis* sp. PCC 6803, b) Trimeric core of *Synechocystis* sp. PCC 6803 c) Trimeric core of *Synechococcus elongatus*, d) Monomeric core of *Spirulina platensis*, e) Trimeric core of *Spirulina platensis*. Linetypes: bulk emission, solid; first red pool emission, dotted; second red pool emission, dashed; free chl emission, dot-dashed.

a long red tail. Except for a 12 nm red shift, the spectrum is nearly indistinguishable from the free chl emission spectrum.

The SAES of the C708 pool of red chls (dotted) look very similar for all studied species, underpinning the strong similarity between C708 chls contained in the PSI cores of the different species. The maxima of these spectra all appear around 712 nm, and the spectra are considerably broader than those of the bulk chls, reflecting the strong homogeneous and inhomogeneous broadening in these red chl pools.^{17,20,41} The similarity between the emission spectra of the C708 pools of red chls in all PSI species studied is striking, considering the large differences in the red parts of the 6K absorption spectra between the different PSI species.

Even more remarkable are the SAES of the C719 pool (dashed), occurring in *Synechococcus* PSI trimers and *Spirulina* PSI monomers, which are practically identical. The maximum of these spectra occurs at about 720 nm, and the width of these spectra is somewhat larger than for the first (C708) pool of red chls, reflecting the larger (in)homogeneous broadening of these pools.²⁰ The SAES of the C740 pool in *Spirulina* trimers (dashed) is even more red shifted, reaching a maximum at 733 nm, and the spectrum is even broader reflecting an even larger (in)homogeneous broadening of this pool.

The maxima of the room temperature emission spectra of the different pools of red chls occur at wavelengths that are about equal or even shorter than their respective 6K absorption maxima. This remarkable feature can be explained by a significant blue-shift of the absorption maxima of these red pools at room temperature.⁴¹

Energy transfer

The fitted values of the various rates that occur in the model (fig. 3.5) are listed in table 3.2. Both the results of the fit with a fixed bulk trapping rate, and the fit in which this rate was a free parameter of the fit are shown, the latter in parentheses.

We emphasize that the rates of energy transfer and trapping in table 3.2 represent effective rates. The actual values of these rates would change in case a P700 compartment could have been included in the model. However, the ratios between forward and backward rates and the ratios between the various trapping rates are hardly affected by such an additional compartment, and it is these ratios rather than the actual rates, that are important for our conclusions.

The Soret to Q_y rates are not listed, since their individual values do not have a physical significance (see above). The sum of Soret to Q_y rates varied between $(0.4 \text{ ps})^{-1}$ and $(0.8 \text{ ps})^{-1}$, in line with the 400–900 fs lifetimes found in the parallel model.

The characteristics of energy transfer between the bulk and red pools are expressed by the rates k_{B1} , k_{B2} , k_{1B} and k_{2B} . Since the number of chls in this first pool of (C708) chls increases from 3 in *Synechocystis* PSI monomers to 5 in *Synechocystis* PSI trimers and *Synechococcus* PSI trimers and ~ 7 in *Spirulina* PSI, the ratio k_{B1}/k_{1B} is expected to increase correspondingly. The ratio k_{B1}/k_{1B} does indeed follow the stoichiometry of the C708 quite well.

In the C719 pool of red chls that appears in *Synechococcus* trimeric PSI and *Spirulina* monomeric PSI we find a ratio of the forward (k_{B2}) and backward (k_{2B}) rates which only differ by about 25% between these two species. This is in clear contradiction with the estimated numbers of chls contained in this pool (4 in *Synechococcus* trimeric PSI vs. 1 in *Spirulina* monomeric PSI), from which a 75% difference would be expected. These findings strongly

suggest that monomeric PSI from *Spirulina* contains more C719 chls (and consequently less C708 chls) at room temperature than anticipated from the Gaussian fit of the 6K absorption spectrum.

We will use the ratio of the forward and backward energy-transfer rates, and the stoichiometric estimates to calculate the energy difference between the red chl pools and the bulk chls, using the concept of detailed balance, which states that the energy difference between two different pools of chls A and B can be expressed as $\Delta E = k_b T \ln(N_A k_{AB} / N_B k_{BA})$, in which k_b represents Boltzmann's constant ($0.695 \text{ cm}^{-1} \text{ K}^{-1}$), T the absolute temperature, N_x the number of chls in pool x , and k_{xy} the transfer rate from pool x to pool y . Using the stoichiometric values from table 3.1 and the transfer rates from table 3.2 we find for the C708 pool in all studied PSI particles a value of ΔE which varies between 350 and 515 cm^{-1} , corresponding to a room temperature absorption maximum of this pool at around 702 nm , which corresponds well with the $702\text{--}704 \text{ nm}$ value reported by Rätsep et al.,⁴¹ and also seems reasonable in view of the $\sim 712 \text{ nm}$ emission maximum of this pool (see above), and the 10 nm Stokes' shift reported by Gobets et al.¹⁷

The energy difference of the second (C719) pool of red chls in *Synechococcus* PSI is found to be approximately 570 cm^{-1} , corresponding to an absorption maximum of $\sim 708 \text{ nm}$. This value seems to be realistic in view of the emission maximum of this pool which appears at 723 nm . The 11 nm blue-shift of the absorption maximum of the C719 pool from 719 nm to 708 nm upon the increase of the temperature from 6 K to room temperature, is considerably larger than the 4 to 6 nm shift found for the C708 pool,⁴¹ which indicates that the chls in the C719 pool are more strongly coupled to their environment than those in the C708 pool.

Table 3.2 Reciprocal of the rates from target analysis

species	(transfer Rates) ⁻¹ in ps				(transfer Rates) ⁻¹ in ps			k _F ⁻¹ in ns
	k _{B1}	k _{1B}	k _{B2}	k _{2B}	k _{TB}	k _{T1}	k _{T2}	
<i>Synechocystis</i> mon.	31(27)	8.6(8.3)	-	-	18(18)	170(200)	-	4.8(5.0)
<i>Synechocystis</i> tri.	18(20)	8.9(8.4)	-	-	18(17)	38(63)	-	6.7(7.1)
<i>Synechococcus</i> tri.	18(18)	9.3(9.5)	26(22)	17(16)	18(20)	21(13)	<i>inf</i> (<i>inf</i>)	5.3(5.3)
<i>Spirulina</i> mon.	19(15)	7.8(10.2)	43(38)	20(22)	18(29)	48(18)	<i>inf</i> (200)	5.0(4.8)
<i>Spirulina</i> tri.	15(13)	9.7(12.3)	24(28)	27(30)	18(27)	30(22)	450 (260)	4.0(4.3)

Parameters set in italic numbers were fixed or varied manually, plain numbers indicate free fitting parameters. Results are shown both for a fit in which the value of k_{TB} was fixed to a value of $(18 \text{ ps})^{-1}$ and for a fit in which k_{TB} was a free fitting parameter (values in parentheses). For more details, see text

As pointed out above we found a discrepancy between our time-resolved data, and the estimated stoichiometry of the pools of red chls in *Spirulina* PSI monomers. This is also reflected by the unrealistically large value of about 800 cm^{-1} for the calculated energy difference between the bulk and the second pool of red chls in this PSI species, if the C719 pool would consist of only one single chl. If however we propose that instead of 7 C708 and 1 C719 chl, 5 C708 and 3 C719 chls are present in *Spirulina* PSI monomers, the calculated energy difference between the C719 and the bulk chls pool is about 575 cm^{-1} , corresponding to a 708 nm absorption maximum, very comparable to the value found for *Synechococcus* PSI trimers.

The reduction of the number of C708 chls in *Spirulina* monomers from 7 to 5 also leads to a room temperature absorption maximum at 702 nm, which is more in line with the C708 pool in the other PSI cores (table 3.1, values between parentheses).

We must therefore conclude that at room temperature the red chl contents of *Spirulina* PSI monomers must be very comparable to the that of *Synechococcus*, with a slightly lower amount of C719 chls, and that the stoichiometry which was estimated from the 6 K absorption spectrum cannot be applied at room temperature for *Spirulina* monomeric PSI. This explains the remarkable kinetic and spectral similarity between both species at room temperature, as was already mentioned in the results section.

The energy difference between the second red pool in *Spirulina* trimeric PSI (C740) and the bulk, is about 725 cm^{-1} , which corresponds to an absorption maximum at 715 nm. This is a realistic value in view of the emission maximum at 733 nm. The apparent Stokes' shift of 18 nm is comparable to the 20 nm Stokes' shift found at 6K. The blue-shift of 25 nm upon a rise of the temperature from 6K to room temperature is about 5 times more than found in *Synechocystis* PSI⁴¹ (see also above) and about 2 times more than found in *Synechococcus* trimeric PSI (see above), indicating an even stronger coupling of the chls in this extremely red-shifted pool to their local environment.

Trapping

If the bulk trapping rate, k_{TB} , is regarded as a free parameter of the fit, its value varies between $(17 \text{ ps})^{-1}$ and $(29 \text{ ps})^{-1}$ in the different PSI cores. Despite this spread of values, it turns out that the quality of the fit decreases only slightly by fixing this value to $(18 \text{ ps})^{-1}$. This common value of k_{TB} had to be chosen quite close to the value found in both monomeric and trimeric PSI from *Synechocystis* in order to obtain a good fit of the model to the results of these PSI particles. The sensitivity of the model to the *Synechocystis* PSI data upon varying k_{TB} has two reasons. First of all, in our view this species exhibits only one pool of red chls, and hence the model for *Synechocystis* PSI has three degrees of freedom less (Two transfer rates, and a trapping rate) than the species with 2 pools of red chls. Secondly, *Synechocystis* PSI has only very few, not very red-shifted red chls, and therefore the effect that these red chls have upon the energy-transfer and trapping dynamics is relatively limited. This is illustrated by the fact that the $(18 \text{ ps})^{-1}$ bulk trapping rate constant is quite close to the 23 to 24 ps time constant found for *Synechocystis* PSI in the parallel model. Modelling of the dynamics in *Synechocystis* and *Synechococcus* PSI, based on the chl coordinates from the structure of *Synechococcus* PSI,⁴⁵ also showed a 18 ps trapping time upon removal of the two red chls, which strongly suggests that this is indeed the trapping time in a bulk PSI without red chls.

The structure of *Synechococcus* PSI reveals that the bulk of the antenna chls are scattered in an ellipse around the RC. This organisation defines the bulk to RC transfer rate, which in turn largely determines the effective rate of trapping k_{TB} from the bulk chls.⁴⁵ Since the sequence homology is highly conserved between different PSI species^{1,2} this organisation will essentially be the same in all these species. Since also the spectral properties of the bulk and RC chls do not vary significantly between the PSI species investigated in this study (fig. 3.1) it seems quite acceptable to propose that the bulk trapping properties are essentially the same for all PSI species, and that in view of the discussion above, the value of this trapping rate, k_{BT} , should be fixed to approximately $(18 \text{ ps})^{-1}$.

The trapping rates from any pool of antenna chls depend in first order on the (average) distance of these chls to P700, their relative orientation to P700, and the overlap integral of their emission spectrum with the absorption of P700. If the average location and orientation of the chls in a red pool are not very different from the bulk chls, the relative trapping rate from that pool as compared to the bulk chls only depends upon the relative spectral overlap between the emission of these red chls with the absorption of P700. At low temperatures this overlap is very small, resulting in slow trapping from the red chls, and a low quantum efficiency of charge separation. Upon an increase of temperature the overlap increases due to a number of causes. First of all the emission (and absorption) of the strongly coupled red chls blue-shifts quite significantly, towards the absorption of P700.⁴¹ Secondly, the absorption band of P700 and the emission of the red chls broadens with increasing temperature. Finally, in the pools of red chls, which are significantly inhomogeneously broadened, at low temperatures excitations mainly reside on the lower energy chls in the distribution, whereas at higher temperatures, also the higher energy chls in the distribution can be excited, which results in a further blue-shift of the (average) emission of the red chls.

The room temperature trapping rates from the red chl pools may be roughly estimated from the emission spectra found in the target analyses, and a P700 absorption spectrum, which can roughly be approximated by a Gaussian with a FWHM of 20 nm, peaking at 698 nm.²² The direct trapping rates from the pools of red chls that are calculated this way turn out to be quite significant: the direct trapping rates from the C708, C719 and C740 pools are estimated to be about 80%, 30% and 15% of the bulk trapping rate, respectively. The accuracy of the smaller numbers is limited, since they depend strongly upon the exact properties of the extreme blue edge of the calculated emission spectra, and because the spectral resolution of the experimental emission spectra is only 8 nm.

The trapping rates estimated this in way can be compared to the trapping rates resulting from the target analysis. The trapping rates k_{T1} from the first pool of red chls (C708) for the fit with the fixed bulk trapping rate k_{TB} are all of the same order as k_{TB} , roughly matching the 80% estimate. The values of k_{T1} for the fit with free bulk trapping are slightly higher, but still comparable. Monomeric PSI of *Synechocystis* is the only exception with a value of k_{T1} which is only about 10% of k_{TB} . It could be that the preparation of monomeric particles is heterogeneous, in the sense that some particles may contain more red chls, and other less (or none), which results in the generally observed slightly lower red chl content as compared to trimeric PSI from the same species.

The trapping rates k_{T2} from the second pools of red chls measure only 10% of k_{TB} or less, which is lower than the estimates indicated above. It must be noted that, in contrast to the trapping rates from the first pool of red chls, the boundary conditions (equal spectral areas) do not depend too strongly upon these (small) trapping rates, and therefore merely represent an "order of magnitude" estimate.

CONCLUSIONS

In this work we have investigated monomeric and trimeric PSI preparations of *Synechocystis* sp. PCC 6803, *Synechococcus elongatus* and *Spirulina platensis* using room temperature time-resolved fluorescence spectroscopy. The 6K steady state absorption spectra of these preparations reveal pronounced differences in the amounts and energies of their respective red-shifted chl forms. A C708 pool appears to be a common feature of all these particles, and a C719 pool appears in two species (*Synechococcus* trimers, *Spirulina* monomers). A C740 pool is unique for *Spirulina* PSI trimers.

The room temperature time-resolved fluorescence measurements of these five PSI preparations reveal a large diversity of fluorescence kinetics and spectral evolution. A fast equilibration step between the bulk chls and the C708 pool is found to occur in about 3.5 to 5 ps in all these PSI cores. In the species containing a second (C719 or C740) pool of red chls a second equilibration process occurs, along with a considerable amount of non equilibrium trapping, in 10 to 15 ps. Trapping from an equilibrated distribution of excitations occurs in 23 to 50 ps.

A target analysis of these data demonstrates that the kinetic and spectral differences between these particles most probably result exclusively from the differences in amounts and energies of red chls, and that trapping from the bulk chls may be described by a single $(18 \text{ ps})^{-1}$ rate constant.

The direct trapping rate from the C708 pool was found to be only slightly slower than trapping from the bulk chls. Trapping from the other red pools was found to be at least an order of magnitude slower. Since the overall trapping kinetics slows down with an increase of the number of red chls, and a lowering of their energies, we conclude that increasing the trapping efficiency of the system apparently is not a function of the red chls. The trapping rate from the bulk and C708 pools were found to be more or less proportional to the overlap between their emission spectrum and the absorption of P700. This leads us to the conclusion that the C708 chls do not have a location very close to or far away from the reaction centre, in agreement with Byrdin et al.²⁴ The trapping rate from the red-most chl pools seems to be lower than expected from the overlap-based estimate, possibly indicating a more remote location of these chls in the structure.

Clear, well defined spectra were obtained for the different spectral forms, which show that the emission of the bulk chls and the C708, C719 and C740 pools can also be distinguished at room temperature. The room temperature emission spectra of the red chls are very broad, and distinctly different from the bulk chl emission spectrum, reflecting that the homogeneous and/or inhomogeneous broadening of the red chl pools are large, also at room temperature.

The red chl pools are considerably blue-shifted at room temperature, C708 absorbs around 702 nm and emits around 712 nm, C719 absorbs around 708 nm, and emits around 722 nm, and C740 absorbs around 715 nm and emits at 733 nm. The more red-shifted a pool is, the stronger the chls in that pool are coupled to their local environment, which is expressed by a larger temperature dependent blue-shift of this pool.

ACKNOWLEDGMENTS

This research was supported by the Netherlands Organization for Scientific Research via the Dutch Foundation of Earth and Life Sciences (ALW), der Deutsche Forschungsgemeinschaft (DFG, Sonderforschungsbereich 480, C2 and Sonderforschungsbereich 498, TP A1), dem Fonds der Chemischen Industrie and a NATO grant (LST.CLG. 975955). The streak camera and amplified Ti:Sapph laser system were funded by investment grants of ALW.

REFERENCES

- (1) Cantrell, A., and D.A. Bryant. 1987. Molecular cloning and nucleotide sequence of the *psaA* and *psaB* genes of the cyanobacterium *Synechococcus* sp. PCC 7002. *Plant Mol. Biol.* 9:453-468.
- (2) Mühlhoff, U., W. Haehnel, H. Witt, and R.G. Herrmann. 1993. Genes encoding 11 subunits of Photosystem I from the thermophilic cyanobacterium *Synechococcus* sp. *Gene*. 127:71-78.
- (3) Krauss, N., W.-D. Schubert, O. Klukas, P. Fromme, H.T. Witt, and W. Saenger. 1996. Photosystem I at 4Å resolution represents the first structural model of a joint photosynthetic reaction centre and core antenna system. *Nat. Struct. Biol.* 3:965-973.
- (4) Karapetyan, N.V., A.R. Holzwarth, and M. Rögner. 1999. The Photosystem I trimer of cyanobacteria: Molecular organization, excitation dynamics and physiological significance. *FEBS Lett.* 460:395-400.
- (5) Fromme, P., H.T. Witt, W.-D. Schubert, O. Klukas, W. Sängner, and N. Krauss. 1996. Structure of Photosystem I at 4.5 angstrom resolution: A short review including evolutionary aspects. *Biochim. Biophys. Acta.* 1275:76-83.
- (6) Schubert, W.-D., O. Klukas, N. Krauss, W. Saenger, P. Fromme, and H.T. Witt. 1997. Photosystem I of *Synechococcus elongatus* at 4 angstrom resolution: Comprehensive structure analysis. *J. Mol. Biol.* 272:741-769.
- (7) Klukas, O., W.D. Schubert, P. Jordan, N. Krauss, P. Fromme, H.T. Witt, and W. Saenger. 1999. Localization of two phylloquinones, Q(K) and Q(K)', in an improved electron density map of Photosystem I at 4-angstrom resolution. *J. Biol. Chem.* 274:7361-7367.
- (8) Fleming, G.R., and R. van Grondelle. 1997. Femtosecond spectroscopy of photosynthetic light-harvesting systems. *Curr. Opin. Struct. Biol.* 7: 738-748.
- (9) Turconi, S., J. Kruip, G. Schweitzer, M. Rögner, and A.R. Holzwarth. 1996. A comparative fluorescence kinetics study of Photosystem I monomers and trimers from *Synechocystis* PCC 6803. *Photosynth. Res.* 49:263-268.
- (10) Kruip, J., D. Bald, E. Boekema, and M. Rögner. 1994. Evidence for the existence of trimeric and monomeric Photosystem I complexes in thylakoid membranes from cyanobacteria. *Photosynth. Res.* 40:279-286.

- (11) Shubin, V.V., I.N. Bezsmertnaya, and N.V. Karapetyan. 1995. Efficient energy-transfer from the long-wavelength antenna chlorophylls to P700 in Photosystem-I complexes from *Spirulina platensis*. *J. Photochem. Photobiol. B.* 30:153-160.
- (12) Van Grondelle, R., J.P. Dekker, T. Gillbro, and V. Sundström. 1994. Energy transfer and trapping in photosynthesis. *Biochim. Biophys. Acta.* 1187:1-65.
- (13) Shubin, V.V., S.D.S. Murthy, N.V. Karapetyan, and P. Mohanty. 1991. Origin of the 77K variable fluorescence at 758 nm in the cyanobacterium *Spirulina platensis*. *Biochim. Biophys. Acta.* 1060:28-36.
- (14) Wittmershaus, B.P., V.M. Woolf, and W.F.J. Vermaas. 1992. Temperature dependence and polarization of fluorescence from Photosystem I in the cyanobacterium *Synechocystis sp* PCC 6803. *Photosynth. Res.* 31:75-87.
- (15) Van der Lee, J., D. Bald, S.L.S. Kwa, R. van Grondelle, M. Rögner, and J.P. Dekker. 1993. Steady-state polarized-light spectroscopy of isolated Photosystem-I complexes. *Photosynth. Res.* 35:311-321.
- (16) Turconi, S., G. Schweitzer, and A.R. Holzwarth. 1993. Temperature dependence of picosecond fluorescence kinetics of a cyanobacterial Photosystem I particle. *Photochem. Photobiol.* 57:113-119.
- (17) Gobets, B., H. van Amerongen, R. Monshouwer, J. Kruip, M. Rögner, R. van Grondelle, and J.P. Dekker. 1994. Polarized site-selected fluorescence spectroscopy of isolated Photosystem I particles. *Biochim. Biophys. Acta.* 1188:75-85.
- (18) Hastings, G., L.J. Reed, S. Lin, and R.E. Blankenship. 1995. Excited state dynamics in Photosystem I: Effects of detergent and excitation wavelength. *Biophys. J.* 69:2044-2055.
- (19) Hoff, A.J., and J. Amesz. 1991. Visible absorption spectroscopy of chlorophylls. In *Chlorophylls*. H. Scheer, editor. CRC Press, Boca Raton, Florida. 723-738.
- (20) Pålsson, L.-O., J.P. Dekker, E. Schlodder, R. Monshouwer, and R. van Grondelle. 1996. Polarized site-selective fluorescence spectroscopy of the long-wavelength emitting chlorophylls in isolated Photosystem I particles of *Synechococcus elongatus*. *Photosynth. Res.* 48:239-246.
- (21) Shubin, V.V., I.N. Bezsmertnaya, and N.V. Karapetyan. 1992. Isolation from *Spirulina* membranes of two Photosystem I-type complexes, one of which contains chlorophyll responsible for the 77 K fluorescence at 760 nm. *FEBS Lett.* 309:340-342.
- (22) Pålsson, L.-O., C. Flemming, B. Gobets, R. van Grondelle, J.P. Dekker, and E. Schlodder. 1998. Energy transfer and charge separation in Photosystem I: P700 oxidation upon selective excitation of the long-wavelength chlorophylls of *Synechococcus elongatus*. *Biophys. J.* 74:2611-2622.
- (23) Trissl, H.-W., B. Hecks., and K. Wulf. 1993. Invariable trapping times in Photosystem-I upon excitation of minor long-wavelength-absorbing pigments. *Photochem. Photobiol.* 57:108-112.
- (24) Byrdin, M., I. Rimke., E. Schlodder, D. Stehlik, and T.A. Roelofs. 2000. Decay kinetics and quantum yields of fluorescence in Photosystem I from *Synechococcus elongatus* with P700 in the reduced and oxidized state: are the kinetics of excited state decay trap-limited or transfer-limited? *Biophys. J.* 79:992-1007.
- (25) Valkunas, L., G. Trinkunas, V. Liulolia, and R. van Grondelle. 1995. Nonlinear annihilation of excitations in photosynthetic systems. *Biophys. J.* 69:1117-1129.
- (26) Van Grondelle, R. 1985. Excitation energy transfer, trapping and annihilation in photosynthetic systems. *Biochim. Biophys. Acta.* 811:147-195.
- (27) Du, M., X. Xie, Y. Jia, L. Mets, and G.R. Fleming. 1993. Direct observation of ultrafast energy transfer in PSI core antenna. *Chem. Phys. Lett.* 201:535-542.

- (28) Kennis, J.T.M., B. Gobets, I.H.M. van Stokkum, J.P. Dekker, R. van Grondelle, and G.R. Fleming. 2001. Light harvesting by chlorophylls and carotenoids in the Photosystem I complex of *Synechococcus elongatus*: a fluorescence upconversion study. *J. Phys. Chem. B.* 105:4485-4494.
- (29) Holzwarth, A.R., G. Schatz, H. Brock, and E. Bittersmann. 1993. Energy transfer and charge separation kinetics in Photosystem I Part 1: Picosecond transient absorption and fluorescence study of cyanobacterial Photosystem I particles. *Biophys. J.* 64:1813-1826.
- (30) Hastings, G., F.A.M. Kleinherenbrink, S. Lin, and R.E. Blankenship. 1994. Time-resolved fluorescence and absorption-spectroscopy of Photosystem-I. *Biochemistry.* 33:3185-3192.
- (31) Karapetyan, N.V., D. Dorra, G. Schweitzer, I.N. Bezsmertnaya, and A.R. Holzwarth. 1997. Fluorescence spectroscopy of the longwave chlorophylls in trimeric and monomeric Photosystem I core complexes from the cyanobacterium *Spirulina platensis*. *Biochemistry.* 36:13830-13837.
- (32) Savikhin, S., W. Xu, V. Soukoulis, P.R. Chitnis, and W.S. Struve. 1999. Ultrafast primary processes in Photosystem I of the cyanobacterium *Synechocystis* sp. PCC 6803. *Biophys. J.* 76:3278-3288.
- (33) Melkozernov, A.N., S. Lin, and R.E. Blankenship. 2000. Excitation dynamics and heterogeneity of energy equilibration in the core antenna of Photosystem I from the cyanobacterium *Synechocystis* sp. PCC 6803. *Biochemistry* 39:1489-1498.
- (34) Pålsson, L.-O, S.E. Tjus, B. Andersson, and T. Gillbro. 1995. Energy-transfer in Photosystem-I - time-resolved fluorescence of the native Photosystem-I complex and its core complex. *Chem. Phys.* 194:291-302.
- (35) Kruip, J., E.J. Boekema, D. Bald, A.F. Boonstra, and M. Rögner. 1993. Isolation and structural characterization of monomeric and trimeric Photosystem-I complexes (P700F_a/F_b and P700F_x) from the cyanobacterium *Synechocystis* PCC-6803. *J. Biol. Chem.* 268:23353-23360.
- (36) Fromme, P., and H.T. Witt. 1998. Improved isolation and crystallization of Photosystem I for structural analysis. *Biochim. Biophys. Acta.* 1365:175-184.
- (37) Kruip, J., N.V. Karapetyan, I.V. Terekhova, and M. Rögner. 1999. *In vitro* oligomerization of a membrane protein complex. *J. Biol. Chem.* 274:18181-18188.
- (38) Greene, B.J., and R.C. Farrow. 1983. The subpicosecond kerr effect in CS₂. *Chem. Phys. Lett.* 98:273-276.
- (39) Hoff, W.D., I.H.M. van Stokkum, H.J. van Ramesdonk, M.E. van Brederode, A.M. Brouwer, J.C. Fitch, T.E. Meyer, R. van Grondelle, and K.J. Hellingwerf. 1994. Measurement and global analysis of the absorbance changes in the photocycle of the photoactive yellow protein from *Ectothiorhodospira halophila*. *Biophys. J.* 67:1691-1705.
- (40) Holzwarth, A.R. 1996. Data analysis of time-resolved measurements. In *Biophysical techniques in photosynthesis*. J. Amesz, and A.J. Hoff, editors. Kluwer, Dordrecht, the Netherlands. 75-92.
- (41) Rätsep, M., T.W. Johnson, P.R. Chitnis, and G.J. Small. 2000. The red-absorbing chlorophyll-*a* antenna states of Photosystem I: A hole-burning study of *Synechocystis* sp PCC 6803 and its mutants. *J. Phys. Chem. B.* 104:836-847.
- (42) Hayes, J.M., S. Matsuzaki, M. Rätsep, and G.J. Small. 2000. Red chlorophyll-*a* antenna states of Photosystem I of the cyanobacterium *Synechocystis* sp. PCC 6803. *J. Phys. Chem. B.* 104:5625-5633.
- (43) Limantara, L., R. Fujii, J.P. Zhang, T. Kakuno, H. Hara, A. Kawamori, T. Yagura, R.J. Cogdell and Y. Koyama. 1998. Generation of triplet and cation-radical bacteriochlorophyll-*a* in carotenoidless LH1 and LH2 antenna complexes from *Rhodobacter sphaeroides*. *Biochemistry* 37: 17469-17486.

-
- (44) Gobets, B., J.P. Dekker, and R. van Grondelle. 1998. Transfer-to-the-trap limited model of energy transfer in Photosystem I. *In* Photosynthesis: Mechanisms and effects. G. Garab, editor. Kluwer Academic Publishers, Dordrecht, The Netherlands. 1:503-508.
- (45) Gobets, B., I.H.M. van Stokkum, F. van Mourik, M. Rögner, J. Kruip, J.P. Dekker, and R. van Grondelle. 1998. Time-resolved fluorescence measurements of Photosystem I from *Synechocystis* PCC 6803. *In* Photosynthesis: Mechanisms and effects. G. Garab, editor. Kluwer Academic Publishers, Dordrecht, The Netherlands. 1: 571-574.
- (46) Trinkunas, G., and A.R. Holzwarth. 1994. Kinetic modeling of exciton migration in photosynthetic systems. 2. Simulations of excitation dynamics in 2-dimensional photosystem core antenna/reaction center complexes. *Biophys. J.* 66:415-429.
- (47) Peterman, E.J.G., S.O. Wenk, T. Pullerits, L.-O. Pålsson, R. van Grondelle, J.P. Dekker, M. Rögner, and H. van Amerongen. 1998. Fluorescence and absorption spectroscopy of the weakly fluorescent chlorophyll-*a* in cytochrome b(6)f of *Synechocystis* PCC6803. *Biophys. J.* 75:389-398.
- (48) Laible, P.D., W. Zipfel, and T.G. Owens. 1994. Excited-state dynamics in chlorophyll-based antennae - the role of transfer equilibrium. *Biophys. J.* 66:844-860.
- (49) Savikhin, S., D.R. Buck, and W.S. Struve. 1999. The Fenna-Matthews-Olson protein: a strongly coupled photosynthetic antenna. *In* Resonance energy transfer. D.L. Andrews, and A.A. Demidov, editors. John Wiley & Sons, Inc., New York, USA. 399-434.
- (50) Gradinaru, C.C., S. Özdemir, D. Gülen, I.H.M. van Stokkum, R. van Grondelle, and H. van Amerongen. 1998. The flow of excitation energy in LHCII monomers: Implications for the structural model of the major plant antenna. *Biophys. J.* 75:3064-3077.

4

Energy transfer and trapping in Photosystem I

Bas Gobets and Rienk van Grondelle

This chapter has been published in *Biochimica et Biophysica Acta* 1507, 80-99, reproduced with permission. © 2001 Elsevier Science

INTRODUCTION

The primary processes in all photosynthetic systems involve the absorption of energy from (sun) light by chromophores in a light-harvesting antenna, and the subsequent transfer of this energy to a reaction centre (RC) site where the energy is "trapped" by means of a stable charge separation.

Photosystem I (PSI) is one of two such photosystems in oxygenic photosynthesis. When co-operating with Photosystem II (PSII) it uses the energy of light to transfer electrons from plastocyanin or soluble cytochrome c_6 to ferredoxin and eventually to NADP^+ . In an alternative pathway, the electrons from ferredoxin are transferred back to plastocyanin via the Cytochrome b_6f complex. This cyclic electron transport, which does not require the input of free energy by PSII, results in a transmembrane electrochemical gradient that can be used to produce ATP.

In plants and green algae the PSI complex consists of two separable functional units: The PSI core, and the Light-Harvesting Complex I (LHCI) peripheral antenna. The PSI complex in cyanobacteria does not possess the peripheral LHCI antenna, but since the PSI core complexes of cyanobacteria bear a large resemblance to the core complex of plants, a direct comparison of the energy transfer and trapping properties of these complexes is justified.^{1,2}

BASIC FEATURES OF THE PSI COMPLEXES

PSI core

The PSI core is a large pigment-protein complex consisting of 11 to 13 protein subunits,³ the largest two of which, PsaA and PsaB, form a heterodimer to which the majority of the core antenna pigments, as well as most of the reaction centre co-factors are bound. Spectroscopic data indicate that the core antenna and reaction centre contain approximately 90-100 chlorophyll-*a* (chl*a*) and 10-25 β -carotene molecules in total.

The PSI core complexes of cyanobacteria can be isolated both as monomers and trimers, which are both equally efficient in energy transfer and charge-separation.⁴ It is not fully clear which one is the native conformation, although it is very likely that a dynamic equilibrium exists between monomers and trimers in the membrane, which can be regulated by, for instance, the salt-concentration.⁵ In contrast, plant PSI core complexes do not assemble as trimers, although the peripheral LHCI antenna does not cause structural hindrances for the type of trimerization as observed in cyanobacterial PSI.⁶

The structure of the PSI core complex of the cyanobacterium *Synechococcus elongatus* has been resolved up to 4 Å resolution,⁷⁻⁹ and will be discussed below in terms of its energy-transfer capacity.

Light-Harvesting Complex I

The peripheral LHCI antenna complex of plants is composed of four different proteins Lhca1-4, which have molecular masses ranging from 20-24 kDa, and which are thought to be present in approximately equal amounts.¹⁰ The Lhca1-4 proteins, which bind on the average 8 chl*a*, 2 chl*b* and 2 carotenoid molecules,^{11,12} assemble as dimers. Lhca1 and Lhca4 have been

shown to form a heterodimer^{13,14} which exhibits a red-shifted low-temperature steady-state emission maximum at 730 nm,¹⁰ and which has therefore been designated LHCI-730.

Biochemical data suggest that Lhca2 and Lhca3 assemble as homodimers rather than as heterodimers.¹³ The 77K fluorescence of these complexes is usually reported to peak at 680 nm, and therefore they so far have been designated LHCI-680.¹⁰ It has recently been suggested, however, that LHCI-680 represents monomeric Lhca2 and Lhca3, degradation products of the dimers, representing the functional complexes *in vivo*.¹⁵ This idea is further corroborated by recent low-temperature (5K) spectroscopy experiments on a mixture of dimers of Lhca1-4 that, in addition to the 730 nm emission, demonstrate the presence of an emission band at ~702 nm (F702), possibly due to Lhca2/Lhca3 homo/hetero dimers.¹²

The pigment stoichiometry of LHCI is very similar to that found for CP29, one of the minor antenna proteins of PSII. The LHCI proteins show a large sequence homology to CP29 as well as to other plant light-harvesting proteins,¹⁰ such as LHCII, which is presently the only Lhca/b protein for which a high resolution (3.4 Å) structure exists.¹⁶ It may therefore be speculated that the general fold of LHCI resembles that of LHCII and the model proposed for the pigments organization in CP29 may also be applied to LHCI.¹⁷

PSI-200

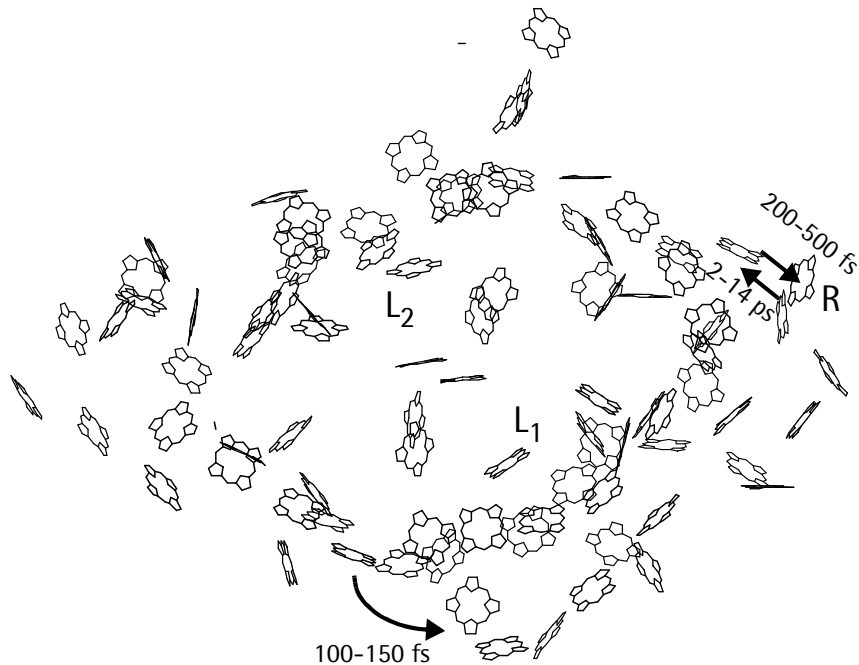
In plants 3-4 or possibly 5 LHCI dimers bind to a PSI core particle to assemble into a complex which contains a total of 170-200 chls and which is designated PSI-200.^{6,11} Earlier results suggested that these LHCI dimers completely surround the core.¹⁸ More recent electron microscopy data indicate, however, that all LHCI dimers are located on one side of the core complex.⁶

Structure of the PSI core

In the 4 Å structure of the PSI core complex of the cyanobacterium *Synechococcus elongatus* 89 chl molecules were identified so far, including the 6 chl a molecules of the electron transfer chain.⁷⁻⁹ These chlorophyll sites are shown in figure 4.1, in which the direction of view is perpendicular to the membrane plane. The porphyrin rings which are shown in figure 4.1 indicate the planes in which the rings lie, rather than the exact orientation, which could not be derived from the 4 Å structure.

The RC, i.e. those chlorophylls and cofactors involved in primary electron transfer, is located in the centre of the structure, bound between PsaA and PsaB. The two parallel oriented chls, which are located in the middle of the structure, constitute the primary electron donor P700. The pairs of chls which are located on both sides in the direct vicinity of P700 represent the primary electron acceptor, A₀, and the accessory chls. Also other components of the electron-transfer chain, including three Fe₄S₄ iron-sulphur clusters F_x, F_A and F_B, could be assigned in the structure. The location of the two phylloquinones, which constitute A₁, was determined by combining the structural data with single crystal EPR results.^{19,20}

The remaining 83 core antenna chls are found to be arranged in a more or less elliptically shaped bowl-like structure surrounding the reaction centre. The distance of most antenna chls to any of the RC chls is found to be larger than 20Å. However, two antenna chls located at ~14Å from the closest RC pigments stand out in the structure, forming a structural, and possibly functional bridge between the other antenna chls and the RC.



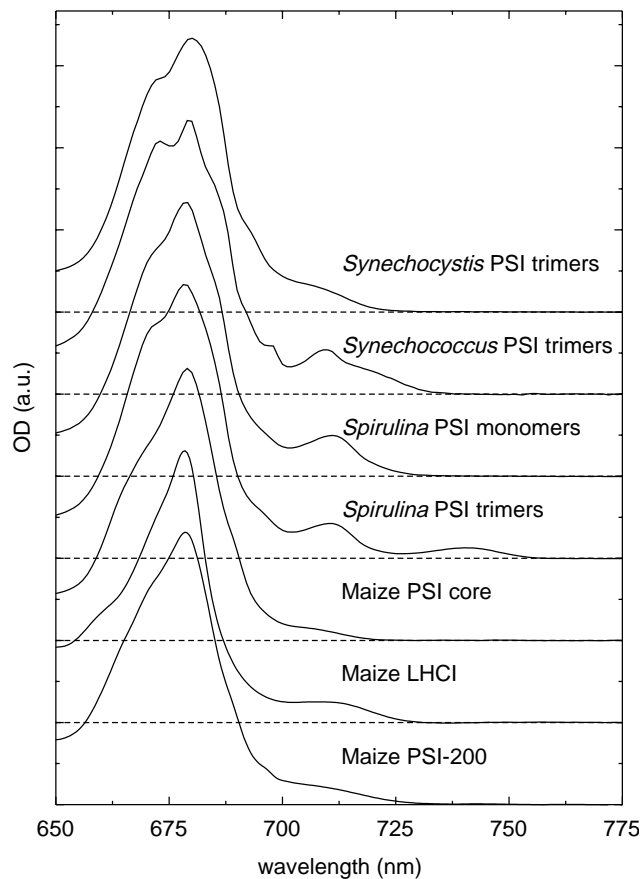
4.1 Positions of chls in PSI as found in the 4 Å structure. The porphyrin rings indicate the plane of the chls rather than the exact orientation in the plane. L1 and L2 indicate the proposed "linker" chls. The indicated rates were calculated as described in the text. R represents a hypothetical red chl.

Previously, in the absence of a structure, the modelling of the energy-transfer dynamics in PSI was often based on square or cubic lattices.²¹⁻²⁴ For a given configuration, these models generally involve 2 separate rates: the energy transfer ("hopping") rate between two sites, and the intrinsic trapping rate from a site representing the primary electron donor P700. This has led to two limiting cases for the dynamics in PSI. In the first, transfer limited case, the energy-transfer rate determines the decay of the excited state due to trapping, while in the second, trap limited case, the intrinsic rate of charge separation from P700 governs these dynamics. The structure in figure 4.1 shows, however, that the primary electron donor, P700, is not just another site on a lattice. The distance between P700 and the antenna chls is significantly larger as compared to the distance between adjacent antenna chls. Therefore a model describing the energy transfer in PSI should include (at least) two energy-transfer rates instead of one: a high rate between the antenna chls, and a lower rate from the antenna to the reaction centre. This leads to a third limiting case; the so-called transfer-to-the-trap limited case, in which the energy transfer from the antenna to the RC is limiting the overall dynamics.²⁵ Such a model, in which two distinctly different distance scales appear, was already proposed before the availability of the structure, based upon an analogy with the arrangement in purple bacteria^{26,27} in which the bacterial RC is surrounded by the LHI ring. Such a ring-like organization of the antenna around the RC appears to be a common feature in photosynthesis. It can easily be shown that such an organization is a prerequisite for an efficient photosystem including a bulky reaction centre. A system in which the RC is located in

the centre of a ring-like structure, with a relatively large average distance to each antenna chl, but in contact with many of them collects excited state energy much more efficiently than a system in which the RC would be located at the periphery of the antenna to which it is linked by only a few antenna chls.

LOW-ENERGY ("RED") CHLOROPHYLLS

Both the Photosystem I core and the peripheral LHCI antenna are spectrally highly heterogeneous, as can clearly be seen from figure 4.2 in which the low-temperature (6 K) absorption spectra of the Q_y -region of a number of PSI core complexes, LHCI and PSI-200 are displayed. The major part of the core antenna chlorophylls, which we refer to as "bulk" chls, absorb in a broad band which shows a maximum at 680 nm. This has to be compared to the absorption profile of isolated chl a which displays a single broad maximum at ~670 nm in organic solvents.²⁸ The low-temperature absorption spectra (figure 4.2) clearly exhibit shoulders both on the blue and the red flanks.^{4,29-34} An even more striking feature of all (intact) PSI complexes, is the presence of a relatively small number of red-shifted chlorophylls



4.2 6K absorption spectra of various cyanobacterial PSI cores and the different plant PSI complexes.

that absorb at energies lower than that of the primary electron donor P700. Although the number of these low-energy chls is small, 3% to 10% of the total number of chls, they have a very pronounced effect on the energy transfer and trapping in the whole PSI system, which is evident from both time-resolved and steady-state spectroscopy experiments. The function of these red chls and the nature of their extreme red shift, are some of the key issues in the spectroscopy of PSI.

Properties of the red chl pools

Red chls in cyanobacterial PSI cores

In PSI cores of cyanobacteria, the amounts and energies of the low-energy chls appear to be highly species-dependent^{29-31,33,35} (see figure 4.2). Moreover, the red chl forms are also affected by the aggregation state of the cyanobacterial core complexes: in monomeric PSI core preparations the number of red chls is generally found to be lower than in trimers. Especially the amplitude of the most red-shifted chl band may depend strongly upon the aggregation state, which is easily observed upon comparison of the 6 K absorption spectra of isolated monomeric and trimeric PSI from *Spirulina platensis* (spectra 3 and 4 in figure 4.2). It has been shown that upon trimerization of isolated monomers of *Spirulina platensis* the trimer red chl absorption emerges,³⁶ indicating that the difference between monomers and trimers is not so much the actual loss of chls in the monomers, but rather that the red shift is due to an interaction induced by trimerization. This effect suggests that these red chls are located in the periphery of the PSI core, in the region where the monomers within the trimer are in contact.³⁷

Since the absorption bands of red chls are quite distinct at 4 K, the maxima of these bands and the number of chls contained in them can be estimated by Gaussian decomposition of the absorption spectra (table 1). For trimeric PSI core particles from the cyanobacterium *Synechocystis* PCC 6803 (figure 4.2, spectrum 1) this procedure reveals an inhomogeneously broadened absorption band with a maximum at 708 nm (C708) which carries an oscillator strength of 4-5 *chl*a molecules.³⁸ Hayes et al.,³⁹ however, have suggested on the basis of holeburning experiments, that 2 chls contribute to C706 and another 2 chls contribute to C714. We, however, do not find any spectroscopic evidence for the presence of two distinct pools of red chls in the PSI core of *Synechocystis*. The low-temperature absorption spectra of *Synechocystis* PSI displayed in figure 4.2 do not show any structure in the red tail. Also in the analysis³⁸ of our time-resolved streak camera data nothing hints at a heterogeneity of the red chls in *Synechocystis* PSI. We therefore favour the picture of a single, inhomogeneously broadened band of (C708) chls in *Synechocystis* PSI,³³ although this band could result from two separate *chl*a dimers. We note that monomers of *Synechocystis* exhibit about 30% less red chls as compared to trimers.^{38,40}

Two separate red absorption bands are found in the 4 K absorption spectrum of the trimeric core particles of the cyanobacterium *Synechococcus elongatus* (figure 4.2, spectrum 2) with maxima at 708 nm (C708, corresponding to 4-6 *chl*a's) and 719 nm (C719, corresponding to 4 *chl*a's).³⁵ The monomers show a 50% reduction of C719 (not shown).⁴¹ In trimeric PSI cores of the cyanobacterium *Spirulina platensis* (figure 4.2, spectrum 4) two red bands are found peaking at ~708 nm (C708, corresponding to ~7 *chl*a) and 740 nm (C740,

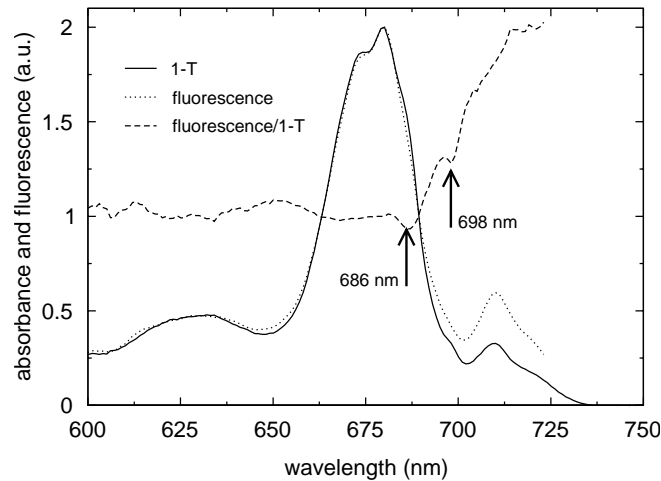
Table 4.1 6K and room temperature low-energy chl*a* absorption and emission

species	pool #1					pool #2				
	absorption (nm)		emission (nm)		# chls /100	absorption (nm)		emission (nm)		# chls /100
	6K	RT	6K	RT		6K	RT	6K	RT	
<i>Synechocystis</i> mon.	708	703	720	712	~3	-	-	-	-	-
<i>Synechocystis</i> tri.	708	702	720	711	~5	-	-	-	-	-
<i>Synechococcus</i> tri.	708	702		707	~5	719	708	730	723	~4
<i>Spirulina</i> mon.	708	702		712	5-7	719	708	730	721	1-3
<i>Spirulina</i> tri.	708	703		714	~7	740	715	760	730	~3
Maize PSI core	705		720		3	-	-	-	-	-
Maize LHCI	693		702		5	711		730		5

corresponding to ~3 chl*a*), the latter constituting the red-most absorbing species reported in any PSI complex. This very red-shifted form is absent in monomeric complexes,⁴² although 1-3 C719 chls seem to be present (figure 4.2, spectrum 3).³⁸ Careful comparison of the *Spirulina* monomeric and trimeric PSI spectra in figure 4.2, suggests that the increase of the C740 band is accompanied by the disappearance of an absorption band which peaks above 712 nm, suggesting that the C719 pool present in monomers may be further red shifted to 740 nm upon trimerization. Thus, all these PSI core particles share the presence of a C708 pool, while additional red forms are variable, both in amount and in spectral properties.

The presence of the low-energy chls has a strong effect on the (steady-state) emission properties of the PSI core complexes. In *Synechocystis* PSI core complexes, containing only 3-5 C708 red chlorophylls, the room temperature fluorescence emission spectrum exhibits a peak around 685-690nm (F685) with a broad shoulder due to red chls at ~710 nm.³⁰ In contrast, in *Synechococcus* and *Spirulina* PSI which contain more and longer wavelength absorbing red chls, the room temperature emission peaks above 700 nm, with F685 only appearing as a shoulder.^{43,44}

At low temperatures the emission from the red pigments fully dominates all fluorescence spectra, which peak at ~720 nm in *Synechocystis* (F720) and ~730 nm in *Synechococcus* (F730) (trimers). In trimers of *Spirulina* at low temperatures one emission band is always present, peaking at ~730 nm (F730). A second emission band, with a maximum at ~760 nm (F760), may or may not be observed, depending on the oxidation state of P700: if P700 is pre-oxidized (using ferri-cyanide) F760 is absent, whereas it is present if the primary electron donor is reduced. The relatively strong spectral overlap of the F760 fluorescence with the absorption spectrum of P700⁺ is thought to be the cause of this remarkable quenching of



4.3 6K fluorescence excitation spectrum of trimeric PSI core complexes of *Synechococcus elongatus*, detected above 780nm (dotted), the 1-T spectrum (solid) and their ratio (dashed). The indicated "dips" in our view represent the RC chls P700 and A_0 .

F760 emission.⁴⁵ Monomeric PSI cores of *Spirulina*, which do not exhibit the extreme C740 long-wavelength chls, only show F730 fluorescence.

At room temperature the quantum yield of fluorescence of all PSI core particles is low,²⁵ and the quantum yield of charge separation is more than 95%. A decrease of the temperature, however, induces a dramatic increase of the fluorescence quantum yield of these PSI particles,^{33,41,46} since a large fraction of excitations is trapped at the low-energy chls at low temperatures. This is elegantly demonstrated in a long-wavelength fluorescence excitation spectrum measured for PSI of *Synechococcus* at low temperature (fig. 4.3). Excitation of the bulk antenna yields about 50% of the fluorescence as compared to direct excitation of the red chls, indicating that only about half of the excitations in this species are quenched in the RC without passing through the red chls. We note the clear 'dips' in the excitation spectrum at 686 and 698 nm, which in our view correspond to RC absorption bands of the primary electron acceptor A_0 and P700, which, upon excitation, have a very low probability of transferring energy to the emitting red chls.

Red chls in plant PSI complexes

In plants, the PSI complex PSI-200 can be separated into the PSI core and the peripheral light-harvesting complex LHCl.¹¹ Each of these constituents contains a specific set of long-wavelength chls. The PSI core of maize (figure 4.2, spectrum 5) mostly resembles the core of *Synechocystis*: At 4 K it exhibits one absorption band of red chls peaking around 705 nm (C705, ~3 chl a) (Gobets and Ihalainen, unpublished data) and has a low temperature emission maximum around ~720 nm (C720).¹¹ LHCl (figure 4.2, spectrum 6) appears as a mixture of the LHCl-730 dimer and homo/hetero dimers of Lhca2 and Lhca3 (see above). Recent experimental results indicate that a red chl pool with an absorption maximum at 711 nm is responsible for the low-temperature emission of LHCl-730.¹² Furthermore, recent fluorescence excitation and emission experiments on a mixture of Lhca1-4 have revealed another, new, low-temperature

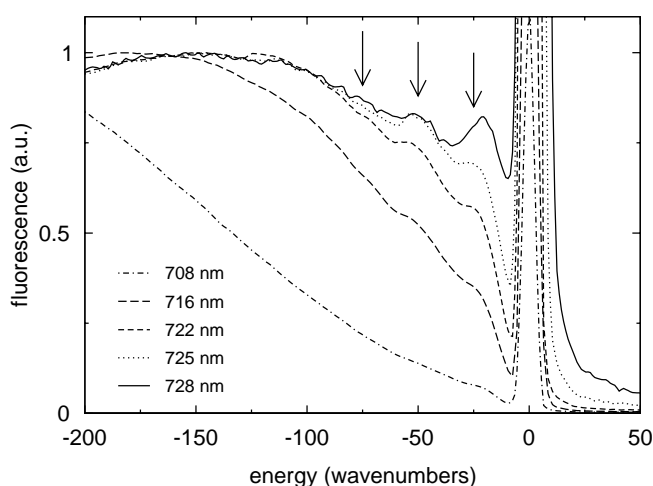
emission band at 702 nm, corresponding to a pool of (relatively) red chls absorbing around 693 nm. These new spectral features may be the fingerprint of another dimer in LHCl.¹² Room temperature time-resolved fluorescence measurements on the same preparation also indicate the presence of (at least) two spectroscopically different dimers in LHCl.⁴⁷

In PSI-200 the spectroscopic characteristics of the plant PSI core and LHCl are combined, resulting in a broad, featureless band of red chl absorption (figure 4.2, spectrum 7). At low temperatures the fluorescence of PSI-200 is dominated by emission from LHCl-730, resulting in the emission maximum at 730-735 nm that is characteristic of plant PSI.

The nature of the long-wavelength chls

Energy selective fluorescence emission experiments at low temperature (6K) have been performed to determine the homogeneous and inhomogeneous line-widths of the bands of red chl, and to obtain their homogeneous line-shape.^{33,35,48} In all cases it was found that the Stokes' shift of the red chls is remarkably large. To illustrate this, in figure 4.4, energy selective emission spectra are presented for monomeric PSI cores of *Synechocystis*, which contain 3 to 4 C708 chls. The spectra are plotted on an energy scale, and are shifted relative to the wavelength of excitation, marked by a sharp scattering peak. For increasingly red-shifted excitation wavelengths, the emission band converges to the homogeneous line-shape, which exhibits a broad phonon wing. This phonon wing shows a maximum at 150 cm^{-1} , corresponding to a Stokes' shift of about 300 cm^{-1} (15 nm). Superimposed on the smooth phonon wing, a distinct progression can be discerned, at 25 cm^{-1} intervals. Both the large Stokes' shift and this progression are unique for the red pigments in PSI and are not observed in other chl *a* containing photosynthetic systems, such as LHClI, Cyt *b*₆*f* and the PSII RC.⁴⁹⁻⁵¹

Preliminary modelling of the emission spectra in figure 4.4 indicates that the Huang Rhys factor *S* for the phonons equals 3 or even more.⁴⁸ In a recent holeburning study by Rätsep et



4.4 6K energy selective emission spectra of monomeric PSI core complexes of *Synechocystis* PCC6803 for increasingly red-shifted excitation wavelengths. The spectra were shifted such that the scatter of the excitation light coincides with zero. The arrows at 25 cm^{-1} intervals indicate the phonon progression (see text).

al.⁴⁰ on *Synechocystis* PSI this S-value was estimated to be 2. This should be compared to for instance LHClI for which an S-value of 0.6 was found.⁴⁹ The most straightforward interpretation of this remarkable difference is that the emitting species in *Synechocystis* is not a monomeric chl a , but for example (a) strongly coupled chl a dimer(s) or maybe even a larger aggregate of chl a .³³ For PSI complexes from *Synechococcus* and *Spirulina*, which exhibit even more red-shifted chl pools, we find that these S-values are even larger and consequently we propose that also in these systems the red chls correspond to dimers or larger aggregates of chl a , in view of the further red shift and the larger number of chls involved in these red bands.

The function of the long-wavelength chls

The function of the red chl species is still a topic of much debate. Intuitively it would appear that the effect of their presence would be a decrease of the overall efficiency of energy transfer to the reaction centre by forming local traps for excitations. Some authors have suggested, however, that in a non-equilibrium situation they may help increasing the efficiency of the system by concentrating excitations close to P700.^{23,43,52-54} Others argue that the red chls may have a role in photoprotection.^{37,52} The above mentioned quenching of excitations located on the red-most pools of chls by P700⁺ could provide a pathway to prevent the formation of chl triplet states, which can lead to the formation of harmful singlet oxygen, under strong illumination conditions.^{37,45}

Another function of the low-energy chls that has been proposed could simply be the increase of the cross-section for absorption of red light by the PSI antenna.^{55,56} In a recent publication Rivadossi et al. investigated the importance of the long-wavelength chls of PSI in photosynthetic light harvesting by leaves. It was demonstrated that although the PSI red forms account for only a few percent of the total light absorption in a normal 'daylight' environment, in a different "shadelight" environment, depleted in ~680 nm light, the long-wavelength pigments may be responsible for up to 40% of total photon capture.⁵⁷

Alternatively, the red chls may simply be a consequence of the relatively dense packing of chls in the PSI core antenna: the chlorophyll concentration in the PSI core is significantly larger than in other photosynthetic antenna complexes. If chl is dissolved in an organic solvent at such a high concentration, such a solution exhibits some extraordinary properties: the fluorescence quantum yield decreases dramatically, whereas the absorption spectrum remains unchanged compared to lower concentrations.⁵⁸ This is thought to be the result of extensive energy transfer in the concentrated chl solution followed by quenching due to for instance a few unfavourably organized (sandwiched) chl a dimers. Such sites are apparently not present in PSI, since they would dramatically decrease the efficiency of the system. As a side-effect the constraint of avoiding sandwiched pairs could result in the occurrence of some excitonically coupled head-to-tail dimers or larger head-to-tail aggregates with a strongly red-shifted absorption maximum. A striking example of a system in which dense head-to-tail packing of pigments results in strong excitonic coupling are chlorosomes, the antenna complexes of green sulphur bacteria, which contain several thousands of Bchl c molecules. These antennae have a maximal absorption at 740 nm whereas monomeric Bchl c has a absorption maximum at 660 nm. In addition it was shown that the effective oscillator strength of Bchl c in chlorosomes was 7-8 times that of monomeric chls.⁵⁹

DYNAMIC EXPERIMENTS

Experimental considerations

The core antenna of PSI is intimately bound to the PSI reaction centre and unlike in antenna-RC complexes of Photosystem II and bacterial photosystems it is not possible to biochemically separate the core antenna from the reaction centre. Therefore time-resolved experiments on native PSI have to be performed on systems with a large number (~100) of chl*a* molecules, all connected by energy transfer. Time-resolved spectroscopic experiments on such large antenna-RC complexes require the use of very low-energy excitation pulses, to avoid the process of singlet-singlet annihilation (see refs. 60 and 61 for a review). This process can occur in complexes in which simultaneously two or more excitations are present: due to efficient energy transfer two excitations may collide at one single chl, which will then be raised to its second singlet excited state (S_2), from which rapid (< 100 fs) internal conversion to the first singlet excited state (S_1) occurs. Singlet-singlet annihilation thus effectively removes excitations from the system resulting in additional non-physiological decay components. It must be stressed that in order to prevent singlet-singlet annihilation from occurring it is by far not sufficient to match the number of absorbed photons to the number of complexes in the sample volume. Since the distribution of absorbed photons is governed by Poisson statistics it can easily be shown that the fraction of excited complexes with more than one excitation, is given by $P(>1)/P(>0) = (e^\mu - 1 - \mu)/(e^\mu - 1)$ in which μ is the average number of excitations per complex. For $\mu=1$ this yields 41% multiple excitations. In order to get this fraction below 10% each laser shot should excite less than 1 out of every 4 complexes, or to put it differently: only 1 out of 400 chls should be excited by each pulse. In practice this implies that pulse energies of a nJ or less have to be used. With such low energies a high repetition rate laser is required to limit the data acquisition time. Yet the repetition rate in its turn is limited by the requirement that before each new laser pulse the sample has to be either completely recovered from the previous excitation event, or has to be replaced by "fresh" sample. Reduction of P700⁺ in the presence of sodium ascorbate and PMS takes about 2 ms,⁴⁶ thus limiting the repetition rate to ~500 Hz in case no sample refreshment is performed. This is almost always the case in low-temperature experiments, since (rapid) sample refreshment in a cryostat is practically impossible. On the other hand at room temperature the sample can be refreshed using a spinning cell or a flowcell with a (peristaltic) pump. With the former a repetition rate of about 100 kHz can be used safely, for a flowcell the repetition rate can generally not exceed 10 kHz, if total sample refreshment is required.

Even if experiments are performed very carefully, the detail of the processes that can be distinguished is limited. In an antenna-RC complex containing 100 chl molecules, in principle 100 separate lifetimes are present in the excitation decay process. One can at best resolve a fraction of those lifetimes, but only if relatively selective excitation and detection is possible. Since the individual absorption and emission spectra of the 100 chls in PSI cores are strongly overlapping, this condition of selectivity can only be met to a very limited extent, and consequently only a small number of (average) kinetic processes can be discerned.

Table 4.2 Observed rate constants for different PSI complexes after aselective excitation at physiological temperature

species	single step transfer (fs)	equilibration in bulk	equilibration with red (ps)	trapping (ps)	ref.	technique*
<i>Chlamydomonas reinhardtii</i> PSI core	180 fs	5.4 ps			69	UPC
<i>Synechocystis</i> monomeric and trimeric PSI cores			4.4-4.7	23-24	38	SSC
		500 fs	2.3	25	64	PP
		400 fs	4.8 or 2, 6.5	22-24	63	PP
			3.7	24	34	PP
<i>Synechococcus</i> trimeric core	130 fs	360 fs	3.6, 9.6	38	70	UPC/SSC
			3.8, 9.6	36	38	SSC
			7-12	30-35	43	SPT/PP
			14	38	46	SPT
<i>Spirulina</i> monomeric core			3.7, 12.9	38	38	SSC
			9	28, 69	68	SPT
<i>Spirulina</i> trimeric core			4.3, 15.1	51	38	SSC
			9	31, 65	68	SPT
Plant core			8	22	#	SSC
PSI-200			5.4, 15	67	#	SSC
			11	57, 130	96	SPT

* UPC=Fluorescence Upconversion, SSC=Synchroscan Streakcamera, PP=Pump-Probe, SPT=Single Photon Timing. # (Gobets and Ihalainen, unpublished data)

Spectral-temporal processes in PSI.

During the past decade, PSI complexes of a wide variety of species have been studied by several groups using (sub-)picosecond time-resolved spectroscopic techniques including pump-probe,^{23,34,43,62-67} Single Photon Timing (SPT),^{4,32,43,46,68} Fluorescence Upconversion^{69,70} and the use of a Synchroscan Streakcamera.^{38,48,71} The values of the time constants which have been found for aselective or bulk excitation at room temperature and which have been

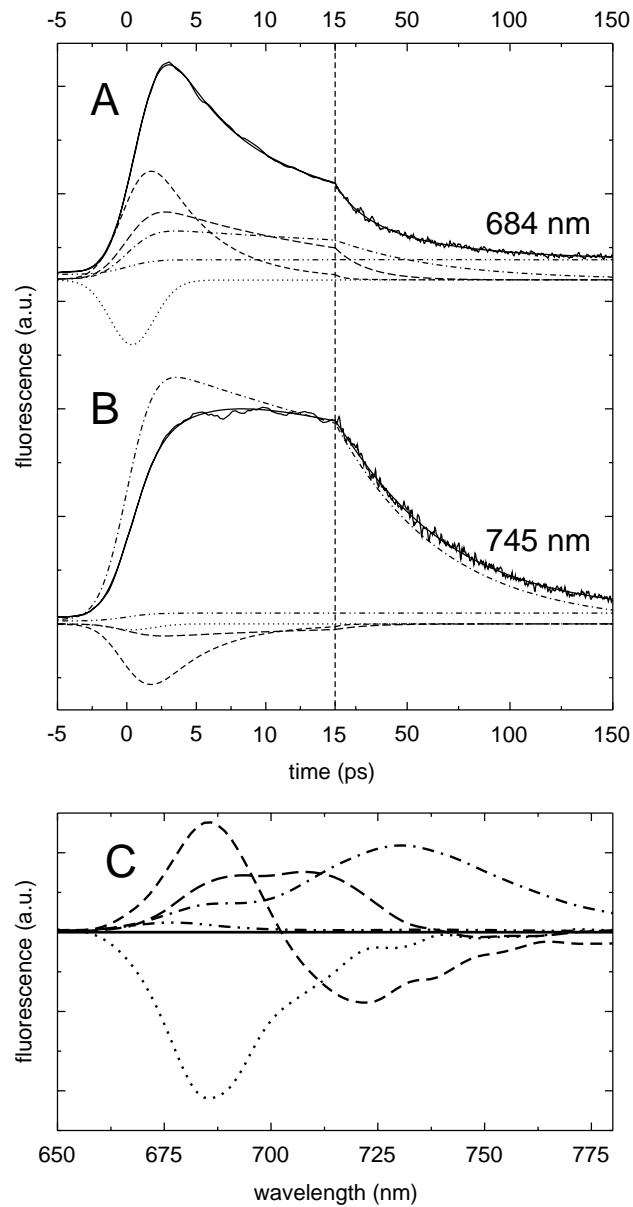
ascribed to various steps in the energy transfer and trapping processes in PSI are summarized in table 2. We will illustrate the different processes that occur using figure 4.5, in which streak camera fluorescence emission data are shown for *Spirulina* trimeric PSI, along with the results of a global analysis fitting procedure.³⁸ In figure 4.5a and b, traces are shown for bulk (684 nm) and red chl (745 nm) emission, and the different lifetime components that contribute to the emission. Figure 4.5c displays the decay-associated spectra that resulted from a global analysis of these data.

The individual energy-transfer steps between two chls are the fastest energy-transfer events that occur in PSI. Since the excited state energy levels of these two chls are not necessarily different, it may not be possible to resolve these steps in isotropic measurements. Anisotropic pump-probe or fluorescence upconversion techniques can reveal energy transfer between such iso-energetic pigments, provided that the absorption and emission dipole moments of donor and acceptor are not parallel. The lifetimes of these single step transfer processes in the PSI core antenna range between 100 and 200 fs.^{69,70} The streak camera measurements displayed in figure 4.5 do not reveal these ultrafast processes. The fastest process recorded in these measurements (dotted), which is fitted with a 0.4 ps timeconstant does not reflect energy transfer, but represents the ingrowth of Q_y fluorescence upon relaxation from the initially excited Soret band³⁸ (We note that the instrument response of 3 ps limited the accuracy with which this lifetime could be determined).

Energy redistribution processes, during which the initial distribution of excited antenna molecules transforms into a thermally more equilibrated distribution take place on a (somewhat) slower time-scale. Since such equilibration processes involve energy transfer between chls absorbing at different energies, they appear as a decrease of fluorescence or bleaching in one part of the spectrum, and an increase of fluorescence or bleaching in another. In figure 4.5a-c the 3.9 ps (dashed) and 15.0 ps (long-dashed) components represent such spectral equilibration components. It must be stressed that equilibration lifetimes generally do not correspond to single step energy-transfer processes, but reflect the overall result of a (large) number of those steps. Often equilibration components are not "pure" in the sense that they also account for some non-equilibrium trapping, resulting in non-conservative energy-transfer spectra, since the total decay exceeds the ingrowth. The 15.0 ps equilibration spectrum in figure 4.5c, which is only slightly negative above 740 nm, represents a clear example of such a non-conservative spectrum.

In order to accurately record the equilibration processes in PSI, high time-resolution spectrally resolved techniques are required such as multicolour pump-probe, fluorescence upconversion or the use of a synchroscan streak camera.

Spectral equilibration between the bulk chls, absorbing between 660 nm and 690 nm, occurs in about 500 fs which, in view of the timeconstant for a single hop (100-200 fs), implies that only a few (<5) hops are required to complete spectral equilibration among bulk chl's in PSI.^{63,64,70} The lifetimes of the equilibration components between the bulk antenna and the various pools of red chls are species dependent and vary between 2 and 15 ps. For *Synechocystis* PSI, which we propose to exhibit only one single pool of red chls, usually only one single bulk to red equilibration component is reported, with a lifetime of 4 to 5 ps.^{4,34,38,48,63,65} However, recently equilibration lifetimes of about 2 ps were reported.^{63,64}



4.5 Room temperature time-resolved emission of trimeric PSI particles of *Spirulina platensis* for excitation at 400nm. A) bulk emission trace taken at 684 nm (noisy solid), the global analysis fit (solid) and the various lifetime contributions. Notice the trace is plotted on a linear-logarithmic scale. B) As A, but for detection of red chl emission at 745 nm. C) Decay-associated Spectra resulting from the global analysis fit. The fitted lifetimes were: 0.4 ps (dotted), 3.9 ps (dashed), 15.0 ps (long-dashed), 50.1 ps (dot-dashed) and 4.9 ns (double-dot-dashed).

Savikhin et al.⁶³ even report a second equilibration component with a lifetime of 6.5 ps. Such bi-exponential equilibration between bulk and red chls seems to be consistent with the two distinct red pools that have been proposed by Hayes et al.³⁹ (see above), but contradicts with other time-resolved spectroscopy results. This apparent discrepancy so far remains unsolved.

In *Synechococcus* PSI cores, which exhibit two distinct pools of red chls, clearly two distinctly different equilibration components are observed, with lifetimes of 3.8 and 9.6 ps.³⁸ These two separate lifetimes could not be resolved in earlier SPT experiments, which have yielded only a single lifetime of 12–14 ps.^{43,46} We note that this single lifetime and its associated spectrum have been the inspiration for a series of serious modelling attempts.^{24,43,46,72}

Like *Synechococcus* PSI, both *Spirulina* monomeric and trimeric PSI particles also exhibit two distinct bands of red chls, and consequently also in these systems equilibration with the red chls is bi-exponential.³⁸ In *Spirulina* monomeric PSI, fast equilibration between the bulk and the red chls occurs in 3.4 ps, and slower equilibration including a considerable amount of non-equilibrium trapping, occurs in 11.6 ps. In the trimeric PSI particles from *Spirulina*, the lifetimes of both equilibration components are somewhat slower, 3.9 ps and 15 ps respectively (figure 4.5). Also for these complexes the SPT technique has failed to accurately disentangle these two equilibration processes.

The excitation dynamics in the PSI core of plants seems to be quite similar to that of *Synechocystis*: since it contains only one pool of red chls, it exhibits only one single equilibration component with these red chls, with a lifetime of 8 ps, which is somewhat slower than observed in *Synechocystis* PSI (Gobets and Ihalainen, unpublished data). In PSI-200 a 5.4 ps equilibration lifetime is observed, which we assign to equilibration processes taking place both in the core and in LHCl. A second, 15 ps component probably represents a mixture of equilibration between the core and LHCl, equilibration within LHCl, and trapping from the core (Gobets and Ihalainen, unpublished data).

The general trend in all these complexes is that the rate of equilibration between the bulk chls and a pool of red chls increases with the size of the red pool, and the excited state energy of the chls contained in it, which is qualitatively consistent with the concept that these times reflect on one hand the search time in the PSI antenna and on the other hand the spectral overlap factor between the bulk and red chls.

The slowest process observed in all PSI cores is the trapping kinetics, representing the overall rate at which excitations disappear from the system by charge separation in the RC, after all spectral evolution processes have been completed. In time-resolved fluorescence spectroscopy experiments, trapping appears as the slowest component of the system, showing a fluorescence decay at all wavelengths of detection. In pump-probe experiments trapping is observed as the rate at which the spectrum of P700⁺ is formed (which generally lives infinitely on the time scale of these experiments). Since the trapping component typically has a lifetime of (several) tens of ps, it can be recorded quite accurately even with relatively low time-resolution techniques such as SPT. In figure 4.5 trapping is reflected by the 50.1 ps process (dot-dashed), which exhibits an all positive spectrum (figure 4.5c). The relative ease of recording the trapping kinetics is reflected by the consistency of the values, both for the trapping times in PSI cores from *Synechocystis* (22–25 ps) and *Synechococcus* (30–38 ps)

using a variety of techniques. In *Spirulina* PSI core monomers, which has a red chl composition quite similar to that of *Synechococcus* trimeric PSI cores, trapping occurs in 38 ps, while in the trimeric PSI cores from *Spirulina* which exhibit the extreme C740 red chls, the observed trapping time is 50 ps (figure 4.5).³⁸ Trapping in the plant core is similar to that of *Synechocystis*, and occurs in 22 ps, in agreement with the similar spectral properties of both cores.

These results clearly demonstrate the trend that a larger number and lower energies of red chls result in a slower trapping component. Whereas red chl contents and spectral properties constitute the key difference between the various core complexes, PSI-200 is a structurally different system due to the presence of the peripheral LHCl-complexes. Therefore the observed relatively slow 67-130 ps trapping time is not only the result of the large number of red chls, but also reflects the much larger average distance between the antenna chls in LHCl and the RC.

The slow 4.9 ns process (double-dot-dashed) in the fit displayed in figure 4.5 represents a contribution by some free chls in the preparation and therefore does not reflect a process in the PSI-core.

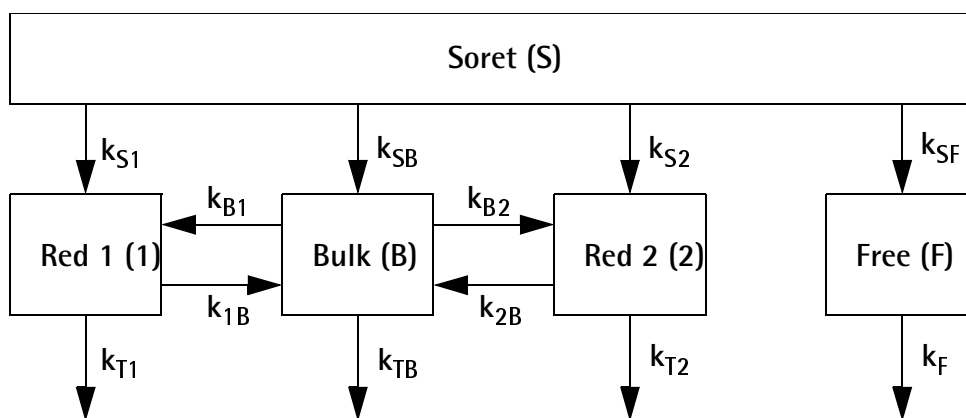
QUANTITATIVE (TARGET) ANALYSIS

So far we have made some qualitative remarks about the relation between the observed lifetimes in the various PSI-core complexes and the amounts and energies of the red chls present. Also the energies of the red pools, and their respective emission spectra have only been characterized at non-physiological, low temperatures. In order to make more quantitative statements about the effects of the red chls upon the energy transfer and trapping in PSI cores, and their absorption and emission properties under physiological conditions, we have recorded the fluorescence dynamics and spectral evolution of both monomeric and trimeric PSI core complexes from *Synechocystis* and *Spirulina*, and trimeric PSI core complexes of *Synechococcus* under identical experimental conditions at room temperature, and performed a target analysis of this data.³⁸

Model

We used the target analysis to test the hypothesis that the observed large kinetic differences between the different cyanobacterial core complexes can all be explained entirely in terms of the differences in the content and spectral properties of the red chls, implying that the properties of the bulk chl antenna do not differ significantly between these core complexes.

The time-resolved fluorescence experiments were performed with a synchroscan streak camera with a spectrograph, which has an instrumental response of ~3 ps, allowing us to resolve kinetics occurring significantly faster than 1 ps.³⁸ Using other techniques, either time-traces are measured sequentially for different detection wavelengths, or spectra are measured sequentially for different delay times. In contrast, the streak camera setup records spectral and temporal data simultaneously resulting in time-resolved fluorescence spectra of unprecedented quality allowing for a quantitative target analysis.



4.6 Compartmental model describing the kinetics of different cyanobacterial PSI core particles upon excitation at 400 nm.

Here we will summarize the procedure and results presented in ref. 38. The compartmental model used to analyse the time-resolved fluorescence data is presented in figure 4.6 and consists of 5 compartments, representing the Soret state (S) of all spectral forms, and the Q_y states of the bulk chl pool (B), two red-shifted chl pools (1 and 2) and a pool representing free chls which are not connected to the PSI core (F), but which have to be accounted for. The RC chls were not included in a separate compartment, since we aim to describe the energy transfer in the antenna rather than the intricate details of charge separation in the RC. Moreover, the number of RC pigments is small, and their spectral properties differ relatively little from those of the bulk chls. Therefore the (fast) kinetics of charge separation are not revealed directly by our data. For the modelling of *Synechocystis* PSI, one of the pools of red-shifted chls was omitted from the scheme.

The following rate constants were included in the model:

1. From the Soret compartment irreversible energy transfer occurs to the three or four Q_y compartments with the rate constants k_{SB} , k_{S1} , k_{S2} and k_{SF} . The sum of these rate constants, which represents the observed Soret- Q_y relaxation rate, measured 1.2 to 2.5 ps⁻¹. The four individual rates do not have an actual physical meaning, they merely account for the initial distribution of the excitations over the different compartments, and were adjusted such that all chls had an equal probability to be excited (aselective excitation);
2. Uphill and downhill energy transfer occurs between the red chl compartments and the bulk chl compartment with rate constants k_{B1} , k_{B2} , k_{1B} and k_{2B} . We have not included direct energy transfer between different pools of red chls since low-temperature fluorescence emission spectra of *Spirulina* trimeric PSI indicate that energy transfer between different pools of red chls is not very efficient,⁴² although energy transfer may occur between the two red pools in *Synechococcus* trimeric PSI.³⁵ At this point we discard it as a secondary effect;
3. Trapping occurs from the bulk chls and the red chl compartments with rate constants k_{TB} , k_{T1} and k_{T2} . It was found that all data sets could be described well using a fixed

value of k_{TB} of $(18 \text{ ps})^{-1}$, in accordance with our hypothesis that the properties of the bulk antenna are very similar for all PSI core complexes;

4. Free chl emission decays with a rate constant k_F , which measured about 0.2 ns^{-1} .

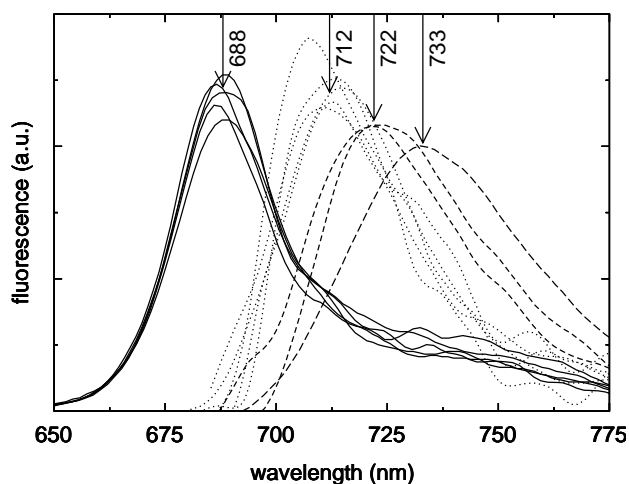
Since discrete spectral pools are used, inhomogeneous broadening, although known to be large for the long-wavelength chls,^{33,35} is not explicitly included in our model. The model described above was used to analyse our data, and we will discuss some specific results. More details of this analysis are reported in ref. 38.

Various kinetic models have been proposed to model time-resolved fluorescence or transient absorption measurements of PSI.^{32,43,63,73-75} In most of these models a "funnel"-like configuration of the various spectral types was proposed,^{32,43,63,74,75} in which the bulk antenna chls transfer energy to the red chls, which subsequently transfer energy to P700. Holzwarth et al.⁴³ and Savikhin et al.⁶³ also proposed a model in which trapping occurred exclusively from the bulk chls.

All these models explicitly assume the red chl forms to be located either very close to, or very distant from P700. Only Searle et al.⁷³ proposed a model, similar to our model presented in figure 4.6, which allowed for trapping both from the bulk chls and the red chls. We note, however, that only Turconi et al.³² and Holzwarth et al.⁴³ actually used their models to perform a target analysis of their data.

Species-associated emission spectra

The species-associated emission spectra (SAES) of the different pools of chls, resulting from the target analysis of the five different PSI preparations are presented in figure 4.7. All spectra are simply plotted together to demonstrate the striking similarities between the results obtained for different PSI particles. In all species the emission from the bulk compartment is represented by a spectrum (solid), which exhibits a maximum around 688 nm and which shows a distinct long red tail, extending beyond the window of observation. Except for a



4.7 Species-Associated Emission Spectra of target analysis of fluorescence decay of different cyanobacterial PSI core particles upon excitation at 400 nm. Arrows indicate the approximate maximum of the bulk spectra (solid), C708 spectra (dotted), C719 spectra (dashed) and C740 spectrum (long-dashed).

12 nm red shift, the spectra are nearly indistinguishable from the emission spectrum corresponding to the free chl compartment (not shown), which in its turn is very characteristic for the emission of monomeric chl a in solution.²⁸ The fact that the bulk spectra are indistinguishable between the different PSI species, underlines the absence of clear differences in the dominating band of the absorption spectra between different PSI core particles.

Also the spectra corresponding to the first (C708) pool of red chls (dotted), present in all studied cyanobacterial PSI core complexes, appear quite similar for all studied species, underpinning the strong similarity between C708 chls contained in the PSI cores of the different species. The C708 spectra are considerably broader than those of the bulk chls, reflecting the strong homogeneous and inhomogeneous broadening in this red chl pool.^{33,35,40} Note that the maxima of these spectra all appear around 712 nm, at significantly higher energy as compared to the low-temperature emission.

Probably even more remarkable are the emission spectra corresponding to the C719 pool (dashed), which represents the second pool of red chls occurring in *Synechococcus* PSI trimers and *Spirulina* PSI monomers, and which are practically identical. The maxima of these spectra occur at about 722 nm, and their width is somewhat larger than for the first (C708) pool of red chls, reflecting the even larger (in)homogeneous broadening of these pools.³⁵ The emission spectrum of the C740 pool (long-dashed), representing the second pool of red chls in *Spirulina* PSI trimers, reaches a maximum at 733 nm, and the spectrum is again broader than for the C719 pool, reflecting an even larger (in)homogeneous broadening of this pool.

The maxima of the all room temperature emission spectra of the different pools of red chls occur at wavelengths that are considerably blue shifted with respect to their low-temperature emission spectra. Part of this may be due to emission from higher energy red chls within the inhomogeneous distribution, which are not populated at low temperatures. Another part may be explained by a significant blue shift of the absorption maxima of these red pools at room temperature (see also below).⁴⁰

Energies of red chls at room temperature

The forward and backward energy-transfer rates³⁸ between the red and the bulk chl pools resulting from the target analysis, together with the stoichiometric estimates listed in table 1, were used to calculate the energy difference between the red chl pools and the bulk chls. To do so we applied the concept of detailed balance, stating that the energy difference between two different pools of chls, A and B, can be expressed as $\Delta E = k_b T \ln(N_A k_{AB} / N_B k_{BA})$, in which k_b represents Boltzmann's constant ($0.695 \text{ cm}^{-1} \text{ K}^{-1}$), T the absolute temperature, N_x the number of chls in pool x , and k_{xy} the transfer rate from pool x to pool y . Doing so, we find for the C708 pool in all studied PSI particles a value of ΔE which varies between 350 and 515 cm^{-1} , corresponding to a room temperature absorption maximum of this pool at around 702 nm, which is consistent with the 702–704 nm value reported by Rätsep et al.⁴⁰, and also seems reasonable in view of the ~ 712 nm emission maximum of this pool (see above) and the 10 nm Stokes' shift we reported previously.³³

Applying the stoichiometry listed in table 1, the energy difference of the second (C719) pool of red chls in *Synechococcus* trimeric and *Spirulina* monomeric PSI is found to be approximately 570 cm^{-1} , corresponding to an absorption maximum of ~ 708 nm. This value

seems to be realistic in view of the emission maximum of this pool which appears around 722 nm. The 11 nm blue shift of the absorption maximum of the C719 pool from 719 nm to 708 nm upon increasing the temperature from 6K to room temperature is considerably larger than the 4 to 6 nm shift found for the C708 pool;⁴⁰ see above, which indicates that the chls in the C719 pool are more strongly coupled to their environment than those in the C708 pool.

The energy difference between the second red pool in *Spirulina* trimeric PSI (C740) and the bulk is about 725 cm^{-1} , which corresponds to an absorption maximum at 715 nm. Also this value we consider realistic in view of the emission maximum at 733 nm. The apparent Stokes' shift of 18 nm is comparable to the 20 nm Stokes' shift found at 6K. The blue shift of 25 nm upon a rise of the temperature from 6K to room temperature is about 5 times more than found for the C708 chls,⁴⁰ and about 2 times more than found for the C719 chls, indicating an even stronger coupling of the chls in this extremely red-shifted pool to their local environment.

In all cases we observe that the energy of the red chls is considerably higher at room temperature as compared to low temperatures. This could be caused by the breakdown of the coherence length in the chl aggregates responsible for the red chl forms, due to dynamic disorder at higher temperatures. A second mechanism responsible for the temperature dependence of the red shift could be a (local) contraction of the protein at low temperatures, causing a change of the distances between the chls. A similar mechanism was proposed to account for the temperature-dependent shift of the energy of the special pair in the bacterial photosynthetic reaction centre.⁷⁶

Trapping

If the bulk trapping rate, k_{TB} , is regarded as a free parameter of the fit, its value varies between $(17 \text{ ps})^{-1}$ and $(29 \text{ ps})^{-1}$ in the different PSI cores. Despite this spread of values, it turns out that the quality of the fit decreases only slightly by fixing this value to $(18 \text{ ps})^{-1}$. Earlier modelling of the dynamics in *Synechocystis* and *Synechococcus* PSI, based on the chl coordinates from the structure of *Synechococcus* PSI,⁷¹ also resulted in a 18 ps trapping time upon removal of two putative red chls, which strongly suggests that this is indeed the trapping time in a bulk PSI without red chls.

The trapping rates from any pool of antenna chls depend in first order on the weighed (average) distance of these chls to P700, their relative orientation to P700, and the overlap integral of their emission spectrum with the absorption of P700. If the average location and orientation of the chls in a red pool are not very different from the bulk chls, the relative trapping rate from that pool as compared to the bulk chls only depends upon the relative spectral overlap between the emission of these red chls with the absorption of P700 as compared to the bulk chls. At low temperatures this overlap is very small, resulting in slow trapping from the red chls, and a low quantum efficiency of charge separation. Upon an increase of temperature the overlap increases due to a number of causes. First of all the emission (and absorption) of the strongly coupled red chls blue shifts quite significantly, towards the absorption of P700 (see also above).⁴⁰ Secondly, in the pools of red chls, which are significantly inhomogeneously broadened, at low temperatures excitations mainly reside on the lower energy chls in the distribution, whereas at higher temperatures, also the higher energy chls in the distribution can be excited, resulting in a further blue shift of the (average)

emission of the red chls. Finally, the absorption band of P700 and the intrinsic emission of the individual red chls broaden with increasing temperature.

The relative overlap integrals of the various chl pools with P700 may be estimated from the emission spectra resulting from the target analyses, and a P700 absorption spectrum, which we approximate by a Gaussian with a full width at half of the maximum of 20 nm, peaking at 698 nm.⁴¹ The overlap integrals of the pools of red chls with P700 that are calculated this way, turn out to be quite significant: overlap integrals of the C708, C719 and C740 pools with the P700 absorption spectrum are estimated to be about 80%, 30% and 15% of the overlap of the bulk emission with the P700 absorption spectrum, respectively. The accuracy of the smaller numbers is limited, since they depend strongly upon the exact properties of the extreme blue edge of the emission spectra obtained from the target analysis.

The relative overlap integrals thus estimated may be compared to the (relative) trapping rates which result from the target analysis. The trapping rates k_{T1} from the first pool of red chls (C708) are all of the same order as k_{TB} , and therefore roughly match the 80% relative overlap integral.³⁸ Monomeric PSI of *Synechocystis* is the only exception with a value of k_{T1} which is only about 10% of k_{TB} . Since these monomers contain approximately 30% less C708 chls as compared to trimeric PSI from the same species, possibly the preparation of monomeric particles is heterogeneous, in the sense that some particles may contain as many red chls as the trimers.

The trapping rates k_{T2} from the second pools of red chls measure only 10% of k_{TB} or less, which is lower than expected from the decrease in overlap integral indicated above. It must be noted that, in contrast to the trapping rates from the first pool of red chls, the quality of the fit does not depend too strongly upon these (slow) trapping rates, and therefore they merely represent an "order of magnitude" estimate.

These results indicate that the C708 chls are probably located neither exceptionally close to the RC, nor at great distance. In other words, in our view C708 could be two dimers of chl_a, located somewhere in the ring of bulk chls, not necessarily in some "special" position. On the other hand, our results are still consistent with a more peripheral location of the more red-shifted pools (C719 and C740), in accordance with biochemical data.

STRUCTURE-BASED SIMULATION

In the absence of a 3 dimensional structure, modelling was until recently essentially limited to square or cubic lattice-models (see for instance refs. 21, 24 and 77). One of the key problems in these earlier simulations was the positioning of the trap, relative to the surrounding antenna. Moreover, the quality of the data at that point did not really allow for an extensive quantitative analysis.

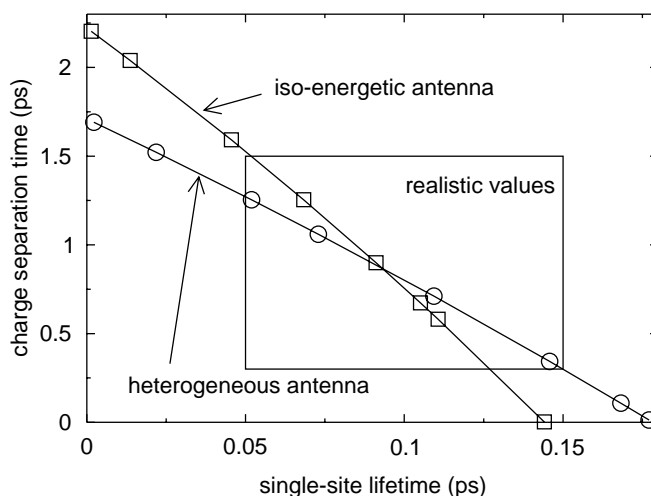
Since the recent publication of a 4 Å resolution three dimensional structure of trimeric PSI core particles from the cyanobacterium *Synechococcus elongatus* by X-ray diffraction on crystals,^{7,8} more realistic modelling has become possible,^{46,48,63,71,79} although a full calculation of energy transfer in PSI based on this structure is still not straightforward. First of all information about the orientation of the transition dipole moments of the chls is currently missing. Secondly, the positions of the different chl spectral forms are unknown. Finally the

structure is known only for *Synechococcus* PSI. In view of the spectroscopic differences, small variations of the protein structure and chl binding sites must be present between the different PSI species that we have investigated, although the global organisation of different PSI species is expected to be conserved to a high degree. Even if these difficulties are overcome (by obtaining high resolution structures of the relevant proteins), relating the structure of a photosynthetic protein to spectroscopic data has proven to be very difficult, even for systems with a much smaller number of chls such as for instance the FMO antenna complex^{80,81} or LHCII.⁸²

Here we will show, however, that some general features of the kinetics in the PSI core system can be derived from a simulation based on the 4 Å structure. The results of the target analysis, which were presented above, can be used as an input for such a simulation: overlap integrals can be estimated from the room temperature absorption and emission properties of the different pools of (red) chls and, moreover, the target analysis has learned us that the kinetics of a (hypothetical) PSI core particle without low-energy chls will exhibit a slowest decay component (trapping time) of approximately 18 ps. Here we will investigate the dynamics of such a PSI core particle, which has the great advantage that it relieves us from the problem of locating the red chls in the structure (such as in refs. 46, 48, 63, 71, 78 and 79). The resulting values of the fitting parameters can subsequently be used as a constraint for the simulation of "real" PSI core particles, which do contain red chls.

The simulations were performed basically as described in ref. 71. We have assumed the Förster mechanism to be the dominant mechanism for the energy transfer in PSI. We calculated the 89×89 k-matrix of Förster transfer rates between each pair of chls *i* and *j*, k_{ij} , using the expression $k_{ij}=F A_{ij} r_{ij}^{-6}$, in which r_{ij} , the distance between chl *i* and *j*, was obtained from the structure. A_{ij} represents the overlap factor between the absorption spectrum of acceptor chl *i* and the emission spectrum of donor chl *j*. The overlap factors for downhill energy transfer were obtained from the shifted absorption and emission spectra of free chls, except for the absorption spectrum of P700 which was approximated by a Gaussian shaped absorption band peaking at 698 nm and a full width at half of the maximum of 19 nm. The reverse, uphill rates were calculated using the constraint of detailed balance (see above). The absorption maxima of the other RC chls were primary electron acceptor (A_0), 686 nm and accessory chls, 680 nm. For the antenna two spectral compositions were investigated: an iso-energetic antenna with an absorption at 680 nm, and a heterogeneous antenna which contained equal ratios of chls absorbing at 670, 680 and 690 nm, which were distributed randomly. The factor *F* is a scaling factor, that accounts for all other factors in the Förster formula (orientations, index of refraction) and which effectively determines the average single site lifetime, τ_{ss} , defined as the time needed for an excitation to hop away from a chl site, averaged over all possible sites. The scaling factor *F* and the intrinsic trapping time τ_{trap} , from the chls identified as P700, are the only two parameters of the simulation. The lifetimes in the system were obtained by calculating the eigen values of the k-matrix.

For both spectral compositions of the antenna, we have looked for combinations of the average single site lifetime τ_{ss} (which is determined by *F*) and τ_{trap} that result in a slowest time constant of 18 ps in the kinetics of the system. This results in the curves plotted in figure 4.8. It immediately strikes the eye that the relation between τ_{ss} and τ_{trap} is almost (but not



4.8 Combinations of the intrinsic trap time and single site lifetime that result in a 18 ps observed trap time. The circles represent the curve for a heterogeneous antenna whereas the squares represent the homogeneous antenna (see text). The box encloses the region of the graph which in our view represents realistic values of the parameters.

perfectly) linear. Such a linear relationship was predicted by Pearlstein,⁸³ Kudzmauskas et al.⁸⁴ and den Hollander et al.,⁸⁵ but we note that such relations were derived for a regular (square) lattice of iso-energetic chromophores, and that it is thus not straightforward that such a linear relation also holds for a non-regular three-dimensional lattice, such as the PSI core antenna, especially in the case of the (slightly) heterogeneous bulk antenna. Furthermore, the equation contains a so-called structure factor, which can be calculated for a regular lattice (see e.g. Somsen et al.⁸⁶), but which is unknown for the PSI structure.

The two lines in figure 4.8 provide upper limits for both τ_{ss} and τ_{trap} , of 200 fs and 2.4 ps, respectively. More realistically the value of τ_{trap} should not be less than ~ 350 fs, and likewise the value of τ_{ss} should be more than 50 fs. This restricts the parameters to the values within the box drawn in figure 4.8. This limits τ_{ss} between 50 and 140 fs, which is somewhat faster than the measured fluorescence depolarisation times of 130-180 fs,^{69,70} but since these measurements do not necessarily reflect the real single step transfer time, but are in fact expected to show a somewhat longer time, the agreement between the simulation and the experiment can be considered as rather good. The box in figure 4.8 limits the intrinsic trapping time, τ_{trap} , between 350 fs and 1.5 ps, which is somewhat faster than the 1.4 to 3 ps values reported earlier,^{65,66,78} but consistent with more recent reports.^{48,67,72,79} It is fast compared to for instance the purple bacterial RC, in which charge separation from the primary electron donor occurs in 3 ps,⁸⁷ but comparable to the 400 fs charge separation as found by Groot et al.⁸⁸ in PSII. In PSII the coupling of the two chl α 's constituting the primary electron donor P680 is less strong as compared to the bacterial primary electron donor, and comparable to the coupling with the other RC chls. Therefore a so-called multimer model that was proposed for PSII,⁸⁹ which may also be applicable for PSI.⁹⁰

Recently it was shown that multiple pathways of charge separation exist in the purple bacterial RC, i.e. electron transfer cannot not only take place from P*, but also from B*.⁹¹⁻⁹³

Similar results were obtained for the RC complex of green sulphur bacteria, which resembles the RC of PSI.^{94,95} Such pathways may prove to be a universal feature of photosynthetic RCs. However, whereas in purple bacteria and green sulphur bacteria the excited state energy levels of respectively B and chl α 670 are too high to be accessible from the antenna, all energy levels of the exciton manifold in a multimer PSI or PSII RC are more or less degenerate with the antenna, and therefore alternative pathways of electron transfer would all sum up to one fast effective rate of electron transfer, even for a selective excitation of the antenna.

In figure 4.1, we have indicated some typical transfer rates, which were derived from the simulation with a trapping time τ_{trap} of ~ 500 fs. This is within the realistic regime, and the simulations with either a iso-energetic or a heterogeneous antenna both yield approximately the same values. The hopping between nearest neighbours in the antenna on the average takes 150-200 fs, a value that agrees with those found in fluorescence depolarisation experiments.^{69,70} Tens to hundred of these elementary steps are required to reach a specific site in the antenna, such as a cluster of red chlorophylls, which therefore takes about 2 to 15 ps, dependent on the exact location and spectral properties of such a cluster. The transfer rate from a bulk chl to a neighbouring red chl is only slightly lower (35-75%) as compared to the transfer between two neighbouring bulk chls, but the rate of back-transfer from the red chls is dramatically lower (1-8%).

The average time needed for an excitation to hop from a bulk chl directly to the RC amounts several tens of ps. However, the effective trapping time in a PSI core particle, lacking red chls, is as low as 18 ps. This implies that hopping to the RC does not occur directly from an average bulk antenna chl, but rather from a selection of chls that are relatively close to the RC.

The "linker" chls, two antenna chls which are located relatively close to the RC (L1 and L2 in figure 4.1), have been proposed to play an important role in guiding excitations from the antenna to the RC.⁹ Within our model we can investigate how important these two chls actually are for the energy transfer in PSI. First of all we can determine which fraction of excitations passes through the linker chls, by setting all reverse rates from the linker chls to zero, we can determine that the fraction of excitations which passes at least once through each of the linker chls is 60 to 70%. This seems to be a large fraction, but in fact this number is not unlike the values found for the other antenna chls, which is not surprising if one realizes that in the 18 ps before trapping, about 100-250 "hops" occur.

A more easy way of determining the importance of the linker chls is simply by leaving them out, and see how this affects the overall trapping time. Both for an iso-energetic and heterogeneous antenna, for realistic values of τ_{ss} and τ_{trap} , removal of the linker chls slows down trapping only by about 6%, and for more extreme cases up to 16%. This of course is negligible compared to the effect that the red chls have upon trapping, slowing it down by almost a factor of 3 in the case of *Spirulina* PSI.

CONCLUDING REMARKS

We have shown that the dynamics of different PSI preparations can be described by a single unifying model, consisting of a bulk compartment of which the properties are species

independent and a number of compartments representing the red chls, the properties of which vary between different species. Consequently the total dynamics are governed by both system dependent and system independent parameters. First of all the transfer from the bulk chls to the RC is mainly governed by the average distance between the antenna and the RC, since equilibration in the bulk antenna takes place on a sub-ps time scale. This parameter together with the intrinsic rate of charge separation by P700, fully determines the dynamics of a PSI core system without red chls, and thus represent the system independent parameters contributing to the dynamics of any PSI core particle. The (large) kinetic differences between the various PSI particles arise from differences in the red chl content. Both the number of red chls and their excited state energies are found to be the basic system dependent parameters that determine the dynamic variety between different PSI core particles.

REFERENCES

- (1) Cantrell, A., and D.A. Bryant. 1987. Molecular cloning and nucleotide sequence of the *psaA* and *psaB* genes of the cyanobacterium *Synechococcus* sp. PCC 7002. *Plant Mol. Biol.* 9:453-468.
- (2) Mühlenhoff, U., W. Haehnel, H. Witt, and R.G. Herrmann. 1993. Genes encoding 11 subunits of Photosystem I from the thermophilic cyanobacterium *Synechococcus* sp. *Gene*. 127:71-78.
- (3) Scheller, H.V., H. Naver, and B.L. Moller. 1997. Molecular aspects of Photosystem I. *Physiol. Plant.* 100:842-851.
- (4) Turconi, S., J. Kruij, G. Schweitzer, M. Rögner, and A.R. Holzwarth. 1996. A comparative fluorescence kinetics study of Photosystem I monomers and trimers from *Synechocystis* PCC 6803. *Photosynth. Res.* 49:263-268.
- (5) Kruij, J., D. Bald, E. Boekema, and M. Rögner. 1994. Evidence for the existence of trimeric and monomeric Photosystem I complexes in thylakoid membranes from cyanobacteria. *Photosynth. Res.* 40:279-286.
- (6) Boekema, E.J., P.E. Jensen, E. Schlodder, J.F.L. van Breemen, H. van Roon, H.V. Scheller and J.P. Dekker. 2001. Green plant Photosystem I binds light-harvesting complex I on one side of the complex. *Biochemistry*. 40:1029-1036.
- (7) Fromme, P., H.T. Witt, W.-D. Schubert, O. Klukas, W. Sängner, and N. Krauss. 1996. Structure of Photosystem I at 4.5 angstrom resolution: A short review including evolutionary aspects. *Biochim. Biophys. Acta.* 1275:76-83.
- (8) Krauss, N., W.-D. Schubert, O. Klukas, P. Fromme, H.T. Witt, and W. Saenger. 1996. Photosystem I at 4Å resolution represents the first structural model of a joint photosynthetic reaction centre and core antenna system. *Nat. Struct. Biol.* 3:965-973.
- (9) Schubert, W.-D., O. Klukas, N. Krauss, W. Saenger, P. Fromme, and H.T. Witt. 1997. Photosystem I of *Synechococcus elongatus* at 4 angstrom resolution: Comprehensive structure analysis. *J. Mol. Biol.* 272:741-769.
- (10) Jansson, S. 1994. The light-harvesting chlorophyll-*a/b* binding-proteins. *Biochim. Biophys. Acta.* 1184:1-19.
- (11) Croce, R., G. Zucchelli, F.M. Garlaschi, and R.C. Jennings. 1998. A thermal broadening study of the antenna chlorophylls in PSI-200, LHCI, and PSI core. *Biochemistry*. 37:17355-17360.

- (12) Ihalainen, J.A., B. Gobets, K. Sznee, M. Brazzoli, R. Croce, R. Bassi, R. van Grondelle, J.E.I. Korppi-Tommola, and J.P. Dekker. 2000. Evidence for two spectroscopically different dimers of light-harvesting complex I from green plants. *Biochemistry*. 39:8625-8631.
- (13) Jansson, S., B. Andersen, and H.V. Scheller. 1996. Nearest-neighbor analysis of higher-plant Photosystem I holocomplex. *Plant Physiology*. 112:409-420.
- (14) Schmid, V.H.R., K.V. Cammarata, B.U. Bruns, and G.W. Schmidt. 1997. *In vitro* reconstitution of the Photosystem I light-harvesting complex LHCI-730: Heterodimerization is required for antenna pigment organization. *Proc. Natl. Acad. Sci. U.S.A.* 94:7667-7672.
- (15) Croce, R., and R. Bassi. 1998. The light-harvesting complex of Photosystem I: Pigment composition and stoichiometry. In *Photosynthesis: Mechanisms and effects*. G. Garab, editor. Kluwer Academic Publishers, Dordrecht, The Netherlands. 1:421-424.
- (16) Kühlbrandt, W., D.N. Wang, and Y. Fujiyoshi. 1994. Atomic model of plant light-harvesting complex by electron crystallography. *Nature*. 367:614-621.
- (17) Simonetto, R., M. Crimi, D. Sandona, R. Croce, G. Cinque, J. Breton, and R. Bassi. 1999. Orientation of chlorophyll transition moments in the higher-plant light-harvesting complex CP29. *Biochemistry*. 38:12974-12983.
- (18) Boekema, E.J., R.M. Wynn, and R. Malkin. 1990. The structure of spinach Photosystem-I studied by electron-microscopy. *Biochim. Biophys. Acta*. 1017:49-56.
- (19) Klukas, O., W.D. Schubert, P. Jordan, N. Krauss, P. Fromme, H.T. Witt, and W. Saenger. 1999. Localization of two phylloquinones, Q(K) and Q(K)', in an improved electron density map of Photosystem I at 4-angstrom resolution. *J. Biol. Chem.* 274:7361-7367.
- (20) Deligiannakis, Y., J. Hanley, and A.W. Rutherford. 1998. Spin-lattice relaxation of the phyllosemiquinone radical of Photosystem I. *Biochemistry*. 37:3329-3336.
- (21) Owens, T.G., S.P. Webb, L. Mets, R.S. Alberte, and G.R. Fleming. 1987. Antenna size dependence of fluorescence decay in the core antenna of Photosystem I: estimates of charge separation and energy transfer rates. *Proc. Natl. Acad. Sci. USA*. 84:1532-1536.
- (22) Beauregard, M., I. Martin, and A.R. Holzwarth. 1991. Kinetic modeling of exciton migration in photosynthetic systems. 1. Effects of pigment heterogeneity and antenna topography on exciton kinetics and charge separation yields. *Biochim. Biophys. Acta*. 1060:271-283.
- (23) Werst, M., Y.M. Jia, L. Mets, and G.R. Fleming. 1992. Energy-transfer and trapping in the Photosystem-I core antenna - A temperature study. *Biophys. J.* 61:868-878.
- (24) Trinkunas, G., and A.R. Holzwarth. 1994. Kinetic modeling of exciton migration in photosynthetic systems. 2. Simulations of excitation dynamics in 2-dimensional photosystem core antenna/reaction center complexes. *Biophys. J.* 66:415-429.
- (25) Van Grondelle, R., J.P. Dekker, T. Gillbro, and V. Sundström. 1994. Energy transfer and trapping in photosynthesis. *Biochim. Biophys. Acta*. 1187:1-65.
- (26) Valkunas, L., V. Liuolia, J.P. Dekker, and R. van Grondelle. 1995. Description of energy migration and trapping in Photosystem I by a model with two distance scaling parameters. *Photosynth. Res.* 43:149-154.
- (27) Somsen, O.J.G., L. Valkunas, and R. van Grondelle. 1996. A perturbed two-level model for exciton trapping in small photosynthetic systems. *Biophys. J.* 70:669-683.
- (28) Hoff, A.J., and J. Ames. 1991. Visible absorption spectroscopy of chlorophylls. In *Chlorophylls*. H. Scheer, editor. CRC Press, Boca Raton, Florida. 723-738.

- (29) Shubin, V.V., S.D.S. Murthy, N.V. Karapetyan, and P. Mohanty. 1991. Origin of the 77K variable fluorescence at 758 nm in the cyanobacterium *Spirulina platensis*. *Biochim. Biophys. Acta.* 1060:28-36.
- (30) Wittmershaus, B.P., V.M. Woolf, and W.F.J. Vermaas. 1992. Temperature dependence and polarization of fluorescence from Photosystem I in the cyanobacterium *Synechocystis* sp PCC 6803. *Photosynth. Res.* 31: 75-87.
- (31) Van der Lee, J., D. Bald, S.L.S Kwa, R. van Grondelle, M. Rögner, and J.P. Dekker. 1993. Steady-state polarized-light spectroscopy of isolated Photosystem-I complexes. *Photosynth. Res.* 35:311-321.
- (32) Turconi, S., G. Schweitzer, and A.R. Holzwarth. 1993. Temperature dependence of picosecond fluorescence kinetics of a cyanobacterial Photosystem I particle. *Photochem. Photobiol.* 57:113-119.
- (33) Gobets, B., H. van Amerongen, R. Monshouwer, J. Kruip, M. Rögner, R. van Grondelle, and J.P. Dekker. 1994. Polarized site-selected fluorescence spectroscopy of isolated Photosystem I particles. *Biochim. Biophys. Acta.* 1188:75-85.
- (34) Hastings, G., L.J. Reed, S. Lin, and R.E. Blankenship. 1995. Excited state dynamics in Photosystem I: Effects of detergent and excitation wavelength. *Biophys. J.* 69:2044-2055.
- (35) Pålsson, L.-O., J.P. Dekker, E. Schlodder, R. Monshouwer, and R. van Grondelle. 1996. Polarized site-selective fluorescence spectroscopy of the long-wavelength emitting chlorophylls in isolated Photosystem I particles of *Synechococcus elongatus*. *Photosynth. Res.* 48:239-246.
- (36) Kruip, J., N.V. Karapetyan, I.V. Terekhova, and M. Rogner. 1999. *In vitro* oligomerization of a membrane protein complex - Liposome-based reconstitution of trimeric Photosystem I from isolated monomers. *J. Biol. Chem.* 274:18181-18188.
- (37) Karapetyan, N.V., A.R. Holzwarth, and M. Rögner. 1999. The Photosystem I trimer of cyanobacteria: molecular organization, excitation dynamics and physiological significance. *FEBS Lett.* 460:395-400.
- (38) Gobets, B., I.H.M. van Stokkum, M. Rögner, J. Kruip., E. Schlodder, N.V. Karapetyan, J.P. Dekker, and R. van Grondelle. 2001. Time-resolved fluorescence emission measurements of Photosystem I particles of various cyanobacteria: a unified compartmental model. *Biophys. J.* 81:407-424.
- (39) Hayes, J.M., S. Matsuzaki, M. Rätsep, and G.J. Small. 2000. Red chlorophyll-*a* antenna states of Photosystem I of the cyanobacterium *Synechocystis* sp. PCC 6803. *J. Phys. Chem. B.* 104:5625-5633.
- (40) Rätsep, M., T.W. Johnson, P.R. Chitnis, and G.J. Small. 2000. The red-absorbing chlorophyll-*a* antenna states of Photosystem I: A hole-burning study of *Synechocystis* sp PCC 6803 and its mutants. *J. Phys. Chem. B.* 104:836-847.
- (41) Pålsson, L.-O., C. Flemming, B. Gobets, R. van Grondelle, J.P. Dekker, and E. Schlodder. 1998. Energy transfer and charge separation in Photosystem I: P700 oxidation upon selective excitation of the long-wavelength chlorophylls of *Synechococcus elongatus*. *Biophys. J.* 74:2611-2622.
- (42) Shubin, V.V., I.N. Bezsmernaya, and N.V. Karapetyan. 1992. Isolation from *Spirulina* membranes of two Photosystem I-type complexes, one of which contains chlorophyll responsible for the 77 K fluorescence at 760 nm. *FEBS Lett.* 309:340-342.
- (43) Holzwarth, A.R., G. Schatz, H. Brock, and E. Bittersmann. 1993. Energy transfer and charge separation kinetics in Photosystem I Part 1: Picosecond transient absorption and fluorescence study of cyanobacterial Photosystem I particles. *Biophys. J.* 64:1813-1826.

- (44) Koehne, B., and H.W. Trissl. 1998. The cyanobacterium *Spirulina platensis* contains a long wavelength-absorbing pigment C-738 (F-760(77K)) at room temperature. *Biochemistry*. 37:5494-5500.
- (45) Shubin, V.V., I.N. Bezsmertnaya, and N.V. Karapetyan. 1995. Efficient energy-transfer from the long-wavelength antenna chlorophylls to P700 in Photosystem-I complexes from *Spirulina platensis*. *J. Photochem. Photobiol. B*. 30:153-160.
- (46) Byrdin, M., I. Rimke., E. Schlodder, D. Stehlik, and T.A. Roelofs. 2000. Decay kinetics and quantum yields of fluorescence in Photosystem I from *Synechococcus elongatus* with P700 in the reduced and oxidized state: are the kinetics of excited state decay trap-limited or transfer-limited? *Biophys. J.* 79:992-1007.
- (47) Gobets, B., J.T.M. Kennis, J.A. Ihalainen, M. Brazzoli, R. Croce, I.H.M. van Stokkum, R. Bassi, J.P. Dekker, H. van Amerongen, G.R. Fleming, and R. van Grondelle. 2001. Excitation energy transfer in dimeric light-harvesting complex I: a combined streak camera/fluorescence upconversion study. *J. Phys. Chem. B*. 105:10132-10139.
- (48) Gobets, B., J.P. Dekker, and R. van Grondelle. 1998. Transfer-to-the-trap limited model of energy transfer in Photosystem I. In *Photosynthesis: Mechanisms and effects*. G. Garab, editor. Kluwer Academic Publishers, Dordrecht, The Netherlands. 1:503-508.
- (49) Peterman, E.J.G, T. Pullerits, R. van Grondelle, and H. van Amerongen. 1997. Electron-phonon coupling and vibronic fine structure of light-harvesting complex II of green plants: Temperature dependent absorption and high-resolution fluorescence spectroscopy. *J. Phys. Chem. B*. 101:4448-4457.
- (50) Peterman, E.J.G, S-O. Wenk, T. Pullerits, L-O. Pålsson, R. van Grondelle, J.P. Dekker, M. Rögner, and H. van Amerongen. 1998. Fluorescence and absorption spectroscopy of the weakly fluorescent chlorophyll-*a* in cytochrome *b₆f* of *Synechocystis* PCC6803. *Biophys. J.* 75:389-398.
- (51) Peterman, E.J.G., H. van Amerongen, R. van Grondelle, and J.P. Dekker. 1998. The nature of the excited state of the reaction center of Photosystem II of green plants: A high-resolution fluorescence spectroscopy study. *Proc.Natl. Acad. Sci. USA*. 95:6128-6133.
- (52) Mukerji, I., and K. Sauer. 1990. A spectroscopic study of a Photosystem I antenna complex. In *Current research in photosynthesis*. M. Baltscheffsky, editor. Kluwer Academic Publishers, Dordrecht, The Netherlands. 2: 321-324.
- (53) Van Grondelle, R., and V. Sundström. 1988. Excitation energy transfer in photosynthesis. In *Photosynthetic light-harvesting systems*. H. Scheer and S. Schneider, editors. De Gruyter, Berlin. 403-438.
- (54) Van Grondelle, R., H. Bergström, V. Sundström, R.J. van Dorssen, M. Vos, and C.N. Hunter. 1988. In *Photosynthetic light-harvesting systems*. H. Scheer and S. Schneider, editors. De Gruyter, Berlin. 519-530.
- (55) Trissl, H.-W. 1993. Long-wavelength absorbing antenna pigments and heterogeneous absorption-bands concentrate excitons and increase absorption cross-section. *Photosynth. Res.* 35:247-263.
- (56) Trissl, H.-W., and C. Wilhelm. 1993. Why do thylakoid membranes from higher-plants form grana stacks? *Trends Biochem. Sci.* 18:415-419.
- (57) Rivadossi, A., G. Zucchelli, F.M. Garlaschi, and R.C. Jennings. 1999. The importance of PSI chlorophyll red forms in light-harvesting by leaves. *Photosynth. Res.* 60:209-215.
- (58) Beddard, G.S., and G. Porter. 1976. Concentration quenching in chlorophyll. *Nature*. 260:366.

- (59) Savikhin, S., D.R. Buck, W.S. Struve, R.E. Blankenship, A.S. Taisova, V.I. Novoderezhkin, and Z.G. Fetisova. 1998. Excitation delocalization in the bacterio-chlorophyll-*c* antenna of the green bacterium *chloroflexus aurantiacus* as revealed by ultrafast pump-probe spectroscopy. *FEBS Lett.* 430:323-326.
- (60) Valkunas, L., G. Trinkunas, V. Liulolia, and R. van Grondelle. 1995. Nonlinear annihilation of excitations in photosynthetic systems. *Biophys. J.* 69:1117-1129.
- (61) Van Grondelle, R. 1985. Excitation energy transfer, trapping and annihilation in photosynthetic systems. *Biochim. Biophys. Acta.* 811:147-195.
- (62) Pålsson, L.-O, S.E. Tjus, B. Andersson, and T. Gillbro. 1995. Energy-transfer in Photosystem-I - time-resolved fluorescence of the native Photosystem-I complex and its core complex. *Chem. Phys.* 194:291-302.
- (63) Savikhin, S., W. Xu, V. Soukoulis, P.R. Chitnis, and W.S. Struve. 1999. Ultrafast primary processes in Photosystem I of the cyanobacterium *Synechocystis* sp. PCC 6803. *Biophys. J.* 76:3278-3288.
- (64) Melkozernov, A.N., S. Lin, and R.E. Blankenship. 2000. Excitation dynamics and heterogeneity of energy equilibration in the core antenna of Photosystem I from the cyanobacterium *Synechocystis* sp. PCC 6803. *Biochemistry* 39:1489-1498.
- (65) Hastings, G., F.A.M. Kleinherenbrink, S. Lin, and R.E. Blankenship. 1994. Time-resolved fluorescence and absorption-spectroscopy of Photosystem-I. *Biochemistry.* 33:3185-3192.
- (66) Kumazaki, S., H. Kandori, H. Petek, K. Yoshihara, and I. Ikegami. 1994. Primary photochemical processes in P700-enriched Photosystem-I particles - Trap-limited excitation decay and primary charge separation. *J. Phys. Chem.* 98:10335-10342.
- (67) Kumazaki, S., I. Ikegami, H. Furusawa, S. Yasuda, and K. Yoshihara. 2001. Observation of the excited state of the primary electron donor chlorophyll (P700) and the ultrafast charge separation in the spinach Photosystem I reaction center. *J. Phys. Chem. B.* 105:1093-1099.
- (68) Karapetyan, N.V., D. Dorra, G. Schweitzer, I.N. Bezmertnaya, and A.R. Holzwarth. 1997. Fluorescence spectroscopy of the longwave chlorophylls in trimeric and monomeric Photosystem I core complexes from the cyanobacterium *Spirulina platensis*. *Biochemistry* 36:13830-13837.
- (69) Du, M., X. Xie, Y. Jia, L. Mets, and G.R. Fleming. 1993. Direct observation of ultrafast energy transfer in PSI core antenna. *Chem. Phys. Lett.* 201:535-542.
- (70) Kennis, J.T.M., B. Gobets, I.H.M. van Stokkum, J.P. Dekker, R. van Grondelle, and G.R. Fleming. 2001. Light harvesting by chlorophylls and carotenoids in the Photosystem I complex of *Synechococcus elongatus*: a fluorescence upconversion study. *J. Phys. Chem. B.* 105:4485-4494.
- (71) Gobets, B., I.H.M. van Stokkum, F. van Mourik, M. Rögner, J. Kruij, J.P. Dekker, and R. van Grondelle. 1998. Time-resolved fluorescence measurements of Photosystem I from *Synechocystis* PCC 6803. *In* Photosynthesis: Mechanisms and effects. G. Garab, editor. Kluwer Academic Publishers, Dordrecht, The Netherlands. 1: 571-574.
- (72) Trinkunas, G., and A.R. Holzwarth. 1996. Kinetic modeling of exciton migration in photosynthetic systems. 3. Application of genetic algorithms to simulations of excitation dynamics in three-dimensional Photosystem I core antenna/reaction center complexes. *Bioph. J.* 71:351-364.
- (73) Searle, G.F.W., R. Tamkivi, A. van Hoek, and T.J. Schaafsma. 1988. Temperature-dependence of antennae chlorophyll fluorescence kinetics in Photosystem-I reaction center protein. *J. Chem. Soc. Faraday Trans. 2.* 84:315-327.

- (74) Wittmershaus, B.P. 1987. Measurements and kinetic modeling of picosecond time-resolved fluorescence from Photosystem I and chloroplasts. *In* Progress in Photosynthesis Research. J. Biggins, editor. Martinus Nijhoff Publishers, Dordrecht. 75-82.
- (75) Wittmershaus, B.P., D.S. Berns, and C. Huang. 1987. Picosecond time-resolved fluorescence from detergent-free Photosystem I particles. *Biophys. J.* 52:829-836.
- (76) Friesner, R.A., and Y.D. Won. 1989. Spectroscopy and electron-transfer dynamics of the bacterial photosynthetic reaction center. *Biochim. Biophys. Acta.* 977:99-122.
- (77) Laible, P.D., W. Zipfel, and T.G. Owens. 1994. Excited-state dynamics in chlorophyll-based antennae - The role of transfer equilibrium. *Bioph. J.* 66:844-860.
- (78) White, N.T.H., G.S. Beddard, J.R.G. Thorne, T.M. Feehan, T.E. Keyes, and P. Heathcote. 1996. Primary charge separation and energy transfer in the Photosystem I reaction center of higher plants. *J. Phys. Chem.* 100:12086-12099.
- (79) Beddard, G.S. 1998. Excitations and excitons in Photosystem I. *Phil. Trans. R. Soc. Lond. A.* 356:421-448.
- (80) Louwe, R.J.W., J. Vrieze, A.J. Hoff, and T.J. Aartsma. 1997. Toward an integral interpretation of the optical steady-state spectra of the FMO-complex of *Prosthecochloris aestuarii*. 2. Exciton simulations. *J. Phys. Chem. B.* 101:11280-11287.
- (81) Savikhin, S., D.R. Buck, and W.S. Struve. 1999. The Fenna-Matthews-Olson protein: a strongly coupled photosynthetic antenna. *In* Resonance energy transfer. D.L. Andrews, and A.A. Demidov, editors. John Wiley & Sons, Inc., New York, USA. 399-434.
- (82) Gradinaru, C.C., S. Özdemir, D. Gülen, I.H.M. van Stokkum, R. van Grondelle, and H. van Amerongen. 1998. The flow of excitation energy in LHClI monomers: Implications for the structural model of the major plant antenna. *Biophys. J.* 75:3064-3077.
- (83) Pearlstein, R.M. 1982. Exciton migration and trapping in photosynthesis. *Photochem. Photobiol.* 35:835-844.
- (84) Kudzmauskas, S.P., L.L. Valkunas, and A.Y. Borisov. 1983. A theory of excitation transfer in photosynthetic units. *J. Theor. Biol.* 105:13-23.
- (85) Den Hollander, W.T.F., J.G.C. Bakker, and R. van Grondelle. 1983. Trapping, loss and annihilation of excitations in a photosynthetic system. I. Theoretical aspects. *Biochim. Biophys. Acta.* 725:492-507.
- (86) Somsen, O.J.G., F. van Mourik, R. van Grondelle, and L. Valkunas. 1994. Energy migration and trapping in a spectrally and spatially inhomogeneous light-harvesting antenna. *Biophys. J.* 66:1580-1596.
- (87) Parson, W.W. 1991. Reaction centers. *In* Chlorophylls. H. Scheer, editor. CRC Press, Boca Raton, Florida. 1153-1180.
- (88) Groot, M.L., F. van Mourik, C. Eijkelhoff, I.H.M. van Stokkum, J.P. Dekker, and R. van Grondelle. 1997. Charge separation in the reaction center of Photosystem II studied as a function of temperature. *Proc. Natl. Acad. Sci. USA.* 94:4389-4394.
- (89) Durrant, J.R., D.R. Klug, S.L.S. Kwa, R. van Grondelle, G. Porter, and J.P. Dekker. 1995. A multimer model for P680, the primary electron-donor of Photosystem-II. *Proc. Natl. Acad. Sci. USA.* 92:4798-4802.
- (90) Beddard, G.S. 1998. Exciton coupling in the Photosystem I reaction center. *J. Phys. Chem. B.* 102:10966-10973.

-
- (91) Van Brederode, M.E., and R. van Grondelle. 1999. New and unexpected routes for ultrafast electron transfer in photosynthetic reaction centers. *FEBS Lett.* 455:1-7.
- (92) Van Brederode, M.E., I.H.M. van Stokkum, E. Katilius, F. van Mourik, M.R. Jones, and R. van Grondelle. 1999. Primary charge separation routes in the BChl : BPhe heterodimer reaction centers of *Rhodobacter sphaeroides*. *Biochemistry.* 38:9556-9556.
- (93) Van Brederode, M.E., F. van Mourik, I.H.M. van Stokkum, M.R. Jones, and R. van Grondelle. 1999. Multiple pathways for ultrafast transduction of light energy in the photosynthetic reaction center of *Rhodobacter sphaeroides*. *Proc. Natl. Acad. Sci. USA.* 96:2054-2059.
- (94) Neerken, S., K.A. Schmidt, T.J. Aartsma, and J. Amesz. 1999. Dynamics of energy conversion in reaction center core complexes of the green sulfur bacterium *Prosthecochloris aestuarii* at low temperature. *Biochemistry.* 38:13216-13222.
- (95) Neerken, S., T.J. Aartsma, and J. Amesz. 2000. Pathways of energy transformation in antenna reaction center complexes of *Heliobacillus mobilis*. *Biochemistry.* 39:3297-3303.
- (96) Croce, R., D. Dorra, A.R. Holzwarth, and R.C. Jennings. 2000. Fluorescence decay and spectral evolution in intact Photosystem I of higher plants. *Biochemistry.* 39:6341-6348.

5

Bridging the gap between structural and lattice-models: a parametrization of energy transfer and trapping in Photosystem I

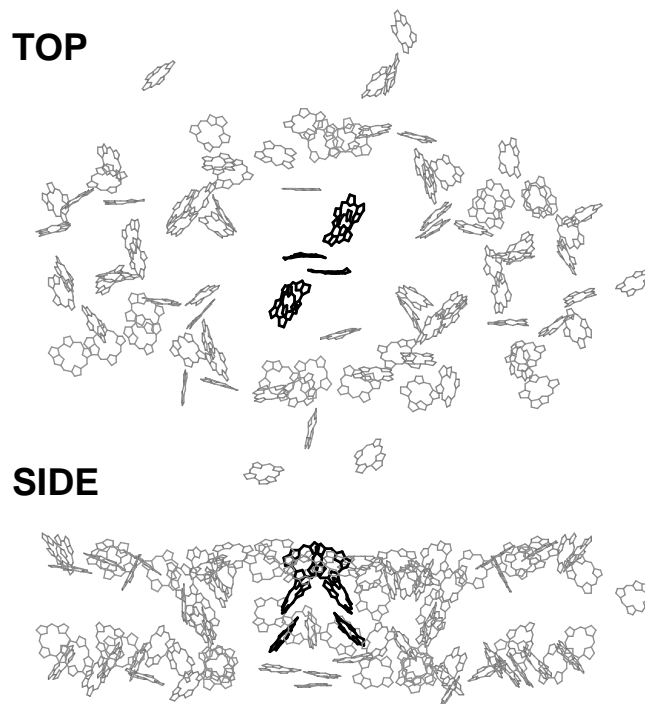
Bas Gobets, Leonas Valkunas and Rienk van Grondelle

In the absence of an accurate structural model, the excited state dynamics of energy-transferring systems is often modelled using lattice-models. To demonstrate the validity and other potential merits of such an approach we present the results of the modelling of the energy transfer and trapping in Photosystem I (PSI) based upon the 2.5 Å structural model, and show that these results can be reproduced in terms of a lattice model with only a few parameters. Recently we have shown that the dynamics of a hypothetical PSI particle, not containing any red chls, is characterized by a longest (trapping) lifetime of 18 ps.¹ The structure-based modelling of the dynamics of this particle yields an almost linear relationship between the possible values of the intrinsic charge-separation time at P700, $1/\gamma$, and the average single-site lifetime in the antenna, τ_{ss} . Lattice-based modelling, using the approach of a perturbed two-level model,² reproduces this linear relation between τ_{ss} and $1/\gamma$. Moreover, this approach results in a value of the (modified) structure-function corresponding to a structure exhibiting a mixture of the characteristics of both a square and a cubic lattice, consistent with the structural model. These findings demonstrate that the lattice model describes the dynamics of the system appropriately. In the lattice model, the total trapping time is the sum of the delivery time to the reaction centre (RC) and the time needed to quench the excitation after delivery. For the literature value of $\tau_{ss} = 150$ fs, both these times contribute almost equally to the total trapping time of 18 ps, indicating that the system is neither transfer- nor trap-limited. The value of ~ 9 ps for the delivery time is basically equal to the excitation-transfer time from the bulk chls to the red chls in *Synechococcus elongatus*, indicating that energy transfer from the bulk to the RC and to the red chls are competing processes. These results are corroborated by independent low-temperature time-resolved and steady-state fluorescence measurements. We conclude that lattice-models can be used to describe the global energy-transfer properties in complex chromophore-networks, with the advantage that such models deal with only a few global, intuitive parameters rather than the many microscopic parameters obtained in structure-based modelling.

INTRODUCTION.

The primary processes in all photosynthetic systems involve the absorption of energy from (sun) light by chromophores in a light-harvesting antenna, and the subsequent transfer of this energy to a RC-site where the energy is "trapped" by means of a stable charge-separation. PSI is one of two such photosystems present in oxygenic photosynthesis. It uses the energy of light to transfer electrons from plastocyanin or soluble cytochrome c_6 to ferredoxin and eventually to NADP^+ . The PSI core is a large pigment-protein complex consisting of 11 to 13 protein subunits,³ the largest two of which, PsaA and PsaB, form a heterodimer to which the majority of the core antenna pigments, as well as most of the RC co-factors are bound. Spectroscopic data indicate that the core antenna and RC contain approximately 90-100 chlorophyll-*a* (chl*a*) and 10-25 β -carotene molecules in total.

In plants and green algae the PSI core complex binds additional Light-Harvesting Complex I (LHCI) antenna proteins. These accessory chl binding antenna proteins are not present in cyanobacteria. The PSI core complexes of cyanobacteria can be isolated both as monomers and trimers, and probably both aggregation states are native, co-existing in the membrane in a dynamic equilibrium.⁴



5.1 Top (upper) and side (lower) view of the spatial arrangement of chl*a* molecules in the PSI core of *Synechococcus elongatus*, as derived from the 2.5 Å structural model. The grey molecules represent the antenna chls whereas the black molecules represent the chls in the RC. For clarity the phytol tails of the molecules have been omitted.

The structure of the PSI core complex of the cyanobacterium *Synechococcus elongatus* has been resolved up to 2.5 Å resolution.⁵ The structural model includes 96 chl molecules, as well as 22 carotenoids, 2 phylloquinones and 3 Fe₄S₄ clusters.

Figure 5.1 displays the organization of the chl molecules in the structural model. For clarity only the porphyrin rings are displayed, although for most chls the complete phytol tail was resolved. The top-view clearly shows how the 90 chl molecules that constitute the core antenna (grey) encompass the RC containing the remaining 6 chls (black). Although located in the middle of the structure, the distance of any of RC chls to most of the antenna chls is larger than 20 Å. The side-view clearly demonstrates that the antenna chls are not distributed homogeneously throughout the whole protein-volume. Whereas the central domain consists of a more or less space-filling three-dimensional chl distribution, the chls in the peripheral domains are concentrated at both the luminal and stromal side of the protein, with an empty layer in between. The spatial distribution of the chls in the protein is one of the major factors contributing to the energy-transfer characteristics of the system.

The dynamics of PSI is determined not only by the structural organization of the antenna, but also by the spectral properties of the chls in the antenna and the RC, in particular since the PSI antenna exhibits a number of low-energy, or "red" chls that absorb maximal at wavelengths longer than that of the primary electron donor, P700.⁶⁻¹⁰ Despite the fact that the number of these low-energy chls is small, less than 10% of the total chl content of the antenna, it has been shown by both time-resolved and steady-state spectroscopy experiments that their effect upon the energy-transfer and trapping characteristics of the PSI system is considerable.^{1,8,10-13} In PSI cores of cyanobacteria, the amounts and energies of the low-energy chls appear to be highly species-dependent.^{1,10} Moreover, the red chl forms are also affected by the aggregation state of the cyanobacterial core complexes: in monomeric PSI core preparations the number of red chls is generally found to be lower than in trimers. The spectral properties of the various pools of (red) chls in PSI and their location in the protein are important parameters in the modelling of the dynamics in PSI.

Previously, in the absence of a structural model, the modelling of the energy-transfer dynamics in PSI was often based on square or cubic lattices.¹⁴⁻²⁰ The dynamics was calculated either analytically,¹⁴ using the equations derived by Pearlstein,^{21,22} or numerically by calculating transfer rates between individual pigments using the Förster mechanism for energy transfer²³ and the subsequent solution of the Pauli master equation.¹⁵⁻²⁰ In some cases only energy transfer between the nearest neighbouring pigments was taken into account, whereas in other cases all pairwise energy-transfer rates were calculated. All these modelling attempts suffered from a number of the following problems:

1. The spectral heterogeneity of PSI, and especially the presence of the red chls has to be taken into account for proper modelling of the kinetics of intact PSI particles. The analytical approach is only applicable to a homogeneous antenna (all antenna chls absorb at the same energy). In contrast, the numerical approach does allow for the inclusion of different spectral forms via the overlap integral appearing in the Förster formula. Two problems arise, however. First of all the spectral properties of the different antenna pools need to be known in order to calculate the overlap integrals. In most cases the overlap integrals are calculated using shifted absorption and emission

spectra of chl a in organic solvents, which is reasonable for most chl pools, except for the pools of red chls, the spectral properties of which have been shown to differ significantly from those of chls in solution.^{1,8,9,24} Another problem is that the dynamics depends strongly upon the location of the different spectral forms in the antenna, which is unknown. This leads to an enormous number of possible permutations of the different chl forms, which is quite impossible to sample, both for the reason of computation time, as well as for the fact that the problem is underdetermined, that is, the amount and quality of the data do not allow to select the best configuration. The latter also relates to the next problem:

2. The experimental input for the modelling frequently consisted of Single Photon Counting data.^{14,18,20} This technique is characterized by an instrument response function with a full width at half maximum (FWHM) of typically 40–80 ps, allowing for a quite accurate recording of the slowest lifetime component, that reflects the overall decay of excitations due to trapping. However, the shorter lifetime components that reflect the energy transfer between the different pools of chls, are generally too fast to be recorded by this technique. Even if such a component was recorded it usually did not help to improve the simulations due to the lack of accuracy with which it could be registered.

Moreover, the PSI preparations used in these experiments were often damaged during isolation, due to the use of harsh detergents, resulting in the loss of (most) the red chl forms and possibly a part of the bulk antenna.

3. The main distinguishing feature of most lattice-models is that they are 2-dimensional with the RC (or P700) occupying one of the sites of the lattice. In these models, for a given spectral composition of the antenna, the dynamics are defined by only two fitting parameters: the rate of charge-separation from P700 and one single distance scaling parameter, the lattice constant. This has led to two limiting cases for the dynamics in PSI. In the transfer limited case the dynamics are mainly determined by the energy-transfer rate in the antenna, due to relatively slow diffusion of excitations to the RC, whereas in the trap limited case, a relatively slow intrinsic rate of charge-separation from P700 would govern the dynamics. Structural data now reveal (fig. 5.1) that the structure is clearly 3-dimensional and, moreover, the RC is not just another site on a lattice. The distance between the RC and the antenna chls is significantly larger as compared to the distance between adjacent antenna chls. Therefore a model describing the energy transfer in PSI should include (at least) two distinct energy-transfer rates: a larger rate for energy transfer between antenna chls, and a smaller rate for energy transfer from the antenna to the RC. This results in a third limiting case, the transfer-to-the-trap limited case, in which the dynamics is limited by a relatively slow energy-transfer rate from the antenna to the RC.¹¹ Already before sufficiently detailed structural data became available Valkunas et al.^{11,25} proposed a model with an organization similar to the bacterial LH1-RC complexes, in which two distinct scaling parameters are present: a short inter-pigment distance between adjacent antenna chls, and a larger distance between the antenna and the RC.

In this contribution we will model PSI using both the analytical (Pearlstein) and the numerical (Förster) approach such that the problems listed above are overcome. Recently we have presented time-resolved fluorescence data of various PSI particles containing different amounts and types of red chls.¹ These experiments were performed using a synchroscan streak camera with a time resolution of about 1 ps, significantly better than in single photon counting experiments. Depending on the type of PSI, one or two fast equilibration components could clearly be distinguished besides the slowest, trapping component. All the different PSI particles used in this study were isolated using mild detergents and were very well characterized. Earlier, we proposed a unified compartmental scheme that described the dynamics of all PSI particles studied.¹ Global target analysis of the various data sets indicated that from the compartment representing the bulk chls, absorbing around 680 nm, trapping occurred in 18 ps. We concluded that in a hypothetical PSI particle, containing no red chls, trapping should occur in 18 ps. In the numerical modelling of the energy transfer in such a hypothetical particle, with a homogeneous (or slightly inhomogeneous) antenna, one is relieved from the problem of locating the red chl forms, thereby greatly reducing the amount of free model-parameters. Since the locations and orientations of the chls can be taken from the structural model, no artificial regular lattice needed to be assumed for the numerical modelling.

For the PSI core “without red chls” we can compare the numerical results with those obtained from an analytical approach. This allows us to formulate a few general concepts that can be intuitively applied to describe the (global) energy-transfer dynamics of a complex system like PSI.

NUMERICAL, STRUCTURE-BASED SIMULATION

To model the kinetics of PSI, not containing red chls, we performed a simulation based upon the recent 2.5 Å structural model of trimeric PSI from *Synechococcus elongatus*.⁵ Although for some pairs of chls in the PSI core strong excitonic effects may exist, most interactions are small, and for that reason we chose for a simulation based on Förster energy-transfer.

Procedure

We calculated all pairwise energy-transfer rates between the 96 different chls in the system using the Förster equation:^{23,26,27}

$$k_{DA} = \frac{k_r^D}{n^4} \cdot \frac{\kappa_{DA}^2}{R_{DA}^6} \cdot I_{DA} \quad 5-1$$

in which k_{DA} is the rate of transfer of an excitation from a donor chl D to an acceptor chl A in ps^{-1} , k_r^D is the radiative rate of chl a , for which we use the value $5.4 \cdot 10^{-5} \text{ps}^{-1}$.²⁶ n is the index of refraction of the protein. R_{DA} is the distance between donor and acceptor in nm. R_{DA} was determined by taking the distance between the centres of the 4 coordinating nitrogen atoms N_A - N_D for each pair of chls in the structure. κ_{DA} is an orientational factor defined by:

$$\kappa_{DA} = (\hat{\mu}_A \cdot \hat{\mu}_D) - 3(\hat{\mu}_A \cdot r_{AD})(\hat{\mu}_D \cdot r_{AD}) \quad 5-2$$

in which $\hat{\mu}_D$ and $\hat{\mu}_A$ represent the Q_y transition dipole moment unit vectors of the donor and the acceptor and r_{AD} represents the unit vector along the line connecting the centres of both transition dipole moments. For each chl α molecule in the structure the vector connecting the nitrogen atoms N_B and N_D was taken to represent the direction of the Q_y transition dipole moment vectors. r_{AD} was calculated as the unit vector along the line connecting the centres of the 4 coordinating nitrogen atoms N_A - N_D for each pair of chls in the structure.

The factor I_{DA} in equation 5-1 represents the overlap integral between the donor emission spectrum and the acceptor absorption spectrum defined by:²⁶

$$I_{DA} = 8.8 \times 10^{17} \cdot \int \frac{\epsilon_A(\nu) \cdot F_D(\nu)}{\nu^4} d\nu \quad 5-3$$

$\epsilon_A(\nu)$ represents the acceptor absorption spectrum scaled to the value of the extinction coefficient (in $M^{-1}cm^{-1}$) in the absorption maximum and $F_D(\nu)$ represents the emission spectrum of the donor, normalized to unit area. Both spectra are recorded on a frequency scale (cm^{-1}).

For all chls, except P700, the overlap integrals I_{DA} were calculated using shifted absorption and emission spectra of chl α in acetone. The absorption spectrum of the two chls constituting P700 was approximated by a Gaussian peaking at 698 nm, with a FWHM of 19 nm. Two different cases were considered: that of a truly homogeneous antenna, with all the antenna chl α molecules absorbing maximal at 680 nm, and that of a heterogeneous antenna in which equal amounts of chls absorbing at 670, 680 and 690 nm were randomly distributed. In all cases the two chlorophylls at the position of A_0 were chosen to absorb at 686 nm, while the two accessory chls were put at 680 nm. We used $7.7 \cdot 10^4 M^{-1}cm^{-1}$ as the value of the maximum of the extinction coefficient of the bulk pools, which is the value reported by Lichtenthaler²⁸ for chl α in 80% acetone. The absorption spectrum of the P700 pool was scaled to that of the other pools by requiring it to have the same area.

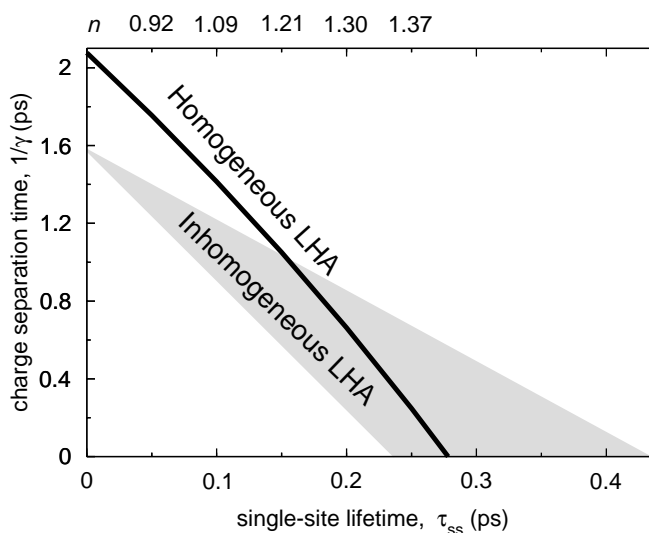
The energy-transfer rates were calculated using equation 5-1 for downhill energy-transfer only, i.e. pairs DA in which the absorption of D peaks at higher or equal energy as compared to the absorption of A . The complementary, uphill rates had to comply with the concept of detailed balance and were thus calculated as: $k_{ij} = k_{ji} \cdot e^{-(E_j - E_i)/k_B T}$.

So far this leaves only one free parameter in the simulation, i.e. the index of refraction, n , which effectively scales the average single-site lifetime τ_{ss} , defined as the time needed for an excitation to hop away from a chl site, averaged over all possible sites. We have to introduce a second free parameter, the trapping parameter γ , the rate at which excitations disappear from the system when they reach one of the two chls constituting P700.

For a particular set of values for n and γ , we can now construct the 96×96 matrix of pairwise energy-transfer and decay rates, the eigenvalues of which correspond to the 96 different lifetimes of the system.

Relation between n and $1/\gamma$

As pointed out above, the simulation only contains two adjustable parameters n and γ . We have recently demonstrated that a hypothetical PSI particle void of red chls exhibits a trapping time of 18 ps.¹ This slowest lifetime of 18 ps can be modelled using different combinations of n and γ (or τ_{ss} and $1/\gamma$). The solid line displayed in figure 5.2 represents all the combinations of the intrinsic trapping time $1/\gamma$ and τ_{ss} (which is \sim proportional to $1/n^4$ for a given spectral composition of the antenna) that yield a 18 ps trapping time. The upper axis also shows the actual values of n for the homogeneous antenna. It immediately strikes the eye that the relation between τ_{ss} and $1/\gamma$ is almost (but not perfectly) linear. The line in figure 5.2 readily provides upper limits for both τ_{ss} and $1/\gamma$, of ~ 275 fs and ~ 2 ps, respectively. However, these values correspond to infinitely fast trapping ($\gamma = \infty$) and transfer ($\tau_{ss} = 0$), respectively, and therefore are not physically realistic. Time-resolved fluorescence depolarisation measurements indicate that τ_{ss} has a value of 130 to 180 fs,^{29,30} corresponding to a charge-separation time $1/\gamma$ of between 0.9 and 1.2 ps. This value of $1/\gamma$ is fast compared to for instance the 3 ps charge-separation time reported for the purple-bacterial RC,³¹ but somewhat slower than the 400 fs charge-separation time as found by Groot et al.³² in PSII. For some more considerations regarding the differences between the rate of charge-separation in plant- and bacterial photosynthesis see refs. 10 and 33.



5.2 Solid line: combinations of the charge-separation time $1/\gamma$ and the average single-site lifetime τ_{ss} that result in a longest lifetime of 18 ps in PSI modelled with a homogeneous antenna. The upper axis shows the values of the index of refraction, n that correspond to the values of τ_{ss} on the lower axis (only for homogeneous antenna). The grey area encloses the interval in which similar relationships between $1/\gamma$ and τ_{ss} occurred for 16 random representations of a heterogeneous antenna (see text for details).

Earlier, a figure similar to figure 5.2 was produced based on the "old" 4 Å structure.¹⁰ In this simulation, the upper limit of the single-site lifetime was found to be about 150 fs, significantly faster than the 275 fs found for the new structure. The most important difference between both these structures is the fact that in the 2.5 Å structure the orientations of the pigments, and thus the approximate transition dipole moment orientations could be distinguished, whereas in the 4 Å structure a value of $2/3$ was used for the orientation factor κ^2 (the average value for randomly oriented chromophores in three dimensions). Applying the value of $2/3$ to the 2.5 Å structure (ignoring orientational information) leads to an upper limit for τ_{ss} of 160 fs, very close to that found for the 4 Å structure, indicating that the actual organization of the orientations of the antenna chls has an profound effect on the energy-transfer dynamics in the antenna. If we compare the simulations for the average and real orientations for the same values of n and γ we find that τ_{ss} is shorter in the case of an average orientation, but that the trapping time is in fact longer as compared to the case of the real orientations. In reality the antenna chls are apparently organized such that, although τ_{ss} is decreased with respect to random orientation, the excitations are "guided" such that excitations arrive to the RC faster than in case of randomly orientated antenna chls.

Applying a correction of a factor 2 to the vertical axis in figure 8 in ref. 10 (Gobets et al., in preparation) the upper limit for the trapping time is approximately the same for the 4 Å and the 2.5 Å structure. Since equilibration is infinitely fast in this case, this value of $1/\gamma$ simply reflects the relative population of excitations on P700 in a thermally-equilibrated state, times 18 ps. This relative population is slightly lower in the simulation based on the 2.5 Å structure as compared to the simulation based on the 4 Å structure, since in the former structure 96 chls were assigned, whereas in the latter only 89 chls could be distinguished.

In reality the bulk absorption band of the antenna in PSI is not completely homogeneous, but consists of several sub-bands, as evidenced by the absorption spectrum.¹⁰ To estimate the extent to which inhomogeneity leads to differences with the homogeneous case described above, we also performed the structure-based simulation using an antenna consisting of equal amounts of chls with absorption maxima at 670, 680 and 690 nm. The grey area in figure 5.2 represents the interval containing the relations between $1/\gamma$ and τ_{ss} leading to an 18 ps trapping time, for 16 different random compositions of the antenna. All antenna compositions result in the same intersection with the vertical axis, demonstrating that for $\tau_{ss} = 0$ the locations of the various spectral forms don't matter because the system is always in thermal equilibrium. The intersection is at a lower value of $1/\gamma$ as compared with the homogeneous antenna, reflecting that the thermal-equilibrium distribution of excitations is shifted towards the antenna in the case of the heterogeneous antenna.

According to figure 5.2, in case of a homogeneous antenna, n would reasonably have a value around 1.2, with an absolute upper limit of about 1.4. For all 16 compositions of the heterogeneous antenna a similar upper value of 1.3 -1.4 was found. This is consistent with values ranging between 1.22 and 1.34 as found for CPC and APC as discussed in van Amerongen et al.,²⁷ although significantly smaller than the 1.6 ± 0.1 value reported for PCP²⁶ and the value of 1.51 ± 0.04 for CP47.³⁴

Of course the values of k_r^D and the maximum of the extinction coefficient need not be the same for chl a in the PSI protein as compared to chl a in solution, which could account for a significant variation of the actual value of n .³⁵ Also the value of the Stokes' shift may actually be different in the protein.

ANALYTICAL, LATTICE MODEL SIMULATION

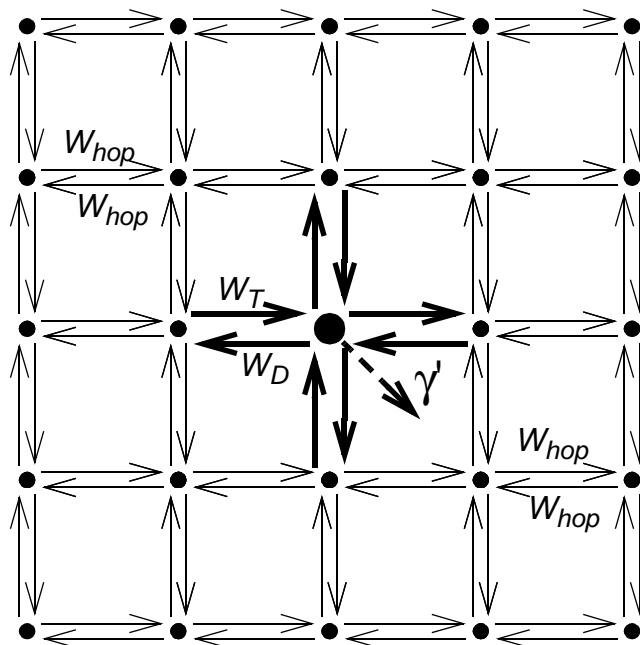
We will now discuss the results of the numerical structure-based analysis in terms of a lattice model in the analytical (Pearlstein) approach. Since this model involves only a limited number of parameters, it represents a simplified view of the system under consideration. However, it is just this kind of simplification that may result in more insight in the global energy-transfer features between the antenna and the RC in PSI than would be obtained by just inspecting the $96 \times 95 + 1$ individual rates or the 96 eigenvalues present in the structure-based calculation of energy transfer. Moreover, a comparison of the results of the lattice model with the results obtained from structure-based calculations may shed some light on the general validity of the application of lattice-models not only to photosynthetic systems, but to any (large) energy-transferring system, such as dendrimers,^{36,37} films of dyes,³⁸ and dye-networks contained in zeolite crystals,³⁹ mesoporous silica,⁴⁰ or (polystyrene) microspheres.⁴¹

Perturbed two-level approach: theory

In figure 5.3 we give a schematic representation of the lattice model used to describe PSI. Every lattice-site indicated by a dot represents a chl site in the antenna, except for one site, indicated by the larger dot, which represents the whole of the RC. Energy transfer occurs between any of the antenna chls and its nearest neighbours with the rate W_{hop} . We start out considering a homogeneous antenna for which all antenna chls have the same energy and consequently, W_{hop} is a constant. In that case the single-site lifetime of an antenna chl site, τ_{ss} , equals $(zW_{hop})^{-1}$, in which z , the coordination number, represents the number of nearest neighbours of a lattice site. The energy transfer between the RC and its nearest neighbours occurs with separate rates W_T and W_D respectively. The RC is the only site in the system where excitations can be quenched, which occurs at a rate of charge-separation γ' . In reality the RC does not consist of only one single chl site, but contains 6 chl a molecules. In the structure-based simulation, charge-separation is presumed only to take place from the two chls constituting P700, at a rate γ . The rates γ' and γ therefore differ by a factor which accounts for the population of excitations on P700 relative to the other RC chls. By assuming that excitation equilibration among the chls within the RC is very fast γ' and γ are related by:

$$\gamma' = \gamma \times \frac{e^{-E_{P700}/k_B T}}{e^{-E_{P700}/k_B T} + e^{-E_{A0}/k_B T} + e^{-E_{acc}/k_B T}} \quad 5-4$$

in which E_{P700} , E_{A0} and E_{acc} represent the energies of the chl dimer constituting P700, the two chls at the position of the primary electron acceptor and the two accessory chls, respectively. k_B is Boltzmann's constant and T is the absolute temperature. The model in figure 5.3 is



5.3 Schematic representation of the lattice model. The small dots represent antenna chl sites, the large dot in the middle represents the RC. W_{hop} is the hopping rate between two "normal" neighbours, W_T and W_D represent the rates of energy-transfer to and from the RC. γ' is the rate of charge-separation from the RC.

presented as a square lattice, but we note that we do not make any *a priori* assumptions regarding the type of lattice. The specific lattice properties will be accounted for by a structure-function $g_d(N)$, the value of which will be compared to that of known, regular lattices (see below).

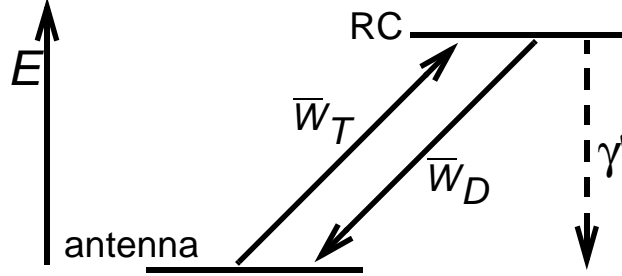
Since the average inter-pigment distance in the antenna is significantly shorter than the distance between the RC and the antenna, it seems reasonable to assume that equilibration within the antenna is faster than the transfer of excitations to the RC. Therefore, as a first order approximation, we take the energy migration in the antenna to be infinitely fast, and subsequently we account for the finite time of the migration in a perturbative way.^{2,27}

In the case of infinitely fast migration in the antenna, i.e. $\tau_{ss} = 0$, the lattice model can be treated as the two-level system shown in figure 5.4, with the upper level representing the RC and the lower level representing the antenna. Here \bar{W}_T and \bar{W}_D are trapping (delivery) and de-trapping (escape) rates of the two level system, which are related to the microscopic trapping and delivery rates W_T and W_D by:^{2,27}

$$\bar{W}_T = \frac{zW_T}{N}$$

5-5

and



5.4 Energy scheme on which the perturbed two level model is based. The two levels represent the antenna and the RC. \bar{W}_T and \bar{W}_D represent the forward and backward energy-transfer rates between both levels and γ' is the rate of charge-separation from the RC.

$$\bar{W}_D = zW_D, \quad 5-6$$

in which N is the total number of antenna chls. In the case of a homogeneous antenna, \bar{W}_T can be regarded as the average energy-transfer rate from any chl site in the antenna to the RC, and \bar{W}_D as the total rate of energy-transfer from the RC to the antenna.

In case $\tau_{ss} = 0$ the antenna and the RC must be in Boltzmann equilibrium and therefore \bar{W}_T and \bar{W}_D are related by:

$$\bar{W}_D = \beta \times \bar{W}_T, \quad 5-7$$

with

$$\beta = \frac{\sum e^{-E_{ant,i}/k_B T}}{\sum e^{-E_{RC,i}/k_B T}}, \quad 5-8$$

in which $E_{ant,i}$ and $E_{RC,i}$ represent the energy levels of the individual antenna and RC chls, and the summations are over all antenna and RC chls respectively.

The two-level system exhibits two rate constants the values of which are given by:

$$\lambda_{\pm} = \frac{\gamma' + \bar{W}_T + \bar{W}_D \pm \sqrt{(\gamma' + \bar{W}_T + \bar{W}_D)^2 - 4\gamma'\bar{W}_T}}{2}, \quad 5-9$$

where λ_+ represents the excitation equilibration rate between the antenna and the RC, and λ_- the excitation decay rate from the equilibrated distribution.

Taking the finite time of excitation migration into account perturbatively results in an additive excitation migration time, τ_{mig} , for the equilibration (τ_+) and decay (τ_-) times:^{2,27}

$$\tau_{\pm} = \frac{1}{\lambda_{\pm}} + \tau_{mig} \quad 5-10$$

The excitation migration time within the antenna is given by:^{2,27}

$$\tau_{mig} = \frac{N\bar{W}_T\bar{W}_D}{(\bar{W}_T + \lambda_{\pm})^2 + \bar{W}_T\bar{W}_D} g_d(N) z\tau_{ss} \quad 5-11$$

in which $g_d(N)$ is the structure-function of the antenna system which depends on the type of lattice (i.e. linear, square, hexagonal, cubic, etc.) (see refs. 2 and 27).

Combining equation 5-9 with equation 5-7, and replacing the square root by the first two terms of its Taylor expansion ($4(\bar{W}_T/\gamma)/(1 + (\beta + 1)\bar{W}_T/\gamma)^2 < 1$ since $\beta > 4$) we can approximate $1/\lambda_-$ by:

$$\frac{1}{\lambda_-} = \frac{1}{\bar{W}_T} + \frac{\beta + 1}{\gamma} \quad 5-12$$

If we substitute this expression for λ_- into equation 5-11 we find that the first term in the denominator of equation 5-11 can be neglected since $\bar{W}_T^2 \ll \beta \bar{W}_T^2 = \bar{W}_T\bar{W}_D$ and therefore $((\beta + 1)\bar{W}_T/\gamma)^2 / (1 + (\beta + 1)\bar{W}_T/\gamma)^2 \ll \bar{W}_T\bar{W}_D$. Therefore we can approximate τ_{mig} by:

$$\tau_{mig} = Nzg_d(N)\tau_{ss}. \quad 5-13$$

Substitution of equations 5-12 and 5-13 into equation 5-10 results in:

$$\tau_- = \tau_{del} + \tau_q \quad 5-14$$

in which

$$\tau_{del} = \left(Nzg_d(N) + \frac{1}{\bar{W}_T\tau_{ss}} \right) \tau_{ss} \quad 5-15$$

can be regarded as the average time needed to deliver an excitation from the antenna to the RC, analogous to the first passage time, τ_{fpt} as defined for local trap models.^{2,21,27} Note that

since \bar{W}_T and $1/\tau_{ss}$ are proportional, $\bar{W}_T\tau_{ss}$ is a constant depending on the structure only, and therefore remains unchanged upon variation of τ_{ss} . The second term in equation 5-14,

$$\tau_q = (\beta + 1)\left(\frac{1}{\gamma}\right) \quad 5-16$$

can be regarded as the average time needed to quench the excitation after delivery.

Since the value of τ_- is fixed to 18 ps, equations 5-14, 5-15 and 5-16 result in the following linear relationship between τ_{ss} and $1/\gamma$:

$$1/\gamma = \frac{1}{\beta + 1}\left(\tau_- - \left(Nzg_d(N) + \frac{1}{\bar{W}_T\tau_{ss}}\right)\tau_{ss}\right) \quad 5-17$$

Thus we have shown that the perturbed two-level approach actually predicts the (almost) linear relation between τ_{ss} and $1/\gamma$, as obtained from the structure-based numerical simulations, displayed in figure 5.2.

Perturbed two-level approach: results

Homogeneous antenna

The solid curve in figure 5.2, which represents the relation between τ_{ss} and $1/\gamma$ for a homogeneous antenna can be approximated by a straight line which intersects both axes at the coordinates $(0, (1/\gamma)_{max})$ and $(\tau_{ss,max}, 0)$. Using $(1/\gamma)_{max}$ rather than $(1/\gamma)_{max}$ this yields:

$$(1/\gamma) = (1/\gamma)_{max} - \frac{(1/\gamma)_{max}}{\tau_{ss,max}}\tau_{ss} \quad 5-18$$

Equating this expression to equation 5-17 yields:

$$\beta = \frac{\tau_-}{(1/\gamma)_{max}} - 1 \quad 5-19$$

and

$$zg_d(N) = \frac{1}{N}\left(\frac{(1/\gamma)_{max}}{\tau_{ss,max}}(\beta + 1) - \frac{1}{\bar{W}_T\tau_{ss}}\right) \quad 5-20$$

The value of $(1/\gamma)_{max}$ for the homogeneous antenna measures 2.08 ps and using equation 5-4 with values for E_{P700} , E_{A0} and E_{acc} corresponding to 698 nm, 686 nm and 680 nm this

yields $(1/\gamma)_{max} = 3.03$ ps. Inserting this value in equation 5-19, using $\tau_- = 18$ ps, yields $\beta = 4.94$, which is identical to the value found applying equation 5-8 with $E_{ant,i}$ corresponding to 680 nm. This confirms that in the limit of $\tau_{ss} = 0$ both the two-level model and the structure-based simulation result in the same equilibrium between the antenna and the RC.

In order to make an estimate of $zg_d(N)$ we need to make an estimate of the constant $\bar{W}_T\tau_{ss}$, that is, estimate \bar{W}_T for a particular value of τ_{ss} . As mentioned above \bar{W}_T for a homogeneous antenna can be regarded as the average energy-transfer rate from any antenna chl to any chl in the RC. The estimate can therefore be obtained from the structure-based simulation by calculating:

$$\bar{W}_T = \frac{1}{N} \sum_{i=1}^N \sum_{j=1}^6 k_{ij} \quad 5-21$$

in which k_{ij} represents the transfer rate from antenna chl i to RC chl j , and the summations are over all antenna chls and all RC chls, respectively. For $\tau_{ss} = 0.15$ ps this yields $\bar{W}_T = 0.227$ ps⁻¹ and therefore $\bar{W}_T\tau_{ss} = 0.034$ and $zg_d(N) = 0.39$.

Since $\bar{W}_T\tau_{ss}$ equals $\bar{W}_D\tau_{ss}/\beta$ we can also estimate this constant if we can make an estimation of \bar{W}_D based upon the structure-based simulation. According to equation 5-6, \bar{W}_D is the total transfer rate from the RC to the antenna. Because in the lattice model we treat the RC as a single site rather than the six chls it consists of in reality, we estimate \bar{W}_D as a weighted sum of the rates from all 6 RC chls to the antenna. If we assume that the equilibration within the RC is fast with respect to transfer to the antenna, the weighing factor is just a Boltzmann factor and

$$\bar{W}_D = \left(\sum_{i=1}^N \sum_{j=1}^6 e^{E_j/k_B T} k_{ji} \right) / \sum_{j=1}^6 e^{E_j/k_B T}, \quad 5-22$$

in which E_j represents the energy of RC chl j , k_{ji} represents the transfer rate from RC chl j to antenna chl i , and the summations are again over all antenna chls and all RC chls, respectively. For $\tau_{ss} = 0.15$ ps and the RC energies used above, this yields $\bar{W}_D = 0.925$ ps⁻¹ and $\bar{W}_D\tau_{ss}/\beta = 0.028$. The difference between this value and the value of $\bar{W}_T\tau_{ss} = 0.034$, estimated above, indicates that our assumption of infinitely fast equilibration within the RC is not fully correct. The value of $\bar{W}_D\tau_{ss}/\beta = 0.028$ corresponds to $zg_d(N) = 0.32$. Since the estimation of $zg_d(N)$ based upon \bar{W}_T did not require any assumptions regarding equilibration in the RC we consider the first estimation as more reliable.

Inhomogeneous antenna

The grey triangle in figure 5.2 indicates the variation in the relation between τ_{ss} and $1/\gamma$ that was found for 16 heterogeneous compositions of the antenna, under the condition that

$\tau_{\perp} = 18$ ps (see above). All antenna compositions result in the same intersection with the vertical axis, at a value of $(1/\gamma)_{max} = 1.58$, corresponding to $\beta = 6.83$, once more identical to the value obtained using equation 5-8. The value of β is larger as compared to the case of a homogeneous antenna, expressing that with this choice of the antenna composition the equilibrium is shifted towards the antenna.

Estimations of $zg_d(N)$ were obtained in a similar way as for the homogeneous antenna, with the exception that for the estimation of the value of \bar{W}_T equation 5-21 was modified with a weighing factor to obtain

$$\bar{W}_T = \frac{1}{N} \left(\sum_{i=1}^N \sum_{j=1}^6 e^{E_{LHA,i}/k_B T} k_{ij} \right) / \sum_{i=1}^N e^{E_{LHA,i}/k_B T} \quad 5-23$$

Here we account for the relative occupancies of the antenna chls, assuming the antenna to be spectrally equilibrated. For \bar{W}_D we can just apply equation 5-22. For $\tau_{ss} = 0.15$ ps, we thus find $\bar{W}_T = 0.29 \pm 0.08$ ps⁻¹ and $\bar{W}_D = 1.6 \pm 0.4$ ps⁻¹, corresponding to values of $g_d(N)z$ of 0.33 ± 0.06 and 0.28 ± 0.06 .

Perturbed two-level approach: discussion

We have applied the perturbed two-level approach to model the kinetics of PSI. The aim of this study is twofold: first, the comparison with the structural model allows to judge the applicability of this approach to other systems for which no structural information is available, second, the perturbed two-level model provides a framework for describing the system in terms of a few global, intuitive parameters, rather than the many microscopic parameters resulting from structure-based modelling. We will discuss some of these global parameters and comment on the application of the perturbed two-level model to other systems

The delivery and escape times τ_{del} and \bar{W}_D^{-1} .

Here we discuss in some detail the value of the delivery time, τ_{del} , defined in equation 5-15, and how its value relates to other, independent experimental observations. τ_{del} is the sum of two contributions, $Nzg_d(N)\tau_{ss}$ and \bar{W}_T^{-1} . Analogous to definitions used in local-trap models²⁷ it is tempting to equate these two factors to τ_{mig} and τ_T . However, in the definition of τ_{mig} in the local-trap model the structure-function $g_d(N)$ is replaced by a structure-function $h_d(N)$, which is larger. In the perturbed 2-level model therefore part of the migration through the antenna is accounted for by the factor \bar{W}_T^{-1} .

Time-resolved depolarisation measurements indicate a value of $\tau_{ss} \sim 0.15$ ps,^{29,30} and recent modelling of the experimentally observed excitation-wavelength dependence of the fluorescence kinetics in PSI indicates a similar value for τ_{ss} .¹³ For this value of τ_{ss} we find a value of \bar{W}_T of 0.227 ps⁻¹ for the homogeneous antenna and somewhat faster, ~ 0.29 ps⁻¹ for the inhomogeneous antenna. The value of \bar{W}_T^{-1} therefore amounts to about 4 ps. The difference between the homogeneous and inhomogeneous antenna reflects that the overlap

integrals of the inhomogeneous antenna with the RC are on the average 28% better than for the homogeneous antenna.

Using equation 5-13, and applying $g_d(N)z \sim 0.33$ we calculate that $\tau_{mig} \sim 4.5$ ps, and therefore τ_{del} is of the order of 8.5 ps.

This estimated value of τ_{del} happens to be basically equal to the effective time needed to transfer energy from the bulk antenna to any of the two pools of red chls in *Synechococcus* trimeric PSI¹ $((18^{-1}+17^{-1})^{-1} = 9.2$ ps) showing that energy transfer from the bulk to the RC on the one hand, and the red chls on the other hand, are two competing processes. These findings are corroborated by low-temperature steady-state and time-resolved spectroscopy experiments: the 4K excitation spectrum of *Synechococcus* trimeric PSI shows that 50% of the excitations are directed to the RC, resulting in a charge-separation, and the remaining 50% of the excitations are transferred to the red chls, were they remain trapped because uphill transfer is blocked at this temperature¹⁰ indicating that transfer from the bulk antenna to either the RC or the red chls is equally likely. Also time-resolved streak camera measurements performed at 77 K show an initial 5 ps process, representing energy transfer from the bulk antenna chls to the red chls and photochemical quenching in the RC (Gobets et al., manuscript in preparation), which is the lifetime expected to result from these two competing processes. We do note, however, that the bands of red chls are shifted significantly at low temperatures, as compared to room temperature, and therefore it is not straightforward to assume that all downhill transfer rates remain the same upon cooling.

The escape rate from the RC is given by the rate \bar{W}_D , which is 0.925 ps⁻¹ for the homogeneous antenna and ~ 1.6 ps⁻¹ for the inhomogeneous antenna; 73% faster than the for homogeneous antenna. This demonstrates that the inhomogeneity of the antenna greatly increases the backtransfer from the RC, which must be caused by an enhanced overlap of P700 with the antenna. In any case the de-trapping occurs in the order of 0.8 ps, and thus competes with charge-separation ($1/\gamma' \sim 1.5$ ps).

Obviously the values of \bar{W}_T and \bar{W}_D should differ between the homogeneous and inhomogeneous antenna, due to the shift of the equilibrium between antenna and RC (i.e., the value of β in equation 5-7). The major difference occurs in the value of \bar{W}_D , since \bar{W}_D depends mainly on the energy difference between the antenna and the RC, whereas \bar{W}_T to a large extent depends on the migration through the antenna (see above), and not so much on this energy difference.

The structure-function

For regular lattice-models (i.e. square, hexagonal, cubic) in which only nearest neighbour-interactions are considered, the value of z , the coordination number is well defined. However, the real structure of PSI is irregular, and energy transfer is not considered to be limited to nearest neighbours only. In order to make an estimation of the value of the structure-function, $g_d(N)$, we attempted to make a definition of z which would also be applicable to an irregular structure. A reasonable proposal would be to regard z as the ratio between the rate from an antenna chl to its nearest neighbour, and the sum of all the rates away from this antenna chl (τ_{ss}^{-1}), averaged over all antenna chls. This, however, led to a rather low value of $z = 1.7$, (compare to $z = 4$ for a square lattice and $z = 6$ for a cubic lattice) and since $g_d(N)$ is inversely proportional to z , this led to high values of $g_d(N)$. We concluded

that in order to compare the effective value of the structure-function of PSI, resulting from the application of the lattice model to the structure-based simulations with the values of the structure-function of regular lattices, it is more appropriate to consider the value of $zg_d(N)$, than the value of $g_d(N)$.

We estimated a value of $0.32 < zg_d(N) < 0.39$ for a homogeneous antenna, and a somewhat lower value of $0.28 < zg_d(N) < 0.33$ for an inhomogeneous antenna. Comparing this to the values of ~ 0.24 , for a cubic lattice and ~ 0.64 for a square lattice^{2,27} we conclude that the PSI structure exhibits a mixture of the characteristics of a two-dimensional, square lattice, and a three-dimensional, cubic lattice. This is in agreement with the structural data, which show that the antenna consists of a central domain which is essential three-dimensional, and a peripheral domain that exhibits a bi-planar architecture.

The validity of model

We have shown that the application of the perturbed two-level model reproduces the linear relation between τ_{ss} and $1/\gamma$ that was found in the structure-based simulation and that the comparison of both models results in a realistic value for the structure-function $zg_d(N)$. Also the resulting value for $\tau_{fpt} = \bar{W}_T + \tau_{mig} \sim 8.5$ ps for a realistic value of $\tau_{ss} = 0.15$ ps is consistent with independent time-resolved and steady-state fluorescence measurements. Since the perturbed two-level model approach works well for PSI, there seems to be no reason why this approach should not be used in other (artificial) antenna-trap systems such as dendrimer systems,^{36,37} films of dyes,³⁸ or systems of dye molecules attached to some kind of substrate such as for instance zeolite crystals,³⁹ mesoporous silica,⁴⁰ or polystyrene microbeads,⁴¹ for which structures have not been resolved, or which are inherently chaotic. It may not be feasible to follow the exact same approach (i.e. varying τ_{ss} and $1/\gamma$ such that τ_- remains constant), but we note that equation 5-17 in fact defines a plane in $(\tau_{ss}, 1/\gamma, \tau_-)$ -space, and that sections through that plane, other than shown in figure 5.2, also yield the required parameters. In particular one could consider varying τ_{ss} by varying the dye concentration and recording the corresponding values of τ_- ($1/\gamma$ remains unchanged).

CONCLUSIONS

Using a structure-based numerical simulation of energy transfer, we have shown that in a PSI particle without red chls the possible combinations of τ_{ss} and $1/\gamma$ follow an (almost) linear relationship, and that upper limits of these parameters are ~ 400 fs and ~ 2 ps respectively. A realistic value is $\tau_{ss} = 150$ fs, for which $1/\gamma$ measures about one ps. The value of the index of refraction was found to be ~ 1.2 , with an upper limit of 1.4. Interestingly, we find that the relative orientations of the antenna chls are organized such that excitations are directed to the RC faster than could be achieved for a random orientation of these chls, despite the fact that this organization results in a longer single-site lifetime. Using a lattice-based model, the perturbed two-level model, to describe the energy transfer and trapping in this system the linear relation between τ_{ss} and $1/\gamma$ could be reproduced. Equating this linear relationship to the one obtained by the structure-based simulation results in a value of the (modified) structure-function $zg_d(N)$, which lies in between that for cubic and square lattice,

indicating correctly that the actual structure exhibits characteristics of both these structures. We conclude that for realistic values of τ_{ss} and $1/\gamma$, τ_q and τ_{del} are both about 9 ps, demonstrating that the system is neither transfer- nor trap-limited. We have shown that these values are consistent both with time-resolved fluorescence measurements and fluorescence excitation measurements at low temperatures. We finally conclude that, since the perturbed two-level model appropriately describes the global energy-transfer properties of a complex photosynthetic RC-antenna complex such as PSI, it may also be applied to other (artificial) systems.

ACKNOWLEDGMENTS

We thank dr. Herbert van Amerongen for helpful discussions and suggestions. L.V. was supported by a grant from the European Union (Improving Human Potential Contract Nr. HPRI-CT-1999-00064)

REFERENCES

- (1) Gobets, B., I.H.M. van Stokkum, M. Rögner, J. Kruij, E. Schlodder, N.V. Karapetyan, J.P. Dekker, and R. van Grondelle. 2001. Time-resolved fluorescence emission measurements of Photosystem I particles of various cyanobacteria: a unified compartmental model. *Biophys. J.* 81:407-424.
- (2) Somsen, O.J.G., L. Valkunas, and R. van Grondelle. 1996. A perturbed two-level model for exciton trapping in small photosynthetic systems. *Biophys. J.* 70:669-683.
- (3) Scheller, H.V., H. Naver, and B.L. Moller. 1997. Molecular aspects of Photosystem I. *Physiol. Plant.* 100:842-851.
- (4) Kruij, J., D. Bald, E. Boekema, and M. Rögner. 1994. Evidence for the existence of trimeric and monomeric Photosystem I complexes in thylakoid membranes from cyanobacteria. *Photosynth. Res.* 40:279-286.
- (5) Jordan, P., P. Fromme, H.T. Witt, O. Klukas, W. Saenger, and N. Krauss. 2001. Three-dimensional structure of cyanobacterial Photosystem I at 2.5 Angstrom resolution. *Nature.* 411:909-917.
- (6) Shubin, V.V., S.D.S. Murthy, N.V. Karapetyan, and P. Mohanty. 1991. Origin of the 77K variable fluorescence at 758 nm in the cyanobacterium *Spirulina platensis*. *Biochim. Biophys. Acta.* 1060:28-36.
- (7) Van der Lee, J., D. Bald, S.L.S. Kwa, R. van Grondelle, M. Rögner, and J.P. Dekker. 1993. Steady-state polarized-light spectroscopy of isolated Photosystem-I complexes. *Photosynth. Res.* 35:311-321.
- (8) Gobets, B., H. van Amerongen, R. Monshouwer, J. Kruij, M. Rögner, R. van Grondelle, and J.P. Dekker. 1994. Polarized site-selected fluorescence spectroscopy of isolated Photosystem I particles. *Biochim. Biophys. Acta.* 1188:75-85.
- (9) Pålsson, L.-O., J.P. Dekker, E. Schlodder, R. Monshouwer, and R. van Grondelle. 1996. Polarized site-selective fluorescence spectroscopy of the long-wavelength emitting chlorophylls in isolated Photosystem I particles of *Synechococcus elongatus*. *Photosynth. Res.* 48:239-246.
- (10) Gobets, B., and R. van Grondelle. 2001. Energy transfer and trapping in Photosystem I. *Biochim. Biophys. Acta.* 1507:80-99.

- (11) Van Grondelle, R., J.P. Dekker, T. Gillbro, and V. Sundström. 1994. Energy transfer and trapping in photosynthesis. *Biochim. Biophys. Acta.* 1187:1-65.
- (12) Pålsson, L.-O., C. Flemming, B. Gobets, R. van Grondelle, J.P. Dekker, and E. Schlodder. 1998. Energy transfer and charge separation in Photosystem I: P700 oxidation upon selective excitation of the long-wavelength chlorophylls of *Synechococcus elongatus*. *Biophys. J.* 74:2611-2622.
- (13) Gobets, B., I.H.M. van Stokkum, F. van Mourik, M. Rögner, J. Kruij, E. Schlodder, J.P. Dekker, and R. van Grondelle. 2002. Excitation wavelength dependence of fluorescence kinetics in Photosystem I particles from *Synechocystis* PCC 6803 and *Synechococcus elongatus*. *Submitted*.
- (14) Owens, T.G., S.P. Webb, L. Mets, R.S. Alberte, and G.R. Fleming. 1987. Antenna size dependence of fluorescence decay in the core antenna of Photosystem I: estimates of charge separation and energy transfer rates. *Proc. Natl. Acad. Sci. USA.* 84:1532-1536.
- (15) Jean, J.M., C.-K. Chan, G.R. Fleming, and T.G. Owens. 1989. Excitation transport and trapping on spectrally disordered lattices. *Biophys. J.* 56:1203-1215.
- (16) Beauregard, M., I. Martin, and A.R. Holzwarth. 1991. Kinetic modeling of exciton migration in photosynthetic systems. 1. Effects of pigment heterogeneity and antenna topography on exciton kinetics and charge separation yields. *Biochim. Biophys. Acta.* 1060:271-283.
- (17) Jia, Y., J.M. Jean, M.M. Werst, C.-K. Chan, and G. R. Fleming. 1992. Simulations of the temperature dependence of energy transfer in the PSI core antenna. *Biophys. J.* 63:259-273.
- (18) Trinkunas, G., and A.R. Holzwarth. 1994. Kinetic modeling of exciton migration in photosynthetic systems. 2. Simulations of excitation dynamics in 2-dimensional photosystem core antenna/reaction center complexes. *Biophys. J.* 66:415-429.
- (19) Laible, P.D., W. Zipfel, and T.G. Owens. 1994. Excited-state dynamics in chlorophyll-based antennae - The role of transfer equilibrium. *Bioph. J.* 66:844-860.
- (20) Trinkunas, G., and A.R. Holzwarth. 1996. Kinetic modeling of exciton migration in photosynthetic systems. 3. Application of genetic algorithms to simulations of excitation dynamics in three-dimensional Photosystem I core antenna/reaction center complexes. *Bioph. J.* 71:351-364.
- (21) Pearlstein, R.M. 1982. Exciton migration and trapping in photosynthesis. *Photochem. Photobiol.* 35:835-844.
- (22) Den Hollander, W.T.F., J.G.C. Bakker, and R. van Grondelle. 1983. Trapping, loss and annihilation of excitations in a photosynthetic system I. Theoretical aspects. *Biochim. Biophys. Acta.* 725:492-507.
- (23) Förster, T. 1948. Zwischenmolekulare Energiewanderung und Fluoreszenz. *Ann. Physik* 6(2): 55-74.
- (24) Rätsep, M., T.W. Johnson, P.R. Chitnis, and G.J. Small. 2000. The red-absorbing chlorophyll-*a* antenna states of Photosystem I: A hole-burning study of *Synechocystis* sp PCC 6803 and its mutants. *J Phys. Chem. B.* 104:836-847.
- (25) Valkunas, L., V. Liuolia, J.P. Dekker, and R. van Grondelle. 1995. Description of energy migration and trapping in Photosystem I by a model with two distance scaling parameters. *Photosynth. Res.* 43:149-154.
- (26) Kleima, F.J., E. Hofmann, B. Gobets, I.H.M van Stokkum, R. van Grondelle, K. Diederichs, and H. van Amerongen. 2000. Förster excitation energy transfer in peridinin-chlorophyll-*a*-protein. *Biophysical J.* 78:344-353.
- (27) Van Amerongen, H., L. Valkunas, and R. van Grondelle. 2000. Photosynthetic Excitons, World Scientific, London. 347-352.

- (28) Lichtenthaler, H.K. 1987. Chlorophylls and carotenoids: pigments of photosynthetic membranes. *Methods Enzymol.* 148:350-382.
- (29) Du, M., X. Xie, Y. Jia, L. Mets, and G.R. Fleming. 1993. Direct observation of ultrafast energy transfer in PS I core antenna. *Chem. Phys. Lett.* 201:535-542.
- (30) Kennis, J.T.M., B. Gobets, I.H.M. van Stokkum, J.P. Dekker, R. van Grondelle, and G.R. Fleming. 2001. Light harvesting by chlorophylls and carotenoids in the Photosystem I complex of *Synechococcus elongatus*: a fluorescence upconversion study. *J. Phys. Chem. B.* 105:4485-4494.
- (31) Parson, W.W. 1991. Reaction centers. In Chlorophylls. H. Scheer, editor. CRC Press, Boca Raton, FL. 1153-1180.
- (32) Groot, M.L., F. van Mourik, C. Eijkelhoff, I.H.M. van Stokkum, J.P. Dekker, and R. van Grondelle. 1997. Charge separation in the reaction center of Photosystem II studied as a function of temperature. *Proc. Natl. Acad. Sci.* 94:4389-4394.
- (33) Van Brederode, M.E., and R. van Grondelle. 1999. New and unexpected routes for ultrafast electron transfer in photosynthetic reaction centers. *FEBS Lett.* 455:1-7.
- (34) Renge, I., R. van Grondelle, and J.P. Dekker. 1996. Matrix and temperature effects on absorption spectra of β -carotene and pheophytin- a in solution and in green plant Photosystem II. *J. Photochem. Photobiol. A: Chem.* 96:109-121.
- (35) Knox, R.S., and H. van Amerongen. 2002. Refractive index dependence of the Förster resonance excitation transfer rate. *J. Phys. Chem. B.* 106:5289-5293.
- (36) Neuwahl, F.V.R., R. Righini, A. Adronov, P.R.L. Malenfant, and J.M.J. Frechet. 2001. Femtosecond transient absorption studies of energy transfer within chromophore-labeled dendrimers. *J. Phys. Chem. B.* 105:1307-1312.
- (37) Benites, M.D., T.E. Johnson, S. Weghorn, L.H. Yu, P.D. Rao, J.R. Diers, S.I. Yang, C. Kirmaier, D.F. Bocian, D. Holten, and J.S. Lindsey. 2002. Synthesis and properties of weakly coupled dendrimeric multiporphyrin light-harvesting arrays and hole-storage reservoirs. *J. Mater. Chem.* 12:65-80.
- (38) Yatskou, M.M., H. Donker, R.B.M. Koehorst, A. van Hoek, and T.J.A. Schaafsma. 2001. Study of energy transfer processes in zinc-porphyrin films using Monte Carlo simulation of fluorescence decay. *Chem. Phys. Lett.* 345:141-150.
- (39) Calzaferri, G., M. Pauchard, H. Maas, S. Huber, A. Khatyr, and T. Schaafsma. 2002. Photonic antenna system for light harvesting, transport and trapping. *J. Mater. Chem.* 12:1-13.
- (40) Murata, S., H. Furukawa, and K. Kuroda. 2001. Effective inclusion of chlorophyllous pigments into mesoporous silica modified with alpha,omega-diols. *Chem. Mater.* 13:2722-2729.
- (41) Roberts, D.V., B.P. Wittmershaus, Y.Z. Zhang, S. Swan, and M.P. Klinosky. 1998. Efficient excitation energy transfer among multiple dyes in polystyrene microspheres. *J. Lumin.* 79:225-231.

6

Excitation wavelength dependence of the fluorescence kinetics in Photosystem I particles from *Synechocystis* PCC 6803 and *Synechococcus elongatus*

Bas Gobets, Ivo H.M. van Stokkum, Frank van Mourik, Matthias Rögner, Jochen Kruij, Eberhard Schlodder, Jan P. Dekker and Rienk van Grondelle

The excitation-wavelength dependence of the excited-state dynamics of monomeric and trimeric Photosystem I (PSI) particles from *Synechocystis* PCC 6803 as well as trimeric PSI particles from *Synechococcus elongatus* has been studied at room temperature using time-resolved fluorescence spectroscopy. For aselective (400 nm), carotenoid (505 nm) and bulk chlorophyll (~ 650 nm) excitation in all species a downhill energy-transfer component is observed corresponding to a lifetime of 3.4 to 5.5 ps. For selective red excitation (702-719 nm) in all species a significantly faster, ~ 1 ps, uphill transfer component was recorded. In *Synechococcus* PSI an additional ~ 10 ps downhill energy-transfer component is found for all wavelengths of excitation, except 719 nm. Each of the species exhibits its own characteristic trap spectrum, the shape of which is independent of the wavelength of excitation. This trap spectrum decays in ~ 23 ps in both monomeric and trimeric *Synechocystis* PSI and in ~ 35 ps in trimeric *Synechococcus* PSI. The data were simulated based on the 2.5 Å structural model of PSI of *Synechococcus elongatus* using the Förster equation for energy transfer, and using the 0.6-1 ps charge separation time and the value of 1.2-1.3 for the index of refraction that were obtained from the dynamics of a hypothetical PSI particle without red chls.¹ The experimentally obtained lifetimes and spectra were reproduced well by assigning three of the chlorophyll-*a* (chl*a*) dimers observed in the structure to the C708/C702RT pool of red chls present in PSI from both species. Essential for the simulation of the dynamics of *Synechococcus* PSI is the assignment of the single chl*a* trimer in the structure to the C719/C708RT pool present in this species.

INTRODUCTION

PSI is one of two photosystems in oxygenic photosynthesis. It uses light energy to transfer electrons from plastocyanin or soluble cytochrome c_6 to NADP^+ .

The PSI core is a large pigment-protein complex consisting of 11-13 protein subunits,^{2,3} the largest two of which, PsaA and PsaB, form a heterodimer to which the majority of the core antenna pigments (chl a and β -carotene) and as well as the reaction centre (RC) cofactors are bound. In cyanobacteria the PSI core complexes can be isolated both as monomers and trimers, and both forms may exist *in vivo* in a dynamic equilibrium, depending on the salt,⁴ the Ca^{2+} concentration and the pH.⁵

Trimeric PSI core particles from the cyanobacterium *Synechococcus elongatus* have been crystallized, and using X-ray diffraction the structure has been obtained at 2.5 Å resolution.^{6,7} In this structural model, 96 chl a 's, 22 β -carotene molecules, 2 phylloquinones and 3 Fe_4S_4 clusters can be distinguished at atomic resolution. About half of the antenna chls form a roughly elliptical bowl-shaped structure around the RC, which is extended by two groups of peripheral antenna molecules. Although the RC is located in the middle of the complex, the distance of any of the antenna chls to the RC cofactors is more than $\sim 18\text{Å}$, except for two chls that seem to form a "bridge" between the RC and the antenna. It has been suggested that these chls could play an important role in delivering excitations to the RC.^{8,9}

The PSI absorption spectrum is spectrally highly heterogeneous (see ref. 10). The different chl forms result from differences in the pigment-pigment and pigment-protein interactions, responsible for the shift of the absorption bands. The strongest shifts occur in the "red" or "long-wavelength" chls, which absorb at energies lower than that of the primary electron donor P700. It has been proposed that these red states are the result of strong pigment-pigment interactions between two or more chl molecules.¹¹ The number and absorption maxima of the red pools and the number of chls contained in them are highly species-dependent.^{10,12} Moreover, the red chl forms are also affected by the aggregation state of the cyanobacterial core complexes: in monomeric PSI core preparations the number of red chls is generally lower than in trimers.

PSI core particles from the cyanobacterium *Synechocystis* PCC 6803 at low temperatures show one single inhomogeneously broadened absorption band with a maximum at 708 nm (C708) with an oscillator strength of ~ 3 chl a molecules in monomers and 4-5 chl a molecules in each monomeric unit in trimers.^{11,13} On the basis of holeburning experiments Hayes et al.,¹⁴ concluded that in the trimers 2 chls contribute to C706, and another 2 chls contribute to C714. However, the fluorescence line-narrowing experiments, presented by Gobets et al.,¹¹ are not consistent with the presence of two distinct pools of red chls in the PSI core of *Synechocystis*, and in this paper we will regard this absorption as due to a single band. At room temperature the C708 pool is blue shifted to peak at about 702 nm (C702RT).^{13,15}

The 4K absorption spectrum of the trimeric core particles of the cyanobacterium *Synechococcus elongatus* clearly reveals two red chl bands with maxima at 708 nm (C708, corresponding to 4-6 chl a 's) and 719 nm (C719, corresponding to ~ 4 chl a 's).¹⁶ Like in PSI from *Synechocystis*, the C708 pool in *Synechococcus* PSI is blue shifted at room temperature to ~ 702 nm (C702RT), whereas the C719 pool is shifted to 708 nm (C708RT).¹³ In their

structural model of *Synechococcus* trimeric PSI Jordan et al.⁶ point out three dimers and one trimer of chl *a* as putative candidates for strongly coupled red chl sites. The trimer, consisting of the chls designated as aC-B31, aC-B32 and aC-B33, is located in the periphery of the antenna, whereas the dimers consisting of the chl pairs aC-A32/aC-B7, aC-A38/aC-A39 and aC-B37/aC-B38 are located closer to the RC. The dimer aC-A32/aC-B7 is located at the luminal side of the trimerization domain, and forms hydrophobic contacts with PsaL of the adjacent monomer, and has therefore been suggested to represent the C719 pool.⁶

The function of the red chl species is still a topic of debate. Some authors have suggested that in a non-equilibrium situation they may help to increase the efficiency of the system by concentrating excitations close to P700.¹⁷⁻²¹ Recent studies have shown, however, that the red chls actually slow down the effective rate of trapping.¹³ Others argue that the red chls may have a role in photoprotection,^{17,22} or that they simply increase the cross-section for absorption of red light by the PSI antenna,²³ important in shadelight environments.²⁴ Although the total number of low-energy chls is small, 3% to 10% of the total number of chls in the PSI core antenna, they have a very pronounced effect on the energy-transfer and trapping dynamics in the whole PSI system, which is evident from both time-resolved and steady-state spectroscopy experiments (for a review see ref. 10).

PSI from *Synechocystis* has been the subject of many room temperature time-resolved spectroscopy experiments.^{13,25-29} In all these studies one or two so-called equilibration components were observed in the dynamics. These components, that account for the energy transfer between the bulk chls and the low-energy chls, exhibited lifetimes between 2 and 6.5 ps. Trapping was consistently found to occur with a lifetime of 22-25 ps. In the few cases in which selective excitation of the low-energy chls was considered,^{25,29} no significant differences between the lifetimes and (decay-associated) spectra of the downhill (bulk or aselective excitation) and uphill (red excitation) energy-transfer components was found, other than the sign of the spectrum. The room temperature dynamics of *Synechococcus* PSI has been studied less extensively. Both Holzwarth et al. and Byrdin et al. have reported a single energy-transfer component of 7-14 ps for *Synechococcus* PSI,^{21,30} whereas Gobets et al.¹³ and Kennis et al.³¹ report two distinctly separate energy-transfer components with lifetimes of 3-4 and ~ 10 ps. All studies report a trapping lifetime of 30-38 ps in this species. So far no experiments have been reported involving selective excitation of the two pools of red chls present in this species.

Here we present a systematic time-resolved fluorescence study of monomeric and trimeric PSI from *Synechocystis*, as well as of trimeric PSI from *Synechococcus* for both aselective (see also ref. 13) and selective excitation of the red chls. Previously we simulated the kinetics of PSI from both *Synechocystis*³², and *Synechococcus*³³ using the 4 Å structural model.⁸ A major difficulty in these simulations was that the precise orientations of the chl molecules, and in particular the directions of the transition dipole moments, were not known. The new 2.5 Å model⁶ does provide the precise chl orientations as well as the assignment of 7 additional chls that could not be distinguished in the 4 Å model. We will show that our kinetic data of PSI from *Synechococcus* can, indeed, be simulated quite well using the 2.5 Å model of PSI from this species. Also the kinetics of PSI from *Synechocystis* could be reproduced quite well using the structural model of PSI from *Synechococcus*.

MATERIALS AND METHODS

The *Synechocystis* sp. PCC 6803 PSI monomers and trimers were prepared as in ref. 34 and contain 85 ± 10 chl a /P700. The trimeric PSI complexes from the thermophilic cyanobacterium *Synechococcus elongatus* were isolated as in ref. 35 and contain ~ 100 chl a /P700.

For the fluorescence experiments the samples were diluted to an OD₆₈₀ of 0.6/cm with a buffer containing 20 mM CaCl₂, 20 mM MgCl₂, 10 mM 2-(N-morpholino)ethane sulfonic acid (MES) and 0.05% W/V dodecyl- β -D-maltoside at a pH of 6.5. 10 mM Sodium ascorbate and 10 μ M phenazine meta sulphate (PMS) were added to all samples to prevent accumulation of P700⁺. To avoid multiple excitation of the same sample volume by successive laser flashes the sample was contained in a spinning cell (diameter 10 cm) rotating at 20 Hz. All experiments were performed at room-temperature (293 K). The experimental setup and procedures as well as the data processing were described in detail in ref. 13. In short, the samples were excited using 150–200 fs pulses at 400, 505, 650/660, 702, 710 and 719 nm which were generated at a 100 kHz repetition rate using a Titanium:sapphire based oscillator (Coherent MIRA), a regenerative amplifier (Coherent REGA) and a double pass optical parametric amplifier (Coherent OPA-9400).

The excitation light was focused with a 15 cm focal length lens, resulting in a focal diameter of 150 μ m in the sample. Fluorescence was collected at right angle to the excitation using achromatic lenses and detected through a sheet polarizer set at magic angle (54.7°), or perpendicular to the polarization of the excitation light, using a Hamamatsu C5680 synchroscan streak camera and a Chromex 250IS spectrograph. The streak-images were recorded on a Hamamatsu C4880 CCD camera which was cooled to -55°C. The full width at half maximum of the overall time-response of this system is 3–3.5 ps. The spectral resolution was 8 nm. One streak image covers 315 nm in the spectral domain (1018 pixels) and 200 ps (1000 pixels) in the time-domain. The applied pulse energy was varied between 1 and 4 nJ, depending on the wavelength of excitation, such that typically only 0.25% of all chls present in the focus was excited by each pulse, thus avoiding singlet-singlet annihilation.

In the data analysis a Gaussian shaped instrument response function (IRF) was assumed. The width of this Gaussian was a free parameter of the fit (typically 3–3.5 ps). In some cases the fit was improved by allowing for a small additional contribution ($\sim 5\%$) of a broader Gaussian to the instrument response.

All measurements were analysed using a model with a number of parallel compartments, which yields Decay-Associated Spectra (DAS). Some restrictions were imposed on the instantaneous spectrum (see table 6.1). For measurements in which a (Raman) scattering contribution was present, a pulse-limited contribution was included in the fit, in addition to the exponentially decaying components. In some of these measurements a small (5–10%) pulse-limited contribution was present at a time later than time zero. This contribution, which was assigned to a reflection, was fitted by allowing for a second pulse in the analysis, which exhibited the same width as the instrument response, but which was delayed by a certain time.

The periodicity of the synchroscan with a period of 13.4 ns results in a "back and forth" sweeping of long lived (> 1 ns) components, evident from the signal present before time zero

(the time of the maximum of the IRF). By taking this into account in the analysis, the lifetime and spectrum of a (single) long-lived component (such as some free chl present in the sample) could be estimated accurately on the 200 ps time-scale.

RESULTS

Room temperature absorption spectra

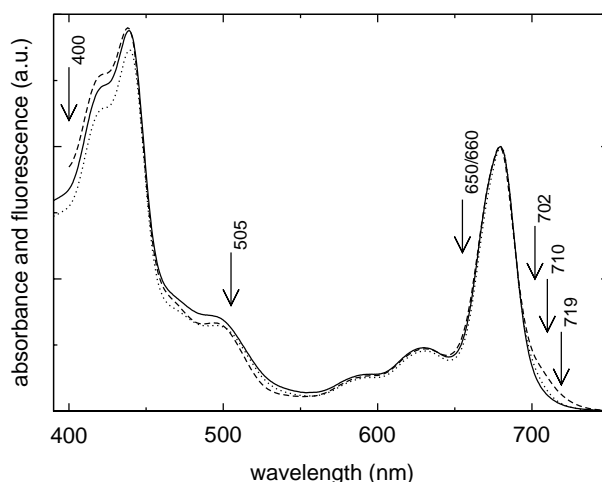
Figure 6.1 displays the room temperature absorption spectra of the three PSI preparations that were studied. Clearly the spectra are very similar; the only significant differences occur in the red edge of the Q_y absorption band, at wavelengths longer than ~ 700 nm, reflecting the variation in the amounts and energies of red-shifted chlorophylls (chls) between the three species.

Monomeric PSI from *Synechocystis* (solid) exhibits the least amount of these red chls. The trimeric PSI from the same species (dotted) shows slightly more red chl absorption, while trimeric PSI from *Synechococcus* (dashed) clearly contains considerably more red chls than the other two preparations. These observations are consistent with other room- and low-temperature estimates of the numbers of red chls contained in these PSI particles.¹³

Figure 6.1 also indicates the wavelengths of excitation used in the time-resolved fluorescence measurements. At 400 nm mainly the Soret-band of chl a is excited, and excitation is considered to be aselective at this wavelength. With 505 nm light the β -carotene molecules are predominantly excited. These molecules are known to transfer energy efficiently to chl a .^{31,36} The blue edge of the bulk Q_y absorption band is excited at 650/660 nm. At 702 nm the excitation is relatively selective both for P700 and the C708/C702RT pool of red chls. More selective excitation of the red-most chl pools is achieved at 710 nm and 719 nm.

Table 6.1 Restrictions used in global analysis

Sample	λ_{ex} (nm)	(raman) scatter zero		time zero spectrum zero	
		below (nm)	above (nm)	below (nm)	above (nm)
<i>Synechocystis</i> monomers	400	-	-	-	665
	505	-	640	-	665
	660	-	670	660	695
	702	688	713	688	-
	710	685	730	685	-
<i>Synechocystis</i> trimers	400	-	-	-	665
	702	688	713	688	-
	710	685	730	685	-
<i>Synechococcus</i> trimers	400	-	-	-	665
	650	-	-	-	-
	710	690	725	675	-
	719	710	730	690	-



6.1 Room temperature absorption spectra of monomeric (solid) and trimeric (dotted) PSI from *Synechocystis* PCC6803 and trimeric PSI from *Synechococcus elongatus* (dashed). Note the clear differences in red chl content. Arrows indicate the wavelengths of excitation that were used in the experiments. The spectra were normalised to the maximum in the Q_y region.

For some excitation wavelengths scattered excitation light was recorded, along with the fluorescence. In these experiments the polarisation of the detection was chosen perpendicular to the polarisation of the exciting laser light, in order to reduce the amount of scattering. In principle this could result in anisotropic lifetime components in the measurements. However, since the major fraction of depolarization is fast (~ 150 fs)^{31,37} and most of the observed lifetime components are not related to a single transfer step between two specific chromophores, but rather to an ensemble average of many different transfer steps between many differently oriented chls, the polarisation effects will to a large extent average out for these components. We will discuss the possibility of polarisation effects for the fastest components. For the wavelengths of excitation that were outside the fluorescence detection range (i.e. 400 nm and 505 nm) the polarisation of the detection was at magic angle (54.7°) to the polarisation of the excitation light.

Time-resolved fluorescence measurements

Figures 6.2-6.4 show the Decay-Associated Spectra (DAS) that result from the global analysis of the time-resolved fluorescence data for the three PSI preparations, for the different wavelengths of excitation. Data for 400 nm excitation have been reported before but have now been analysed requiring the absence of instantaneous fluorescence in the Q_y region.¹³ Fast rise components in the Q_y region are also found in the analysis without this explicit restriction, but the DAS-es improve significantly upon applying these constraints. For other wavelengths of excitation similar restrictions were imposed in the analysis, which are listed in table 6.1. In the cases for which a significant difference occurs between the shown, restricted analysis and the fit without restrictions (not shown) this will be addressed. The pulse-limited (Raman)scatter contributions were also restricted to the wavelength range in which they are expected (table 6.1). All the lifetimes of the global analysis of the three preparations for all wavelengths of excitation used are listed in table 6.2.

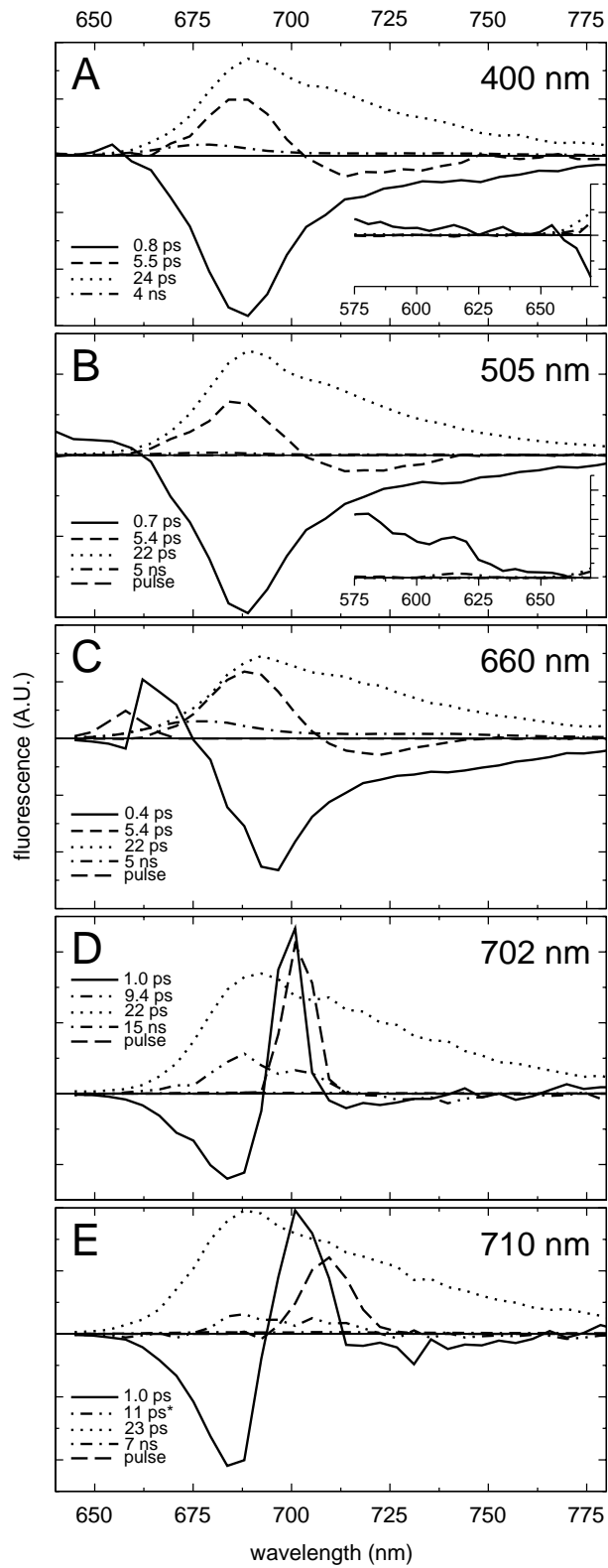
Synechocystis PSI monomers

The 400 nm light preferentially excites the Soret band of chl a , which relaxes to the lowest excited singlet (Q_y) state in a few hundred fs. The Soret- Q_y ingrowth is reflected by a component which is represented by a DAS (figure 6.2a, solid) which is negative throughout the whole Q_y region with a minimum at 688 nm, and which is fitted with a lifetime of 0.8 ps. The second component exhibits a lifetime of 5.5 ps and is represented by a DAS (dashed) which is positive in the blue part of the spectrum, peaks around 687 nm and drops below zero at wavelengths longer than 703 nm (In an analysis without restrictions this equilibration component was fitted with a somewhat shorter lifetime of 4.4 ps).¹³ Such a DAS which represents a decay of fluorescence in one part of the spectrum and a rise of fluorescence in another part, is indicative of energy transfer between spectrally different chromophores. This component therefore reflects energy transfer from bulk chls emitting around 687 nm, to red-shifted chls emitting around 712 nm,¹³ thus creating a thermally (more) equilibrated distribution of excitations. However, the DAS is not conservative, i.e. the positive area is somewhat larger than the negative area, indicating that effectively some excitations disappear during this process. For a "pure" transfer component no loss of excitations would occur, therefore we conclude that this component also includes some non-equilibrium trapping.¹³ The third component is fitted with a lifetime of 24 ps, and an all-positive DAS

Table 6.2 Lifetimes observed in PSI of *Synechocystis* and *Synechococcus*

λ_{ex} (nm)	energy-transfer components (ps)				trapping (ps)		long-lived (ns)
	Soret and Car to Q_y	within bulk Q_y	bulk to red	red to bulk	fast	normal	
<i>Synechocystis</i> monomers							
400	0.8	-	5.5	-	-	24	4
500	0.7	-	5.4	-	-	22	5
650	-	0.4	5.4	-	-	22	5
700	-	-	-	1.0	9.4	22	15 [#]
710	-	-	-	1.0	11*	23	7 [#]
<i>Synechocystis</i> trimers							
400	0.9	-	5.2	-	-	22	5
700	-	-	-	0.7	13	23	24 [#]
710	-	-	-	0.7	11*	23	100 [#]
<i>Synechococcus</i> trimers							
400	0.2	-	4.3 and 8.7	-	-	35	5
650	-	-	3.4 and 10	-	-	38	5
710	-	-	10	0.7	-	33	6 [#]
719	-	-	-	1.6	-	37	4 [#]

* Fixed value. [#]Minor amplitudes



(dotted) that peaks around 690 nm and exhibits a broad shoulder around 712 nm. This component represents the decay of excitations from a more or less thermally equilibrated distribution of excitations, due to trapping of the excited state energy by charge-separation in the RC. This component will therefore be referred to as the trap component.

The slowest component, representing a small fraction of uncoupled chls in the preparation, is fitted with a 4 ns lifetime, and a DAS (dot-dashed) which peaks at 678 nm and has a shape which is typical for chl*a* in solution.

The inset shows the DAS-es in the 575–675 nm region, which are all zero, except for the fastest (0.8 ps) component. The small positive amplitude of this component may indicate some carotenoid excitation at 400 nm (see below).

Excitation at 505 nm (figure 6.2b) preferentially excites β -carotene, which efficiently transfers excitations to chl*a*.^{31,36} The results are almost identical to those for 400 nm excitation, although at this excitation wavelength the sub-ps ingrowth in the Q_y region (solid) is accompanied by a large positive contribution in the region below 660 nm (see inset), indicating that this component represents energy transfer from β -carotene to chl*a* rather than Soret to bulk equilibration. Raman scattering of the excitation light by water (at 3600 cm^{-1} from the excitation wavelength) results in a pulse-limited contribution (long-dashed) around 615 nm. The amplitude of the component representing uncoupled chls (dot-dashed) is significantly reduced with respect to 400 nm excitation, due to the low absorption of chl at 505 nm.

The main results for 660 nm excitation (figure 6.2c) are almost identical to those for 400 nm and 505 nm excitation. The difference in excitation wavelength is mainly expressed by the fastest lifetime component (0.4 ps, solid), which shows a decay around 665 nm, and therefore represents energy transfer (equilibration) within the Q_y absorption band.^{31,37} This energy-transfer spectrum is non-conservative (the area of the positive part of the spectrum is smaller than that of the negative part), which may to a large extent be attributed to depolarization, since only the perpendicular fraction of the fluorescence was recorded for this wavelength of excitation (see above).

The 5.4 ps component (dashed), representing energy transfer between the bulk and red chls, exhibits a spectrum which shows a significantly larger amplitude in the positive region, which may reflect that the amount of non-equilibrium trapping is larger for 660 nm excitation, as compared to excitation at 400 nm and 505 nm. A pulse-limited contribution (long dashed) accounts for the scatter contribution present around the excitation wavelength.

The results for 702 nm excitation (figure 6.2d), selective for both P700 and the red chls of the C708/C702RT pool, differ substantially from the results for the three excitation wavelengths discussed so far. The fastest process (solid), is fitted with a 1 ps lifetime and a spectrum which is negative around 685 nm, positive around 700 nm, and again slightly negative in the red part of the spectrum. This component reflects the uphill energy-transfer from the initially excited red-shifted chl forms to the bulk antenna chls. The lifetime of this uphill energy-transfer is remarkably short compared to the ~ 5.5 ps downhill energy-transfer

6.2 (opposite page) Decay-Associated Spectra of fluorescence decay of monomeric PSI from *Synechocystis* PCC6803 for excitation at 400 nm (A), 505 nm (B), 660 nm (C), 702 nm (D) and 710 nm (E). Note that the scaling of the y-axis of each of the insets corresponds to that of the main graph.

lifetime observed for the previously discussed wavelengths of excitation and (apart from the sign) also the shape of the uphill transfer spectrum differs significantly from the downhill spectra. These differences cannot be explained in terms of simple compartmental models.¹³ The results for 702 nm excitation also feature a process characterized by a 9.4 ps lifetime and an all-positive spectrum (double-dot-dashed) exhibiting a double banded structure with maxima at 688 nm and 702 nm. The origin of this component is not clear. It does not emerge from compartmental¹³ nor structure-based modelling (ref. 32, and see below). Since the spectrum is positive at all wavelengths, it seems to be a fast trapping component. However, for this wavelength of excitation also a "normal" trapping component is recorded (dotted), with a lifetime and spectrum identical to those found for the other wavelengths of excitation. The fit also includes a component with a lifetime of 15 ns, with an almost negligible amplitude (dot-dashed) and a pulse-limited contribution (long-dashed) to account for the scattered excitation light.

Excitation with 710 nm light, leads to an almost exclusive excitation of the red chls. The results for this wavelength of excitation (figure 6.2e) are very similar to those for 702 nm excitation. Uphill energy-transfer occurs in 1 ps. The corresponding spectrum (solid) has more or less the same shape as for 702 nm excitation, but has a larger amplitude: the more red-shifted excitation wavelength leads to a larger non-equilibrium initial distribution of excitations, resulting in a larger amplitude of the equilibration component. The remarkable 9.4 ps component that appeared in the analysis for 702 nm excitation, does not appear directly in the analysis for 710 nm excitation. However, it was found that the introduction of a component with a fixed 11 ps lifetime resulted in an improved fit, and a spectrum similar to the 9.4 ps component found for 702 nm excitation, albeit with a smaller amplitude (figure 6.2e double-dot-dashed). Since no ~ 10 ps component could be found for the other wavelengths of excitation, it seems that the ~ 10 ps process is somehow related to the direct excitation of chls absorbing around 700 nm.

Also for this wavelength of excitation the trapping component (23 ps, dotted), appears identical to that for the other wavelengths of excitation. The scattered excitation light at 710 nm was accounted for by a pulse-limited contribution (long dashed).

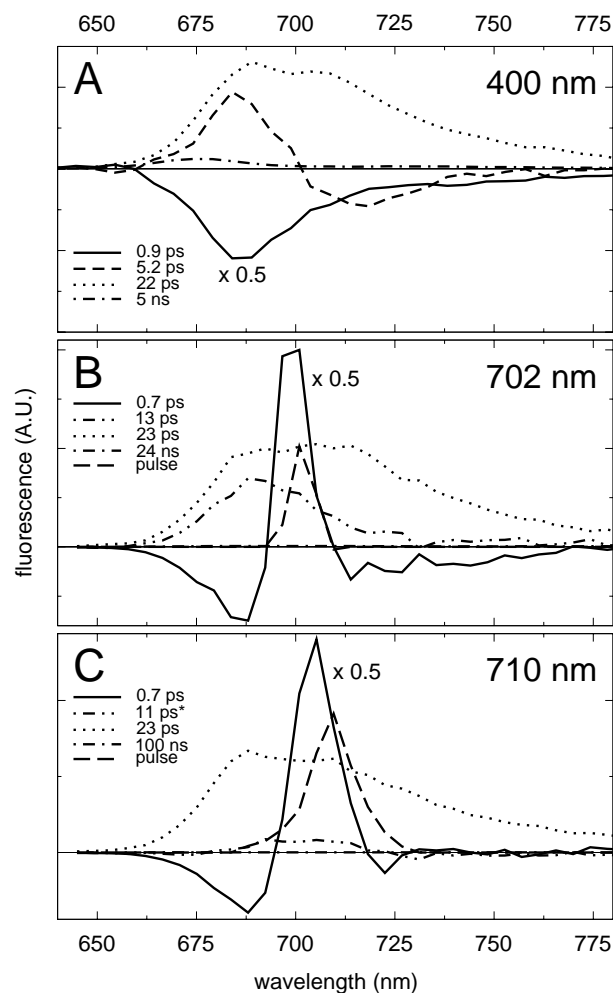
Synechocystis PSI trimers

The results for the PSI trimers of *Synechocystis* for excitation at 400, 702 and 710 nm are displayed in figure 6.3. All the lifetimes and spectra are very similar to those observed for the monomers for the corresponding wavelengths of excitation. However, the amplitude of both the uphill (figure 6.3a, dashed) and downhill (figure 6.3b/c, solid) energy-transfer spectra appear to be somewhat larger in trimers than in monomers, and also the trapping spectra (figure 6.3a-c, dotted) display a more pronounced shoulder around 710 nm in the trimers. Both these observations are attributed to the larger number of red chls contained in the trimers as compared to the monomers. Also for trimers, the analysis for 702 nm excitation yields a ~ 10 ps component with an all-positive spectrum (figure 6.3b, double-dot-dashed, 13 ps), ruling out the possibility that this component results from monomerisation. For 710 nm excitation, as for monomers, the introduction of a fixed 11 ps component lead to an improved fit, and an all-positive spectrum with a small amplitude (figure 6.3b, double-dot-dashed).

Synechococcus PSI trimers

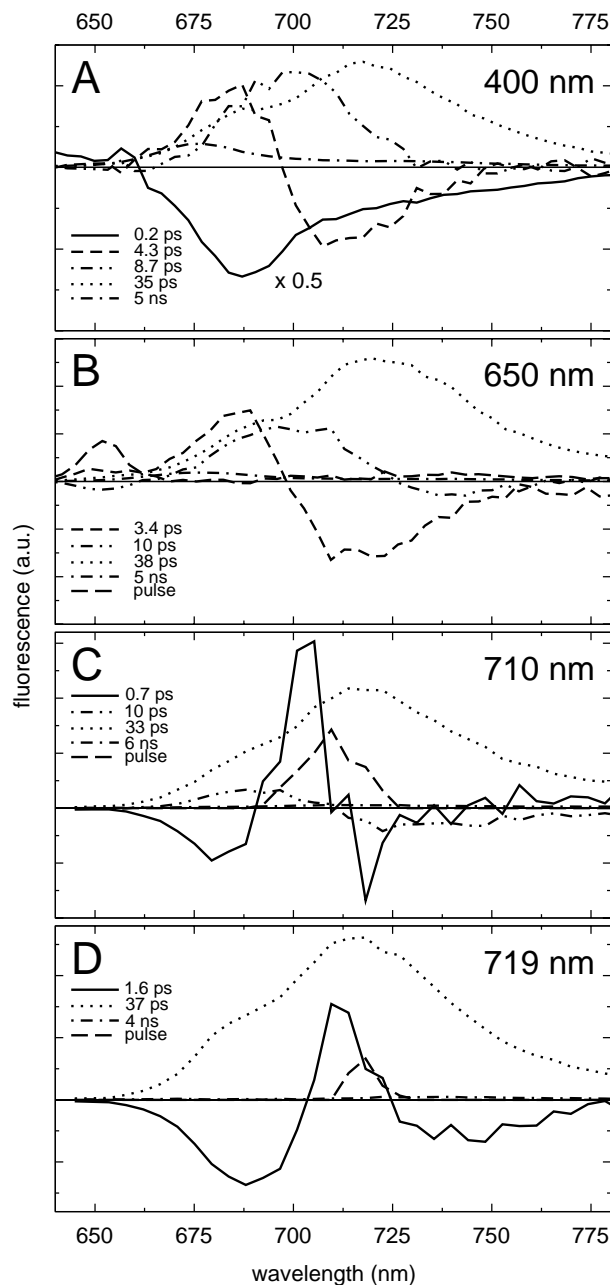
PSI trimers from *Synechococcus elongatus* contain a significantly larger number of red chls as compared to PSI from *Synechocystis*. Moreover, they appear in two distinct pools, one of which is significantly lower in energy as compared to the PSI particles from *Synechocystis*. Consequently, the energy-transfer and trapping dynamics in *Synechococcus* PSI differ substantially from those of PSI from *Synechocystis* (figure 6.4).

In figure 6.4a, the results are shown for excitation of the chl a Soret transition at 400 nm. The fastest component is fitted with a 0.2 ps lifetime, and expresses the Soret to Q_y relaxation (solid). As for *Synechocystis* PSI, this ingrowth shows a distinct minimum around 687 nm, yet it features a much more pronounced wing above ~ 700 nm, reflecting the larger number and lower energies of the red chls contained in this species. A process with a 4.3 ps lifetime features an energy-transfer spectrum (dashed) that displays a significantly deeper and more



6.3 Decay-Associated Spectra of fluorescence decay of trimeric PSI from *Synechocystis* PCC6803 for excitation at 400 nm (A), 702 nm (B) and 710 nm (C).

pronounced minimum in the negative region of the spectrum than the ~ 5.5 ps downhill energy-transfer spectra of *Synechocystis* PSI. Therefore, in contrast to *Synechocystis* PSI, the total spectrum is basically conservative. The minimum of this spectrum appears at about the same wavelength as in *Synechocystis* PSI, which indicates that this component mainly



6.4 Decay-Associated Spectra of fluorescence decay of trimeric PSI from *Synechococcus elongatus* for excitation at 400 nm (A), 650 nm (B), 710 nm (C) and 719 nm (D).

accounts for equilibration of the bulk chls with the C708/C702RT pool of red chls present in both species.

A third component, with a lifetime of 8.7 ps, exhibits a spectrum (double-dot-dashed) which peaks around 700 nm, and drops only slightly below zero at wavelengths longer than 730 nm. We assign this component to equilibration between the equilibrated bulk and C708/C702RT pools on the one hand and C719/C708RT red chl pool on the other hand, together with a significant amount of non-equilibrium trapping (see also ref 13).

A fourth component, with a 35 ps lifetime, exhibits a spectrum which is positive at all wavelengths and reflects the trapping from the equilibrated distribution of excitations. The maximum of this spectrum (dotted) appears at about 719 nm, reflecting that due to the larger number, and lower energies of the red chls in *Synechococcus* PSI the equilibrium distribution is red shifted considerably with respect to *Synechocystis* PSI. The contribution of the bulk chls is reduced to just a shoulder around 690 nm. A small fraction of uncoupled chls present in the preparation is represented by a small 5 ns contribution (dot-dashed).

The results for 650 nm excitation, presented in figure 6.4b, are very similar to those for 400 nm excitation. The 3.4 ps and 10 ps equilibration components (dashed and double-dot-dashed) correspond to the 4.3 ps and 8.7 ps components for 400 nm excitation. The 10 ps component more clearly reveals its energy-transfer character, it is, beyond doubt, negative above ~ 725 nm. The 38 ps trapping component (dotted) is identical to that for 400 nm excitation, and some uncoupled chls are evident from a small 5 ns component (dot-dashed). The scattered excitation pulse is accounted for by a pulse-limited contribution (long dashed) peaking at 650 nm.

With 710 nm excitation light, both pools of red chls are selectively excited (figure 6.4c). The results for this wavelength of excitation differ significantly from those for 400 nm and 650 nm excitation. The fastest equilibration component is fitted with a 0.7 ps lifetime and a spectrum (solid) resembling that for the ~ 1 ps components found for 702 nm and 710 nm excitation of *Synechocystis* PSI. Since the negative part to the red side of the excitation light is only small, it seems that this fast energy-transfer component mainly involves equilibration of the first pool of red chls with the bulk chls, like the 3-4 ps components found for 400 nm and 650 nm excitation. A second equilibration component, fitted with a 10 ps lifetime, (double-dot-dashed) bears resemblance to the ~ 10 ps component observed for 400 nm and 650 nm excitation. The amplitude of the spectrum is smaller, however, and the zero crossing seems to be significantly blue shifted. The spectrum also seems much more conservative. Nevertheless we assign this component to the same processes as the ~ 10 ps component observed for 400 nm and 650 nm excitation. The trapping component, fitted with a 33 ps lifetime (dotted), is identical to that of the other wavelengths of excitation. Also at this wavelength of excitation a small 6 ns component was present. The scattered excitation light is accounted for by a pulse-limited contribution (long-dashed).

Excitation at 719 nm is mostly selective for the C719/C708RT pool of red chls. For this wavelength of excitation only one equilibration component can be distinguished. This component is fitted with a 1.6 ps lifetime and a spectrum (solid) which exhibits a positive contribution around 712 nm and negative contributions around 690 nm and at wavelengths longer than 725 nm. This component therefore represents both uphill and downhill

energy-transfer, effectively resulting in a broadening of the initially excited distribution to the equilibrated distribution. Trapping from the equilibrated distribution (dotted) occurs in 37 ps, and the equilibrated spectrum (dotted) is identical to the trapping DAS-es found at other wavelengths of excitation. Also for this wavelength of excitation a very small 4 ns component was found (dot-dashed). The scattered excitation light is accounted for by a pulse-limited contribution (long-dashed).

Summary of results

Synechocystis PSI contains a single pool of red chls with an absorption maximum at 702 nm at room temperature (C702RT). For all wavelengths of excitation *Synechocystis* PSI (both monomers and trimers) exhibits a single equilibration component, which is directed downhill for aselective excitation (400, 505 and 660 nm) and uphill for selective excitation in the red chl region (702 and 710 nm). The uphill transfer components are distinctly different from the downhill transfer components, both in lifetimes (0.7–1 ps uphill vs. ~ 5.5 ps downhill) and in spectral shape.

From the analysis for excitation at 702 nm and 710 nm a ~ 10 ps component emerges that exhibits an all-positive (double-banded) spectrum. The nature of this component remains unclear, but it seems to be related to excitation of chls absorbing around 700 nm.

For all wavelengths of excitation *Synechocystis* PSI exhibits a trapping component that decays in ~ 23 ps. The spectrum of this component exhibits a maximum around 690 nm and a shoulder around 710 nm, which is more pronounced in trimers than in monomers, due to the larger red chl content of the trimers.

In contrast to PSI from *Synechocystis*, PSI from *Synechococcus* exhibits two distinct pools of red chls with room temperature absorption maxima at 702 and 708 nm (C702RT and C708RT). Consequently, for 400nm, 650 nm and 719 nm excitation, two separate energy-transfer components were distinguished in *Synechococcus* PSI, with distinctly different lifetimes. The fastest of these two components in all cases seems to reflect the equilibration between the bulk chls and the C702RT pool, whereas the slower component is associated with both non-equilibrium trapping and the equilibration between on the one hand the equilibrated distribution on the bulk chls and the C702RT pool, and on the other hand the C708RT pool.

For relatively aselective excitation (400 and 650 nm) the fastest equilibration component is directed downhill, and exhibits a lifetime of 3–4 ps, and a spectrum that resembles the downhill equilibration spectra found for *Synechocystis* PSI, albeit more conservative. For excitation at 710 nm the fastest equilibration component, is directed (mainly) uphill, and is fitted with a much shorter lifetime of 0.7 ps, similar to *Synechocystis* PSI. For all three wavelengths of excitation the slow energy-transfer is directed downhill with a lifetime of about 10 ps. The amplitude of this component is significantly lower for 710 nm excitation than for aselective excitation.

The data for 719 nm excitation reveals only one single equilibration component reflecting both up and downhill transfer with a lifetime of 1.6 ps.

For all wavelengths of excitation an identical trapping component was resolved with a lifetime of ~ 35 ps and a spectrum that exhibits a broad band with a maximum around 719 nm, and a shoulder around 690 nm.

In the next section we will numerically simulate most of these results.

SIMULATIONS

In order to understand the processes that were summarized above and the time scales on which they occur, we performed a simulation of the kinetic data based upon the recent 2.5 Å structural model of trimeric PSI from *Synechococcus elongatus*.⁶ Although the dipole-dipole approximation may not hold for all pairs of chls in the PSI and in some cases the interaction strength between chls may be considerable, we chose for a simulation based on Förster energy-transfer.

Procedure

We calculated the transfer rates between the 96 different chls in the system using the Förster equation:³⁸⁻⁴⁰

$$k_{DA} = \frac{k_r^D}{n^4} \cdot \frac{\kappa_{DA}^2}{R_{DA}^6} \cdot I_{DA} \quad 6-1$$

in which k_{DA} is the rate of transfer of an excitation from a donor chl (D) to an acceptor chl (A) in ps^{-1} and k_r^D is the radiative lifetime of chl a , for which we use the value $5.4 \cdot 10^{-5} \text{ ps}^{-1}$.³⁹ n is the index of refraction of the protein. R_{DA} is the distance between donor and acceptor in nm. R_{DA} was determined by taking the distance between the centres of the 4 coordinating nitrogen atoms N_A-N_D for each pair of chls in the structure. κ is an orientational factor defined by:

$$\kappa = (\hat{\mu}_A \cdot \hat{\mu}_D) - 3(\hat{\mu}_A \cdot \hat{r}_{AD})(\hat{\mu}_D \cdot \hat{r}_{AD}) \quad 6-2$$

in which $\hat{\mu}_A$ and $\hat{\mu}_D$ represent the normalized Q_y transition dipole moment vectors and \hat{r}_{AD} represents the vector connecting the centres of both transition dipole moments, normalised to unity. For each chl a molecule in the structure the vector connecting the nitrogen atoms N_B and N_D was taken to represent the direction of the Q_y transition dipole moment vectors. \hat{r}_{AD} was calculated as the normalised vector connecting the centres of the 4 coordinating nitrogen atoms N_A-N_D for each pair of chls in the structure.

The factor I_{DA} in equation 1 represents the overlap integral between the donor chl emission spectrum and the acceptor chl absorption spectrum defined by:³⁹

$$I_{DA} = 8.8 \times 10^{17} \cdot \int \frac{\epsilon_A(\nu) \cdot F_D(\nu)}{\nu^4} d\nu \quad 6-3$$

$\epsilon_A(\nu)$ represents the acceptor absorption spectrum scaled to the value of the extinction coefficient (in $M^{-1}cm^{-1}$) in the absorption maximum and $F_D(\nu)$ represents the emission spectrum of the donor, normalized to unit area. Both spectra are on a frequency scale (cm^{-1}). The overlap integral I_{DA} was calculated for 5 spectrally different chl pools; a bulk chl pool with an absorption maximum at 680 nm, a pool at 686 nm representing the two chls at the A_0 position, a pool representing P700 peaking at 698 nm and 2 red chl pools with room temperature absorption maxima at 702 and 708 nm.^{10,13} The spectra that were used to calculate the overlap integrals are listed in table 6.3. The overlap integrals were calculated using equation 3 for downhill energy-transfer only, i.e. for pairs DA in which the absorption of D peaks at higher or equal energy as compared to the absorption of A . The complementary, downhill rates had to comply with the concept of detailed balance and were thus calculated as: $k_{ij} = k_{ji} \cdot e^{-(E_j - E_i)/k_B T}$. We used $7.7 \cdot 10^4 M^{-1}cm^{-1}$ as the value of the maximum of the extinction coefficient of the bulk pools, which is the value reported by Lichtenthaler for chl*a* in 80% acetone.⁴¹ The absorption spectra of the other pools were scaled to those of the bulk pools by requiring them to have equal areas.

Using the same procedure as outlined above, we have performed a simulation of the dynamics of a PSI particle not containing any red chls.¹ Previously it was found that such a PSI particle should exhibit a 18 ps trapping time.¹³ This condition could only be met for certain combinations of the index of refraction, n , (corresponding to a certain value of the single site lifetime τ_{ss}) and the rate of charge separation from each of the two chls constituting P700, γ . Consistent with the experimental results reported in ref. 31 and 37, we use a value for τ_{ss} of

Table 6.3 Absorption and emission spectra used for overlap integrals

Pool	Absorption Spectrum	Absorption max (nm)	Emission Spectrum	Emission max (nm)
Bulk C680	chl <i>a</i> in acetone	680 [#]	chl <i>a</i> in acetone	687 [#]
A_0 , C686		686 ^{#10}		693 [#]
P700	Gaussian, 19 nm FWHM	698 ¹⁰	C702 emission ¹³	708 [#]
Red pool C702RT*	Gaussian, 12 nm FWHM	702	C702 emission ¹³	712
Red pool C708RT*	Gaussian, 19 nm FWHM	708	C708 emission ¹³	722

*The red pools C702 and C708 represent the respective room temperature equivalents of the C708 and C719 red pools found at low temperatures in cyanobacterial PSI.¹³
[#]Shifted to this wavelength.

150 fs, corresponding to a value of γ of 1 ps^{-1} . This leaves us with no free parameters, except for the spectral composition of the antenna, which we construct by assigning each of the 96 chls to one of the five pools. In the simulations we assigned P700 and A_0 to their respective pools, and all the chls that were not assigned to one of the red chl pools were assigned to the bulk pool. Differences between the (simulated) dynamics of different PSI particles therefore arise solely due to the differences in red chl assignments. Once the red chls have been assigned we can calculate all 96×96 pairwise energy-transfer rate constants using equation 1. These energy-transfer rate constants and γ are subsequently used to construct the 96 coupled linear differential equations describing the dynamics of the system. Solving these equations one obtains the 96 different eigenvalues (lifetimes) of the system. By subsequently choosing the distribution of excitations at time *zero* (i.e. aselective excitation, preferential excitation of a red pool) one imposes boundary conditions to the system which enable the calculation of the DAS-es corresponding to each of these lifetimes.

Because we only consider processes occurring in the Q_y region, and since we do not include heterogeneity in the bulk, the sub-ps processes of Soret- Q_y relaxation as well as bulk equilibration are not considered in the simulation.

Simulation of the dynamics in *Synechococcus* PSI

In the framework of the structure-based simulation, outlined above, we only have to assign the red chls in the structure to calculate the dynamics of the *Synechococcus* PSI. Jordan et al.⁶ point out three dimers and one trimer of chl a in their structural model for PSI of *Synechococcus* as being putative candidates for strongly coupled red chl sites. The trimer, consisting of the chls designated as aC-B31, aC-B32 and aC-B33, is located in the periphery of the antenna, whereas the dimers consisting of the chl pairs aC-A32/aC-B7, aC-A38/aC-A39 and aC-B37/aC-B38 are located closer to the RC. The dimer aC-A32/aC-B7 is located at the luminal side of the trimerization domain, and forms hydrophobic contacts with PsaL of the adjacent monomer, and has therefore been suggested to represent (part of) the C719 pool, since the amplitude of this pool depends on the aggregation form of the complex.⁴² An important parameter determining the coupling strength between a pair of chls is the distance, R , that separates them. However, also the relative orientation is an important parameter. We have therefore for each pair of chls considered the value of κ^2/R^6 (See eq. 1) as a measure of the coupling strength (of course pigment-protein interactions also play an important role, but this is not considered here). The κ^2/R^6 criterion yields P700 as being (by far) the most strongly coupled dimer in the complex. The two pairwise couplings in the trimer are the second and third strongest couplings according to this criterion. It is therefore likely that the trimer constitutes the C719/C708RT pool rather than the aC-A32/aC-B7 dimer proposed by Jordan et al. Moreover, we were not able to obtain an acceptable simulation of the data with the aC-A32/aC-B7 dimer included in the C719/C708RT pool (see below). Interestingly, this is at odds with the idea that the C719/C708RT pool should be located within the trimerization domain. We also note that according to the κ^2/R^6 criterion there are three more dimers in the periphery of the structure that are at least as strongly coupled as the dimers proposed by Jordan et al.,⁶ i.e. chl pairs aC-A12/aC-A14, aC-A10/aC-A18 and aC-B09/aC-B17. However, for now we will perform the simulation using the trimer and dimers indicated by Jordan et al.⁶ with the trimer representing the C719/C708RT pool and the three dimers representing the

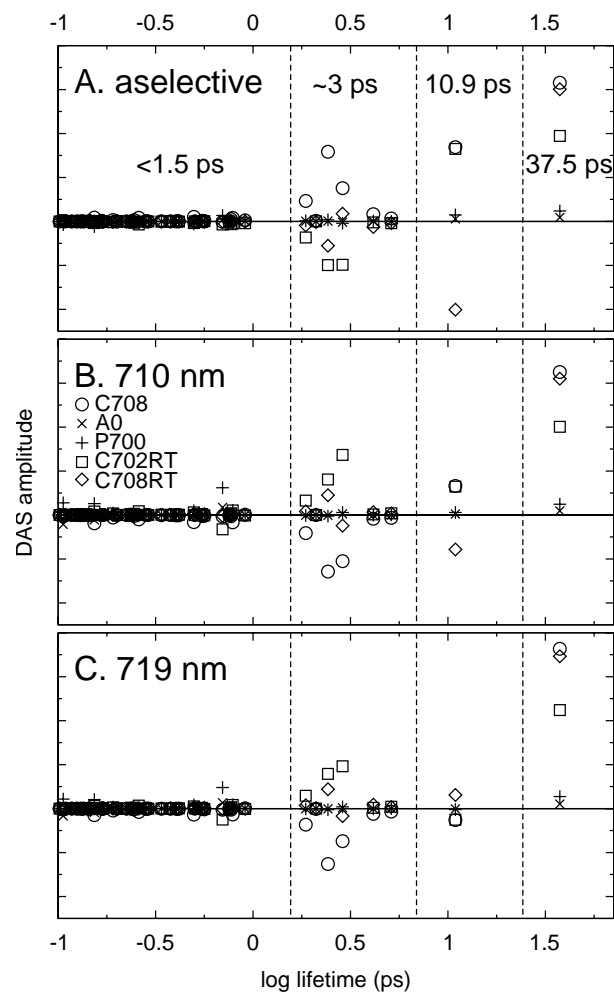
C708/C702RT pool. We considered three different excitation conditions: aselective (corresponding to 400 nm excitation and more or less to 650 nm: all chls have equal probability to be excited at time zero), 710 nm excitation (corresponding to the excitation of a mixture of the P700, C708/C702RT and C719/C708RT pools in a 1:1:1 probability ratio of excitation of the chls in each of these pools), and 719 nm excitation (corresponding to a 1:1:2 probability ratio of excitation of the chls in each of these pools). The 96 lifetimes resolved in the simulation each correspond to a separate DAS. However, if no significant increase or decay of the excitation density in any of the pools occurs with a particular lifetime, the corresponding DAS will be negligible. Also if the values of two or more lifetimes are close together, they may not be separated in the experiment, and effectively the sum of the respective DAS-es is observed. This is enhanced if the shapes of the respective DAS-es are similar.

In figure 6.5 we have plotted the amplitudes of the contribution to the DAS-es of each of the 5 pools for each of the 96 lifetimes in the system (note the logarithmic time-base). Clearly only a few lifetimes correspond to DAS-es with a significant amplitude. Four (clusters of) lifetimes dominate the dynamics of the system for all excitation conditions: 37.5 ps, 10.9 ps, ~ 3 ps and <1.5 ps. The number of lifetimes and their values correspond remarkably well to the experimentally observed lifetimes of 35–38 ps, 8.7–10 ps, 3.4–4.3 ps and 0.7–1.6 ps. The relative contributions of the various pools to the slowest (37.5 ps) component are the same for each excitation wavelength, consistent with the observation that the shape of the trapping spectrum is independent of the wavelength of excitation. Note that the absolute amplitude of the trapping component does depend slightly on the wavelength of excitation, indicating an excitation-wavelength dependence of the amount of non-equilibrium trapping. The 10.9 ps component in figure 6.5 shows energy transfer between on the one hand the bulk and C708/C702RT pools (circles and squares) and on the other hand the C719/C708RT pool (diamonds), consistent with the idea that the former pools equilibrate on a shorter time-scale. This is confirmed by the components contributing to the ~ 3 ps lifetime components, which mainly display energy transfer between the bulk (circles) and the C708/C702RT pool (squares), and does not involve a significant contribution of the C719/C708RT pool (diamonds). The <1.5 ps component is composed of the sum of a large number of short lifetime components. This component shows an enhancement of the amplitude of the P700 (crosses) and C708/C702RT pools (squares) for 710/719 nm excitation as compared to aselective excitation.

In figure 6.6 we present the actual dominant DAS-es resulting from the simulation, which were constructed using the emission-spectra of the various PSI pools as reported in ref. 10 and 13. The DAS-es were summed over the intervals indicated by the dashed vertical lines in figure 6.5, to obtain four effective DAS-es corresponding to the four lifetimes indicated above. This allows for a direct comparison between the simulated DAS-es of figure 6.6 and the measured DAS-es of figure 6.4. Figure 6.6a corresponds to aselective excitation and should be compared to figure 6.4a (and b). The fastest two downhill energy-transfer components of the simulation have a similar shape, but the ~ 3 ps contribution (dashed) dominates the sub-ps equilibration (solid) in amplitude, in accordance with the measurements. The shape and total amplitude of the fast downhill transfer component are quite similar to those observed in the measurements. The experimental data show a distinct very non-conservative 8.7 ps

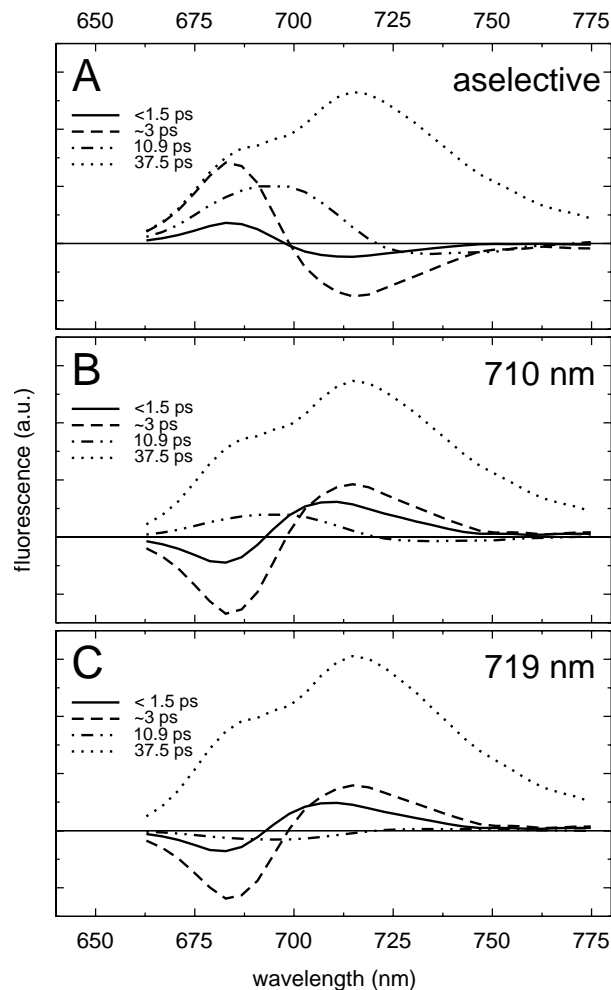
component that accounts for both downhill energy-transfer and non-equilibrium trapping. This striking feature is reproduced remarkably well by the simulated 10.9 ps component (double-dot-dashed) in figure 6.6a, which is clearly highly non-conservative. The trap spectrum (dotted) resembles the measured trap spectrum quite well, although the shoulder representing the bulk antenna chls is somewhat high. This may be the result of employing a spectrally homogeneous bulk antenna. For a heterogeneous bulk antenna the bulk emission would be broader, and therefore the shoulder would be less distinct.

For excitation at 710 nm, the fast equilibration components are both uphill. The sub-ps contribution is considerably larger as compared to aselective excitation conditions, and therefore the mixture of the sub ps and ~ 3 ps DAS-es is fitted in the experiment with a faster



6.5 Amplitudes of the Decay-Associated Spectra of all 96 lifetimes occurring in the simulation of *Synechococcus elongatus*, for excitation at 400 nm (A), 710 nm (B) and 719 nm (C). Pools: C680 (circles), C708/C702RT (squares), C719/C708RT (diamonds), P700 (plusses), and A₀ (crosses). Note the four distinct dominant lifetimes that occur, i.e. 37.5 ps, 10.9 ps, ~ 3 ps, and <1.5 ps. The dashed vertical lines mark the lifetime intervals over which the DAS-es were summed to obtain the DAS-es in figure 6.6. For details see text.

lifetime as for aselective excitation. The spectral differences between the fastest DAS-es in the simulation and the experiment occur because we do not include inhomogeneous broadening in the simulation. The excitation pulse in the experiment has a spectral width of approximately 10 nm and selectively excites an energetic sub-fraction of the inhomogeneous distributions of the various pools. Energy transfer within the inhomogeneously broadened pools results in the much narrower positive region of the fast energy-transfer DAS and the slightly negative region in the red that are not present in the simulated spectrum. Very similar to the experiment, the 10.9 ps DAS shows downhill energy-transfer with the same characteristics as for aselective excitation, albeit with a lower amplitude. As pointed out above, the trapping component has the same shape and approximate amplitude as for the simulation for aselective excitation.



6.6 Simulated Decay-Associated Spectra of fluorescence decay of trimeric PSI from *Synechococcus elongatus* for excitation at 400 nm (A), 710 nm (B) and 719 nm (C).

For extremely red excitation at 719 nm, the fast uphill transfer component is very similar to that found for 710 nm excitation, i.e. a mixture of a ~ 3 ps and a sub-ps component. Differences between the experimental and simulated spectrum result from inhomogeneous broadening in a similar way as described above. The amplitude of the 10.9 ps component is negligible in the simulation, consistent with the experiment in which no such slow transfer component could be distinguished at all. The shape of the trapping spectrum is identical to that for the other wavelengths of excitation, but the amplitude is significantly higher, indicating that the amount of non-equilibrium trapping is lower with respect to shorter wavelength excitation.

We would like to emphasize that the simulation lifetimes and the DAS-es in figure 6.6 resemble the experimental lifetimes and DAS-es of figure 6.4 remarkably well, especially considering the fact that the simulation did not contain any "free" parameters, with the exception of the choice of the red chl sites (which was in fact also restricted by only using the most strongly coupled chl*a* dimers/trimer appearing in the structure).

We also attempted to perform the simulations using other assignments of the red chls. This included different permutations of the dimers/trimer indicated by Jordan et al., as well as the inclusion of the three additional dimers that were introduced above. From these simulations it appeared that out of all these aggregates, the trimer is the only suitable candidate for the C719/C708RT pool. The use of any of the dimers (either alone or in combination with another dimer) to represent the C719/C708RT pool did not result in a distinct separation of a ~ 10 ps transfer component from the faster transfer components. It appears that the whole C719/C708RT pool needs to be located in one single cluster in the periphery of the antenna. We therefore propose that the aC-A32/aC-B7 dimer does not constitute (part of) the C719/C708RT pool, as suggested previously by Jordan et al, but that instead the trimer consisting of chls aC-B31/B32/B33 is a much better candidate. The assignment of the trimer of chlorophylls (aC-B31/B32/B33) to C719 is further supported by structural and biochemical data for *Synechococcus elongatus* and *Synechocystis* PCC 6803 PSI, based on the observation that *Synechocystis* PCC 6803 PSI lacks a C719 pool. A luminal loop structure in PsaB which stabilizes the chlorophyll trimer is shorter in *Synechocystis*, subunit PsaX which interacts with one of the chlorophylls is probably not present in *Synechocystis*, and the axial ligand to aC-B31 (His-B470)⁷ is not conserved in *Synechocystis*. According to these observations, the presence of a complete trimer like in *Synechococcus elongatus* PSI seems to be unlikely for *Synechocystis* PCC 6803 PSI (N. Krauss, P. Jordan and P. Fromme, personal communication).

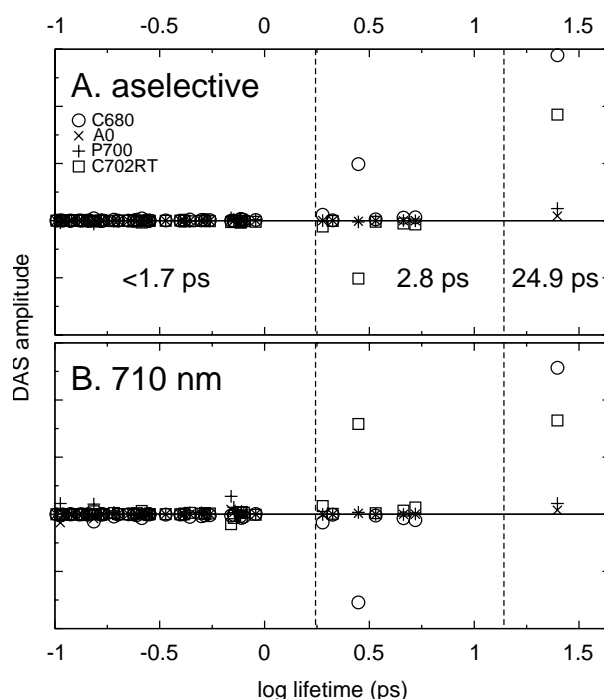
The assignment of the chls constituting the C708/C702RT pool appears to be less unambiguous: different selections of 3 out of the total of the 6 candidate dimers generally resulted in an acceptable simulation.

In order to investigate whether the so-called linker-chls, aC-A40 and aC-B39, perform an important bridging role in the excitation transfer to the RC, we performed the simulation under exactly the same conditions as discussed above, with the only difference that these linker-chls were removed. The resulting simulation appeared very similar to the one in which the linker chls were included, with only slightly increased values of the dominant lifetimes and a trapping time which was slowed down by only 2%. Therefore we conclude that the linker chls do not perform a very special role in the energy transfer to the RC.

Simulation of the dynamics in trimeric *Synechocystis* PSI

Since a structural model is only available for PSI from *Synechococcus* PSI, we have to assume that the differences with *Synechocystis* PSI are sufficiently small to allow for a simulation based upon the *Synechococcus* structure. We do know that *Synechocystis* PSI, like *Synechococcus* trimeric PSI, contains a pool of C708/C702RT chls and that it lacks the C719/C708RT pool present in this species.¹⁰ Since the number of C708/C702RT chls in *Synechocystis* trimeric PSI and *Synechococcus* trimeric PSI is about the same, the most straightforward way of simulating the kinetics in *Synechocystis* trimeric PSI is simply to "remove" the C719/C708RT trimer, i.e. treat those as "normal" antenna chls. *Synechocystis* monomeric PSI contains fewer C708/C702RT chls than the trimers, but since its dynamics is very similar, we refrain from a separate simulation of the excitation transfer dynamics in the monomers.

We consider two excitation conditions: aselective and selective at 710 nm (excitation of the chls in the P700 and C708/702RT pools with equal probability). This results in the DAS-amplitude versus lifetime plots of figure 6.7, which is the *Synechocystis* PSI trimers equivalent of figure 6.5. In contrast to the simulation of *Synechococcus* PSI, which exhibits four distinct time-scales, only three lifetimes are dominant in *Synechocystis* PSI: 24.9 ps, 2.8 ps and <1.7 ps, corresponding to the ~ 23 ps, ~ 5 ps and ~ 1 ps dominant components



6.7 Amplitudes of the Decay-Associated Spectra of all 96 lifetimes occurring in the simulation of (trimeric) *Synechocystis* PCC6803, for excitation at 400 nm (A) and 710 nm (B). Pools: C680 (circles), C702RT (squares), P700 (plusses), and A₀ (crosses). Note that only three distinct dominant lifetimes occur, i.e. 24.9 ps, 2.8 ps, and <1.7 ps. The dashed vertical lines mark the lifetime intervals over which the DAS-es were summed to obtain the DAS-es in figure 6.8. For details see text.

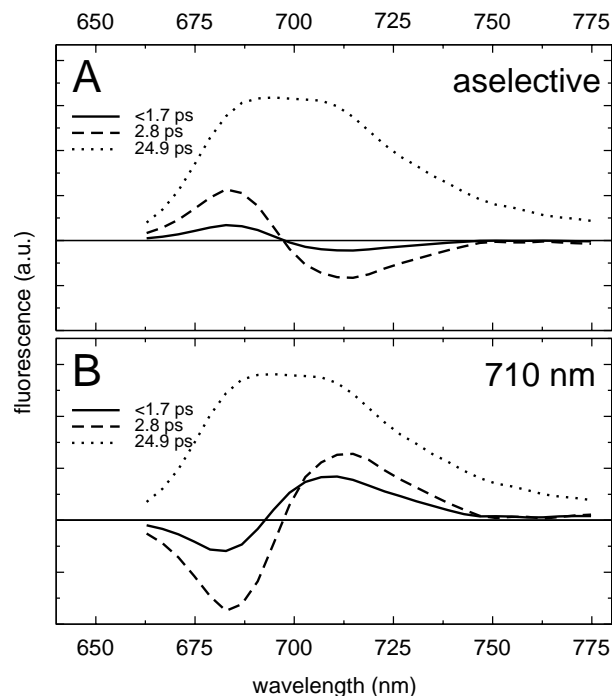
that are observed in the data. In figure 6.8 we present the DAS-es resulting from the simulation.

For aselective excitation (figure 6.8a) the slower 2.8 ps downhill transfer component dominates the faster <1.7 ps component, consistent with the measurements. The shape and amplitude of the total energy transfer also correspond reasonably well with the energy-transfer component in figures 6.2a-c and 6.3a. Both the lifetime and the spectrum of the trapping component (dotted) match the experimental trapping component very well.

For 710 nm excitation both energy-transfer components are directed uphill. The contribution of the sub-ps component is significantly larger, as compared to aselective excitation, consistent with the faster lifetime observed in the experiment. The shape of the trapping spectrum is identical to that found for aselective excitation, but the amplitude is slightly higher, indicating that somewhat less non-equilibrium trapping occurs for selective excitation in the red.

The 2.8 ps lifetime in the simulation of *Synechocystis* PSI is slightly too fast compared to the ~ 5 ps lifetime that was found in the experiments. The use of other dimers to constitute the C708/C702RT pool did not significantly improve the simulations. Some improvement could be made by using a slightly higher value of n , which resulted in lifetimes of 24.3 ps, 3.7 ps and sub-ps, for the spectral composition discussed above.

The ~ 10 ps component observed for excitation at 702 nm, and to a lesser extent at 710 nm in both monomers and trimers of PSI of *Synechocystis*, could not be reproduced in the simulation. The lifetime and spectrum of this component resemble that of the ~ 10 ps



6.8 Simulated Decay-Associated Spectra of fluorescence decay of trimeric PSI from *Synechocystis* PCC6803 for excitation at 400 nm (A) and 710 nm (B).

component in *Synechococcus* PSI, but there it is clearly associated with the presence of the C719/C708RT pool of red chls, which is not present in *Synechocystis* PSI. One could argue that the 10 ps component in *Synechocystis* PSI reflects equilibration with the low-energy fraction of the inhomogeneously broadened C708/C702RT pool,¹¹ which is not accounted for in the simulations. However, this does not explain why the 10 ps component is absent in the dynamics observed upon aselective excitation. The fact that the 10 ps component in *Synechocystis* PSI is large for 702 nm excitation, suggests that the process may be linked to the direct excitation of a considerable fraction of P700. One might think about charge recombination fluorescence from the $P700^+A_0^-$ state which is expected to have a lifetime in the order of 10 ps. However, the energy difference between $P700^*$ and $P700^+A_0^-$ is so large that no significant amount of recombination fluorescence is expected.⁴³ The low light intensities and laser repetition rates used, rule out that the 10 ps component is the result of singlet-singlet annihilation or the accumulation of $P700^+$.

In both PSI species the simulations show a significant difference in the ratio between the ~ 3 ps component and the sub-ps component, for aselective and selective (red) excitation. This observation is in accordance with the experimental results, but the difference may not be enough to account for a factor of 3 to 6 difference in the measured lifetimes. We note that the amplitude of the sub-ps component strongly depends on the initial density of excitations on P700. As expressed above, in the experiments with selective red excitation the polarization of detection was perpendicular to the exciting light. We therefore also calculated polarized DAS-es (not shown) to determine if the large lifetime-difference could be due to depolarization, but we found that the differences between the polarized DAS-es and the magic angle DAS-es presented above are very small.

CONCLUSIONS

We have shown that the excitation dynamics in PSI from *Synechocystis* and *Synechococcus* differ significantly. Furthermore, for each species the dynamics depends strongly on the initially excited distribution of pigments.

For aselective excitation the fastest downhill energy-transfer occurred between the bulk and the C702RT pool with a lifetime of 3.4–5.5 ps. For selective excitation of the red chl pools uphill transfer between the same two pools occurs much faster, in about 1 ps. Such a difference between the uphill- and downhill energy-transfer lifetimes in PSI has not been reported before. By interpreting both lifetimes as a mixture of lifetimes this compelling difference could to a certain extent be explained in a structure-based simulation, which demonstrated that the amplitude ratio between the faster and slower contributions shifts towards the faster lifetimes upon red chl excitation, especially if some direct excitation of P700 is taken into account.

In *Synechococcus* PSI an additional, significantly slower equilibration process occurs in about 10 ps, which is mainly associated with energy transfer between the bulk and C702RT pool on the one hand, and the C719/C708RT pool on the other hand, and which also accounts for a significant amount of non-equilibrium trapping. For all wavelengths of excitation both the lifetime and the non-conservative spectrum of this component were reproduced very well

in the simulation, provided that the chls aC-B31, aC-B32 and aC-B33 constituting the trimer reported by Jordan et al.⁶ were used for the C719/C708RT pool. The choice of this dimer was corroborated by structural and biochemical data for *Synechococcus* and *Synechocystis* PSI (N. Krauss, P. Jordan and P. Fromme, personal communication). The assignment of the chls constituting the C702RT pool was less crucial; combinations of the three dimers reported by Jordan et al. (aC-A32/aC-B7, aC-A38/aC-A39 and aC-B37/aC-B38) and three more dimers proposed in this contribution (aC-A12/aC-A14, aC-A10/aC-A18 and aC-B09/aC-B17) all resulted in more or less reasonable lifetimes and spectra.

Each of the species exhibits its own characteristic trap spectrum, the shape of which is independent of the wavelength of excitation. This trap spectrum decays in ~ 23 ps in both monomeric and trimeric *Synechocystis* PSI and in ~ 35 ps in trimeric *Synechococcus* PSI. These lifetimes and spectra were reproduced very well in the simulation.

The presence of a significant ~ 10 ps component upon 702 nm excitation in *Synechocystis* PSI, exhibiting an all-positive spectrum, could not be reproduced in the simulation

Furthermore, the simulation revealed that the so-called linker chls do not perform a very special role in the process of energy transfer to the RC.

ACKNOWLEDGMENTS

We thank N. Krauss, P. Jordan and P. Fromme, for sharing unpublished work. This research was supported by the Netherlands Organization for Scientific Research via the Dutch Foundation of Earth and Life Sciences (ALW). The streak camera and amplified Ti:Sapph laser system were funded by investment grants of ALW.

REFERENCES

- (1) Gobets, B., L. Valkunas, and R. van Grondelle. 2002. Bridging the gap between structural and lattice models: a parametrization of energy transfer and trapping in Photosystem I. *Submitted*.
- (2) Scheller, H.V., H. Naver, and B.L. Moller. 1997. Molecular aspects of Photosystem I. *Physiol. Plant.* 100:842-851.
- (3) Scheller, H.V., P.E. Jensen, A. Haldrup, C. Lunde, and J. Knoetzel. 2001. Role of subunits in eukaryotic Photosystem I. *Biochim. Biophys. Acta.* 1507:41-60.
- (4) Kruip, J., D. Bald, E. Boekema, and M. Rögner. 1994. Evidence for the existence of trimeric and monomeric Photosystem I complexes in thylakoid membranes from cyanobacteria. *Photosynth. Res.* 40:279-286.
- (5) Schwabe, T.M.E., E.J. Boekema, S. Berry, P.R. Chitnis, E. Pistorius, and J. Kruip. 2001. Dynamics of Photosystem I: Ca²⁺-based oligomerization and response to iron deficiency by induction of a new antenna built by IsiA. In Proceedings of the 12th International congress on photosynthesis. B. Osmond, editor. CSIRO Publishing, Brisbane, Australia. S6:003.
- (6) Jordan, P., P. Fromme, H.T. Witt, O. Klukas, W. Saenger, and N. Krauss. 2001. Three-dimensional structure of cyanobacterial Photosystem I at 2.5 angstrom resolution. *Nature.* 411:909-917.
- (7) Fromme, P., P. Jordan, and N. Krauss. 2001. Structure of Photosystem I. *Biochim. Biophys. Acta.* 1507:5-31.

- (8) Krauss, N., W.-D. Schubert, O. Klukas, P. Fromme, H.T. Witt, and W. Saenger. 1996. Photosystem I at 4Å resolution represents the first structural model of a joint photosynthetic reaction centre and core antenna system. *Nat. Struct. Biol.* 3:965-973.
- (9) Schubert, W.-D., O. Klukas, N. Krauss, W. Saenger, P. Fromme, and H.T. Witt. 1997. Photosystem I of *Synechococcus elongatus* at 4 Å Resolution: Comprehensive structure analysis. *J. Mol. Biol.* 272:741-769.
- (10) Gobets, B., and R. van Grondelle. 2001. Energy transfer and trapping in Photosystem I. *Biochim. Biophys. Acta*, 1507:80-99.
- (11) Gobets, B., H. van Amerongen, R. Monshouwer, J. Kruip, M. Rögner, R. van Grondelle, and J.P. Dekker. 1994. Polarized site-selected fluorescence spectroscopy of isolated Photosystem I particles. *Biochim. Biophys. Acta.* 1188:75-85.
- (12) Van Grondelle, R., J.P. Dekker, T. Gillbro, and V. Sundström. 1994. Energy transfer and trapping in photosynthesis. *Biochim. Biophys. Acta.* 1187:1-65.
- (13) Gobets, B., I.H.M. van Stokkum, M. Rögner, J. Kruip, E. Schlodder, N.V. Karapetyan, J.P. Dekker, and R. van Grondelle. 2001. Time-resolved fluorescence emission measurements of Photosystem I particles of various cyanobacteria: a unified compartmental model. *Biophys. J.* 81:407-424.
- (14) Hayes, J.M., S. Matsuzaki, M. Rätsep, and G.J. Small. 2000. Red chlorophyll-*a* antenna states of Photosystem I of the cyanobacterium *Synechocystis* sp. PCC 6803. *J. Phys. Chem. B.* 104:5625-5633.
- (15) Rätsep, M., T.W. Johnson, P.R. Chitnis, and G.J. Small. 2000. The red-absorbing chlorophyll-*a* antenna states of Photosystem I: A hole-burning study of *Synechocystis* sp PCC 6803 and its mutants. *J. Phys. Chem. B.* 104:836-847.
- (16) Pålsson, L.-O., J.P. Dekker, E. Schlodder, R. Monshouwer, and R. van Grondelle. 1996. Polarized site-selective fluorescence spectroscopy of the long-wavelength emitting chlorophylls in isolated Photosystem I particles of *Synechococcus elongatus*. *Photosynth. Res.* 48:239-246.
- (17) Mukerji, I., and K. Sauer. 1990. A spectroscopic study of a Photosystem I antenna complex. *In* Current Research in Photosynthesis. M. Baltscheffsky, editor. Kluwer Academic Publishers, Dordrecht, The Netherlands. 2:321-324.
- (18) Van Grondelle, R., and V. Sundström. 1988. Excitation energy transfer in photosynthesis. *In* Photosynthetic Light-Harvesting Systems. H. Scheer and S. Schneider, editors. De Gruyter, Berlin. 403-438.
- (19) Van Grondelle, R., H. Bergström, V. Sundström, R.J. van Dorssen., M. Vos, and C.N. Hunter. 1988. *In* Photosynthetic Light-Harvesting Systems. H. Scheer and S. Schneider, editors. De Gruyter, Berlin. 519-530.
- (20) Werst, M., Y.W. Jia, L. Mets, and G.R. Fleming. 1992. Energy-transfer and trapping in the Photosystem-I core antenna - A temperature study. *Biophys. J.* 61:868-878.
- (21) Holzwarth, A.R., G. Schatz, H. Brock, and E. Bittersmann. 1993. Energy transfer and charge separation kinetics in Photosystem I. Part 1: Picosecond transient absorption and fluorescence study of cyanobacterial Photosystem I particles. *Biophys. J.* 64:1813-1826.
- (22) Karapetyan, N.V., A.R. Holzwarth, and M. Rögner. 1999. The Photosystem I trimer of cyanobacteria: molecular organization, excitation dynamics and physiological significance. *FEBS Lett.* 460:395-400.
- (23) Trissl, H.-W., and C. Wilhelm. 1993. Why do thylakoid membranes from higher-plants form grana stacks? *Trends Biochem. Sci.* 18:415-419.

- (24) Rivadossi, A., G. Zucchelli, F.M. Garlaschi and R.C. Jennings. 1999. The importance of PSI chlorophyll red forms in light-harvesting by leaves. *Photosynth. Res.* 60:209-215.
- (25) Hastings, G., L.J. Reed, S. Lin, and R.E. Blankenship. 1995. Excited state dynamics in Photosystem I: effects of detergent and excitation wavelength. *Biophys. J.* 69: 2044-2055.
- (26) Turconi, S., J. Kruip, G. Schweitzer, M. Rögner, and A.R. Holzwarth. 1996. A comparative fluorescence kinetics study of Photosystem I monomers and trimers from *Synechocystis* PCC 6803. *Photosynth. Res.* 49:263-268.
- (27) Savikhin, S., W. Xu, V. Soukoulis, P.R. Chitnis, and W.S. Struve. 1999. Ultrafast primary processes in Photosystem I of the cyanobacterium *Synechocystis* sp. PCC 6803. *Biophys. J.* 76: 3278-3288.
- (28) Savikhin, S., W. Xu, P.R. Chitnis, and W.S. Struve. 2000. Ultrafast primary processes in PS I from *Synechocystis* sp. PCC 6803: Roles of P700 and A(0). *Biophys. J.* 79:1573-1586.
- (29) Melkozernov, A.N., S. Lin, and R.E. Blankenship. 2000. Excitation dynamics and heterogeneity of energy equilibration in the core antenna of Photosystem I from the cyanobacterium *Synechocystis* sp. PCC 6803. *Biochemistry.* 39:1489-1498.
- (30) Byrdin, M., I. Rimke., E. Schlodder, D. Stehlik, and T.A. Roelofs. 2000. Decay kinetics and quantum yields of fluorescence in Photosystem I from *Synechococcus elongatus* with P700 in the reduced and oxidized state: are the kinetics of excited state decay trap-limited or transfer-limited? *Biophys. J.* 79:992-1007.
- (31) Kennis, J.T.M., B. Gobets, I.H.M. van Stokkum, J.P. Dekker, R. van Grondelle, and G.R. Fleming. 2001. Light harvesting by chlorophylls and carotenoids in the Photosystem I complex of *Synechococcus elongatus*: a fluorescence upconversion study. *J. Phys. Chem. B.* 105:4485-4494.
- (32) Gobets, B., I.H.M. van Stokkum, F. van Mourik, M. Rögner, J. Kruip, J.P. Dekker, and R. van Grondelle. 1998. In *Photosynthesis: Mechanisms and effects*. G. Garab, editor. Kluwer Academic Publishers, Dordrecht, The Netherlands. 1:571-574.
- (33) Gobets, B., J.P. Dekker, and R. van Grondelle. 1998. Transfer-to-the-trap limited model of energy transfer in Photosystem I. In *Photosynthesis: Mechanisms and effects*. G. Garab, editor. Kluwer Academic Publishers, Dordrecht, The Netherlands. 1:503-508.
- (34) Kruip, J., E.J. Boekema, D. Bald, A.F. Boonstra, and M. Rögner. 1993. Isolation and structural characterization of monomeric and trimeric Photosystem-I complexes (P700F_a/F_b and P700F_x) from the cyanobacterium *Synechocystis* PCC-6803. *J. Biol. Chem.* 268:23353-23360.
- (35) Fromme, P., and H.T. Witt. 1998. Improved isolation and crystallization of Photosystem I for structural analysis. *Biochim. Biophys. Acta.* 1365:175-184.
- (36) Van der Lee, J., D. Bald, S.L.S. Kwa, R. van Grondelle, M. Rögner, and J.P. Dekker. 1993. Steady-state polarized-light spectroscopy of isolated Photosystem-I complexes. *Photosynth. Res.* 35:311-321.
- (37) Du, M., X. Xie, Y. Jia, L. Mets, and G.R. Fleming. 1993. Direct observation of ultrafast energy transfer in PS I core antenna. *Chem. Phys. Lett.* 201:535-542.
- (38) Förster, T. 1965. In *Modern Quantum Chemistry*. O. Sinanoglu, editor. Academic Press, New York. 2:93-137.
- (39) Kleima, F.J., E. Hofmann, B. Gobets, I.H.M. van Stokkum, R. van Grondelle, K. Diederichs, and H. van Amerongen. 2000. Förster excitation energy transfer in peridinin-chlorophyll-*a*-protein. *Biophysical J.* 78:344-353.
- (40) Van Amerongen, H., L. Valkunas, and R. van Grondelle. 2000. *Photosynthetic Excitons*. World Scientific, London. 347-352.

- (41) Lichtenthaler, H.K. 1987. Chlorophylls and carotenoids: pigments of photosynthetic membranes. *Methods Enzymol.* 148:350-382.
- (42) Pålsson, L.-O., C. Flemming, B. Gobets, R. van Grondelle, J.P. Dekker, and E. Schlodder. 1998. Energy transfer and charge separation in Photosystem I: P700 oxidation upon selective excitation of the long-wavelength chlorophylls of *Synechococcus elongatus*. *Biophys. J.* 74:2611-2622.
- (43) Brettel, K., and W. Leibl. 2001. Electron transfer in Photosystem I. *Biochim. Biophys. Acta.* 1507:100-114.

7

Light harvesting by chlorophylls and carotenoids in the Photosystem I core complex of *Synechococcus elongatus*: a fluorescence upconversion study

John T.M. Kennis, Bas Gobets, Ivo H.M. van Stokkum, Jan P. Dekker, Rienk van Grondelle and Graham R. Fleming

The Photosystem I (PSI) core complex of oxygenic photosynthesis is an integral pigment-protein complex that incorporates both the antenna and the reaction centre (RC). It binds about 100 chl a and 20 β -carotene molecules. In the PSI core complex of the cyanobacterium *Synechococcus elongatus*, a total of about 9 antenna chl a molecules are red-shifted with respect to the primary electron donor, which absorbs at 700 nm. We have studied energy transfer and trapping processes in trimeric PSI complexes of this species at femtosecond resolution by means of the fluorescence-upconversion technique. By simultaneously analysing the fluorescence upconversion results and those obtained with a streak camera with picosecond resolution and multichannel detection,¹ we have mapped out the energy-transfer processes that follow immediately after photon absorption. Equilibration among chl a pigments in the bulk antenna was found to occur with a time constant of 360 fs. A major energy equilibration phase between bulk chl a and the red-shifted antenna chls occurs in 3.6 ps. A slow phase in energy equilibration takes place in 9.8 ps, after which the excitations are trapped by the RC in 38 ps. Fluorescence anisotropy measurements indicated an initial anisotropy of 0.30, which decayed biphasically with a major fast phase of 160 fs and a minor slow phase of 1.8 ps to a final anisotropy of 0.06. The 160 fs phase is assigned to elementary energy-transfer steps in the bulk chl a antenna, and the 1.8 ps phase to further equilibration processes, possibly involving energy transfer to or among red-shifted chls. Energy transfer from β -carotene to chl a was found to proceed both from the S₂ state and the S₁ state, with the majority of transferred excitations (60%) originating from the S₂ state, resulting in an estimated overall yield of ~90%. A comparison is made with the PSII core antenna protein CP47, which binds the same pigments but has a substantially lower carotenoid-chl a energy transfer yield of ~35%.²

INTRODUCTION

The core complex of Photosystem I (PSI) of oxygenic photosynthesis is a large, multisubunit integral membrane pigment-protein complex that uses light energy to catalyse electron transfer from cytochrome c_6 or plastocyanin to NADP^+ . It binds about 100 chlorophyll- a (chl a) and 20 β -carotene molecules,³ and, in that sense, forms the largest and most complex known photosynthetic energy converting protein complex. A 4 Å structure of the PSI core complex of the cyanobacterium *Synechococcus elongatus* in its trimeric form has been available for some years now.^{3,4} Each monomeric unit in the trimeric structure comprises 11 subunits termed PsaA through PsaF and PsaL through PsaM. PsaA and PsaB are the largest and most important subunits, and are arranged in a pseudo C_2 symmetry at the centre of the complex. PsaL, PsaM and PsaN lie at the periphery of the core complex near the trimerization domain. A total of 89 chl a molecules were resolved in the entire complex. At the centre, 6 chls are bound to PsaA and PsaB close to the pseudo- C_2 axis, and were assigned as the redox-active chromophores of the reaction centre (RC). They are arranged in a fashion that is reminiscent of the purple bacterial RC, with two chl a 's as a special pair, two 'monomeric' chl a and two chl a 's at the position of the bacteriopeheophytins.³

The other 83 chl a molecules resolved in the complex constitute the PSI core's light-harvesting system. A majority of 77 of them are bound to PsaA and PsaB. The core antenna chls form an ellipsoidically shaped, irregular bowl around the reaction centre at distances ranging between 15 and 40 Å. The chl a molecules in the core antenna are densely packed at distances from 8 to 16 Å. The 4 Å structure resolution did not allow for an identification of any of the about 20 β -carotene molecules.

A conspicuous feature of the light-harvesting system of cyanobacterial PSI in general is the presence of several chl a molecules that have their excited state energies red shifted significantly below that of the primary donor (P700) of the RC. In the PSI core, the number of red chls and the extent of red shifting depend on the species and the aggregation state (monomeric or trimeric) of the complex. A pool that absorbs maximal at 708 nm at low temperature (4 K), hereafter referred to as C708, appears to be a common feature to all cyanobacterial PSI core particles. It was proposed some years ago that in the cyanobacterium *Synechocystis* PCC6803, C708 corresponds to the lower excitonic state of a strongly coupled dimer or trimer of chl a molecules.⁵ Studies on a series of mutants of *Synechocystis*, which each had one of their peripheral subunits deleted, indicated that C708 is most likely bound to the periphery of PsaA and/or PsaB, near the L and M subunits.^{6,7} Some species have an additional red pool which absorbs more to the red than C708. These generally suffer loss of absorption upon monomerisation of the complexes, which suggests that they are located at the periphery of the core complex near the trimerization domain.⁸

The function of the red pigments is a matter of considerable debate. In fact, the presence of different pools in the various species may indicate that they have different functions. It has been suggested that they could increase the efficiency of energy trapping by concentrating excitations near the RC.^{9,10} However, this is contradicted by recent experiments which demonstrated that PSI preparations with a progressively increasing number of red chls exhibit increasing lifetimes in the core antenna.¹¹ A more likely explanation would be that the

absorption cross section of far red light is increased by the presence of the red pigments, which in the case of considerable shading of leaves or cyanobacterial mats may significantly¹² increase the photochemical turnover rate.¹³ Alternatively, the red chls may be involved in photoprotective mechanisms.¹⁴

PSI core particles bind about 20 β -carotene molecules per monomer, which give rise to a broad absorption band in the blue and green parts of the solar spectrum. They are the only PSI core pigments that absorb significantly in that wavelength region, which may imply an important role for β -carotene as accessory light-harvesting pigments. We remark that cyanobacteria employ phycobilisomes, which are extra-membrane light-harvesting complexes, to fill the spectral gaps left open by chl*a*. These complexes absorb yellow and orange, and in some cases blue-green light, but under most circumstances they transfer their excited state energy primarily to PSII.¹⁵

The light-harvesting function of β -carotene in the PSI core is exemplified by the high energy-transfer efficiency to chl*a* of about 85%.¹⁶ Such a high efficiency, often seen in photosynthetic systems, is remarkable in the light of the short lifetime of carotenoid excited states. The optically allowed S_2 state of carotenoids generally relaxes to the optically forbidden S_1 state in 100–200 fs by internal conversion (IC), after which the S_1 state internally converts to the ground state on a picosecond time scale.^{17,18} For an efficient light-harvesting function of carotenoids, these IC processes must be counteracted by faster energy transfer to chl. Indeed, it has recently been shown that in photosynthetic antennae, sub-ps and ps energy transfer from both the S_2 and S_1 state to (B)chl can effectively compete with IC to the ground state.^{19–24}

Energy-transfer and trapping processes in the PSI core have been studied quite extensively by time-resolved absorption and fluorescence techniques for many years now^{9,25–28} (for a review of early work see ref. 10). Only recently, however, the time resolution and sensitivity of the measuring equipment have come to a point that all relevant energy-transfer steps can be mapped out in an annihilation-free regime. Low-energy transient absorption studies with fs time-resolution have focused on PSI cores of the cyanobacterium *Synechocystis* PCC6803.^{29–31} Recent time-resolved fluorescence measurements with ps resolution utilizing a streak camera with multi-wavelength detection have compared the excited state dynamics of PSI cores of several cyanobacterial species.^{11,32,33} All this research has exclusively addressed chl*a* dynamics, and thus far, the light-harvesting process that involves energy transfer from β -carotene to chl*a* has remained uninvestigated.

In this paper we present a fluorescence upconversion study on trimeric PSI particles of the cyanobacterium *Synechococcus elongatus*. The trimeric PSI core of this species contains two pools of red chls, the common pool C708 and an additional pool C719 after its absorption maximum at low temperature.^{34,35} By combining spectrally-resolved upconversion data with femtosecond resolution with those obtained by means of a multichannel streak camera, we have mapped out energy equilibration components between bulk chl*a* molecules, between bulk chl*a* and the red pools, and subsequent trapping by the RC. Furthermore, we present time-resolved fluorescence anisotropy measurements, which indicate the time scale of elementary energy-transfer steps in the PSI core antenna. Finally, we have characterized the dynamic aspects of the energy-transfer process from β -carotene to chl*a*.

EXPERIMENTAL

Trimeric complexes from the cyanobacterium *Synechococcus el.* were prepared as described previously.³⁶ For the fluorescence measurements, the concentrated samples were diluted to an absorbance at 680 nm of 0.3 per mm with a buffer containing 20 mM CaCl₂, 20 mM MgCl₂, 10 mM 2-(N-morpholino)ethane sulfonic acid (MES) and 0.05% W/V dodecyl- β -D-maltoside at a pH of 6.5. Although we were working with closed (oxidized) RCs (see below), 10 mM sodium ascorbate and 10 μ M Phenazine Meta Sulphate (PMS) were added to the samples. We found that addition of these chemicals slowed down photo-degradation of the sample during the measurements by a factor of at least three, enabling us to utilize longer data collection times. The sample was flowed through a 1 mm path length quartz cell using a peristaltic pump and maintained at 8-10 °C by a recirculating bath that flowed around the sample reservoir. The sample was exchanged for a fresh one after every \sim 3 hrs. of data collection. The absorption spectra of the used samples revealed no significant degradation.

Fluorescence upconversion measurements were carried out with an apparatus described previously.²¹ At its basis was a regeneratively amplified Ti:sapphire laser system (Coherent Mira-Rega), operating at 250 kHz with a pulse duration of about 50 fs. Excitation pulses at 400 nm were provided by frequency-doubling the output of the laser system in a 2 mm long BBO crystal. Excitation pulses at 650 nm or 510 nm were generated by means of an optical parametric amplifier (OPA, Coherent 9450). The instrument response function of the upconversion apparatus ranged between 280 fs and 350 fs. The polarization of the excitation beam with respect to the polarization of the upconverted fluorescence was set to either parallel, perpendicular, or at the magic angle (54.7°) by means of an achromatic waveplate (CVI). For fluorescence anisotropy measurements, the polarization was alternately switched between parallel and perpendicular many times to avoid any possible effect of long-term fluctuations in the laser and detection system or sample conditions. A test measurement of the anisotropy in the dye LDS 720 upon excitation at 650 and detection at 725 nm gave a non-decaying anisotropy of 0.36, which is close to the expected value of 0.4.

Initially, it was our goal to perform the measurements with P₇₀₀ in the open (reduced) state. However, we found that this would require unattainable low excitation powers. To achieve reasonable count rates (\sim 40 counts/second) necessary for efficient data collection, we had to employ 2 mW of excitation energy, corresponding to a pulse energy of 8 nJ. At such pulse energies, and estimating a focal diameter of 100 μ m, we expect that about 1 out of 100 chls is excited in the focal volume, which corresponds to about 1 chl in every PSI monomer, and thus all RCs are oxidized after the sample in the excited volume has received a few shots. Given a 250 kHz repetition rate of the laser system and a flow speed of 0.5 m/s, a given volume of PSI particles resides 0.2 ms in the focus and is exposed to about 50 laser shots while moving through. During this time, P₇₀₀⁺ is not reduced by the combination of sodium ascorbate and PMS, as this process takes place on a ms time scale.³⁷ Hence, these circumstances will lead to a vast majority of $>90\%$ oxidized RCs in the excited volume.

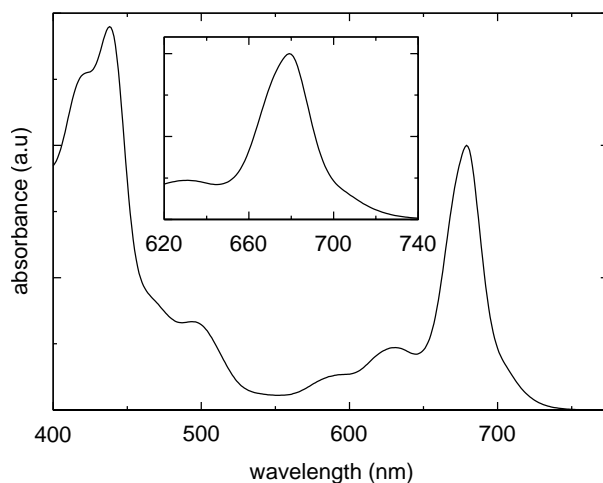
The above estimate of the excitation density indicates that we are near the threshold for singlet-singlet annihilation. To test for annihilation effects, the excitation power was varied between 0.3 mW and 3 mW. This did not alter the upconverted trace (data not shown), from

which we conclude that we were measuring in a regime where singlet-singlet annihilation does not play a significant role. We note that our pulse energies are below those given by Savikhin et al. for the onset of annihilation.²⁹ Singlet-triplet annihilation is unlikely to arise given the low triplet yield of chl a in the PSI core (by virtue of the short chl a antenna lifetime of ~ 40 ps). Moreover, any chl a triplet will likely be rapidly quenched by β -carotene.

Some of the time-resolved data were analysed with a global fitting program as described in.³⁸ Species-associated emission spectra (SAES) were determined assuming a sequential, irreversible model $A \rightarrow B \rightarrow C \rightarrow D$. The arrows symbolize increasingly slower mono-exponential decays, with time constants that can be regarded as the species lifetimes. This procedure enables us to visualize clearly the evolution of the excited states in the system. Note, however, that the thus obtained species A through D are not necessarily pure, but may represent mixtures of pure states. The anisotropy measurements were analysed following the method of Cross and Fleming by simultaneously fitting the polarized and magic angle traces with sums of exponential functions, convoluted with the instrument response function.³⁹

RESULTS AND DISCUSSION

Figure 7.1 shows the absorption spectrum of trimeric PSI particles of *Synechococcus elongatus* at room temperature. The absorption features at wavelengths longer than 600 nm result exclusively from the Q_y transition of chl a , and are shown on an expanded scale in the inset. The absorption band with a maximum at 680 nm is associated with bulk chl a pigments in the core antenna. This band is markedly asymmetric and shows a shoulder near 670 nm, indicating significant spectral heterogeneity among bulk antenna chls. Near 630 nm a vibronic band of chl a is located. At wavelengths longer than 700 nm the spectrum shows a distinct long tail, which is due to the two pools of red-shifted chls, C708 and C719. These two pools contain 4-5 and 4 chls respectively.³⁴ It is important to note that at room temperature,



7.1 Absorption spectrum of trimeric PSI particles of *Synechococcus elongatus* at room temperature. The inset shows the chl a Q_y absorption region on an expanded scale.

the absorption maxima of C708 and C719 are probably located at 702 nm and 708 nm, respectively.^{6,11} In the blue region, the absorption spectrum shows a maximum at 440 nm, which can be assigned to the Soret band of chl a . The absorption band near 500 nm is associated with β -carotene, of which about 20 molecules are bound per PSI monomer. All absorption features shown in figure 7.1 are similar to those published earlier for this preparation.^{34,35}

The room temperature steady-state fluorescence spectrum of *Synechococcus* trimers was published previously.³⁵ It shows a maximum at 720 nm, which can primarily be attributed to fluorescence from the red pools C708 and C719, and a pronounced shoulder at 690 nm, which originates from bulk chl a in thermal equilibrium with the red pools.

Isotropic time-resolved fluorescence

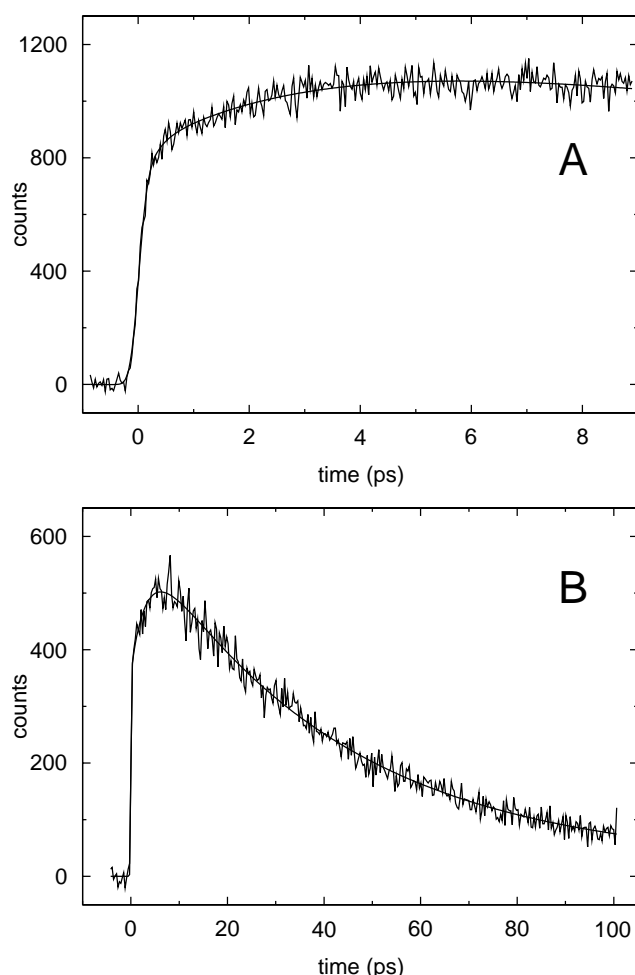
We characterized energy-transfer processes between bulk chl a , the red pools C708 and C719 and the RC by performing fluorescence upconversion measurements with excitation in the vibronic band of bulk chl a at 650 nm, and detection at 725 nm, where we primarily observe fluorescence from the two pools of red pigments, C708 and C719, which contribute roughly equally here.¹¹ Figure 7.2 shows the upconverted fluorescence detected at the magic angle in *Synechococcus* trimers with closed RCs on a short (A) and long time axis (B), respectively. Several distinct time scales ranging from instantaneous to tens of picoseconds can be discerned in this measurement. A simultaneous fit to the traces yields an instantaneous component, a rise-time of 210 fs with a minor amplitude, a major rise-time of 3.3 ps, a decay component time of 41 ps and a minor long-lived end level.

The instantaneous component can be assigned to emission from the directly excited bulk chl a molecules, which have a significant vibronic tail at this wavelength.¹¹ The amplitude of the 210 fs rise component is small (18% with respect to the overall 41 ps decay component), and from this measurement alone we cannot deduce its origin. The 3.3 ps rise time can readily be ascribed to energy equilibration between bulk chl a and the red pools C708 and C719. It closely matches the value of 3.8 ps that has been determined before on the same species by means of a streak camera with ps resolution.¹¹ It is significantly shorter than the equilibration times of 7 ps reported by Holzwarth et al.⁹ and 13 ps by Byrdin et al.³⁷ for *Synechococcus* trimers, but the determination of these values were severely hampered by the limited time-resolution of both experiments. The 3.3 ps equilibration time is similar to the corresponding time constants reported recently with fs transient absorption spectroscopy for PSI particles of *Synechocystis* PCC6803.^{29,31}

The 41 ps component can be assigned to excitation quenching by the oxidized RCs. It agrees well with the lifetime of 37 ps which has been reported in recent photon counting measurements on closed RCs in *Synechococcus* trimers by Byrdin et al.³⁷ and is virtually indistinguishable from that reported for open RCs in this species.^{9,11,37} The lifetime of 41 ps is significantly longer than that found in plant PSI cores (22 ps) (B. Gobets, unpublished results) and the PSI core of *Synechocystis* (25 ps).^{11,28,32,33} Gobets et al. have recently shown that an increasing number of red chls leads to longer trapping times, as is the case with *Synechococcus*. The species with the highest red chl content known to date, *Spirulina platensis*, has a lifetime of 50 ps.¹¹ The long-lived component has minor amplitude (4%) and

can be attributed to a small fraction of unbound chl a , which has a lifetime in the order of 5 ns.

To obtain a more complete picture of excited state equilibration in the core antenna of *Synechococcus*, we performed fluorescence upconversion experiments with excitation in the chl a Soret band at 400 nm and detection at 8 different wavelengths from 668 nm to 738 nm, which covers the fluorescence emitted from all spectral forms in the PSI core. It would have been desirable to perform these wavelength-resolved measurements with direct excitation in the Q $_y$ band, but as a result of strong scattering by the pump beam at 650 nm, it was not possible to upconvert the fluorescence at wavelengths shorter than about 710 nm. With excitation in the Soret band, all chl a molecules, including the red pigments, have an equal

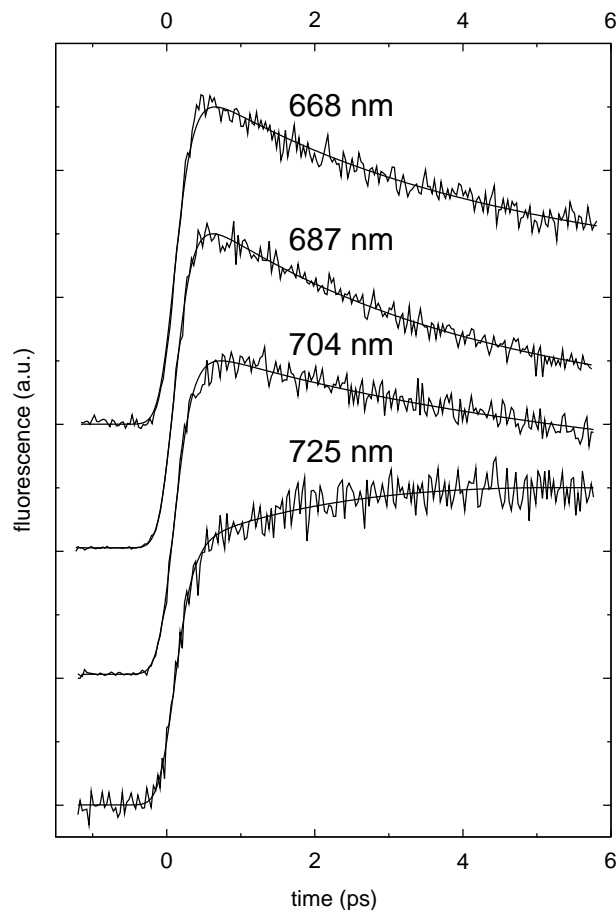


7.2 A: Time-resolved isotropic fluorescence in trimeric *Synechococcus elongatus* PSI particles, detected at 725 nm upon excitation at 650 nm, collected on a time basis of 9 ps. B: Time-resolved trace collected under the same conditions as A), on a time basis of 100 ps. The traces are fitted with a 4-component exponential function with time constants of 210 fs, 3.3 ps, 41 ps and a long-lived end level with relative amplitudes - 0.18:-0.39:1:0.04. See text for details.

excitation probability, and they will relax to the Q_y state in ca. 100 fs.⁴⁰ Figure 7.3 shows four selected traces at 668 nm, 687 nm, 704 nm and 725 nm.

The trace at 725 nm, which monitors fluorescence from the red pools C708 and C719, is very similar to the trace presented in figure 7.2a upon excitation at 650 nm and detection at 725 nm. It exhibits a rapid rise of the fluorescence, which mainly represents bulk chl α fluorescence following relaxation from the Soret to the Q_y state. It then rises further on a time scale of a few ps, indicating equilibration between the bulk and the red pigments. Correspondingly, the traces at 668 nm, 687 nm and 704 nm, which probe fluorescence from bulk chl α , display a decay on a picosecond time scale. All traces are fitted well with the time constants of 3.3 ps (with positive amplitude at 668, 687 and 704 nm, and negative amplitude at 725 nm) and 41 ps found in the measurement presented in figure 7.2.

Close inspection of the early time behaviour of the traces in figure 7.3 indicates that the rise of the fluorescence at 704 nm lags that of the trace at 668 nm by a few hundreds of fs. To demonstrate this, we fitted the traces with a single rise time of 140 fs, assuming that the



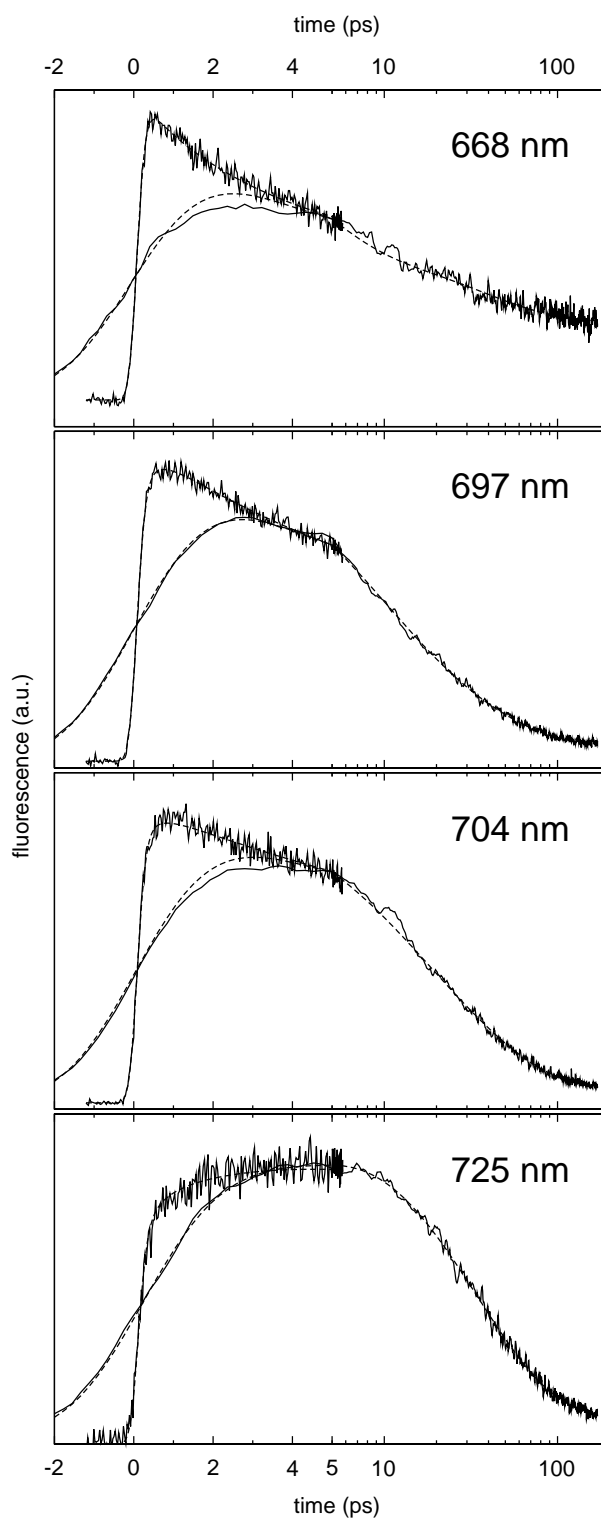
7.3 Time-resolved isotropic fluorescence in trimeric *Synechococcus elongatus* PSI particles upon excitation at 400 nm, detected at 668 nm, 687 nm, 704 nm and 725 nm. The traces are fitted with tri-exponential functions with time constants of 140 fs, 3.3 ps and 41 ps. (see text for details).

sample does not fluoresce at time zero. In principle, 140 fs is not an unreasonable number for Soret- Q_y relaxation. However, at 668 nm the fit undershoots the experimental data at early times, while at 704 nm the fit overshoots the data. If we assume that Soret- Q_y relaxation takes place at a uniform, wavelength-independent rate, this indicates that an additional sub-ps dynamic process is taking place in the PSI core antenna. Because the lag in the rise occurs at the red side of the bulk chl a fluorescence (and not at a wavelength where fluorescence from the red pigments dominates, as evidenced by the positive 3.3 ps component at 704 nm, see also ref. 11), we assign this component to a dynamic process taking place in bulk chl a molecules. We will substantiate this point below.

For a meaningful characterization of the time-dependent fluorescence behaviour in the PSI core antenna, it is highly desirable to apply a global analysis of the spectrally resolved time-dependent traces, and determine the relative intensities across the fluorescence spectrum, in the form of so-called species-associated spectra. However, with the fluorescence upconversion technique, a quantitative determination of the relative fluorescence intensities at different detection wavelengths is cumbersome, which means that the construction of time-resolved or species-associated spectra cannot be reliably conducted. We have noted already the consistency of the present fluorescence upconversion data and the wavelength-resolved streak camera data reported earlier,¹¹ which encouraged us to perform a simultaneous global analysis of these two data-sets. This approach allows us to maximally utilize the spectral and temporal information that is provided by our measurements, and follow the spectrally-resolved dynamics from \sim 100 fs after photon absorption to more than 100 ps, after which all excited states have been trapped by the RC. In this analysis, the early dynamics up to about 1.5 ps are mainly extracted from the fluorescence upconversion measurements. The dynamics between 1.5 ps and 6 ps are extracted from both data-sets, and the dynamics slower than 6 ps are obtained exclusively from the streak camera data. In essence, the overlapping time ranges of both experiments allow us to assign a spectral evolution to the early time window.

We forewarn the reader that the experimental circumstances under which the two data-sets were collected were not identical. The largest difference is that the upconversion data were collected with oxidized RCs, and the streak camera data with reduced RCs. However, thus far all reports dealing with open and closed RCs on PSI particles have indicated a very similar evolution in these two cases.^{30,37} The analysis of the streak camera data was published earlier and indicated that five lifetimes are necessary to describe the data: 400 fs, 3.8 ps, 9.6 ps, 38 ps and 3 ns.¹¹ It is important to note that in this case, the 400 fs component was limited by the instrument response and represented a rise of fluorescence, which was ascribed to chl a Soret- Q_y relaxation.

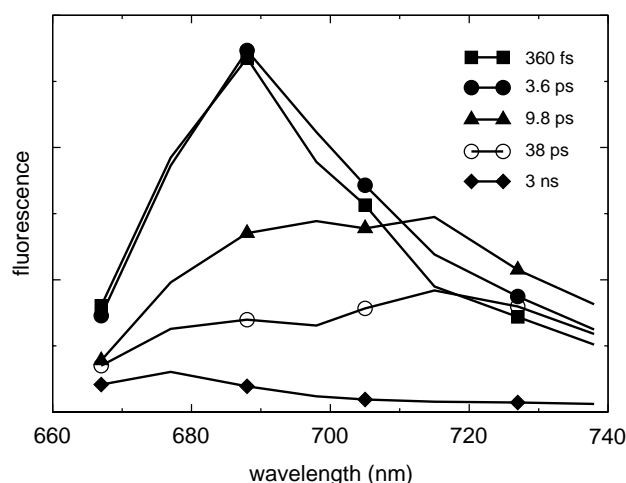
In the new, simultaneous analysis it was assumed that no fluorescence originates from the sample at time zero, and rises with the Soret- Q_y relaxation time. This relaxation time can be estimated to be 100 fs,⁴⁰ which is significantly shorter than that estimated in the earlier analysis of the streak camera data.¹¹ We found that 6 components are required for an adequate description of the complete data-set. Figure 7.5 shows the upconversion traces plotted together with the streak camera traces, along with the results of the global analysis. Note that the time-axis is linear from -2 ps to 5.8 ps, and logarithmic at longer times.



7.4 (Opposite page) Fluorescence upconversion traces obtained in *Synechococcus elongatus* PSI particles combined with those obtained with a streak camera (solid lines),¹¹ plotted on a linear-logarithmic time axis. The dashed lines denote the result of the 6-component simultaneous analysis of the upconversion and streak camera data. The excitation wavelength was 400 nm, the detection wavelengths (from top to bottom) 668 nm, 697 nm, 704 nm and 725 nm. See text for details.

Strikingly, the upconversion traces connect smoothly to the streak camera traces. The time constants that follow from the simultaneous global analysis are 100 fs, 360 fs, 3.6 ps, 9.6 ps, 38 ps and 3 ns. The species-associated emission spectra (SAES) that follow from this analysis are shown in figure 7.4. Note that to obtain these SAES, we have assumed a sequential model in which the first SAES decays into the second SAES, etc. (see the Experimental section). The SAES with a lifetime of 100 fs represents the Soret state of chl a , which we require to be zero in this wavelength region and is not shown.

The first displayed SAES (squares) rises in 100 fs and has a lifetime of 360 fs. It peaks at about 687 nm, and can thus be assigned to fluorescence emanating primarily from bulk chl a pigments. The next SAES (solid circles), which is formed in 360 fs, has a lifetime of 3.6 ps. It is slightly red shifted with respect to the former SAES by a few nm. The extent of the red shift cannot be accurately determined because of the coarse wavelength intervals used. The wavelengths associated with this red shift can be attributed to fluorescence changes that originate from the bulk of the PSI core antenna, not the red pools C708 and C719. We accordingly assert that the 360 fs component represents excited-state energy equilibration among bulk chl a molecules. Similar time constants, assigned to the same process, were observed using fs pump-probe spectroscopy in PSI particles of *Synechocystis* PCC6803 upon excitation at the blue side of the Q $_y$ band.^{29,31} Our measurements thus form the fluorescence-detected counterpart of these observations, and indicate that this process is also discernible upon excitation at 400 nm, which is non-selective and results in a more even initial excited state distribution between the different spectral forms in the core antenna. We note



7.5 Species-associated emission spectra (SAES) that follow from the 6-component simultaneous analysis of the isotropic fluorescence upconversion data presented in Fig. 4 and streak camera data of ref. 11 of trimeric *Synechococcus elongatus* PSI particles.

that the 360 fs time constant is similar to the 210 fs rise component that we detected at 725 nm with excitation at 650 nm (figure 7.2a). The SAES of figure 7.4 (squares vs. solid circles) show that the 360 fs component has the same sign and a similar amplitude, which makes it likely that these components have the same origin.

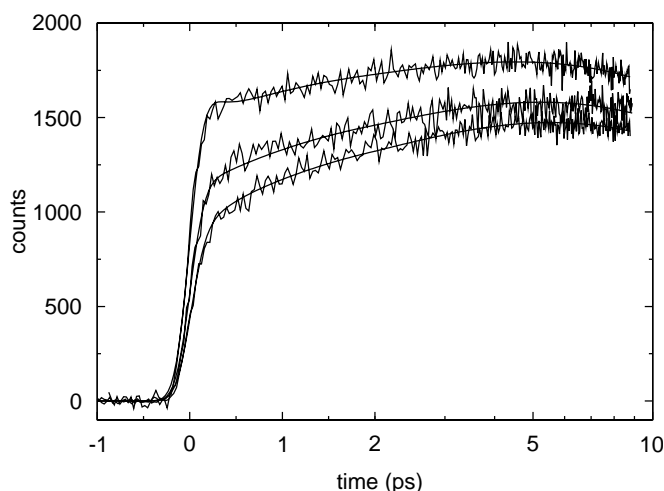
The next SAES (triangles) is formed in 3.6 ps and has a lifetime of 9.8 ps. It represents a large red-shift of about 20 nm, having a shallow maximum near 715 nm and thus implies a drastic shift towards thermal equilibrium in the PSI core antenna. This newly formed fluorescence band is associated with the red pools C708 and C719, therefore the 3.6 ps process can clearly be assigned to equilibration between the bulk chl α and the red pools C708 and C719. Note that the process appears to be non-conservative, i.e. the area under the 360 fs SAES is larger than that under the 3.6 ps component, indicating that some excited states are quenched. This may indicate that some non-equilibrium energy trapping by the RC occurs, as observed before for some PSI preparations.^{11,32} The 3.6 ps component is the only component in this analysis which adopts weight from both the upconversion and streak camera data-sets. The shape of the SAES and the value of the time constant are very similar to what follows from the analysis of the streak camera data alone, which substantiates the consistency of the two data-sets.

The longer-lived components all follow from the streak camera data, and have been characterized previously.¹¹ The next component (open circles) rises in 9.8 ps and has a lifetime of 38 ps. With regard to the previous SADS, it is slightly further red-shifted, along with a significant decrease of fluorescence intensity, which indicates that the 9.8 ps process signals slow energy equilibration with the red pigments and a significant portion of energy transfer to the RC. The 38 ps component represents the transfer-equilibrated state in the core antenna,^{11,33} and is exclusively associated with energy transfer to the RC. Its shape is similar to that of the steady-state fluorescence spectrum reported in ref. 35. The 3 ns component (diamonds) has a small amplitude, peaks near 675 nm and is caused by a fraction of loose, unbound chl α .

We also performed a simultaneous analysis of these data with 5 components, i.e. 1 component less than in the above analysis. We found that the fit becomes slightly worse, by 2%, and the time constants become 140 fs, 2.5 ps, 7.4 ps, 34 ps and 5 ns. The only significant difference with the above analysis lies in the sub-picosecond time constants; the rest of the components remains qualitatively the same. With 5 components, the Soret- Q_y relaxation time constant is fitted to 140 fs, (see figure 7.3), whereas with 6 components, the sub-picosecond times were split in a Soret- Q_y relaxation time of 100 fs and a bulk chl α equilibration component of 360 fs.

Time-resolved fluorescence anisotropy

To further characterize the time scale of elementary energy-transfer steps in the PSI antenna, we performed time-resolved fluorescence anisotropy measurements on trimeric PSI particles of *Synechococcus el.* From top to bottom, figure 7.6 shows the upconverted fluorescence with excitation and detected fluorescence polarized parallel, at the magic angle, and perpendicular, detected at 725 nm upon excitation at 650 nm. (The magic angle trace is reproduced from figure 7.2a). We observe that at early times, especially during the rising part, the trace with parallel polarization has significantly higher intensity than the perpendicular trace, implying a



7.6 Polarized time-resolved fluorescence of trimeric *Synechococcus elongatus* PSI particles, with from top to bottom, excitation and detected fluorescence polarized parallel, at the magic angle, and perpendicular. The excitation wavelength was 650 nm, fluorescence was detected at 725 nm. Note that the time scale is linear from -1 to 2 ps, and logarithmic from 2 ps to 8 ps. The smooth solid lines denote the result of an anisotropy analysis, which yielded an anisotropy decay function $r(t) = 0.14 e^{-t/0.16} + 0.1 e^{-t/1.8} + 0.06$, with the time constants given in ps.

substantial fluorescence anisotropy. Note that although the detection wavelength corresponds to that of the red pigments, the sub-picosecond signals are dominated by fluorescence that originates from the vibronic tail of bulk chl a (see above). At increasing delays, the parallel and perpendicular traces move closer together, indicating fluorescence anisotropy decay.

To determine the time-resolved anisotropy $r(t)$, we analysed these data according to the method of Cross and Fleming by simultaneously fitting the polarized and magic angle traces to a sum of exponential functions, convoluted with the instrument response function.³⁹ In the analysis, we also took into account the long magic angle scan of 100 ps shown in figure 7.2b to properly determine the time constants in the isotropic contribution to the signals. The result of this analysis is shown as the smooth lines in figure 7.6. We find an initial value $r(0)$ of 0.30, which decays biphasically with time constants of 160 ± 60 fs (amplitude 0.14), and 1.8 ± 0.2 ps (amplitude 0.10) to a final, non-decaying value of 0.06 ± 0.015 . A test measurement on a laser dye in solution gave a time-independent anisotropy of 0.36, which is reasonably close to the theoretically expected value of 0.4 for the initially prepared excited state (see the Experimental section). In the PSI core, we observe an initial anisotropy $r(0)$ of 0.30, which is somewhat lower than the reference measurement, indicating that we do not detect the anisotropy decay of the entire initially prepared chl a ensemble. Fixing the initial anisotropy to 0.36 in the analysis gave a fast anisotropy decay of 95 ± 15 fs (amplitude 0.2), a slow one of 1.6 ± 0.14 ps (amplitude 0.1) and a non-decaying component of 0.06. The quality of the fit was similar to that shown in figure 7.6. (Result not shown)

Our results are very similar to the fluorescence upconversion measurements of Du et al. on PSI particles of *Chlamydomonas reinhardtii*, who reported an initial anisotropy of 0.34 which

decayed with a time constant of 180 fs.²⁵ We note that the excitation and detection wavelengths in our and Du's studies were similar, but that the instrument response function of Du's study was significantly shorter (100 fs vs. 280 fs). Savikhin et al. employed polarized femtosecond transient absorption spectroscopy on PSI core particles of *Synechocystis*.²⁹ Upon excitation and probing in bulk chl a , they found an initial anisotropy of 0.27 which decayed mono-exponentially to 0.07 with a time constant of 590 fs, which appears to be at odds with our results. However, Savikhin et al. analysed their data by determining the raw anisotropy $r_{raw}(t) = I_{par} - I_{perp} / (I_{par} + 2I_{perp})$, and subsequently fitting $r_{raw}(t)$ with a sum of exponentials. As pointed out before, this procedure may lead to considerable errors because it does not take into account the effects of a finite instrument response.³⁹ When we apply a similar procedure to our fluorescence upconversion data, and fit the resulting raw anisotropy $r_{raw}(t)$ with a bi-exponential function, we also find an initial anisotropy of 0.27, which decays with a major time constant of 560 fs (0.17 amplitude) and a minor one of 6 ps (0.055 amplitude) to a non-decaying value of 0.046. This suggests that it may be the analysis of the time-resolved data, and not the experimental data themselves that are the source of the apparent incompatibility of our results and those of Savikhin et al.

A fast anisotropy decay of 160 fs would be consistent with the structural information we have for the PSI core: the close packing of chls in the PSI core antenna, with centre-to-centre distances ranging from 7 to 16 Å and an average coordination number of about 3 within this range of distances,³ is expected to lead to site-to-site hopping times (or perhaps excitonic relaxations) in the order of 100 fs, as has been extensively documented by anisotropy measurements on the LH1 and LH2 complexes of purple bacteria⁴¹⁻⁴⁴ and the FMO complex of green sulphur bacteria,^{45,46} which have comparable interpigment distances. Structure-based simulations of energy transfer and trapping in the PSI core have indicated chl a single-site lifetimes in the order of 100 fs.⁴⁷

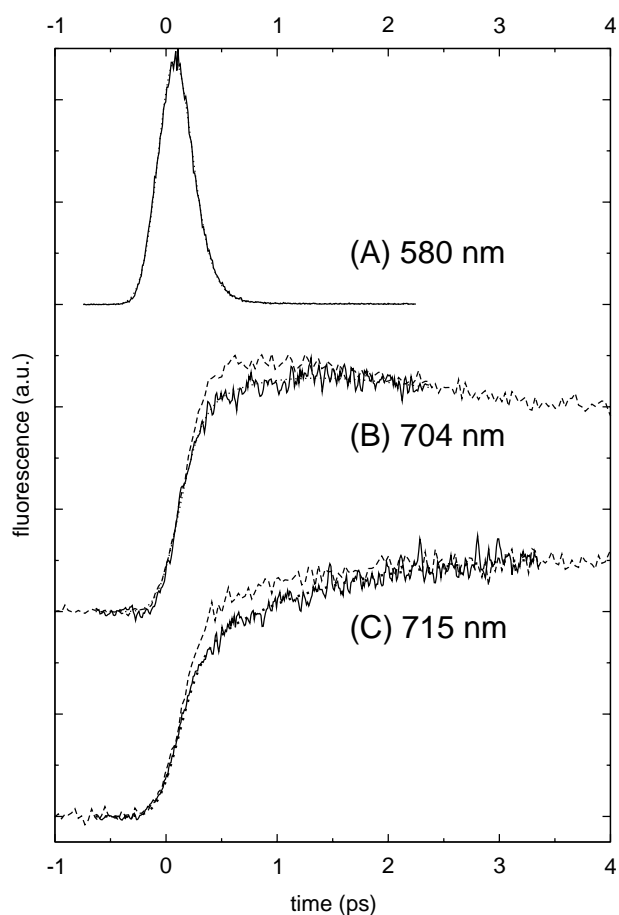
A relatively slow anisotropy decay with an amplitude of 0.1 occurs with a time constant of 1.8 ps. It is not very likely that this component is associated with one specific process; it probably follows from the combined effects of slow energy equilibration in bulk chl a , energy-transfer processes between bulk and red chl a , and perhaps equilibration processes among the red pools C708 and C719, which may all have their specific time scales of which 1.8 ps forms some weighted average. The final anisotropy is 0.06, which is close to zero, as one would expect for an orientationally disordered system as PSI. Note that in the study of Du et al., the final anisotropy did not vanish, but remained constant at 0.2 at long delays.²⁵ This was probably an artifact, possibly caused by the presence of a fraction of unbound, non-transferring chl a in the preparation.

Carotenoid-chl a transfer

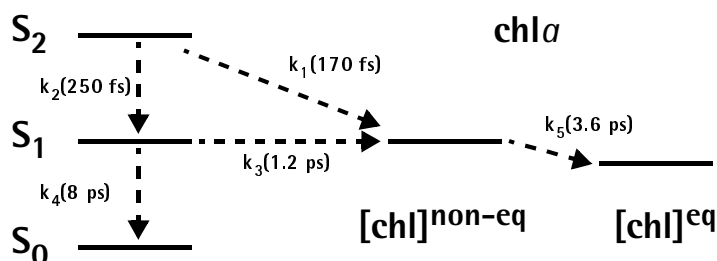
As of yet, no information is available on the dynamics of the carotenoid light-harvesting process in the PSI core. We have studied β -carotene to chl a energy transfer by exciting β -carotene at 510 nm and upconverting the carotenoid fluorescence from the carotenoid S₂ state at 590 nm, and the chl a fluorescence at 704 nm and 715 nm. Figure 7.7a shows the time-resolved fluorescence from the S₂ state of β -carotene at 590 nm. A single exponential fit indicates a lifetime of 105 fs. This lifetime closely corresponds to that recently determined for carotenoids bound to LHCII of plants by means of the fluorescence upconversion technique,²¹

and is almost twice as long as that obtained for rhodopin glucoside in the LH2 complex of the purple photosynthetic bacterium *Rhodospseudomonas acidophila*.¹⁹ The S_2 state of β -carotene in solution has a solvent-dependent lifetime that ranges between 180 fs in non-polar solvents and 120 fs in polar solvents.⁴⁸ The hydrophobic interior of the PSI core protein probably resembles a non-polar solvent, which suggests that the 'intrinsic' S_2 lifetime in PSI may be close to 180 fs. The observed lifetime of 105 fs in PSI is thus shortened, presumably as a result of energy transfer to chl a from the S_2 state.

Figure 7.7b and c show the upconverted fluorescence of chl a at 704 nm and 715 nm (solid lines), respectively, upon excitation at 510 nm. For comparison, we also plotted the corresponding traces upon excitation at 400 nm (dashed lines), which represent the dynamics



7.7 A: Time-resolved fluorescence in *Synechococcus* PSI trimers upon excitation of β -carotene at 510 nm, and detection at 580 nm. The trace is fitted with a single lifetime of 105 fs. B: Solid line: time-resolved fluorescence upon excitation at 510 nm and detection at 704 nm. The dotted line denotes the results of target analysis according to the kinetic scheme depicted in Fig. 8, see text for details. Dashed line: time-resolved fluorescence upon excitation of chl a at 400 nm and detection at 704 nm. C: Solid line: time-resolved fluorescence upon excitation at 510 nm and detection at 715 nm. Dotted line: result of the target analysis. Dashed line: time-resolved fluorescence upon excitation of chl a at 400 nm and detection at 715 nm.



7.8 Kinetic scheme used for a target analysis of the data of Fig. 7 to describe energy-transfer pathways from β -carotene to *chl a* in PSI trimers of *Synechococcus el.* See text for details.

of directly excited *chl a*. The initial part of the fluorescence rises rapidly, which reflects the ~ 100 fs carotenoid-chl transfer from the S_2 state. The signal subsequently rises further on a ps time scale. It is evident that the *chl a* fluorescence at both 704 nm and 715 nm exhibits a slower rise component upon excitation of β -carotene as compared to *chl a* Soret excitation. Our global analysis procedure of the data in figure 7.5 and figure 7.4 indicated a rise component of 360 fs at 704 nm upon 400 nm excitation, which we attributed to equilibration among bulk *chl a* molecules. A fit to the 510 nm excited trace at 704 nm (not shown) yields a distinctly slower rise component of 1.2 ps. This time constant probably originates from carotenoid to *chl a* energy transfer. The only candidate donor state would be the carotenoid S_1 state. However, such a direct assignment is precarious due to the convoluted *chl a* energy-transfer dynamics that follows energy transfer from the carotenoids.

To better characterize the S_1 -*chl a* energy-transfer process, we have conducted a so-called target analysis to our data,⁴⁹ in which we utilize our knowledge of *chl a* dynamics to disentangle the energy-transfer processes among chls and between β -carotene and *chl a*. We analysed the three fluorescence-upconversion traces of figure 7.7 in terms of the kinetic scheme depicted in figure 7.8. In this minimal model, we assume that β -carotene transfers its energy uniformly to all spectral forms of *chl a*, bulk and red pools alike, from both the S_2 state and the S_1 state. This results in a *chl a* excited state distribution after energy transfer from β -carotene identical to that upon non-selective *chl a* excitation at 400 nm. Our analysis is based on the assumption that the time scales of energy-transfer from the S_2 and S_1 states are clearly separated, and lie in the order of 100 fs and 1 ps, respectively. In doing this, we may estimate the branching of excitations that reach *chl a* through S_2 and S_1 by comparing the femtosecond and picosecond rise-times in the signals at 705 and 716 nm, in which the picosecond part is affected by energy transfer among *chl a* molecules. The model does not consider possible heterogeneities in the energy-transfer characteristics of the 20 β -carotenes in the PSI core; it may of course well be that not all β -carotene transfer their energy with equal efficiency, and with the fluorescence upconversion traces at 704 and 715 nm, evidently only those carotenoids are probed that do transfer their excitations to *chl a*.

The energy-transfer rate from the S_2 state to *chl a*, k_1 , and internal conversion rate from S_2 to S_1 , k_2 , were chosen such to produce the observed S_2 lifetime of $1/(k_1+k_2)=105$ fs. The energy-transfer rate constant from the S_1 state of β -carotene to *chl a* is k_3 . We further assume that the intrinsic S_1 lifetime of β -carotene in the protein is the same as in solution, and thus introduce decay into a loss channel at a rate $k_4 = (8 \text{ ps})^{-1}$.^{50,51} The fluorescence originating

from the carotenoid S_2 state is assumed to be zero at the detection wavelengths 705 nm and 716 nm, and we assume that no fluorescence originates from the S_1 state. We take into account the internal chl α dynamics by introducing two chl-compartments: one non-equilibrated bulk chl α -C708/C719 compartment, denoted $[\text{chl}]^{\text{non-eq}}$, which is populated from the S_1 and S_2 states of β -carotene, and one equilibrated bulk chl α -C708/C719 compartment, denoted $[\text{chl}]^{\text{eq}}$. The equilibration rate constant between bulk and red chl α , k_5 , is fixed to $(3.6 \text{ ps})^{-1}$, as found above (see figure 7.4). We did not include the 360 fs bulk chl α equilibration component in our model: our data are too sparse to justify such an increased complexity. An important requirement that we impose on the outcome of the model is that the fluorescence intensity amplitudes associated with the internal chl α equilibration process are similar to those we determined in the SAES of figure 7.4, in which $[\text{chl}]^{\text{non-eq}}$ corresponds to the 3.6 ps SAES (solid circles) and $[\text{chl}]^{\text{eq}}$ to the 9.6 ps SAES (triangles). Thus, when performing this analysis, the adjustable parameters are the β -carotene S_1 -chl α energy-transfer rate constant k_3 , and the relative rates of energy-transfer from S_2 to chl α , k_1 , and IC from S_2 to S_1 , k_2 .

We found that the most satisfactory result arises when the S_2 state of β -carotene branches into the S_1 state and chl α at a ratio of 0.4: 0.6. In the frame of our model, this would imply an internal conversion rate of $k_2 = (250 \text{ fs})^{-1}$ and an energy-transfer rate $k_1 = (170 \text{ fs})^{-1}$. The rate constant for the S_1 -chl α transfer process k_3 that results from the analysis is $(1.2 \text{ ps})^{-1}$. The resulting amplitude ratio of $[\text{chl}]^{\text{non-eq}} : [\text{chl}]^{\text{eq}}$ is 1.5 : 1 in the 705 nm trace, and 0.7 : 1 in the 716 nm trace, in reasonable agreement with the SAES presented in figure 7.4. The fitted curves are shown as the dotted lines in figure 7.7. An S_1 -chl α energy-transfer rate constant of $(1.2 \text{ ps})^{-1}$ would imply an efficiency of 85% from the S_1 state. Taken into account the estimated 60% energy-transfer efficiency from the S_2 state, this would lead to an overall carotenoid-chl energy-transfer efficiency of more than 90%, which is in line with the value found using fluorescence excitation measurements on *Synechocystis*.¹⁶ The resulting carotenoid-chl α energy-transfer rates in PSI are summarized in figure 7.8.

The value of the S_2 - S_1 IC rate constant $k_2 = (250 \text{ fs})^{-1}$ that follows from our analysis is a point of concern. A rate of $(250 \text{ fs})^{-1}$ would lie significantly outside the range of afore-mentioned rates measured for β -carotene in the various solvents. However, if we fix k_2 to $(180 \text{ fs})^{-1}$ in the analysis, which is the IC rate reported for hexane, a S_2 lifetime of 105 fs implies a branching between the S_2 and S_1 pathways of 0.45 : 0.55, and this inevitably leads to an overestimation of the S_1 energy-transfer pathway contribution to the picosecond part of the rise-times in the 705 and 716 nm traces, which translates into unrealistic amplitudes for the 3.6 ps relaxation process of the two chlorophyll compartments. More precisely, in the 716 nm trace $[\text{chl}]^{\text{non-eq}}$ obtains a somewhat larger amplitude than $[\text{chl}]^{\text{eq}}$, and in the 705 nm trace, the $[\text{chl}]^{\text{non-eq}}$ amplitude becomes 3 times larger than that of $[\text{chl}]^{\text{eq}}$, which is clearly at odds with the SAES shown in figure 7.4. In principle, we cannot exclude that the S_2 to S_1 IC rate is slower in the protein than in non-polar solvents. However, an equally sound explanation where we may maintain an IC rate close to $(180 \text{ fs})^{-1}$ is provided by asserting that a fraction of S_1 states may not or very poorly transfer its energy to chl α . Given the lack of structural symmetry in PSI and the ensuing variety in pigment orientations and surroundings,

this is not an unreasonable supposition. In this scenario, the relative contribution of the S_1 pathway could be lower than that of S_2 , consistent with our target analysis.

It is well established that the S_1 lifetime of β -carotene in solution is 8–10 ps and basically solvent-independent.^{50,51} We thus propose that this lifetime is shortened to 1.2 ps in at least a significant fraction of the β -carotene molecules in the PSI core complex as a result of energy transfer to *chl**a*. The situation sketched for PSI (fig. 7.8) is similar to that recently determined for LHClI of plants^{21,23} and for LH2 of purple bacteria,^{22,24} and emphasizes that energy transfer from both S_2 and S_1 is required for an efficient light-harvesting function of carotenoids.

It is interesting to compare the β -carotene dynamics in PSI with those in the PSII core antenna proteins CP43 and CP47. These complexes, which each bind 2 β -carotene molecules as their only carotenoids, are weakly homologous to the inner part of the PSI core antenna⁵² and share structural similarities with it.⁵³ In CP43 and CP47, the energy-transfer efficiency to *chl**a* is 35%,^{51,2} which is dramatically lower as compared to the PSI core complex. The S_1 lifetime of β -carotene in CP43 and CP47 is essentially the same as in solution, indicating that no or very little energy transfer occurs from the S_1 state.⁵¹ This illustrates the very different roles that carotenoids may have in light-harvesting systems that function under vastly different circumstances: PSI is an efficient and robust energy converter relatively insensitive to photo-damage, and β -carotene strongly partakes in the overall goal of collecting as much light as possible. In contrast, the PSII core is a highly regulated light-harvesting system designed to carefully balance energy conversion and minimizing the photo-damage that this process unavoidably accompanies; with relatively long *chl**a* lifetimes in the antenna, it has a relatively high probability of intersystem crossing to the *chl**a* triplet state, which along with the presence of an oxygen evolving complex gives rise to high concentrations of singlet oxygen. Under these perilous circumstances, β -carotene exerts an indispensable protective role by quenching *chl**a* triplets and thus preventing the formation of singlet oxygen, and its light-harvesting purpose may be minute, or even undesirable.

Let us consider the possible physical basis for the differences in energy-transfer characteristics of β -carotene in PSI and PSII. Energy transfer from the S_2 state of β -carotene to *chl**a* in PSI and PSII probably proceeds at similar rates in the order of 100–200 fs, which appears to be a rather universal phenomenon in carotenoid-binding light-harvesting antennae,^{20,21,23,24} and may be understood from the concept of Förster-like energy transfer between molecules having strongly allowed optical transitions. The main difference in overall energy-transfer efficiency between PSI and PSII cores lies in energy transfer from the S_1 state, which accounts for ~40% of the total carotenoid energy-transfer in PSI and is basically non-existent in PSII.

Generally, the energy-transfer rate between a donor and acceptor molecule is proportional to the product of the spectral overlap and the square of the electronic coupling. The 0–0 energy level of the S_1 state of β -carotene in solution has been estimated to lie between 14650 cm^{-1} (682 nm) and 14100 cm^{-1} (709 nm),^{54,55} which is close to the Q_y level of *chl**a*. Considering the large width of the S_1 transition generally found in carotenoids ($\sim 3000\text{ cm}^{-1}$)^{20,21,24,54} and that the Q_y levels of *chl**a* in PSI and PSII are at most a few hundreds of cm^{-1} apart, it seems likely that the spectral overlap of the S_1 state of β -carotene and *chl**a*

is similar in PSI and PSII. However, a definite conclusion regarding this issue must await a determination of the *in vivo* S_1 energy level in PSI and PSII, as has been done for the LH2 complex of purple photosynthetic bacteria and LHCII of plants.^{20,21}

We next consider the possibility that the electronic coupling of the β -carotene S_1 and chl Q_y states may be significantly larger in PSI as compared to PSII. A possible reason for a larger electronic coupling could be the significantly higher pigment density in PSI with respect to PSII; the PSI and PSII cores have approximately equal sizes, but bind 100 and 35 chls, and 20 and 6 β -carotenes, respectively.^{3,56,57} This leads to shorter interpigment distances, and higher coordination numbers of energy accepting chl a molecules.

It has recently been estimated that in the LH2 complex of purple bacteria, the electronic coupling between the S_1 state of carotenoids and Bchl lies in the order of 10's of cm^{-1} , which lead to energy-transfer time scales of a few ps.²² It was concluded from quantum chemical calculations that the 'pure' S_1 state of carotenoids requires mixing with the strongly allowed S_2 state to produce a Coulombic coupling of the magnitude necessary for picosecond energy-transfer rates.^{24,58,59} Symmetry breaking elements, be it in the carotenoid itself, interaction with other pigments or its protein surroundings could be responsible for such a phenomenon. In this respect, it is interesting to note that β -carotene in CP47 experiences an unusual, highly symmetric and non-polar environment,⁶⁰ which may imply a highly forbidden S_1 state for β -carotene in PSII. However, recent time-dependent density functional theoretical calculations have indicated that strictly speaking, the S_1 state of the carotenoid does not need to have a transition moment to efficiently couple to nearby (B)chls, and that the magnitude of the Coulombic coupling may depend more critically on the geometrical details of donor and acceptor than on the extent of planar distortions of the carotenoid backbone.⁶¹

At present, it remains an open question as of what exactly causes the differences in light-harvesting efficiency of β -carotene in PSI and PSII, and it is evident that additional spectroscopic information, combined with high-resolution structural models of the PSI and PSII core complexes and sophisticated structure-based calculations, are required for a better understanding of the versatility of roles that β -carotene can adopt in the PSI and PSII core complexes.

ACKNOWLEDGEMENTS

J.K. acknowledges dr. Cheri Hsu for enlightening discussions. J.K. is grateful to the Human Frontier Science Program Organization (HFSP) for granting a long-term fellowship. This work was supported by the Director, Office of Science, of the U.S. Department of Energy under Contract No. DE-AC03-76SF00098. The research at Vrije Universiteit is supported by the Netherlands Organization for Scientific Research (NWO) via the Foundation of Earth and Life Sciences (ALW).

REFERENCES

- (1) Gobets, B., J.T.M. Kennis, J.A. Ihalainen, M. Brazzoli, R. Croce, I.H.M. van Stokkum, R. Bassi, J.P. Dekker, H. van Amerongen, G.R. Fleming, and R. van Grondelle. 2001. Excitation energy transfer in dimeric light-harvesting complex I: a combined streak camera/fluorescence upconversion study. *J. Phys. Chem. B.* 105:10132-10139.
- (2) Van Dorssen, R.J., J. Breton, J.J. Plijter, K. Satoh, H.J. van Gorkom, and J. Amesz. 1987. Spectroscopic properties of the reaction center and of the 47 kDa chlorophyll protein of Photosystem II. *Biochim. Biophys. Acta.* 893:267-274.
- (3) Krauss, N., W.-D. Schubert, O. Klukas, P. Fromme, H.T. Witt, and W. Saenger. 1996. Photosystem I at 4Å resolution represents the first structural model of a joint photosynthetic reaction centre and core antenna system. *Nat. Struct. Biol.* 3:965-973.
- (4) Schubert, W.-D., O. Klukas, N. Krauss, W. Saenger, P. Fromme, and H.T. Witt. 1997. Photosystem I of *Synechococcus elongatus* at 4 angstrom resolution: Comprehensive structure analysis. *J. Mol. Biol.* 272:741-769.
- (5) Gobets, B., H. van Amerongen, R. Monshouwer, J. Kruip, M. Rögner, R. van Grondelle, and J.P. Dekker. 1994. Polarized site-selected fluorescence spectroscopy of isolated Photosystem I particles. *Biochim. Biophys. Acta.* 1188:75-85.
- (6) Rätsep, M., T.W. Johnson, P.R. Chitnis, and G.J. Small. 2000. The red-absorbing chlorophyll-*a* antenna states of Photosystem I: A hole-burning study of *Synechocystis* sp PCC 6803 and its mutants. *J Phys. Chem. B.* 104:836-847.
- (7) Soukoulis, V., S. Savikhin, W. Xu, P.G. Chitnis, and W.S. Struve. 1999. Electronic spectra of PSI mutants: The peripheral subunits do not bind red chlorophylls in *Synechocystis* sp PCC 6803. *Biophys. J.* 76:2711-2715.
- (8) Karapetyan, N.V., D. Dorra, G. Schweitzer, I.N. Bezsmertnaya, and A.R. Holzwarth. 1997. Fluorescence spectroscopy of the longwave chlorophylls in trimeric and monomeric Photosystem I core complexes from the cyanobacterium *Spirulina platensis*. *Biochemistry* 36:13830-13837.
- (9) Holzwarth, A.R., G. Schatz, H. Brock, and E. Bittersmann. 1993. Energy transfer and charge separation kinetics in Photosystem I Part 1: Picosecond transient absorption and fluorescence study of cyanobacterial Photosystem I particles. *Biophys. J.* 64:1813-1826.
- (10) Van Grondelle R., J.P. Dekker, T. Gillbro, and V. Sundström. 1994. Energy transfer and trapping in photosynthesis. *Biochim. Biophys. Acta.* 1187:1-65.
- (11) Gobets, B., I.H.M. van Stokkum, M. Rögner, J. Kruip., E. Schlodder, N.V. Karapetyan, J.P. Dekker, and R. van Grondelle. 2001. Time-resolved fluorescence emission measurements of Photosystem I particles of various cyanobacteria: a unified compartmental model. *Biophys. J.* 81:407-424.
- (12) Trissl, H.-W. 1993. Long-wavelength absorbing antenna pigments and heterogeneous absorption-bands concentrate excitons and increase absorption cross-section. *Photosynth. Res.* 35:247-263.
- (13) Rivadossi, A., G. Zucchelli, F.M. Garlaschi, and R.C. Jennings. 1999. The importance of PSI chlorophyll red forms in light-harvesting by leaves. *Photosynth. Res.* 60:209-215.
- (14) Karapetyan, N.V., A.R. Holzwarth, and M. Rögner. 1999. The Photosystem I trimer of cyanobacteria: molecular organization, excitation dynamics and physiological significance. *FEBS Lett.* 460:395-400.
- (15) MacColl, R. 1998. Cyanobacterial phycobilisomes. *J. Struct. Biol.* 124:311-334.

- (16) Van der Lee, J., D. Bald, S.L.S Kwa, R. van Grondelle, M. Rögner, and J.P. Dekker. 1993. Steady-state polarized-light spectroscopy of isolated Photosystem-I complexes. *Photosynth. Res.* 35:311-321.
- (17) Frank, H.A., and R.J. Cogdell. 1996. Carotenoids in photosynthesis. *Photochem. Photobiol.* 63:257-264.
- (18) Koyama, Y., M. Kuki, P.O. Andersson, and T. Gillbro. 1996. Singlet excited states and the light-harvesting function of carotenoids in bacterial photosynthesis. *Photochem. Photobiol.* 63:243-256.
- (19) Krueger, B.P., G.D. Scholes, R. Jimenez, and G.R. Fleming. 1998. Electronic excitation transfer from carotenoid to bacteriochlorophyll in the purple bacterium *Rhodospseudomonas acidophila*. *J. Phys. Chem. B.* 102:2284-2292.
- (20) Krueger, B.P., J. Yom, P.J. Walla, and G.R. Fleming. 1999. Observation of the S-1 state of spheroidene in LH2 by two-photon fluorescence excitation. *Chem. Phys. Lett.* 310:57-64.
- (21) Walla, P.J., J. Yom, B.P. Krueger, and G.R. Fleming. 2000. Two-photon excitation spectrum of light-harvesting complex II and fluorescence upconversion after one- and two-photon excitation of the carotenoids. *J. Phys. Chem. B.* 104:4799-4806.
- (22) Walla, P.J., P.A. Linden, C.P. Hsu, G.D. Scholes, and G.R. Fleming. 2000. Femtosecond dynamics of the forbidden carotenoid S-1 state in light-harvesting complexes of purple bacteria observed after two-photon excitation. *Proc. Natl. Acad. Sci. USA.* 97:10808-10813.
- (23) Gradinaru, C.C., I.H.M. van Stokkum, A.A. Pascal, R. van Grondelle, and H. van Amerongen. 2000. Identifying the pathways of energy transfer between carotenoids and chlorophylls in LHCII and CP29. A multicolor, femtosecond pump-probe study. *J. Phys. Chem. B.* 104:9330-9342.
- (24) Zhang, J.P., R. Fujii, P. Qian, T. Inaba, T. Mizoguchi, Y. Koyama, K. Onaka, Y. Watanabe, and H. Nagae. 2000. Mechanism of the carotenoid-to-bacteriochlorophyll energy transfer via the S-1 state in the LH2 complexes from purple bacteria. *J. Phys. Chem. B.* 104:3683-3691.
- (25) Du, M., X. Xie, Y. Jia, L. Mets, and G.R. Fleming. 1993. Direct observation of ultrafast energy transfer in PSI core antenna. *Chem. Phys. Lett.* 201:535-542.
- (26) Hastings, G., F.A.M. Kleinherenbrink, S. Lin, T.J. McHugh, R.E. Blankenship. 1994. Observation of the reduction and reoxidation of the primary electron-acceptor in Photosystem-I. *Biochemistry.* 33:3193-3200.
- (27) White, N.T.H., G.S. Beddard, J.R.G. Thorne, T.M. Feehan, T.E. Keyes, and P. Heathcote. 1996. Primary charge separation and energy transfer in the Photosystem I reaction center of higher plants. *J. Phys. Chem.* 100:12086-12099.
- (28) Dimagno, L., C.-K. Chan, Y. Jia, M.J. Lang, J.R. Newman, L. Mets, G.R. Fleming, and R. Haselkorn. 1995. Energy-transfer and trapping in Photosystem-I reaction centers from cyanobacteria. *Proc. Natl. Acad. Sci. USA.* 92:2715-2719.
- (29) Savikhin, S., W. Xu, V. Soukoulis, P.R. Chitnis, and W.S. Struve. 1999. Ultrafast primary processes in Photosystem I of the cyanobacterium *Synechocystis* sp. PCC 6803. *Biophys. J.* 76:3278-3288.
- (30) Savikhin, S., W. Xu, P.R. Chitnis and W.S. Struve. 2000. Ultrafast primary processes in PSI from *Synechocystis* sp. PCC 6803: Roles of P700 and A(0). *Biophys. J.* 79:1573-1586.
- (31) Melkozernov, A.N., S. Lin, and R.E. Blankenship. 2000. Excitation dynamics and heterogeneity of energy equilibration in the core antenna of Photosystem I from the cyanobacterium *Synechocystis* sp. PCC 6803. *Biochemistry* 39:1489-1498.

- (32) Gobets, B., I.H.M. van Stokkum, F. van Mourik, M. Rögner, J. Kruip, J.P. Dekker, and R. van Grondelle. 1998. Time-resolved fluorescence measurements of Photosystem I from *Synechocystis* PCC 6803. *In* Photosynthesis: Mechanisms and effects. G. Garab, editor. Kluwer Academic Publishers, Dordrecht, The Netherlands. 1: 571-574.
- (33) Gobets, B., J.P. Dekker, and R. van Grondelle. 1998. Transfer-to-the-trap limited model of energy transfer in Photosystem I. *In* Photosynthesis: Mechanisms and effects. G. Garab, editor. Kluwer Academic Publishers, Dordrecht, The Netherlands. 1:503-508.
- (34) Pålsson, L.-O., J.P. Dekker, E. Schlodder, R. Monshouwer, and R. van Grondelle. 1996. Polarized site-selective fluorescence spectroscopy of the long-wavelength emitting chlorophylls in isolated Photosystem I particles of *Synechococcus elongatus*. *Photosynth. Res.* 48:239-246.
- (35) Pålsson, L.-O., C. Flemming, B. Gobets, R. van Grondelle, J.P. Dekker, and E. Schlodder. 1998. Energy transfer and charge separation in Photosystem I: P700 oxidation upon selective excitation of the long-wavelength chlorophylls of *Synechococcus elongatus*. *Biophys. J.* 74:2611-2622.
- (36) Fromme, P., and H.T. Witt. 1998. Improved isolation and crystallization of Photosystem I for structural analysis. *Biochim. Biophys. Acta.* 1365:175-184.
- (37) Byrdin, M., I. Rimke., E. Schlodder, D. Stehlik, and T.A. Roelofs. 2000. Decay kinetics and quantum yields of fluorescence in Photosystem I from *Synechococcus elongatus* with P700 in the reduced and oxidized state: are the kinetics of excited state decay trap-limited or transfer-limited? *Biophys. J.* 79:992-1007.
- (38) Van Stokkum, I.H.M., L.M.P. Beekman, M.R. Jones, M.E. van Brederode, and R. van Grondelle. 1997. Primary electron transfer kinetics in membrane-bound *Rhodobacter sphaeroides* reaction centers: A global and target analysis. *Biochemistry* 36:11360-11368.
- (39) Cross, A.J., and G.R. Fleming. 1984. Analysis of time-resolved fluorescence anisotropy decays. *Biophys. J.* 46:45-56.
- (40) Donovan, B., L.A. Walker, C.F. Yocum and R.J. Sension. 1996. Transient absorption studies of the primary charge separation in Photosystem II. *J. Phys. Chem.* 100:1945-1949.
- (41) Bradforth, S.E., R. Jimenez, F. van Mourik, R. van Grondelle, and G.R. Fleming. 1995. Excitation transfer in the core light-harvesting complex LH-1. of *Rhodobacter-sphaeroides* - an ultrafast fluorescence depolarization and annihilation study. *J. Phys. Chem* 99:16179-16191.
- (42) Jimenez, R., S.N. Dikshit, S.E. Bradforth, and G.R. Fleming. 1996. Electronic excitation transfer in the LH2 complex of *Rhodobacter sphaeroides*. *J. Phys. Chem.* 100:6825-6834.
- (43) Pullerits, T., M. Chachivilis, and V. Sundström. 1996. Exciton delocalization length in the B850 antenna of *Rhodobacter sphaeroides*. *J. Phys. Chem.* 100:10787-10792.
- (44) Kennis, J.T.M., A.M. Streltsov, S.I.E. Vulto, T.J. Aartsma, T. Nozawa, and J. Amesz. 1997. Femtosecond dynamics in isolated LH2 complexes of various species of purple bacteria. *J. Phys. Chem. B.* 101:7827-7834.
- (45) Savikhin, S., and W.S. Struve. 1994. Ultrafast energy-transfer in FMO trimers from the green bacterium *Chlorobium-tepidum*. *Biochemistry.* 33:11200-11208.
- (46) Vulto, S.I.E., A.M. Streltsov, and T.J. Aartsma. 1997. Excited state energy relaxation in the FMO complexes of the green bacterium *Prosthecochloris aestuarii* at low temperatures. *J. Phys. Chem. B.* 101:4845-4850.
- (47) Gobets, B., L. Valkunas, and R. van Grondelle. 2002. Bridging the gap between structural and lattice models: a parametrization of energy transfer and trapping in Photosystem I. *Submitted*.

- (48) MacPherson, A.N., and T. Gillbro. 1998. Solvent dependence of the ultrafast S-2-S-1 internal conversion rate of beta-carotene. *J. Phys. Chem. A.* 102:5049-5058.
- (49) Holzwarth, A.R. 1996. Data analysis of time-resolved measurements. *In* Biophysical Techniques in Photosynthesis. J. Amesz, and A. J. Hoff, editors. Kluwer, Dordrecht, the Netherlands. 75-92.
- (50) Wasielewski, M.R., D.G. Johnson, E.G. Bradford, and L.D. Kispert. 1989. Temperature-dependence of the lowest excited singlet-state lifetime of all-trans-beta-carotene and fully deuterated all-trans-beta-carotene. *J. Chem. Phys.* 91:6691-6697.
- (51) De Weerd, F.L., I.H.M van Stokkum, and R. van Grondelle. 2002. Subpicosecond dynamics in the excited state absorption of all-trans-beta-Carotene. *Chem. Phys. Lett.* 354:38-43.
- (52) Fromme, P., H.T. Witt, W.-D. Schubert, O. Klukas, W. Sanger, and N. Krauss. 1996. Structure of Photosystem I at 4.5 angstrom resolution: A short review including evolutionary aspects. *Biochim. Biophys. Acta.* 1275:76-83.
- (53) Rhee, K.-H., E.P. Morris, J. Barber, and W. Kuhlbrandt. 1998. Three-dimensional structure of the plant Photosystem II reaction centre at 8 angstrom resolution. *Nature.* 396:283-286.
- (54) Onaka, K., R. Fuji, H. Nagae, M. Kuki, Y. Koyama, and Y. Watanabe. 1999. The state energy and the displacements of the potential minima of the 2A(g)-state in all-trans-beta-carotene as determined by fluorescence spectroscopy. *Chem. Phys. Lett.* 315:75-81.
- (55) Chynwat, V., and H.A. Frank. 1995. The application of the energy-gap law to the S-1 energies and dynamics of carotenoids. *Chem. Phys.* 194:237-244.
- (56) Boekema, E.J., A.F. Boonstra, J.P. Dekker, and M. Rogner. 1994. Electron-microscopic structural-analysis of Photosystem-I, Photosystem-II, and the Cytochrome-b6/f complex from green plants and cyanobacteria. *J. Bioenerg. Biomem.* 26:17-29.
- (57) Van Leeuwen, P.J., M.C. Nieveen, E.J. van der Meent, J.P. Dekker, and H.J. van Gorkom. 1991. Rapid and simple isolation of pure Photosystem-II core and reaction center particles from spinach. *Photosynth. Res.* 28:149-153.
- (58) Nagae, H., T. Kakitani, T. Katoh, and M. Mimuro. 1993. Calculation of the excitation transfer-matrix elements between the S-2 or S-1 state of carotenoid and the S-2 or S-1 state of bacteriochlorophyll. *J. Chem. Phys.* 98:8012-8023.
- (59) Damjanovic, A., T. Ritz, and K. Schulten. 1999. Energy transfer between carotenoids and bacteriochlorophylls in light-harvesting complex II of purple bacteria. *Phys. Rev. E.* 59:3293-3311.
- (60) Renge, I., R. van Grondelle, and J.P. Dekker. 1996. Matrix and temperature effects on absorption spectra of β -carotene and pheophytin-a in solution and in green plant Photosystem II. *J. Photochem. Photobiol. A: Chem.* 96:109-121.
- (61) Hsu, C.P., P.J. Walla, M. Head-Gordon, and G.R. Fleming. 2001. The role of the S-1 state of carotenoids in photosynthetic energy transfer: The light-harvesting complex II of purple bacteria. *J. Phys. Chem. B.* 105:11016-11025.

8

Excitation energy transfer in dimeric Light-Harvesting Complex I: a combined streak camera/fluorescence upconversion study.

Bas Gobets, John T.M. Kennis, Janne A. Ihalainen, Michela Brazzoli, Roberta Croce, Ivo H.M. van Stokkum, Roberto Bassi, Jan P. Dekker, Herbert van Amerongen, Graham R. Fleming and Rienk van Grondelle

The excitation dynamics in isolated dimers of Light-Harvesting Complex I, the peripheral light-harvesting complex associated with Photosystem I in green plants, was studied by time-resolved fluorescence spectroscopy. A unique combination of two techniques, fluorescence upconversion and synchroscan streak camera measurements, revealed the energy transfer and decay of excitations over a time range from hundred femtoseconds up to several nanoseconds, over a spectral range from 570 to 780 nm.

Energy transfer from initially excited carotenoid S_2 states to the chlorophylls was found to occur within 0.15 ps. Energy transfer from chlorophyll-*b* to chlorophyll-*a* occurred with two distinctly different lifetimes of 0.5 and 2-3 ps. The 0.5 ps component mainly reflects transfer to the bulk chl*a*, whereas the 2-3 ps component may also account for direct transfer to the special red-shifted chl*a* forms. Equilibration between the bulk chl*a*'s and these red-shifted forms occurs with lifetimes of 4-8 ps and ~20 ps, which are assigned to intra- and inter-monomer equilibration, respectively. After completion of the energy-transfer processes, the fluorescence decays bi-exponentially. The largest fraction of excitations (75-80%) decays with a 3 ns time constant, which is attributed to both the Lhca1/Lhca4 heterodimer and a homodimer of either Lhca2 or Lhca3, whereas the remaining fraction, which decays in 0.6 ns, is assigned to the remaining homodimer. A comparison is made between the kinetics of LHCI and the more well studied CP29 and LHCI light-harvesting complexes of Photosystem II, which belong to the same family of Lhca/b light-harvesting proteins, but do not feature the unique red-shifted chl*a* forms which are found in LHCI.

INTRODUCTION

Photosystem I (PSI) consists of a core complex containing both the PSI reaction centre and a core antenna consisting of 90-100 chlorophyll-*a* (chl*a*) molecules. In green plants a peripheral antenna complex, Light-Harvesting Complex I (LHCI),¹ is attached to the core complex. LHCI binds another 80-100 antenna chlorophylls, both chl*a* and chlorophyll-*b* (chl*b*).^{1,2} Consequently, about 170-200 chlorophylls are contained in one PSI unit, which is therefore designated PSI-200. LHCI consists of four different proteins Lhca1-4, which have molecular masses ranging from 20-24 kDa, and which are thought to be present in approximately equal amounts.¹ Lhca1 and Lhca4 have been shown to form a heterodimer,^{3,4} which at 77K exhibits a red-shifted steady-state emission maximum at 730 nm,¹ and is therefore designated LHCI-730. The 730 nm emission may originate either from red-shifted chl*a* located in Lhca4 or from pigment-pigment interaction induced upon dimerization.^{5,6} Similar red-shifted chl*a* forms are also found in PSI core complexes and have also been suggested to result from dimers or larger aggregates of chl*a*.^{7,8}

Biochemical data suggest that Lhca2 and Lhca3 assemble as homodimers rather than heterodimers.³ The 77K fluorescence of these complexes has usually been reported to peak at 680 nm, and has therefore so far been designated LHCI-680.¹ It has recently been suggested, however, that the 680 nm form represents monomeric Lhca2 and Lhca3, rather than the dimers of these proteins which represent the functional complexes *in vivo*.⁶ This idea is corroborated by recent low-temperature (5K) spectroscopy data of dimeric LHCI, which instead of a 680 nm emitter show the presence of an emission band at ~702 nm (F702) in addition to the F730 band. It was suggested that F702 arises from an absorption band peaking at ~695 nm, and that Lhca2/Lhca3 homo/hetero dimers are responsible for this band.²

So far it has not been possible to isolate the Lhca2/3 proteins from the Lhca1/4 heterodimers without breaking up the native dimers.

Electron microscopy data indicated that in total about 3-4 LHCI dimers bind to the PSI core complex near the PSI-F and PSI-J subunits.⁹

Measurements of the pigment-to-protein stoichiometry indicated that each LHCI monomer contains 10 chl molecules, of which 8 are chl*a* and 2 are chl*b*.⁶ Besides the chls, each LHCI monomer also contains 2 carotenoid (Car) molecules in a mixture of violaxanthin, lutein and β -carotene.⁶

The pigment stoichiometry of LHCI is almost the same as found for CP29, an antenna protein of Photosystem II. The LHCI proteins show a high sequence homology with CP29, as well as with other plant light-harvesting proteins,¹ such as those of LHCII, the only one of the Lhca/b proteins of which a structure (at 3.4 Å) has been resolved.¹⁰

The main function of these light-harvesting proteins is to absorb light and to transfer the collected energy to the reaction centre of either PSI or PSII. A unique property of LHCI is the presence of the above-mentioned red-shifted chl*a* forms, which absorb around 695-705 nm,^{1,2} and which are expected to have a pronounced influence on the energy-transfer dynamics. In contrast to LHCII and CP29, which have been studied extensively by femtosecond time-resolved spectroscopy,¹¹⁻¹⁴ energy-transfer processes in LHCI have not been studied in much detail so far. Early experiments by Pålsson et al.¹⁵ and Mukerji et al.¹⁶

suffer from a limited time-resolution, and were performed on LHCI preparations that were not very well defined. Recently, Schmid et al.⁴ succeeded in overexpression of Lhca1 and Lhca4 in *E.coli*, and in the reconstitution of these proteins with chlorophylls and carotenoids. A heterodimer LHCI-730 was generated, which quite closely resembled the native dimer. Time-resolved absorption and fluorescence emission experiments performed on these reconstituted Lhca4 monomers and LHCI-730 dimers revealed a ~ 5 ps energy-transfer component within the chl α -band.¹⁷ A second ~ 30 ps energy-transfer component was only observed in the dimer.^{5,17} It was concluded that these two components correspond to intra- and intermonomer energy-transfer between the bulk chl α and the red-shifted chl α forms, respectively. A fast 0.5–0.6 ps component was assigned to chl b to chl α transfer.¹⁷ The decay of excitations both in reconstituted as well as native LHCI-730 was found to be multi-exponential with major ~ 280 ps and 800–850 ps components and a small 2–2.5 ns contribution (see table 8.1).⁵

In this contribution, we present room temperature time-resolved fluorescence data of a well-defined LHCI preparation containing all the (native) LHCI dimers.¹⁸ The combination of fluorescence upconversion and streak camera data provides both a high time resolution (~ 0.1 ps), and the complete spectral evolution in the 570–780 nm wavelength interval. Energy transfer kinetics were recorded for preferential excitation of the carotenoids, chl b and chl α .

MATERIALS AND METHODS

Sample

Dimeric LHCI was isolated from maize as a mixture of dimers of all four Lhca1–4 proteins, using β -DM and sucrose gradient centrifugation as described in ref. 18. Size exclusion chromatography, non-denaturing gel electrophoresis, density gradient ultracentrifugation and cross-linking experiments all confirmed that the preparation indeed consisted of dimers only.⁶ The preparation was treated with antibodies against all four Lhca proteins, which clearly indicated that all four were present. No impurities were detected by SDS-PAGE. The chl α to chl b ratio in this preparation was 3.6–3.8.

Streak camera measurements

The sample was diluted with a buffer containing 10 mM Tricine (pH 7.5), 0.5 M sucrose and 0.03% w/v dodecyl- β -D-maltoside to an OD of 0.12 per 3 mm at the Q_y absorption maximum.

The sample, contained in a spinning cell (optical pathlength = 3 mm), was excited with 100 fs pulses of 400 nm (chl α excitation) or 470 nm (chl b excitation) which were generated at a 125 kHz repetition rate using a Titanium:sapphire based oscillator (Coherent MIRA), a regenerative amplifier (Coherent REGA) and a double pass optical parametric amplifier (Coherent OPA-9400). The applied pulse energy was typically 4 nJ, sufficiently low to avoid singlet-singlet annihilation. Fluorescence was collected at right angle to the excitation beam using achromatic lenses, and detected through a sheet polarizer set at magic angle (54.7°), with a Hamamatsu C5680 synchroscan streak camera and a Chromex 250IS spectrograph.

The streak-images were recorded on a Hamamatsu C4880 CCD camera which was cooled to -55°C .

The streak images measure 315 nm in the spectral domain (1018 pixels, spectral resolution 8 nm) and either 200 ps or 2.2 ns (1000 pixels) in the time domain. The full width at half maximum (FWHM) of the time response of this system was 3–3.5 ps for the 200 ps time range and ~20 ps for the 2.2 ns time range. For more details on the data acquisition and processing we refer to Gobets et al.¹⁹

Fluorescence upconversion measurements (UPC)

The OD₆₈₀ of the sample was 0.3/mm. The sample was pumped through a flow cell (1 x 1 mm) and was thermostatted at 10 °C.

The fluorescence upconversion experiments were performed basically as described by Walla et al.²⁰ Briefly, excitation pulses at 510 nm (Car excitation) and 470 nm (chl*b* excitation) were generated at a 250 kHz repetition rate, using a laser system similar to the one described above. At this repetition rate a given sample volume was exposed to about 25 successive laser pulses during the time it moved through the laser focus. The excitation pulse energy was typically 8 nJ. A part of the amplified 800 nm pulses was used as the gate beam. The excitation pulses were focused into the flowcell, which was placed at one focus of an elliptical mirror. The fluorescence of the sample was collected by the ellipsoid and focused into a 0.5 mm BBO crystal placed at the other focus. Here the fluorescence was mixed with the gate beam to create the upconversion signal. The polarization angle between the excitation light and the gate beam was adjusted to magic angle (54.7°) using a broadband variable waveplate (CVI) which was placed in the excitation beam.

A double monochromator was used to select an ~8 nm band-width spectral window from the upconversion signal, which was detected with a photomultiplier. For chl*b* excitation, detection was at 655 nm (chl*b*), 695 nm (bulk chl*a*) and 723 nm (red chl*a*). For Car excitation, detection was at 591 nm (Car S₂), 655 nm (chl*b*) and 699 nm (bulk chl*a*). The cross-correlation between pump- and gate pulse was 280–300 fs.

Data analysis

For both 400 and 470 nm excitation the upconversion traces at three detection wavelengths were analysed simultaneously, independently of the streak camera data.

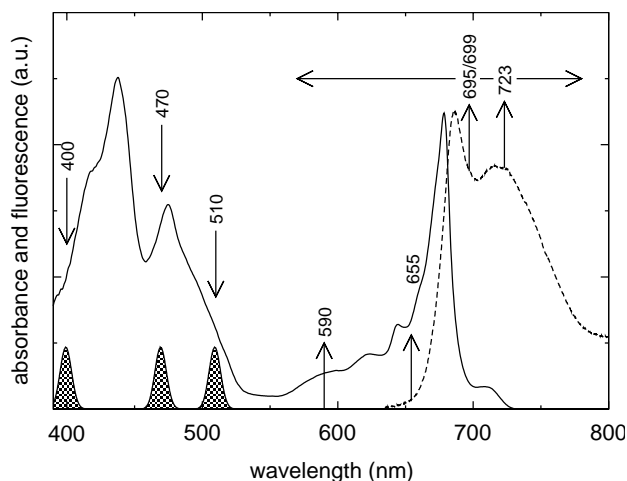
The streak camera measurements were analysed using a model with parallel decaying components, which yields Decay-Associated Spectra (DAS). For 400 nm excitation both the 200 ps and 2.2 ns time range data were analysed simultaneously, and for 470 nm excitation the streak data of both time ranges were analysed simultaneously with the upconversion data for that wavelength of excitation. The amplitude of both upconversion and streak camera traces obtained for the 200 ps time range were scaled to the streak data obtained for the 2.2 ns time range. Since we did not apply direct excitation of the chl Q_y transitions, the analysis was performed under the condition that no fluorescence was present above 665 nm at time zero. The results of the simultaneous fitting were compared to separate fits of the data obtained for the different time ranges. In all cases the instrument response function was assumed to be a Gaussian, the width of which was a free parameter of the fit. All the DAS shown were corrected for the spectral sensitivity of the apparatus.

RESULTS

Steady-state absorption and emission spectrum

The 5 K absorption spectrum of LHCl in figure 8.1 (solid line) reveals the different absorption bands of the chromophores present in the system. In the blue part of the spectrum the Soret bands of *chl**a* and *chl**b* peak at 438 nm and 475 nm, respectively.^{2,16,21} The *chl**b* Soret absorption band overlaps strongly with absorption due to the S_2 transition of the carotenoids (400–525 nm).^{2,21} The maximum at 643.5 nm is assigned to a *chl**b* Q_y transition,^{2,11,16,21,22} and a second *chl**b* band with a maximum at 650 nm was resolved from linear dichroism measurements,² indicating that at least two spectroscopically distinct *chl**b* binding sites are present in LHCl, similar to CP29.^{11,12} The Q_y region of *chl**a* peaks at 678.5 nm, and exhibits a weak shoulder around 671 nm. The red-shifted *chl**a* forms are represented by a broad band around 710 nm.

The wavelengths of excitation used in the time-resolved experiments have been indicated in figure 8.1 by arrows pointing down. The room temperature absorption spectrum was decomposed using (shifted) room temperature absorption spectra of *chl**a* (maximum at 440 nm) and *chl**b* (maximum at 475 nm) in acetone (not shown), to roughly estimate the extent of selectivity for the various pigments for these wavelengths of excitation. *Chl**a* and Car were excited quite selectively using 400 nm (~90% *chl**a*) and 510 nm light (~80% Car), respectively. It was not possible to achieve such selective excitation of *chl**b*; using 470 nm light about 50% *chl**b*, 45% Car and 5% *chl**a* are excited. Figure 8.1 also shows the room temperature steady-state emission spectrum for excitation at 455 nm. This emission spectrum exhibits a sharp maximum at 686 nm, due to the emission of the bulk *chl**a* molecules, and a

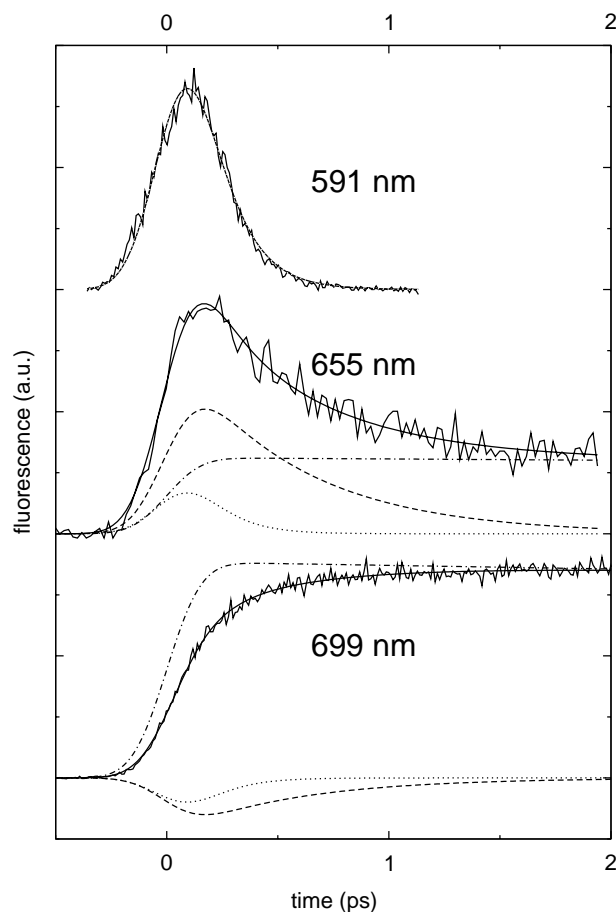


8.1 The 5 K absorption spectrum (solid) and RT steady state emission spectrum (dashed) of the isolated dimeric LHCl particles. Arrows pointing down indicate excitation wavelengths of the time-resolved fluorescence experiments (400, 470 and 510 nm). Representative spectral profiles of the excitation pulses have been indicated. Arrows pointing up indicate detection wavelengths of the fluorescence upconversion experiments (591, 655, 695/699 and 723nm). The horizontal double arrow indicates the fluorescence detection range of the streak camera experiments that was analysed (575–775 nm).

broad side-band with a maximum around 720 nm due to the emission by the red-shifted chl*a* species. The wavelengths of detection used in the fluorescence upconversion experiments are indicated in figure 8.1 by the arrows pointing up: at 591 nm for emission of the carotenoids, at 655 nm for the emission of chl*b*, at 695–699 nm for the emission of bulk chl*a*, and at 723 nm for the emission of the red-shifted chl*a* forms. The analysed fluorescence detection range of the streak camera is indicated by the horizontal double pointed arrow.

Time-resolved fluorescence for carotenoid excitation

In figure 8.2, upconversion traces are shown for preferential excitation of the carotenoid molecules at 510 nm, detected at 591, 655 and 699 nm. Three lifetimes (0.14 ps, 0.5 ps and long-lived) were needed to simultaneously fit the 3 recorded traces. The decay of the fluorescence at 591 nm, representing carotenoid S_2 fluorescence, is very fast. In a free fit, the fastest (0.14 ps) component dominates the fluorescence decay at this wavelength. Forcing the amplitudes of the other two components of the fit to zero for this wavelength did not change



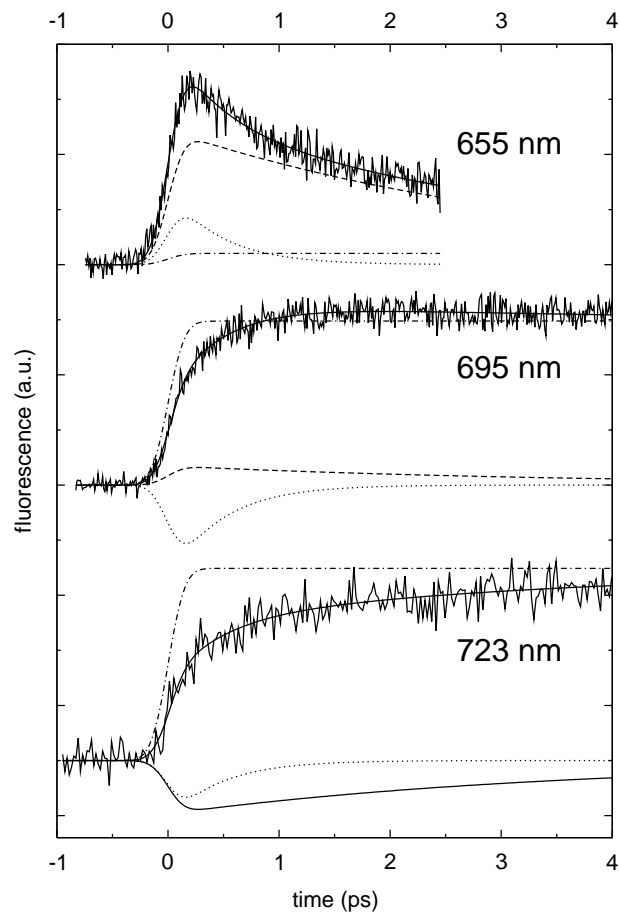
8.2 RT, 510 nm excitation upconversion traces of isolated LHCI detected at 591 nm, 655 nm and 699 nm (noisy solid), the result of the simultaneous fit (solid) and the 0.14 ps (dotted), 0.5 ps (dashed) and long-lived (dot-dashed) lifetime contributions to the fit.

the quality of the total fit (figure 8.2). Therefore, we conclude that practically all carotenoid S_2 fluorescence decay (by energy transfer or internal conversion) occurs with the 0.14 ps time constant.

For detection at 655 nm, the 0.14 ps component only has a small (positive) contribution, reflecting the tail of the carotenoid fluorescence. At 699 nm the contribution of the 0.14 ps component is negative, indicating energy transfer from the carotenoids to chl a , although a small part of this ingrowth may also be attributed to Soret- Q_y relaxation of the small fraction of directly excited chl a 's.

The 0.5 ps component represents the largest decay component of fluorescence at 655 nm (primarily chl b). This component is negative at 699 nm and is therefore attributed to chl b -chl a transfer.

The long-lived component has a positive amplitude both at 655 and 699 nm, and accounts for all slow components.

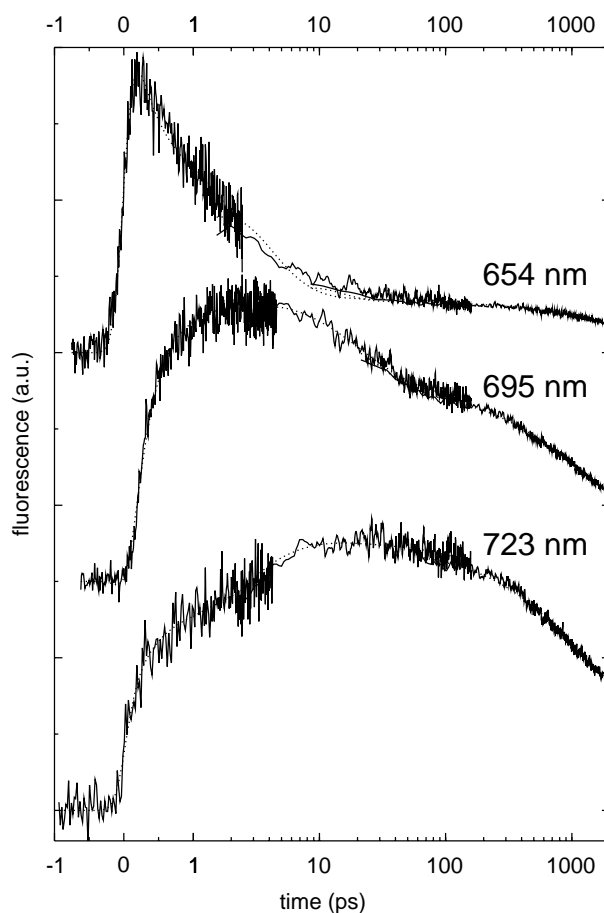


8.3 RT, 470 nm excitation upconversion traces of isolated LHCl detected at 655 nm, 695 nm and 723 nm (noisy solid), the result of the simultaneous fit (solid) and the 0.5 ps (dotted), 4 ps (dashed) and long-lived (dot-dashed) lifetime contributions to the fit.

Time-resolved fluorescence for chlorophyll-*b* excitation

In figure 8.3, the upconversion traces are shown for excitation at 470 nm, which is about 50% selective for chl*b*, detected at 655, 695 and 723 nm. Three lifetimes are needed to simultaneously fit the three traces. The shortest lifetime found is 0.5 ps. The amplitude of this component is positive at 655 nm and negative both at 695 nm and 723 nm, indicating that this component reflects energy transfer from chl*b* to chl*a*. The time constant matches the 0.5 ps transfer component found for 510 nm excitation (see above).

The second component has a lifetime of 4 ps and shows a positive amplitude at both 655 nm and 695 nm, and a negative amplitude at 723 nm, indicating that this component reflects energy transfer from both chl*a* and chl*b* to the red chl*a* forms, although it cannot be ruled out that chl*b* in fact transfers to bulk chl*a* (see below). The remaining dynamics takes place on a time scale that extends beyond the range of the fluorescence upconversion



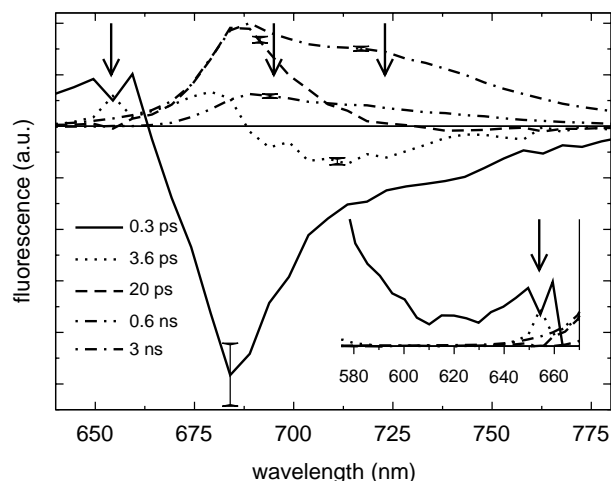
8.4 RT combined 470 nm excitation traces of isolated LHCI of the upconversion experiments and the 200 ps and 2.2 ns time range streak camera experiments (solids) and the simultaneous fit (dotted). The scaling of the time axis is linear from -1 to 1 ps, and logarithmic above 1 ps. The streak camera traces have been plotted from $t \sim 2$ ps and ~ 20 ps for the 200 ps and 2.2 ns time range respectively.

experiments, and is accounted for by the third, long-lived component which exhibits a positive amplitude for all three wavelengths of detection.

Time-resolved fluorescence for chl*b* (470 nm) excitation was also recorded with the streak camera setup. The streak camera measurements provide the dynamics over the whole 570-780 nm wavelength range in the picosecond to nanosecond time range. Sub-picosecond processes can be observed as well, but due to the relatively broad instrument response, the time constants of these processes cannot be determined very precisely from these experiments alone. By performing a simultaneous global analysis of the streak-data at the 200 ps and 2.2 ns time ranges together with the three upconversion traces recorded for 470 nm excitation, lifetimes of hundreds of fs to several ns (4 orders of magnitude in time) could be determined accurately. Figure 8.4 displays the traces recorded at the three wavelengths of detection for which the upconversion and streak camera measurements were combined. It demonstrates that the traces recorded with different experimental techniques join smoothly (note that the traces are plotted on a linear-logarithmic scale).

The Decay-Associated Spectra resulting from the global analysis are shown in figure 8.5. We note that the results of the simultaneous analysis are in agreement with the results obtained for separate analyses of the individual time-ranges (not shown).

The fastest component of the simultaneous analysis is fitted with a 0.3 ps time constant. The corresponding DAS (solid) is positive in the carotenoid emission region (570-630 nm, see inset), shows a maximum around 645-650 nm in the chl*b* region, and exhibits a negative band in the main-band chl*a* region. A DAS that is positive in one region of the spectrum, and negative in another is characteristic for energy transfer between two spectrally different chromophores. We therefore assign this component to energy transfer from the carotenoids (which are receiving a significant fraction of the excitations for 470 nm excitation) and chl*b*



8.5 Decay-Associated Spectra of fluorescence decay of isolated LHCI for 470 nm excitation. 0.3 ps (solid), 3.6 ps (dotted), 20 ps (dashed), 0.6 ns (double-dot-dashed) and 3 ns (dot-dashed). The inset shows a blow-up of the 575-670 nm detection region. The arrows show the wavelengths of the upconversion traces, that were fitted simultaneously with the streak camera data. Rough error-bars have been included at selected wavelengths.

to the bulk chl a . The tail of the rise in the fluorescence above 700 nm is somewhat higher than would be expected for bulk chls, suggesting that a small fraction of the energy transfer from the carotenoid may be directed to the red-shifted chl a 's

The ~ 0.3 ps time constant may in fact represent a mixture of the ~ 0.14 ps carotenoid to chl a component (fig. 8.2) and the ~ 0.5 ps chl b to chl a component (figure 8.2 and figure 8.3) observed in the separate fits of the fluorescence upconversion experiments.

The second component in figure 8.5 exhibits a 3.6 ps time constant. The DAS of this component (dotted) shows maxima at 655 nm (chl b) and 680 nm (bulk chl a), and is negative above 687 nm with a broad minimum around 715 nm. This component represents two energy-transfer processes: both from the bulk chl a to a red-shifted chl a form, and from chl b either to the bulk chl a or the red-shifted chl a form. In view of the 678 nm bulk absorption maximum, the 680 nm emission must result from a relatively blue fraction of the bulk chls, possibly the chls corresponding to the shoulder around 671 nm. We do note that there is a slight discrepancy between the streak camera data and the upconversion trace at 655 nm, apparent from the "dip" in the 0.3 ps DAS and the peak in the 3.6 ps DAS at this wavelength, which probably results from the uncertainty in the estimation of the instrument response of the streak camera.

The lifetime of the third component is about 20 ps, and it exhibits a DAS (dashed) which shows a pronounced peak at 686 nm, and which only slightly drops below zero above ~ 730 nm. This component represents slow transfer from bulk chl a to a red-shifted chl form, and may be attributed to intermonomer transfer within a dimer.⁵ Obviously, the DAS shows a much larger positive area as compared to the negative area, which suggests that either some loss of excitations occurs as well during the 20 ps process, or that the red-shifted state has a lowered oscillator strength, i.e. is somewhat forbidden.

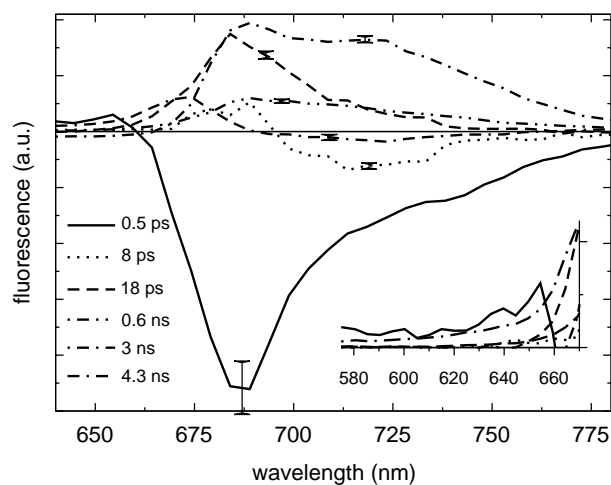
The final two processes which take place with 0.6 ns and 3 ns time constants are represented by all positive Decay-Associated Spectra (double-dot-dashed and dot-dashed) and account for the decay of excitations after the energy-transfer processes are completed.

Time-resolved fluorescence for chlorophyll- a excitation

In figure 8.6 the Decay-Associated Spectra resulting from the simultaneous global analysis of the 200 ps and 2.2 ns time range streak-measurements for 400 nm excitation are shown. At this wavelength of excitation mainly chl a is excited. The results of the simultaneous fit are consistent with the results obtained for fits of the individual time-ranges (not shown).

The fastest component is fitted with a 0.5 ps time constant. The DAS of this component (solid) exhibits a (slightly) positive chl b region, which peaks at 655 nm, and is negative in the bulk chl a region with a minimum around 686 nm. We assign this component to both energy transfer from the small fraction of chl b that is excited at 400 nm to chl a , and chl a Soret to Q_y relaxation. The observation that the DAS has virtually no amplitude in the carotenoid region, indicates that indeed no significant amount of carotenoids is excited at 400 nm. Although the 0.5 ps lifetime corresponds well to the chl b to chl a transfer times reported above, we note that in the absence of upconversion data for 400 nm excitation we cannot accurately determine this time constant.

The second component corresponds to a 8 ps time constant and exhibits a spectrum (dotted) which shows maxima at ~ 680 nm and ~ 690 nm, and a negative region in the red



8.6 Decay-Associated Spectra of fluorescence decay of isolated LHCl for 400 nm excitation. 0.5 ps (solid), 8 ps (dotted), 18 ps (dashed), 0.6 ns (double-dot-dashed) 3 ns (dot-dashed) and 4.3 ns (dot-long-dashed). The inset shows a blow-up of the 575-670 nm detection region. Rough error-bars have been included at selected wavelengths.

wavelength region with a minimum around 719 nm. The negative part of this spectrum is very similar to that of the 3.6 ps transfer component observed for 470 nm excitation (see above), however, the positive part, reflecting decay of "bulk" emission is about ~ 10 nm red shifted with respect to the corresponding decay in the DAS for 470 nm excitation. Also the emission of chl*b* is almost absent for 400 nm excitation, which implies that the chl*b* responsible for the slow chl*b* to chl*a* energy transfer is not excited at 400 nm. The differences in time constants between the 3.6 ps component found for 470 nm excitation and the 8 ps time constant found for 400 nm excitation, suggests that the former represents a mixture of a 2-3 ps chl*b* to *a* transfer component, and (a) slower 4-8 ps bulk chl*a* to red-shifted chl*a* component(s) (see below).

The third component, which is fitted with a 18 ps time constant closely resembles the 20 ps component observed in the analysis of the 470 nm excited data. Therefore, although there is no real negative region in the red part of the spectrum (dashed), we also assign this component to energy transfer from bulk chl*a* to a red-shifted chl*a* form, maybe combined with some decay of excitations.

The 0.6 ns and 3 ns component (double-dot-dashed and dot-dashed) are basically identical to those found for excitation at 470 nm. A small 4.3 ns component (dot-long-dashed) which peaks around 675 nm accounts for some free chl*a* present in the preparation.

DISCUSSION

We summarize our results in the scheme presented in figure 8.7. We note that this scheme should be regarded as a summary of the observed lifetimes rather than a true kinetic scheme, since no backward (uphill) rates have been included, and no explicit separation is made between the different Lhca1-4 dimers. The lifetimes obtained in the different experiments and

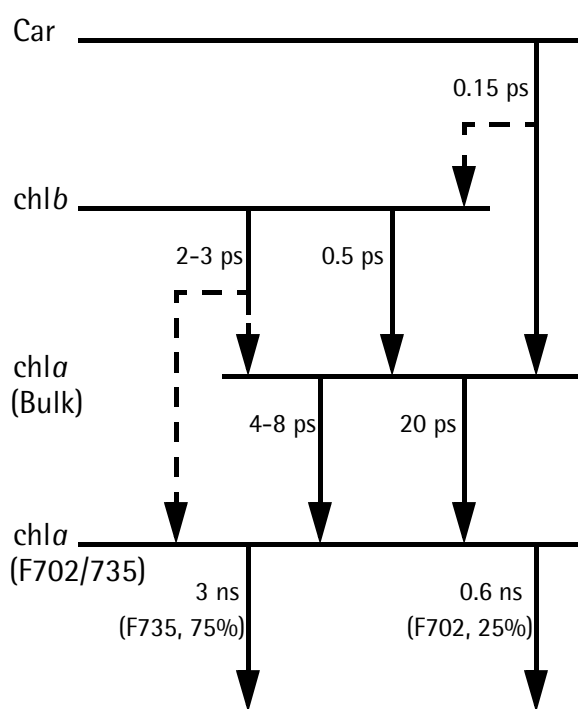
their assignments are summarized in table 8.1. For comparison results obtained by Melkozernov et al. for (reconstituted) LHCI-730,^{5,17} as well as results obtained for LHCII and CP29 are also listed in table 8.1.

Carotenoid to chlorophyll-*a* transfer

Fast energy transfer from the carotenoid S_2 state to chl*a* occurs within about 0.15 ps. This time constant is in the range of fluorescence lifetimes of carotenoids in organic solvents, which is about 0.12–0.18 ps for β -carotene²³ and \sim 0.32 ps for violaxanthin²⁴, and carotenoid S_2 lifetimes found in LHCII, CP29,¹² and the PSI core complex.²⁵ Our data do not permit to determine the Car to chl transfer efficiency, but steady-state fluorescence excitation measurements performed on the same LHCI preparations indicate that this efficiency is at least 80% (Ihalainen et al., unpublished results). For both LHCII and CP29 the overall efficiency of Car to chl transfer was also estimated to be approximately 80%, which included 15–20% transfer via the Car S_1 state occurring on a \sim 1 ps time scale.¹² Although our data on LHCI does not reveal a second, slower, Car to chl transfer component, we can not rule out that a fraction of the Car to chl transfer in LHCI is mediated by the S_1 state.

Carotenoid to chlorophyll-*b* transfer

It is unclear if Car transfers directly to chl*b* in LHCI. The bi-exponential ingrowth at 699 nm upon carotenoid excitation (fig. 8.2) shows a larger amplitude for the 0.5 ps rise attributed to chl*b* to chl*a* transfer, than for the 0.14 ps Car to chl transfer component. This may be an



8.7 Scheme of energy-transfer pathways in LHCI. Dashed lines indicate pathways which presently cannot be decided upon based on our data (see discussion).

indication that direct Car to *chl**b* transfer occurs (followed by *chl**b* to *chl**a* transfer), since the amount of *chl**b* that is directly excited at 510 nm is expected to be 10-fold lower than the amount of Car which is excited at that wavelength. On the other hand, if Car to *chl**b* transfer occurs, the 0.14 ps component is expected to show a negative amplitude for 655 nm detection, since at this wavelength the ingrowth of *chl**b* fluorescence would be larger than the corresponding decay of carotenoid fluorescence. Since the 0.14 ps component shows a positive (decay) amplitude at 655 nm this argues against Car to *chl**b* transfer.

In CP29 the carotenoids transfer exclusively to *chl**a*, in contrast to LHCII in which energy transfer from neoxanthin to *chl**b* does occur.¹² We note that LHCII contains 3 carotenoids per monomer, in contrast to the 2 Cars that are present in both LHCI and CP29 and that LHCI does not contain neoxanthin. Therefore, LHCI is more likely to resemble CP29 in this respect.

Chlorophyll-*b* to chlorophyll-*a* transfer

Fast transfer from *chl**b* to *chl**a* occurs in 0.5 ps, and does, most likely, not involve a significant amount of transfer to the red *chl**a* forms. A similar 0.5–0.6 ps *chl**b* to *a* transfer component was observed in a transient absorption study of reconstituted monomeric Lhca4 polypeptides.¹⁷ Upon *chl**b* excitation a 3.6 ps process is observed that involves a decay both in the *chl**b* region and the bulk *chl**a* region, and a rise in the red *chl**a* region. Upon excitation of *chl**a* (fig. 8.6) a similar component is present, which, however, lacks the decay in the *chl**b* region, and which is associated with a slower, 8 ps, lifetime. This suggests that the observed 3.6 ps component in the global analysis of the *chl**b* excited streak measurements represents a mixture of both a 2–3 ps *chl**b* to (red) *chl**a* transfer component and (a) slower bulk *chl**a* to red *chl**a* transfer component(s) (see also below). This idea is further supported by a separate

Table 8.1 Lifetimes observed in LHCI, LHCII and CP29

experiment	Car (S_2) decay	<i>chl</i> <i>b</i> – <i>chl</i> <i>a</i> transfer		<i>chl</i> <i>a</i> equilibration		decay	
		fast	slow	fast	slow	fast	slow
Car excitation (UPC)	0.14 ps	0.5 ps	-	-	-	-	-
<i>chl</i> <i>b</i> excitation (UPC)	-	0.5 ps	4 ps	4 ps	-	-	-
<i>chl</i> <i>b</i> excitation (UPC + streak)	0.3 ps	0.3 ps	3.6 ps	3.6 ps	20 ps	0.6 ns	3 ns
<i>chl</i> <i>a</i> excitation (streak camera)	-	0.5 ps	-	8 ps	18 ps	0.6 ns	3 ns
concluding	~0.14 ps	0.5 ps	2–3 ps	4–8 ps	~20 ps	0.6 ns	3 ns
Melkozernov et al. ((<i>r</i> -)LHCI-730) ^{5,17}	-	0.5–0.6 ps	-	5 ps	30–50 ps	several, 0.3–7 ns	
LHCII monomers (77K) ^{12,13,14}	0.1 ps	0.2 ps	3 ps	0.3 ps, 0.45 ps, 5 ps 12 ps, 18 ps		-	2.9 ns
CP29 (77K) ^{11,12}	70–90 fs	0.35 ps	2.2 ps	280 fs	10–13 ps	-	-

analysis of the *chl*b region only, which reveals a decay of *chl*b fluorescence in 2.3 ps (not shown). Due to the entanglement of these two processes it is unclear if the 2–3 ps *chl*b to *chl*a transfer component involves transfer either to the bulk or to the red *chl*a forms (or both). Biphasic *chl*b to *chl*a transfer (in \sim 0.2–0.35 ps and 2–3 ps) was, however, also observed in monomers of LHClI¹³ and CP29,¹¹ which do not contain red-shifted chls. For CP29 it was shown that the fast *chl*b to *chl*a transfer component corresponds to transfer from the blue-most *chl*b form, whereas the slower transfer component occurs from the red-most *chl*b form.¹¹ Considering the similarities between CP29 and LHClI a similar separation of the two (C643 and C650) *chl*b to *chl*a transfer components could be expected in the latter, although our data are not conclusive on this issue.

Equilibration between bulk chlorophyll-*a* and red chlorophyll-*a*

Upon 400 nm excitation energy transfer from the bulk *chl*a's to the red *chl*a's is found to occur in 8 ps. A separate analysis of parts of the bulk *chl*a fluorescence decay indicates that the decay time is quite independent of the wavelength. However, upon 465 nm excitation, it is found that the fluorescence decay of bulk *chl*a's around 675 is faster (4–5 ps) than that of the *chl*a emission around 685 (7 ps). This indicates that different pools of bulk *chl*a's may equilibrate with the red chls on different time-scales varying between 4 and 8 ps.

In addition a slower bulk *chl*a to red *chl*a transfer of about 20 ps was observed. Earlier experiments on isolated LHClI showed a 10–45 ps^{5,15,16} and even slower *chl*a equilibration components,¹⁶ but did not reveal the faster 4–8 ps equilibration process.

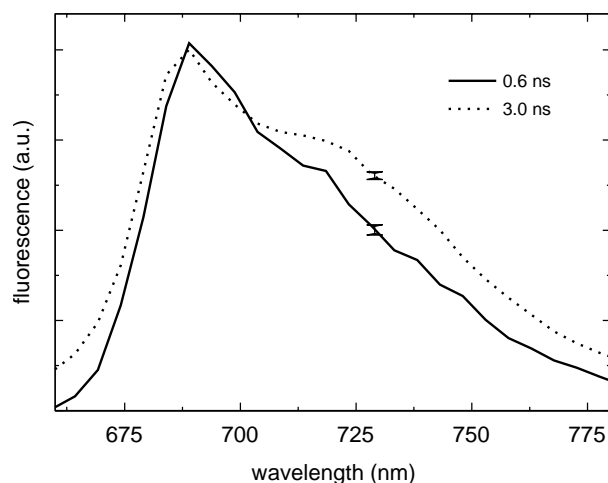
Since it appears that all LHClI dimers exhibit a long-wavelength chl (F730, F702)² (see also below), the observed *chl*a equilibration times most probably represent some average of a larger number of equilibration components. If the red-shifted chl form is assumed to be localized in one of the monomers, the \sim 4–8 ps rates may be interpreted as the intra-molecular equilibration within a monomer and the \sim 20 ps rate as inter-molecular equilibration between the monomers constituting a dimer. This view is in agreement with recent results by Melkozernov et al.,¹⁷ which show a 4–5 ps *chl*a equilibration component present in monomeric reconstituted Lhca4 and reconstituted LHClI-730 heterodimers, whereas a 33 ps equilibration component is only present in the latter. We do note that some mixing of (slow) *chl*b to *chl*a transfer and *chl*a equilibration, may have occurred in these experiments as well, since excitation was performed in the *chl*b region. Both in these and our experiments, the slow (20 ps) bulk to red *chl*a energy-transfer components are strongly non-conservative, suggesting that either a significant loss of excitations occurs with this time constant, or that the acceptor-state exhibits a lowered oscillator strength. We can rule out that the observed non-conservativity results from singlet-singlet or singlet-triplet annihilation, considering the conditions under which our experiments were performed. Moreover, a similar non-conservative, slow energy-transfer component was observed in pump-probe experiments on CP47 (de Weerd et al., unpublished data). Obviously, if there would be an actual loss of excitations on a tens of ps time scale in LHClI bound to the PSI core complex, this would result in a significant decrease in the light-harvesting efficiency of LHClI.

Although LHClI and CP29 do not contain red-shifted *chl*a, several equilibration processes were observed in the bulk *chl*a band, occurring on sub-picosecond and 5–18 ps time scales.^{11,13,14}

Long lifetimes

Both the 400 nm and 470 nm excitation data sets reveal two distinct long lifetime decays of 0.6 ns and 3 ns. For both wavelengths of excitation the respective spectra of these components appear very similar, both with respect to shape and relative amplitude. In figure 8.8 the spectra of the 0.6 ns and 3 ns components are shown for 470 nm excitation, scaled to their maxima. The 0.6 ns component (solid) peaks a few nm red shifted with respect to the 3 ns component (dotted). Although both spectra exhibit a red wing, the wing of the 3 ns component is significantly more pronounced and red shifted than that of the 0.6 ns component. This implies that both "species" possess a different red-shifted chl*a* form. This is in agreement with low-temperature experiments by Ihalainen et al.² which reveal a 702 nm emitting species in addition to the established 730-735 nm fluorescence of LHCl. The spectrum of the 3 ns component quite closely resembles the emission spectrum of LHCl-730 reported by Melkozernov et al.⁵ The ratio of the total areas of the 0.6 ns DAS and ~3 ns DAS is about 1 to 4. This is quite close to the 1 to 3 ratio which would be expected if one out of 4 dimers (one Lhca2 homodimer, one Lhca3 homodimer, and two Lhca1/4 heterodimers) has decay properties that are significantly different from the other three. It has been suggested that either the Lhca2 or Lhca3 homodimer exhibits emission properties similar to those of the Lhca1/Lhca4 heterodimer (i.e. F730), and that the remaining dimer may be responsible for F702 (S. Jansson, personal communication). Therefore we tentatively assign the 0.6 ns component to a homodimer of either Lhca2 or Lhca3, which at low temperatures may be responsible for the observed F702 fluorescence.

Presently we do not have an exclusive explanation why the fluorescence decay of this dimer at room temperature is 5-fold faster as compared to the other dimers, since there are several mechanisms that could result in such a shortening of the fluorescence lifetime. Shortening of the fluorescence lifetime has been observed in many (bacterio)chlorophyll containing systems, such as the bacterial light-harvesting complexes LH1 and LH2,²⁶ the B820 subunit of LH1,²⁷ the primary electron donor in the bacterial reaction centre^{28,29} and the chl*a*



8.8 Normalized Decay-Associated Spectra of the two slowest components for 470 nm excitation with lifetimes of 0.6 ns (solid) and 3 ns (dotted). Rough error-bars have been included at selected wavelengths.

in the Cytochrome b_6f complex of *Synechocystis* PCC6803.³⁰ Various explanations have been proposed for the shortening of lifetimes, such as superradiance of the excitonically coupled (B)chl molecules,²⁶ enhanced internal conversion rates,²⁶⁻²⁸ and quenching of excitations by a nearby amino-acid residue.³⁰ It has also been argued that a moderately strong interaction of the chl Q_y state with the S_1 state of carotenoids can result in a substantial decrease of the fluorescence lifetime.³¹

Melkozernov et al.⁵ observed several long lifetimes both in native and reconstituted LHCI-730, with dominating ~ 300 ps and ~ 800 ps components. Since these preparations were supposed to consist of the Lhca1/Lhca4 heterodimer only, a single decay lifetime is expected. The observed multi-exponential decay must therefore result from some heterogeneity of the sample, possibly the isolation procedures somehow disrupt the sample or maybe some aggregation occurs.

Concluding remarks: why are red chls only found in PSI?

The dynamics of LHCI show some remarkable similarities to the light-harvesting proteins CP29 and LHCII (see table 8.1) of Photosystem II. However, Photosystem II and its light-harvesting proteins do not feature the red-shifted chl α forms which are found in all PSI core complexes and LHCI. Apparently, in the course of evolution, PSI has experienced a net benefit from the presence of red chls, which was not the case for PSII. The cause of this difference may be that PSI is a more efficient photosystem than PSII.^{32,33} A PSI core particle containing no red chls is estimated to exhibit a 18 ps effective trapping time,¹⁹ resulting in a quantum efficiency for charge separation of 99.6% (assuming the rate of losses to be $(5 \text{ ns})^{-1}$). In plant PSI cores the number of red chls is small, and results in an increase of the effective trapping rate to about 20 ps (Gobets et al., unpublished results). However, in some cyanobacterial PSI cores the number of red chls is much larger, resulting in an increase of the effective trapping time of up to threefold.¹⁹ Nevertheless, this causes the estimated quantum efficiency to drop by only 0.7%. The quantum efficiency for charge separation of a PSII core particle, which does not contain red chls, is only 85%.³² A three-fold slow-down of the effective trapping rate similar as in PSI would lead to a 20% decrease of the quantum efficiency in PSII. Clearly, whereas the positive effects of red chls (increased red photon absorption, and possibly photoprotection), could easily justify the minute decrease in quantum efficiency in PSI, it is very likely that the large decrease in efficiency in PSII is not compensated by these positive effects.

The relatively low efficiency of PSII is the result of two effects. First of all, energy transfer to the RC is slower in PSII than in PSI. A comparison of the crystal structures of the two photosystems^{34,35} (P. Fromme, personal communication) shows why: in PSI the volume directly surrounding the reaction centre is densely packed with about 50 chl α molecules, whereas in PSII the same volume is basically empty. Therefore the average distance between the antenna chls and the RC is much larger in PSII than in PSI, resulting in a slower transfer to the RC in the former. The reason why the volume directly surrounding the RC in PSII is empty, may be the risk of damage to the antenna chls because of the high redox-potential involved in oxygen evolution, as well as the need to be able to easily replace the D1 protein.

The second effect responsible for the low efficiency of PSII is the small energy difference between $P680^*Pheo$ and the first charge-separated state $P680^+Pheo^-$, resulting in losses by "delayed fluorescence" due to backtransfer from $P680^+Pheo^-$ to the PSII RC and antenna. The

small energy gap is the consequence of tuning the PSII system to obtain the high redox-potential, needed for the splitting of water.^{32,36}

Thus, the absence of red chls in Photosystem II may very well be a direct result of its ability to split water.

ACKNOWLEDGMENTS

We thank Claudiu C. Gradinaru for the helpful discussions and suggestions, and prof. S. Jansson (Umeå) for sharing unpublished work. B.G. was supported with a grant from the Dutch Science Foundation (SIR beurs NWO). J.K. was supported by the Human Frontier Science Program Organization. J.I. was supported with a short-term fellowship from the ESF Program "Biophysics of Photosynthesis". This work was supported by the Netherlands Organization for Scientific Research (NWO) via the Foundation of Earth and Life Sciences (ALW), and by the Director, Office of Science, of the U.S. Department of Energy under Contract No. DE-AC03-76SF00098.

REFERENCES

- (1) Jansson, S. 1994. The Light-harvesting chlorophyll *a/b* binding-proteins. *Biochim. Biophys. Acta.* 1184:1-19.
- (2) Ihalainen, J.A., B. Gobets, K. Sznee, M. Brazzoli, R. Croce, R. Bassi, R. van Grondelle, J.E.I. Korppi-Tommola, and J.P. Dekker. 2000. Evidence for two spectroscopically different dimers of light-harvesting complex I from green plants. *Biochemistry.* 39:8625-8631.
- (3) Jansson, S., B. Andersen, and H.V. Scheller. 1996. Nearest-neighbor analysis of higher-plant Photosystem I holocomplex. *Plant Physiology.* 112:409-420.
- (4) Schmid, V.H.R., K.V. Cammarata, B.U. Bruns, and G.W. Schmidt. 1997. *In vitro* reconstitution of the Photosystem I light-harvesting complex LHCl-730: Heterodimerization is required for antenna pigment organization. *Proc. Natl. Acad. Sci. USA.* 94:7667-7672.
- (5) Melkozernov, A.N., V.H.R. Schmid, G.W. Schmidt, and R.E. Blankenship. 1998. Energy redistribution in heterodimeric light-harvesting complex LHCl-730 of Photosystem I. *J. Phys. Chem. B.* 102:8183-8189.
- (6) Croce, R., and R. Bassi. 1998. The light-harvesting complex of Photosystem I: Pigment composition and stoichiometry. *In* Photosynthesis: Mechanisms and effects. G. Garab, editor. Kluwer Academic Publishers, Dordrecht, The Netherlands. 1:421-424.
- (7) Gobets, B., H. van Amerongen, R. Monshouwer, J. Kruij, M. Rögner, R. van Grondelle, and J.P. Dekker. 1994. Polarized site-selected fluorescence spectroscopy of isolated Photosystem I particles. *Biochim. Biophys. Acta.* 1188:75-85.
- (8) Pålsson, L.-O., J.P. Dekker, E. Schlodder, R. Monshouwer, and R. van Grondelle. 1996. Polarized site-selective fluorescence spectroscopy of the long-wavelength emitting chlorophylls in isolated Photosystem I particles of *Synechococcus elongatus*. *Photosynth. Res.* 48:239-246.
- (9) Boekema, E.J., P.E. Jensen, E. Schlodder, J.F.L. van Breemen, H. van Roon, H.V. Scheller, and J.P. Dekker. 2001. Green plant Photosystem I binds light-harvesting complex I on one side of the complex. *Biochemistry.* 40:1029-1036.

- (10) Kühlbrandt, W., D.N. Wang, and Y. Fujiyoshi. 1994. Atomic model of plant light-harvesting complex by electron crystallography. *Nature*. 367:614-621.
- (11) Gradinaru, C.C., A.A. Pascal, F. van Mourik, B. Robert, P. Horton, R. van Grondelle, and H. van Amerongen. 1998. Ultrafast evolution of the excited states in the chlorophyll *a/b* complex CP29 from green plants studied by energy-selective pump-probe spectroscopy. *Biochemistry*. 37:1143-1149.
- (12) Gradinaru, C.C., I.H.M. van Stokkum, A.A. Pascal, R. van Grondelle, and H. Amerongen. 2000. Identifying the pathways of energy transfer between carotenoids and chlorophylls in LHCII and CP29. A multicolor, femtosecond pump-probe study. *J. Phys. Chem. B*. 104:9330-9342.
- (13) Kleima, F.J., C.C. Gradinaru, F. Calkoen, I.H.M. van Stokkum, R. van Grondelle, and H. van Amerongen. 1997. Energy transfer in LHCII monomers at 77K studied by sub-picosecond transient absorption spectroscopy. *Biochemistry*. 36:15262-15268.
- (14) Gradinaru, C.C., S. Özdemir, D. Gülen, I.H.M. van Stokkum, R. van Grondelle, and H. van Amerongen. 1998. The flow of excitation energy in LHCII monomers: Implications for the structural model of the major plant antenna. *Biophys. J*. 75:3064-3077.
- (15) Pålsson, L.-O., S.E. Tjus, B. Andersson, and T. Gillbro. 1995. Ultrafast energy-transfer dynamics resolved in isolated spinach light-harvesting complex-I and the LHC-I-730 subpopulation. *Biochim. Biophys. Acta*. 1230:1-9.
- (16) Mukerji, I., and K. Sauer. 1993. Energy-transfer dynamics of an isolated light-harvesting complex of Photosystem-I from spinach - time-resolved fluorescence measurements at 295-K and 77-K. *Biochim. Biophys. Acta*. 1142:311-320.
- (17) Melkozernov, A.N., S. Lin, V.H.R. Schmid, H. Paulsen, G.W. Schmidt, and R.E. Blankenship. 2000. Ultrafast excitation dynamics of low-energy pigments in reconstituted peripheral light-harvesting complexes of Photosystem I. *FEBS Lett*. 471:89-92.
- (18) Croce, R., G. Zucchelli, F.M. Garlaschi, and R.C. Jennings. 1998. A thermal broadening study of the antenna chlorophylls in PSI-200, LHCI, and PSI core. *Biochemistry*. 37:17355-17360.
- (19) Gobets, B., I.H.M. van Stokkum, M. Rögner, J. Kruij, E. Schlodder, N.V. Karapetyan, J.P. Dekker, and R. van Grondelle. 2001. Time-resolved fluorescence emission measurements of Photosystem I particles of various cyanobacteria: a unified compartmental model. *Biophys. J*. 81:407-424.
- (20) Walla, P.J., J. Yom, B.P. Krueger, and G.R. Fleming. 2000. Two-photon excitation spectrum of light-harvesting complex II and fluorescence upconversion after one- and two-photon excitation of the carotenoids. *J. Phys. Chem. B*. 104:4799-4806.
- (21) Peterman, E.J.G., C.C. Gradinaru, F. Calkoen, J.C. Borst, R. van Grondelle, and H. van Amerongen. 1997. Xanthophylls in light-harvesting complex II of higher plants: Light harvesting and triplet quenching. *Biochemistry*. 36:12208-12215.
- (22) Schmid, V.H.R., P. Thome, W. Ruhle, H. Paulsen, W. Kuhlbrandt, and H. Rogl. 2001. Chlorophyll-*b* is involved in long-wavelength spectral properties of light-harvesting complexes LHCI and LHCII. *FEBS Lett*. 499:27-31.
- (23) Macpherson, A.N., and T. Gillbro. 1998. Solvent dependence of the ultrafast S-2-S-1 internal conversion rate of beta-carotene. *J. Phys. Chem. A*. 102:5049-5058.
- (24) Polivka, T., J.L. Herek, D. Zigmantas, H.E. Akerlund, and V. Sundstrom. 1999. Direct observation of the (forbidden) S-1 state in carotenoids. *Proc. Natl. Acad. Sci. USA*. 96:4914-4917.

- (25) Kennis, J.T.M., B. Gobets, I.H.M. van Stokkum, J.P. Dekker, R. van Grondelle, and G.R. Fleming. 2001. Light harvesting by chlorophylls and carotenoids in the Photosystem I complex of *Synechococcus elongatus*: a fluorescence upconversion study. *J. Phys. Chem. B.* 105:4485-4494.
- (26) Monshouwer, R., M. Abrahamsson, F. van Mourik, and R. van Grondelle. 1997. Superradiance and exciton delocalization in bacterial photosynthetic light-harvesting systems. *J. Phys. Chem. B.* 101:7241-7248.
- (27) Helenius, V., R. Monshouwer, and R. van Grondelle. 1997. Temperature-dependent lifetimes and quantum yield of the singlet and triplet states of the B820 subunit of LHI antenna complex of purple bacterium *Rhodospirillum rubrum*. *J. Phys. Chem. B.* 101:10554-10559.
- (28) Breton, J., J.-L. Martin, J.-C. Lambry, S.J. Robles, and D.C. Youvan. 1990. Ground state and femtosecond transient absorption spectroscopy of a mutant of *Rhodobacter capsulatus* which lacks the initial electron acceptor bacteriopheophytin. In *Reaction centers of photosynthetic bacteria*. M.E. Michel-Beyerle, editor. Springer Verlag. 293.
- (29) Van Brederode, M.E., M.R. Jones, F. van Mourik, I.H.M. van Stokkum, and R. van Grondelle. 1997. A new pathway for transmembrane electron transfer in photosynthetic reaction centers of *Rhodobacter sphaeroides* not involving the excited special pair. *Biochemistry.* 36:6855-6861.
- (30) Peterman, E.J.G, S-O. Wenk, T. Pullerits, L.-O. Pålsson, R. van Grondelle, J.P. Dekker, M. Rögner, and H. van Amerongen. 1998. Fluorescence and absorption spectroscopy of the weakly fluorescent chlorophyll-*a* in cytochrome *b₆f* of *Synechocystis* PCC6803. *Biophys. J.* 75:389-398.
- (31) Van Amerongen, H., and R. van Grondelle. 2001. Understanding the energy transfer function of LHCII, the major light-harvesting complex of green Plants. *J. Phys. Chem. B.* 105:604-617.
- (32) Trissl H.-W. and C. Wilhelm. 1993. Why do thylakoid membranes from higher-plants form grana stacks? *Trends Biochem. Sci.* 18:415-419.
- (33) Van Grondelle, R., J.P. Dekker, T. Gillbro, and V. Sundström. 1994. Energy transfer and trapping in photosynthesis. *Biochim. Biophys. Acta.* 1187:1-65.
- (34) Krauss, N., W.-D. Schubert, O. Klukas, P. Fromme, H.T. Witt, and W. Saenger. 1996. Photosystem I at 4Å resolution represents the first structural model of a joint photosynthetic reaction centre and core antenna system. *Nat. Struct. Biol.* 3:965-973.
- (35) Zouni, A., H.T. Witt, J. Kern, P. Fromme, N. Krauss, W. Saenger, and P. Orth. 2001. Crystal structure of Photosystem II from *Synechococcus elongatus* at 3.8 angstrom resolution. *Nature.* 409:739-743.
- (36) Diner, B.A., and G.T. Babcock. 1996. Structure, dynamics, and energy conversion efficiency in PS II. In *Advances in photosynthesis*, vol. 4, oxygenic photosynthesis: The light reactions. D.R. Ort, and C.F. Yocum, editors. Kluwer Academic Publishers, Dordrecht, The Netherlands. 213-247.

Summary

In this thesis the energy transfer and trapping in the Photosystem I (PSI) antenna-reaction centre complex is investigated. A conspicuous feature of practically all Photosystem I complexes is the presence of a number of low-energy or "red" chlorophylls (chls) that absorb at energies lower than that of the primary electron donor (P700) in the reaction centre (RC). Although these red chls are expected to act as low-energy sinks that lower the efficiency of the photosystem, at room-temperature the overall quantum-efficiency of PSI is high, around 99%.

In chapter two of this thesis the spectroscopic properties of these red chls are investigated by energy-selective fluorescence spectroscopy at low (liquid helium) temperatures. It was found that the properties of the red chls are considerably different from those of the "normal" antenna chls. Both the homogeneous line width (electron-phonon coupling) and the Stokes' shift were found to be exceptionally large. We therefore concluded that the red chls in PSI do not represent a monomeric form, but rather excitonically coupled dimers of chl.

In order to study the precise effect of the red chls on the PSI dynamics at room temperature, we investigated the dynamics of five PSI core complexes differing in the number and energies of the red chls that they contained. These investigations, presented in chapter 3, were performed by time-resolved fluorescence measurements. We noted that the trapping-time, the slowest process in the decay of excitations, varied between 23 ps for PSI cores containing the fewest red chls, and 50 ps for PSI cores containing the most, and most red chls. Prior to the trapping of the majority of the excitations, in all PSI core complexes one or two equilibration processes were found to occur between the bulk antenna chls and the red chls. We succeeded in analysing the data in terms of a uniform target-analysis scheme, which indicated that the observed differences in the dynamics of the five PSI core particles are predominantly due to the differences in red chl content. Our model revealed that a hypothetical PSI core particle that does not contain any red chls exhibits a trapping-time of approximately 18 ps.

Recently, the structure of the PSI core from the cyanobacterium *Synechococcus elongatus* was resolved, first at a 4 Å, and later at a 2.5 Å resolution, revealing details of the almost 100 chls present in this PSI core particle. The modelling of energy-transfer of real PSI cores is hampered by the fact that the positions of the few red chls in the structure are in principle unknown. This problem was overcome by modelling the dynamics of our hypothetical red-chl free PSI core, which is described in chapters 4 and 5. It was found that the 18 ps trapping time resulted in an almost linear relation between the values of the average single-site lifetime in the antenna, and the charge-separation time from P700. The experimentally observed single-site lifetime (chapter 7) of about 150 fs corresponds to a charge-separation time of about 1 ps. The results of the structure-based simulation were subsequently used for describing the system in terms of a lattice-model. One of the merits of the lattice model is that it yields parameters that provide insight into the global energy-transfer features of the system, rather than the microscopic parameters that result from the structure-based simulation. It enabled us to explain results from low-temperature steady-state fluorescence measurements presented in chapter 4. Moreover, the comparison of a lattice model with a

structure-based simulation in our view validates application of lattice models to other systems, for which (precise) structural data is lacking.

In chapter 6 the results of the structure-based simulation of the dynamics in a red-chl free PSI core are used to perform a similar simulation of the dynamics in real PSI cores, that do contain red chls. Both the time-resolved fluorescence results presented in chapter 3, as well as additional time-resolved fluorescence results for selective excitation of the red chls could to a large extent be simulated, even though very few degrees of freedom were present in these simulations.

In chapters 7 and 8 the dynamics in PSI complexes are studied with the high time-resolution technique of fluorescence-upconversion. In chapter 7 the energy transfer in the PSI core from *Synechococcus elongatus* is studied with this technique, and permitted resolution of the elementary energy transfer steps (~ 160 fs) and equilibration (~ 360 fs) in the bulk antenna. Energy transfer from β -car to chl was found to proceed both via the S_2 and the S_1 state, resulting in an estimated overall yield of $\sim 90\%$.

Finally, in chapter 8, we study the energy transfer in isolated LHCl dimers, the additional light-harvesting complexes that are bound to the PSI cores of higher plants. Although the analysis of the results was hampered by the fact that the preparation consisted of a mixture of different LHCl dimers (separation is currently not possible), we were able to resolve details of the energy-transfer processes occurring in these systems, by applying different wavelengths of excitation and by combining streak camera and fluorescence-upconversion data. It was concluded that, contrary to earlier reports, all LHCl dimers contain some low-energy chl form. In the analysis two distinct (classes of) LHCl dimers could be distinguished, with different excited-state lifetimes and emission spectra.

Samenvatting

Tijd van leven in Fotosysteem I

de overdracht en vangst van excitatie-energie ontrafeld.

Fotosynthese is het proces dat planten, maar ook algen en sommige bacteriën, in staat stelt te leven van de energie van het zonlicht. Omdat vrijwel alle andere levensvormen, mensen inbegrepen direct, of indirect leven van planten, algen en bacteriën is het fotosynthese proces één van de belangrijkste, zonet het belangrijkste proces in de natuur. Daarbij komt nog dat alle fossiele brandstoffen die wij gebruiken ook ooit geproduceerd zijn door middel van fotosynthese, en ook de zuurstof die wij inademen is door fotosynthese in de atmosfeer gebracht. Als het fotosynthese proces nooit ontstaan was, waren levensvormen die afhankelijk zijn van zuurstof nooit ontstaan, kortom zonder fotosynthese zou de aarde er heel anders uit hebben gezien.

De allereerste stap in de fotosynthese is de absorptie van (zon)licht. Daarvoor zijn kleurstofmolekulen (pigmenten) nodig die het licht kunnen absorberen. Belangrijke kleurstoffen in de fotosynthese zijn chlorofyl en caroteen. Als een pigment licht absorbeert wordt de energie van dat licht opgeslagen in de vorm van een aangeslagen (geëxciteerde) toestand van dat pigment: de licht-energie wordt gebruikt om de electronische structuur van het pigment iets te veranderen. Deze manier van energie-opslag is echter niet erg stabiel: in chlorofyl gaat deze excitatie-energie binnen enkele miljardsten van seconden na het absorberen van het licht verloren. De fotosynthese is ontworpen om de vluchtige excitatie-energie in een reeks stappen om te zetten in steeds stabielere vormen van energie. De eerste stappen na lichtabsorptie richten zich op het transport van de excitatie-energie naar een speciale plaats in het eiwitcomplex, het reactiecentrum, alwaar excitatie-energie omgezet wordt in stabielere vorm van energie. Het transport van de excitatie-energie kan plaatsvinden doordat een pigment zijn excitatie-energie doorgeven aan een ander pigment dat zich in de buurt bevindt. Dit gaat razendsnel, binnen een duizendste van een miljardste van een seconde. Omdat de pigmenten zijn georganiseerd in een groot pigment-netwerk, lichtoogst antenne genoemd, zal, als één van de pigmentmolekulen licht absorbeert, de excitatie-energie vanaf dat pigment razendsnel gaan rondzwerven door de hele lichtoogst antenne. Dit eindigt wanneer de excitatie energie terecht komt op een speciaal paar chlorofylmolekulen dat deel uitmaakt van het reactiecentrum. Als dit speciale paar de excitatie-energie ontvangt, wordt deze energie gebruikt om een electron, een negatief geladen deeltje, van de ene kant van het eiwitcomplex naar de andere te brengen. Een positieve lading blijft achter, en zo wordt de energie gevangen in een moleculaire batterij, een vorm van energie-opslag die stabiel is gedurende milliseconden tot seconden.

De overdracht van excitatie-energie door een lichtoogst antenne en de "vangst" van deze energie in een reactiecentrum vormen in alle soorten fotosynthese de eerste stappen van het proces. In zuurstofontwikkende fotosynthese, zoals die in planten plaatsvindt, werken twee van dit soort ladingscheidende eiwitcomplexen in serie om voldoende "spanning" op te bouwen om water te ontleden in zuurstof en waterstof. Deze complexen worden Fotosysteem I en Fotosysteem II genoemd. In dit proefschrift wordt onderzocht hoe in

Fotosysteem I het transport van excitatie-energie in de lichtoogst antenne en de vangst van excitatie-energie in het reactiecentrum plaatsvindt.

Niet alle pigmenten in de lichtoogst antenne absorberen dezelfde kleur licht. Dat betekent dat energie van hun aangeslagen toestand verschilt: pigmenten die meer blauw absorberen hebben een hogere energie in hun aangeslagen toestand dan pigmenten die meer rood absorberen. De overdracht van excitatie-energie van pigmenten met een hogere energie in de aangeslagen toestand gaat sneller naar pigmenten met een lagere energie in de aangeslagen toestand (bergaf) dan omgekeerd (bergop). In het algemeen zijn fotosynthetische systemen daarom zo georganiseerd dat het speciale paar chlorofylmolekullen waar vanaf in het reactiecentrum de ladingsscheiding plaatsvindt, het laagst in energie is: de lichtoogst antenne vormt als het ware een trechter, met het speciale paar chlorofylmolekullen van het reactiecentrum als tuitje. De lichtoogst antenne in Fotosysteem I vormt echter een uitzondering op dit ontwerp: in deze antenne is een aantal pigmenten aanwezig dat een lagere energie in de aangeslagen toestand heeft dan het speciale paar chlorofylmolekullen in het reactiecentrum. De lichtoogst antenne van Fotosysteem I vormt als het ware een trechter, waarvan het tuitje (het speciale paar chlorofyllen in het reactiecentrum) zich niet in het laagste punt bevindt. De pigmenten met een lagere energie in de aangeslagen toestand dan het speciale paar chlorofylmolekullen in het reactiecentrum worden ook wel "rode" chlorofylmolekullen, of lage-energie chlorofyllen genoemd. De vraag is natuurlijk waarom deze rode chlorofylmolekullen zich in Fotosysteem I bevinden. Intuïtief zou men namelijk verwachten dat ze de efficiëntie van Fotosysteem I verlagen.

Voor dit proefschrift heb ik een aantal Fotosysteem I complexen onderzocht die verschillen in de hoeveelheid rode chlorofylmolekullen die ze bevatten. Ook de energieën van de aangeslagen toestanden van de rode chlorofylmolekullen verschillen tussen de onderzochte Fotosysteem I complexen. Ik heb aangetoond dat de snelheid waarmee de excitatie-energie naar het reactiecentrum wordt getransporteerd inderdaad afneemt naarmate er zich meer rode chlorofylmolekullen in Fotosysteem I bevinden, en naarmate ze een lagere energie van de aangeslagen toestand hebben. Bij kamertemperatuur kán de excitatie-energie echter wel van de rode chlorofylmolekullen bergop getransporteerd naar het speciale paar van het reactiecentrum. Dit kan plaatsvinden door de warmte-energie die bij kamertemperatuur aanwezig is: de trechter wordt als het ware geschud, zodat toch het hoger gelegen tuitje wordt bereikt. Daarom heeft de aanwezigheid van de rode chlorofylmolekullen bij kamertemperatuur geen dramatische gevolgen voor de uiteindelijke efficiëntie van het systeem: de verliesprocessen verlopen nog steeds veel trager dan het bergop transporteren van de excitatie-energie waardoor de efficiëntie van het systeem hoog blijft, rond de 99%. Bij lage temperaturen verandert dit: de hoeveelheid aanwezige warmte-energie neemt af (het schudden van de trechter wordt minder), en het bergop transporteren van excitatie-energie wordt dramatisch vertraagd. Bij 269 graden onder nul, (4 graden Kelvin, dicht bij het absolute nulpunt), kan de excitatie-energie niet meer vanaf de rode chlorofyllen bergop worden getransporteerd. Experimenten die ik heb uitgevoerd bij deze extreem lage temperatuur tonen echter aan dat zelfs bij deze temperatuur van elke keer dat er in de lichtoogst antenne van Fotosysteem I licht wordt geabsorbeerd, dit nog steeds in 50% van de gevallen tot een ladingsscheiding in het reactiecentrum leidt. Dat wil zeggen dat in de merkwaardig gevormde

trechter die de lichtoogst antenne van Fotosysteem I vormt, ook zonder "schudden" nog steeds 50% van de "druppels" die in de trechter valt, tijdens het omlaaggliden langs de trechterwand door het hooggelegen tuitje wordt ingevangen, terwijl de overige 50% verloren gaat in het dal van de rode chlorofylmolekules.

Het eiwitcomplex van Fotosysteem I is minuscule klein, ongeveer een tiende micrometer. Het kan met een lichtmicroscop niet gezien worden, laat staan dat er details van de structuur kunnen worden waargenomen. Een onderzoeksgroep in Duitsland is er echter recent met een speciale techniek in geslaagd een heel gedetailleerd beeld te krijgen van het Fotosysteem I eiwitcomplex. De precieze plaats van elk pigmentmolekuul in het eiwitcomplex kon worden bepaald. Ik heb deze gegevens gebruikt om berekeningen te doen aan de overdracht van excitatie-energie in Fotosysteem I, en ben er in geslaagd de hierboven beschreven experimentele resultaten (en ook andere) te verklaren.

Er blijft echter de vraag van het nut van de rode chlorofyl molekulen. Een aantal verklaringen is gesuggereerd, waarvan ik er enkele met mijn onderzoek heb kunnen weerleggen. De meest waarschijnlijke verklaring lijkt dat de rode chlorofylmolekulen juist belangrijk zijn omdat ze roder licht absorberen dan de andere pigmenten in de lichtoogst antenne. Onder de schaduwrijke omstandigheden die een blad lager aan een boom ondervindt is de hoeveelheid licht van de kleur die "gewone" pigmenten in de lichtoogst antenne absorberen beperkt, omdat dit al in bladeren hoger in de boom geabsorbeerd is. Het licht is daarom relatief rijk aan het rodere licht dat door de rode chlorofylmolekulen kan worden geabsorbeerd. Berekeningen hebben aangetoond dat onder schaduwrijke omstandigheden, een paar procent rode chlorofyl molekulen in de lichtoogst antenne verantwoordelijk kan zijn voor 40 procent van de totale hoeveelheid geabsorbeerd licht!

List of publications

Peer reviewed journals

- (1) Gobets, B., H. van Amerongen, R. Monshouwer, J. Kruip, M. Rögner, R. van Grondelle, and J.P. Dekker. 1994. Polarized site-selected fluorescence spectroscopy of isolated photosystem I particles. *Biochim. Biophys. Acta.* 1188:75-85.
- (2) Pålsson, L.-O., C. Flemming, B. Gobets, R. van Grondelle, J.P. Dekker, and E. Schlodder. 1998. Energy transfer and charge separation in Photosystem I: P700 oxidation upon selective excitation of the long-wavelength chlorophylls of *Synechococcus elongatus*. *Biophys. J.* 74:2611-2622.
- (3) Cordfunke, R., R. Kort, A. Pierik, B. Gobets, G.J. Koomen, J.W. Verhoeven, and K.J. Hellingwerf. 1998. Trans/cis (Z/E) photoisomerization of the chromophore of photoactive yellow protein is not a prerequisite for the initiation of the photocycle of this photoreceptor protein. *Proc. Natl. Acad. Sci. USA.* 95:7396-7401.
- (4) Kleima, F.J., E. Hofmann, B. Gobets, I.H.M. van Stokkum, R. van Grondelle, K. Diederichs, and H. van Amerongen. 2000. Förster excitation energy transfer in peridinin-chlorophyll-*a*-protein. *Biophys. J.* 78:344-353.
- (5) Ihalainen, J.A., B. Gobets, K. Sznee, M. Brazzoli, R. Croce, R. Bassi, R. van Grondelle, J.E.I. Korppi-Tommola, and J.P. Dekker. 2000. Evidence for two spectroscopically different dimers of light-harvesting complex I from green plants. *Biochemistry.* 39:8625-8631.
- (6) Kennis, J.T.M., B. Gobets, I.H.M. van Stokkum, J.P. Dekker, R. van Grondelle, and G.R. Fleming. 2001. Light harvesting by chlorophylls and carotenoids in the Photosystem I complex of *Synechococcus elongatus*: a fluorescence upconversion study. *J. Phys. Chem. B.* 105:4485-4494.
- (7) Gobets, B., I.H.M. van Stokkum, M. Rögner, J. Kruip, E. Schlodder, N.V. Karapetyan, J.P. Dekker, and R. van Grondelle. 2001. Time-resolved fluorescence emission measurements of Photosystem I particles of various cyanobacteria: a unified compartmental model. *Biophys. J.* 81:407-424.
- (8) Gobets, B., and R. van Grondelle. 2001. Energy transfer and trapping in Photosystem I. *Biochim. Biophys. Acta.* 1507:80-99.
- (9) Gobets, B., J.T.M. Kennis, J.A. Ihalainen, M. Brazzoli, R. Croce, I.H.M. van Stokkum, R. Bassi, J.P. Dekker, H. van Amerongen, G.R. Fleming, and R. van Grondelle. 2001. Excitation energy transfer in dimeric light-harvesting complex I: a combined streak-camera/fluorescence upconversion study. *J. Phys. Chem. B.* 105:10132-10139.
- (10) Larsen, O.F.A., I.H.M. van Stokkum, B. Gobets, R. van Grondelle, and H. van Amerongen. 2001. Probing the structure and dynamics of a DNA hairpin by ultrafast quenching and fluorescence depolarization. *Biophys. J.* 81: 1115-1126.
- (11) Yatskou, M.M., B.M. Koehorst, A. van Hoek, H. Donker, T.J. Schaafsma, B. Gobets, and R. van Grondelle. 2001. Spectroscopic properties of a self-assembled zinc porphyrin tetramer. II. Time-resolved fluorescence spectroscopy. *J. Phys. Chem. B.* 105:11432-11440.
- (12) Van den Berg, P.A.W., S.B. Mulrooney, B. Gobets, I.H.M. van Stokkum, A. van Hoek, C.H. Williams Jr., and A.J.W.G. Visser. 2001. Exploring the conformational equilibrium of thioredoxin reductase: Characterization of two catalytically important states by ultra-fast flavin fluorescence spectroscopy. *Protein Science.* 10: 2037-2049.

Submitted manuscripts

- (1) Gobets, B., L. Valkunas, and R. van Grondelle. 2002. Bridging the gap between structural and lattice models: a parametrization of energy transfer and trapping in Photosystem I. *Submitted*.
- (2) Gobets, B., I.H.M. van Stokkum, F. van Mourik, M. Rögner, J. Kruip, E. Schlodder, J.P. Dekker, and R. van Grondelle. 2002. Excitation wavelength dependence of the fluorescence kinetics in Photosystem I particles from *Synechocystis* PCC 6803 and *Synechococcus elongatus*. *Submitted*.

Proceedings

- (1) Gobets, B., J.P. Dekker, and R. van Grondelle. 1998. Transfer-to-the-trap limited model of energy transfer in Photosystem I. *In* Photosynthesis: Mechanisms and effects. G. Garab, editor. Kluwer Academic Publishers, Dordrecht, The Netherlands. 1:503-508.
- (2) Gobets, B., I.H.M. van Stokkum, F. van Mourik, M. Rögner, J. Kruip, J.P. Dekker, and R. van Grondelle. 1998. Time-resolved fluorescence measurements of Photosystem I from *Synechocystis* PCC 6803. *In* Photosynthesis: Mechanisms and effects. G. Garab, editor. Kluwer Academic Publishers, Dordrecht, The Netherlands. 1:571-574.
- (3) Kleima, F.J., E. Hofmann, B. Gobets, I.H.M. van Stokkum, R. van Grondelle, and H. van Amerongen. 1998. Peridinin chlorophyll protein: structure and dynamics related. *In* Photosynthesis: Mechanisms and effects. G. Garab, editor. Kluwer Academic Publishers, Dordrecht, The Netherlands. 1:441-444.
- (4) Frese, R.N., B. Gobets, I.H.M. van Stokkum, R. van Grondelle, and F. Van Mourik. 1998. Dielectric Relaxation on a picosecond time-scale at 77K; a time-resolved Stark fluorescence study on the LH2 B800-820 complex of *Rps. Acidophila*. *In* Photosynthesis: Mechanisms and effects. G. Garab, editor. Kluwer Academic Publishers, Dordrecht, The Netherlands. 1: 41-44.
- (5) Gobets, B., I.H.M. van Stokkum, M. Rögner, J. Kruip, E. Schlodder, N.V. Karapetyan, J.P. Dekker, and R. van Grondelle. 2001. Fluorescence kinetics of Photosystem I core particles with different low energy chlorophyll content: A unified quantitative analysis. *In* Proceedings of the 12th International congress on photosynthesis. B. Osmond, editor. CSIRO Publishing, Brisbane, Australia.

Nawoord

Fotosysteem I: de tijd van m'n leven

Hier ligt dan het resultaat van een dikke zes jaar min of meer noeste arbeid, samengebald in pakweg 200 bladzijden. Maar dit boekje zou niet af zijn zonder "nawoord" (een calvinistisch eufemisme voor dankwoord). Niet alleen omdat deze afsluitende pagina's zondermeer de meestgelezen van elk proefschrift zijn, maar vooral omdat dit boekje er niet zou zijn geweest zonder de bijdragen van vele mensen, binnen en buiten de biofysica groep.

Ik heb een heel plezierige tijd gehad in de vakgroep biofysica, het is niet voor niets dat ik een groot aantal (ex)vakgroepleden inmiddels als mijn vrienden beschouw. Ik heb veel gelachen tijdens de talloze melige en snedige conversaties en eindeloze e-mail-polemieken, maar ook ondervonden dat men er ook voor elkaar is als het even niet meer lollig is. Ik wil iedereen in de vakgroep bedanken voor deze goede sfeer, waarvan ik hoop dat deze in de toekomst behouden blijft.

Jan, jij bent mijn copromotor, en was mijn officiële begeleider gedurende mijn promotie, al vergat ik dat wel eens. Ik heb veel gehad aan jouw grote kennis van PSI (je oude troetelkindje), en je grote ervaring met het schrijven van artikelen. Ik ben altijd onder de indruk van de rust die je uitstraalt, zelfs als je naast mij de auto zit terwijl ik op de Autobahn verwoede pogingen doe om de magische grens van 200 km per uur te overschrijden.

Rienk, ik denk dat het bij weinigen zo prettig promoveren is als bij jou. Je deur staat altijd open (zowel in Amsterdam als in Haarlem), en je bent altijd enthousiast over elk nieuw resultaat, zelfs het meest simpele metinkje. Steevast wordt er dan een vloed aan ideeën, verklaringen, en speculaties door je gespuid, waar je als promovendus (weliswaar na een eerste, zeer noodzakelijke filtering) weer een eind verder mee komt. Bovendien ben je een goed hardlooper. Als ik het hardlopen binnenkort weer oppik, hoop ik nog eens samen met je een loopje te doen. Of anders een potje risken of kolonisten.

Herbert, mijn officieuze begeleider, bij jou kon ik altijd terecht als "sparring partner" om de dingen net even beter op een rijtje te krijgen. Ik heb ook veel gehad aan jouw commentaar op mijn manuscripten. Maar ook aan de gezellige avonden, die steevast eindigden op het moment waarop jij het hoofd op tafel legde en sprak: "Bas, ik ben nu écht hééél errug dronken!"

Ivo, zonder jou was er geen streak camera geweest, en zonder streak camera was dit boekje er niet geweest. Met veel enthousiasme werkte je aan de globale en target analyse van de streakmetingen, die zo'n centrale rol speelt in dit proefschrift. Simultaan analyseren van opconversie en streak-data op twee tijdschalen? Ivo draait z'n hand er niet voor om. Met (mijns inziens) als hoogtepunt de target analyse besproken in hoofdstuk 3.

Frank, in samenspraak met Ivo hebben wij in de vingers gekregen hoe je een streak camera optimaal gebruikt. Met jouw technisch inzicht en je twee rechter handen (in de één een haakse slijper, in de andere een lasapparaat) zijn er weinig dingen die je niet gedaan krijgt. Ook blijkt je te beschikken over onvermoede onderhandelings-kwaliteiten: je presteerde het om bij het kopen van een optische tafel te bedingen dat wij een dagje gingen racen op Zandvoort, en je wist vervolgens mij te strikken voor een vijfdaagse verhuistocht Amsterdam-Mülheim-Lausanne-Parijs-Amstelveen.

I really enjoyed my stay in the laboratory of Graham Fleming in Berkeley, a month well spent, resulting in chapters 7 and 8 of this thesis. John, zonder jouw pragmatische instelling had ik waarschijnlijk geen enkele opconversie trace gemeten, en door na mijn vertrek nog wat aanvullende metingen te doen, voegde je nog een hoofdstuk toe aan dit proefschrift. Ik hoop dat je gelukkige jaren tegemoet gaat met Silvia.

Without the samples provided by Matthias Rögner, Jochen Kruij, Eberhardt Schlodder, Navassard Karapetyan, Roberto Bassi and Roberta Croce, the work presented in this thesis would not have been possible. The collaboration with Leonas Valkunas, the mental father of chapter 5, provided the primary prerequisite for a serious physics thesis: a large number of equations.

Being "the boss" of the streak camera I helped a large number of people with streak measurements on a great variety of different systems. I really liked these collaborations, that broadened my horizon (a little bit) beyond Photosystem I.

Wouter, jij bent de enige "echte" student die ik begeleid heb, maar daar hebben we dan ook goed de tijd voor genomen. Je kunt je in ieder geval beroemen op het mooist uitgevoerde afstudeerverslag dat in onze vakgroep het licht zag. Ik hoop dat je dit boekje ook mooi vindt.

Michael, alhoewel de metingen die we aan PYP probeerden te doen op jou meer overkwamen als een doffe aaneenschakeling van rampen, en ik in Duitsland zat op het moment dat ik beloofd had je verslag te bespreken, hoop ik dat je het toch een beetje leuk hebt gehad. We gaan in ieder geval binnenkort een biertje drinken!

Kinga, although I was your official supervisor during your first visit to Amsterdam I "delegated" most of this task to Janne, although I did not skip your Polish Wodka parties. I wish you a lot of succes with your Phd-work.

Janne, when you first came to Amsterdam, a finnish Phd student to work with was the last thing I was waiting for. You have been very patient with me during this first visit (thanks for supervising Kinga), and eventually everything turned out remarkably well, culminating in us almost freezing to death during our night outside, near the arctic circle, at -25°C .

I thank dr. Fleming, dr. Blankenship, dr. Freiberg, Ivo and of course Rienk for reviewing my thesis. Ook de vele anderen die in de loop van de tijd mijn manuscripten aan een kritische blik hebben onderworpen ben ik dank verschuldigd. Peter, bedankt voor de last-minute (met of zonder streepje?) taalkundige correcties in de inleiding. Alex, bedankt voor het font waarmee dit proefschrift is opgemaakt.

Om rustig wetenschap te kunnen bedrijven is de ondersteuning door niet-wetenschappers onontbeerlijk. Ik wil daarom het secretariaat (met name Sandra van der Kolk en Petra de Gijssel), de administratie, de electronische en fijnmechanische werkplaats en de computergroep bedanken voor de ondersteuning gedurende mijn promotie.

De boog kan niet altijd gespannen staan, en dus wil ik al mijn vrienden en vage kennissen (binnen en buiten de vakgroep) bedanken voor alle biertjes die samen gedronken hebben, en de restaurantjes die we bezocht hebben. Ook de verschillende (ont)spannende (wandel)tochten zijn zeker van belang geweest voor het tot stand komen van dit proefschrift. Het begon natuurlijk allemaal met de onvergetelijke "Dutch Finland expedition", het lage temperatuur experiment in de bossen bij Jyväskylä georganiseerd door Jari-Jari, met L.-O. "one-match" Palsson, Lucas "the animal" Beekman, Vesa ("all the Dutch are arrogant: van Gaal,

Rienk...") Helenius, en natuurlijk mijn (bijna) vaste vakantie-maatjes Erwin en René. Daarna volgden tochten in de Alpen, Pyreneeën, Noorwegen, Zweden, Finland, Californië etc., en het schier oneindige aantal Ardennen-weekenden.

Dankzij Johan, John, Marion, mijn broer Arthur, en Olof heb ik tijdens mijn promotie nooit werkelijk onder een brug hoeven te slapen.

Als laatste, maar beslist niet als minste wil ik mijn ouders bedanken. Jullie hebben me altijd de vrijheid gegeven te doen wat ik wilde, en mij daar ook altijd bij gesteund: tot het einde van de middelbare school was dat zelfs nog inhoudelijk (woordjes Engels overhoren, hè, pap), later meer moreel, en niet te vergeten financieel! Ondanks dat het meeste van het boekje abacadabra voor jullie zal zijn, hoop ik dat jullie uit een gedeelte van de inleiding, en de samenvatting een beetje begrijpen waar ik me de afgelopen jaren mee heb bezighouden. In ieder geval zijn de engelse overhoringen niet voor niets geweest.

